MULTIFRACTALS

AND

THE TEMPORAL STRUCTURE OF RAINFALL

Promotoren:

Dr.-Ing. J. J. Bogardi
Hoogleraar in de hydrologie, hydraulica en kwantitatief waterbeheer

Dr. Ir. J. Grasman
Hoogleraar in de wiskundige methoden en modellen

M. I. P. de Lima

MULTIFRACTALS
AND
THE TEMPORAL STRUCTURE OF RAINFALL

Proefschrift

ter verkrijging van de graad van doctor
op gezag van de rector magnificus
van de Landbouwuniversiteit Wageningen,
Dr. C. M. Karssen,
in het openbaar te verdedigen
op woensdag 23 December 1998
des namiddags te vier uur in de Aula.

The research in this dissertation was funded by the *Junta Nacional de Investigação Científica e Tecnológica* (Portugal) and the Wageningen Agricultural University.

Lima, M. I. P. de

Multifractals and the temporal structure of rainfall. Doctoral Dissertation, Wageningen Agricultural University - With ref. - With summary in Dutch.

ISBN 90-5485-982-2

STATEMENTS

1. Some natural patterns and processes that appear extremely complex can display an underlying simplicity through scale invariance.

2. The temporal structure of rainfall exhibits scale-invariant and multifractal properties over a wide range of scales.

   This thesis.

3. It is important to analyze rainfall with methods that have the potential to assess the full range of rainfall fluctuations.

   This thesis.

4. The algebraic behaviour of the tail of the probability distributions of rainfall intensity is important. It may indicate that the probability of exceeding certain extreme events is greater than the probability predicted by more traditional models such as the one devised by Gumbel.

   This thesis.

5. Breaks in the scaling behaviour of rainfall can be either fundamental in nature or they can be artefacts arising from limitations of the process sample.

   This thesis.

6. Scale-invariant and multifractal analyses can contribute to improving the selection of the resolution for data collection and the type of measuring device. It can also help in evaluating the different procedures that are used to process rainfall records from continuously recording devices.

   This thesis.

7. Data collected by governmental agencies should be made readily available for research. Unfortunately, many data managers still hold on to these data, thinking that they must be 'protected' or traded.

8. Modelling and data collection are not independent processes. Ideally, each drives and directs the other. Therefore, there is a need to improve communication between modellers and data collectors.

9. Protection of soil and water is not only a scientific problem but also an issue of translating scientific knowledge into practical use and legislation.

10. Policies to prevent water pollution from agricultural production should seek to enhance and conserve soil quality as a fundamental step toward improving water quality.

    National Research Council, Board on Agriculture, 1993. Soil and Water Quality — An Agenda for Agriculture. National Academy Press, Washington D.C., U.S.A.

11. Water has already become and will continue to become a critical issue of global importance.

12. Nations must treat their natural resources as invaluable assets.

M. I. P. de Lima
Multifractals and the temporal structure of rainfall
Wageningen, December 23, 1998.

Abstract

Lima, M. I. P. de, 1998. *Multifractals and the temporal structure of rainfall.* Doctoral dissertation, Wageningen Agricultural University, Wageningen, The Netherlands, x+229 pages, 113 Figures, 3 Photographs, 14 Tables, and 2 Appendices (Summary in Dutch).

Rainfall is a highly non-linear hydrological process that exhibits wide variability over a broad range of time and space scales. The strongly irregular fluctuations of rain are difficult to capture instrumentally and to handle mathematically. The purpose of this work is to contribute to a better understanding of the variability of rainfall by investigating the multifractal behaviour that is present in the temporal structure of rainfall. This type of rainfall analysis is based on the invariance of properties across scales, and it takes into account the persistence of the variability of the process over a range of scales.

The dissertation focuses on the analyses of point-rainfall data from four locations in Europe. The data sets differ with respect to climatic origin, type of measuring device used, resolution of the data, and length of the records. The data are from recording and non-recording gauges. The highest resolution of the data is 1 minute, and the lowest is 1 month. The time span of the records varies from 4 years to 90 years.

The presence of scale-invariant and multifractal properties in the rainfall process are investigated with spectral analysis, and by studying the multiple scaling of probability distributions and statistical moments of the rainfall intensity. This study shows that the temporal structure of rainfall exhibits these properties across a wide range of scales. Within the range of scales studied, it analyzes the presence of different scaling regimes and seasonal variation in the statistics of rainfall. The empirical multifractal scaling exponent functions that describe the statistics of the rainfall process are derived. Special attention is given to discontinuities in the empirical scaling functions that are caused by the finite size of the samples, the divergence of moments, and the dynamic and temporal resolutions of the rainfall measuring devices and data. The critical exponents associated with these multifractal phase transitions are studied empirically.

The applicability to rainfall of a theoretical multifractal model based on Lévy stochastic variables is studied. The adequacy of this model in describing the empirical scaling functions of rainfall is examined. Results indicate that it is possible to quantify the statistics of rainfall

over a wide range of scales, and over a range of the process dynamics using only a few parameters. For an analysis of this type, it is essential to recognize the effects of such limitations as the sample size, and the type of acquisition of the experimental data and its resolution.

This dissertation shows that multifractals offer a good framework for the analysis of the temporal structure of rainfall. It provides a good description of both the average and the extreme events. The expectation is that this type of studies will help in solving problems related to the choice of suitable resolutions for data collection and in making a correct assessment of the 'quality' of data sets.

Free descriptors:
Rainfall; time series, multifractals; scale invariance; scaling; 'universal' multifractal model.

Samenvatting

Regenval is een sterk niet-lineair stochastisch proces dat een grote variabiliteit vertoont over een breed spectrum van schalen in tijd en ruimte. De irreguliere fluctuaties van regen laten zich moeilijk vastleggen door meetinstrumenten vanwege de beperkingen van deze apparatuur en zijn ook wiskundig moeilijk te beschrijven. Omdat regenval van directe invloed is op andere processen, vormen de ruimtelijke en spatiële variabiliteit ervan een belangrijk element in vele studies op diverse gebieden van onderzoek. Het gemis van geschikte regenval-data vormt één van de belangrijkste obstakels in verdere ontwikkelingen in de hydrologie, die daarvan afhankelijk zijn.

Het doel van deze studie is om bij te dragen aan een beter inzicht in de variabiliteit van regenval door het multifractaal gedrag te onderzoeken dat aanwezig is in de temporele structuur van regenval. Dit type onderzoek is gebaseerd op de invariantie van eigenschappen over een schaaldomein en richt zich op de persistentie van variabiliteitskarakteristieken over zo'n schaaldomein. Met deze methode is men in staat regenval-fluctuaties vrijwel volledig vast te leggen.

Het onderzoek betreft de analyse van punt-regenval data van vier verschillende locaties in Europa: Vale Formoso en Coimbra in Portugal, Assink (Hupsel) in Nederland en Nancy in Frankrijk. De data verzamelingen verschillen onderling voor wat betreft het plaatselijke klimaat, het type meetinstrument en de resolutie en lengte van de tijdreeks. De gegevens zijn afkomstig van automatisch- en niet-automatisch registrerende regenmeters. De hoogste resolutie was 1 minuut en de laagste 1 maand. De lengte van de reeksen varieert van 4 tot 90 jaar.

De aanwezigheid van schaalinvariante en multifractale eigenschappen van het regenvalproces wordt onderzocht met spectrale analyse en met meervoudige schaling van de waarschijnlijkheidsverdelingen van de regenvalintensiteit. Het onderzoek laat zien dat in de temporele structuur van regenval deze eigenschappen aanwezig zijn over een breed schalingsdomein. Binnen dit domein blijken er verschillende schalingsregimes te bestaan.

Ook is er de seizoensfluctuatie, zoals deze is terug te vinden in de regenvalstatistieken. Het gedrag op de korte tijdschaal en het effect van de methode van acquisitie van punt-regenval data zijn eveneens onderwerp van onderzoek. De empirische multifractale schalingsexponentfuncties die worden gebruikt om de variabiliteit te kwantificeren, worden afgeleid. Speciale aandacht wordt gegeven aan discontinuïteiten in deze functies die veroorzaakt worden door de eindige lengte van de tijdreeksen, de divergentie van statistische momenten en de dynamische eigenschappen en temporele resolutie van de meetinstrumenten. In relatie hiermee worden de kritieke exponenten die behoren bij multifractale fase-overgangen op empirische wijze onderzocht.

De toepasbaarheid van het universele theoretische multifractaal model is vervolgens onderwerp van studie. Dit model, gebaseerd op stochastische variabelen van het Lévy type, is een multiplicatief cascademodel. Het geeft analytische uitdrukkingen voor de multifractale schalingsexponentfunctie die geheel worden vastgelegd door drie parameters. Nagegaan wordt hoe geschikt deze modellen zijn voor de benadering van de empirische schalingsfuncties. Het blijkt dat er belangrijke verschillen optreden voor zowel zeer hoge als zeer lage intensiteiten. Voor lage intensiteiten is er een verschil dat kan worden teruggebracht tot de aanwezigheid van nullen in de data-verzameling, terwijl het model er impliciet van uit gaat dat deze er niet zijn. Voor hoge intensiteiten vertoont het model niet die sterke variabiliteit die wordt gevonden in experimentele data van grote tijd-reeksen. Deze grote variabiliteit geeft aanleiding tot divergentie van statistische momenten vanaf een zekere orde. Dus de waarschijnlijkheid van het voorkomen van hoge regenvalintensiteiten (extreme gebeurtenissen) is groter dan wordt voorspeld door het theoretische model. Ondanks deze verschillen, laten de resultaten zien dat het mogelijk is om de statistische eigenschappen van regenval over een breed spectrum van schalen te kwantificeren met behulp van slechts enkele parameters. Voor een analyse van dit type is het van belang om de beperkingen waarmee men bij deze aanpak wordt geconfronteerd, te onderkennen. Deze betreffen de lengte van de tijdreeks, het type meetinstrument en de resolutie ervan.

Deze studie toont aan dat met multifractale analyse de temporele structuur van regenval gekwantificeerd kan worden, waarbij een goede beschrijving van gemiddelde en meer extreme gebeurtenissen gegeven kan worden. De verwachting is dat dit type onderzoek kan bijdragen tot het oplossen van problemen die te maken hebben met de keuze van de juiste resolutie van te gebruiken tijdreeksen en van het juiste type meetinstrument. Ook kan het helpen bij de beoordeling van de kwaliteit van een gegeven data-verzameling en bij het opstellen van een procedure voor de vervaardiging van tijdreeksen uit continue metingen.

Table of contents

Chapter 1
Introduction

Precipitation is one of the driving forces of the hydrological cycle. It is the hydrological process having perhaps the greatest impact on everyday life. Precipitation is the product of a complex combination of numerous physical processes, which include microphysical cloud processes and precipitation particle growth, and continental and global patterns of airflow. The processes involved in the formation of precipitation operate over a variety of scales in space and time, and interact with surface topography, soil moisture, and vegetation, for example.

Precipitation exhibits a high non-linear variability over a wide range of time and space scales. Precipitation phenomena range from cells (associated with cumulus convection), to synoptic areas (frontal systems). Rain cells have an areal extent of the order of 1-10 km^2 and lifetimes of several minutes. Synoptic rain fields cover areas of 10^4 km^2 and have a lifetime of one to several days. This variability involves a large dynamic range, which in certain cases leads to catastrophic events. Such strongly irregular fluctuations of rainfall are difficult to capture instrumentally (because of technical limitations of the measuring devices) and to handle mathematically. Another difficulty inherent to the precipitation data collection is that it is expensive owing to the high-density network required.

Precipitation is the driving agent of many other processes. Its temporal and spatial variability are important issues in many studies and areas of research (e.g. hydrology, hydraulics, agronomy, soil pollution, water resources). However, information on the amount and distribution of precipitation in space and time is often restricted because of its strong temporal and spatial variation. Therefore, hydrological models have usually to conceptualize processes based on simple, often homogeneous, approximations of nature (e.g. rainfall is expressed as a mean over large areas, and as depths over periods of a day). Such generalized conceptualizations often lack sufficient temporal and spatial resolutions to permit a detailed modelling of complex hydrological processes. The lack of adequate rain data is claimed to be one of the main problems hindering progress in many hydrological studies.

The study of precipitation has been an active area of research in the last two decades. Research has been mainly oriented towards understanding the physical mechanisms producing rainfall, and the incorporation of precipitation dynamics in stochastic rainfall models. A drawback of many existing rainfall models is their unsatisfactory handling of the great temporal and spatial variability of this process. Moreover, empirical scale truncations are made often, and one scale is studied independently of the others. Many models are also often misused because their restricted applicability to different scales is not taken into consideration.

In hydrology, such (scale) issues are very important, and influence the study of other hydrological processes (for reviews of scale issues see e.g. Klemeš, 1983; Rodríguez-Iturbe and Gupta, 1983; Dooge, 1986; Gupta et al., 1986; Wood et al., 1990; Beven, 1991; Kalma and Sivapalan, 1995; Blöschl and Sivapalan, 1995). The 'scale problem' has been identified as a major unresolved problem in hydrology (e.g. NRC, 1991). Quite often, combined work on different components of the earth system requires bridging across scales, in space and/or time. Specifically, hydrological processes are often observed and modelled using short time-scales, whereas estimates are needed for very long time-scales. Similarly, models and theories developed in small space-scale laboratory experiments are expected to hold good for larger scales (for example, at the scale of a catchment area). Conversely, large-scale models are sometimes used for small-scale predictions. This involves some sort of extrapolation or transfer of information across scales. Thus it is pertinent, for example, to know whether there are intrinsically different phenomena as one moves from one scale to the next; and whether results obtained on one scale can be transported to the other. Another question is the adequate temporal and spatial resolution for data collection. Then, even when problems of this type are not addressed explicitly, they are always at the core of research and applications in hydrology. Therefore, there is a general need for a better understanding of the variability in different natural processes.

Recent advances in applied mathematics (stochastics, non-linear dynamics and numerical analysis), supported by developments in computer science and remote sensing technology, have contributed to the development of theories that are based on the invariance of properties across scales. In hydrology, attention is focusing on the search for such invariance, as a basic hidden order in hydrological phenomena.

Theories that hold for a broad range of scales are called *scaling* theories. They apply to processes and systems without a characteristic scale. The term *scaling* (or the term *scale-invariance*) is used to indicate that certain features of a dynamic system are independent of scale. One can think of a scale-invariant process as one in which the same type of elementary dynamics acts at each relevant scale (i.e. a common behaviour is present at different scales). Scale-invariance leads to a class of *scaling rules* (*power laws*) characterized by *scaling exponents*. This allows the *relationship* of variability between

different scales to be quantified. Statistical properties of scale-invariant systems at different scales (i.e. on large and small scales) are related by a scale-changing operation that involves only scale ratios. Scaling theories offer an alternative to ('traditional') approaches that study one scale independent of the other.

The invariance of properties being maintained across scales can be mathematically investigated using *fractal* and *multifractal* theories. In fact, these theories have evolved from a *fractal* theory into a *multifractal* theory. They are based on the recognition that the type of variability of processes and systems exists for a range of scales. An initial contribution was Richardson's well-known poem[1] on self-similar cascades, in 1922. It developed into a theory/geometry that was characterized as being *fractal* by Mandelbrot (1977, 1982). Using fractal theory one deals with *simple scaling*, taking the stand point that the statistical variability does not change with scale. Fractals have the potential to describe complex phenomena by a minimal number of parameters, which makes them an appealing tool. The need to generalize the scaling properties of physical processes has led to the *multifractal* theory (Hentschel and Procaccia, 1983; Grassberger, 1983; Schertzer and Lovejoy, 1983), dealing not with simple scaling but with *multiscaling*. Multifractals are thus more general than simple fractals. Their behaviour is determined not by one, but by an infinity of scaling exponents.

In the last decade, multifractals have been given considerable attention by the scientific community; they have been used to study diverse types of geophysical processes. Many complex physical processes that are governed by highly non-linear dynamics exhibit multifractal behaviour (e.g. turbulence, atmospheric circulation, cloud formation, ocean currents, spread of pollutants, tornadoes, volcanic eruption, and earthquakes). For reviews, see e.g. Schertzer and Lovejoy (1991a, 1993), and Lovejoy and Schertzer (1995b). In these processes non-linear dynamics couples with scaling. This behaviour is the result of (non-linear) interactions between processes at different scales, which lead to a non-linear (i.e. non-proportional) response to a given 'excitation.'

Outline of the research

The large temporal (and spatial) non-linear variability of rainfall usually hampers the measuring and modelling of this process. The invariance of properties and multifractality in the structure of the rainfall process, over a range of scales, may lead to an understanding of its variability that cannot be grasped from other descriptions of the complex dynamics of this process. Such knowledge of scale-invariant behaviour can contribute to improve data collection as it may give an indication of the required temporal

[1] Big whorls have little whorls that feed on their velocity,
and little whorls have smaller whorls and so on to viscosity
— in the molecular sense.

(and spatial) sampling resolution. Moreover, the expectation is that multifractal theory and its application in models offer tools to produce high-resolution synthetic rainfall data. These data can be used in many hydrological applications and studies (e.g. rainfall-runoff, soil erosion, spread of pollutants, urban drainage).

The alternative approach to the study of rain using multifractal theory has been reported in only a few studies (see Section 3.6 for a review), and needs to be investigated further. The applicability of the multifractal theory to rainfall has still not been fully explored.

The purpose of the present study is to contribute to a better understanding of the non-linear variability of rainfall by investigating the scale-invariant and multifractal behaviour that is present in its temporal structure. The study is based on spectral analysis and on investigation into the scaling of probability distributions and statistical moments of the rainfall intensity. It uses point-rainfall data from 4 different locations in Europe. The data sets differ with respect to climatic origin, type of measuring device used, resolution of the data, and time span of the records. The data are from non-recording gauges and recording gauges of both the float and the tipping-bucket types. The length of some records, especially for the high-resolution rainfall data (over a period of 23 years), is an important contribution to the subject. The small-scale behaviour in the rainfall process, and the effects that the different types of acquisition of point-rainfall data have on the analysis, are among the topics that are dealt with in this work. The study includes the investigation of different scaling regimes, and characterization of the multifractal behaviour. Empirical multifractal exponent functions describing the scaling of the probability distributions and the scaling of the moments of the rainfall intensity are determined for different ranges of time scales. Special attention is given to discontinuities in the empirical scaling functions that are caused by the finite size of the samples, the divergence of moments, and the dynamic and temporal resolution of the rainfall measuring device and data. The description of the empirical scaling functions using a multifractal model based on Lévy random variables is investigated. The study also discusses seasonal variations in the multifractal temporal structure of rainfall.

Outline of the dissertation

This dissertation is structured as follows. Chapter 2 reviews some studies of precipitation in hydrology. It describes briefly the physics of precipitation, and some techniques commonly used to measure this process. Special attention is also given to a review of some 'traditional' approaches to the temporal study of rainfall, including analysis, design procedures and modelling. Chapter 3 reviews the fractal and multifractal theories, as well as analysis techniques that are relevant to the study of the temporal structure of rainfall. The inclusion of such an extensive review in the dissertation aims at helping researchers who are not familiar with those theories to understand the topic better. The last section of Chapter 3 discusses the assumptions and motivation to study rainfall using multifractal

theory, and gives a brief review of previous studies. Chapter 4 introduces the point-rainfall data that are analyzed in this work. Chapter 5 presents and discusses the results of the multifractal analysis of the temporal structure of the rainfall described in the previous chapter. Chapter 6 presents some concluding remarks.

Some theoretical topics complementary to the review of the multifractal theory (in Chapter 3) are given in Appendices I and II. Appendix I is dedicated to the role of Lévy variables in the multifractal model known as 'universal' multifractals (this model is discussed in Section 3.4). Appendix II shows the relation between the multifractal ('turbulence') formalism used in this dissertation and the 'strange attractor' formalism.

References are to be found at the end of this work, as well as the list of the symbols and abbreviations that appear throughout this dissertation. In this work, figures, photos, tables, and equations are numbered by chapter.

Chapter 2
Review of rainfall studies in hydrology

2.1 Introduction

Hydrology may be defined as the science that deals with the water of earth, its occurrence, circulation and distribution, and its chemical and physical properties. It includes the cycling of continental water at all scales as well as those biological processes that interact significantly with the hydrological cycle. It also includes the spatial and temporal characteristics of the global water balance in the earth system. Hydrology is an important component in meteorology, geography, agronomy, forestry, geology and biology, for example. Hydrological investigations, including the collection and interpretation of data on such processes as precipitation, evapotranspiration, and discharge, are essential for the practical planning of land use and design of water development schemes.

For hydrology, the most important of the many meteorological processes occurring continuously within the atmosphere are the processes of precipitation and evaporation. These processes are the result of interactions of the atmosphere with surface water. Precipitation occurs in a number of forms. A simple distinction can be made between liquid and solid forms of precipitation, and between vertical and horizontal precipitation. Vertical precipitation falls onto the earth's surface (e.g. rain, snow, hail and other variations such as drizzle and sleet) whereas horizontal precipitation is formed on the earth's surface (e.g. dew, fog, frost). The form of precipitation and its quantity are influenced by the action of such climatic factors as wind, temperature, and atmospheric pressure. Some of the physical characteristics of rainfall (like intensity, raindrop size, raindrop shape and raindrop fall velocity) play an important role in hydrology and other earth sciences (e.g. soil physics). These characteristics are correlated (see e.g. Kohnke and Bertrand, 1959; Chow et al., 1988; Smith, 1993).

Atmospheric processes that produce precipitation operate over a variety of time and space scales, and interact, for example, with surface topography, soil moisture and vegetation. Precipitation displays extreme variability: in time, over intervals of minutes to years; and in

space, from less than one to several thousand square kilometres. One of the major challenges for hydrologists, meteorologists and climatologists is to measure, model and predict the nature of this variability.

The study of precipitation has been an active area of research in the last decades. Precipitation *research* includes: precipitation *measurement* and *estimation*; precipitation *modelling* in space and time; and quantitative precipitation *forecasting* (see e.g. Singh, 82; Georgakakos and Kavvas, 1987; Foufoula-Georgiou and Georgakakos, 1991).

This chapter reviews briefly some studies of precipitation that are relevant to the present work. Section 2.2 deals with the physical characteristics of precipitation, and its space and time distribution. Section 2.3 describes some methods for measuring precipitation. Finally, Section 2.4 reviews some approaches to the study of the temporal structure of precipitation that are used 'traditionally'; the review covers analysis, design procedures, and modelling. The 'alternative' approach to the study of precipitation based on scale-invariance is discussed in more detail in other chapters of this dissertation.

2.2 Space and time distribution of precipitation

Many physical processes are involved in the formation of precipitation (see e.g. Eagleson, 1970; Chow et al., 1988; McIlveen, 1992; Smith, 1993; Jones, 1997). It requires the lifting of an air mass in the atmosphere so that it cools and some of its moisture condenses. Evaporation adds vapour to the lowest atmospheric levels, where the water vapour concentration is highly variable both in space and time. This water vapour is transported upward through the lower troposphere largely by convection. And it is removed, mostly from the mid-troposphere, by the formation of rainfall and snowfall. The upward flux from the earth's surface due to evaporation depends upon the states of the surface and of the adjacent atmosphere (e.g. available moisture, heat). The downward flux is due to precipitation and to direct condensation on the surface (e.g. dew), being here precipitation the most important of these two mechanisms. Conservation of mass demands that there is an equality between evaporation and precipitation when averaged spatially over the earth's surface and temporally over a long period. The amount of atmospheric water vapour over a region is not necessarily related to the resulting precipitation. Atmospheric moisture is a necessary but not sufficient condition for precipitation. Therefore, temporal and spatial variability of precipitation can be expected at all scales.

Three basic stages are necessary for precipitation to occur (see e.g. Eagleson, 1970; Chow et al., 1988; Smith, 1993):

(a) creation of saturation conditions;

(b) phase change of water content from vapour to liquid and/or solid state;

(c) growth of the small water droplets (or ice crystals) to precipitable size.

The conditions for the occurrence of saturation result, almost exclusively, from the cooling that accompanies an ascending movement of moist air. In relation to the mechanisms for cooling a distinction can be made between cyclonic, convective, and orographic cooling. Condensation requires a 'seed' (condensation *nucleus*), which is essential for the 'attachment' of the water molecules. When temperatures are below the freezing point, ice crystals are formed.

At the ground surface, precipitation varies greatly both in space and time. This is a consequence of the different precipitation generating mechanisms (e.g. related to cloud formation and to the different cooling mechanisms), and the general patterns of atmospheric circulation, for example. The following local factors are also important (Eagleson, 1970):

(a) latitude: in general, annual precipitation totals are high in latitudes of predominantly rising air (0 to approximately 60° latitude) and low where the primary vertical motions are descending (from about 30 to about 90°);

(b) altitude: due to orographic cooling there is an increase in precipitation with elevation, up to about 1500 m; and topography or relief (e.g. mountain ranges);

(c) position within, and size of continental land masses (thus, distance from moisture sources);

(d) prevailing wind direction (towards or away from the source of moisture) and wind intensity;

(e) relative temperatures of land and bordering oceans.

Apart from variations in precipitation quantities, their patterns of occurrence are also different in different climatic regimes. In general, the greater the annual precipitation the less variation from year to year (Shaw, 1983). Seasonal variation in precipitation is pronounced where the annual oscillation in the atmospheric circulation changes the amount of moisture inflow over those regions (Chow et al., 1988). As an example of the precipitation variability, Figure 2.1 illustrates the spatial and seasonal differences of precipitation in mainland Portugal. On a global scale the variations of spatial and temporal distribution of precipitation are even more pronounced.

2.3 Precipitation measurements

Precipitation is routinely measured throughout the world. Nevertheless, the solid knowledge of its spatial and temporal distribution is hampered by the existing diversity of observation standards and the erratic pattern of observing networks. A variety of methods have been developed for measuring precipitation, mainly as a result of the time and space variability exhibited by this process. These techniques range from point gauge measurements to methods based upon the interpretation of indirect data obtained from space-based instrumentation. Descriptions of precipitation measurement methods can be found in e.g. Seyhan (1977), Engman and Gurney (1991), Collier (1997), Jones (1997). A problem that results from the methods and instrumentation used to measure precipitation is the suitability of the data

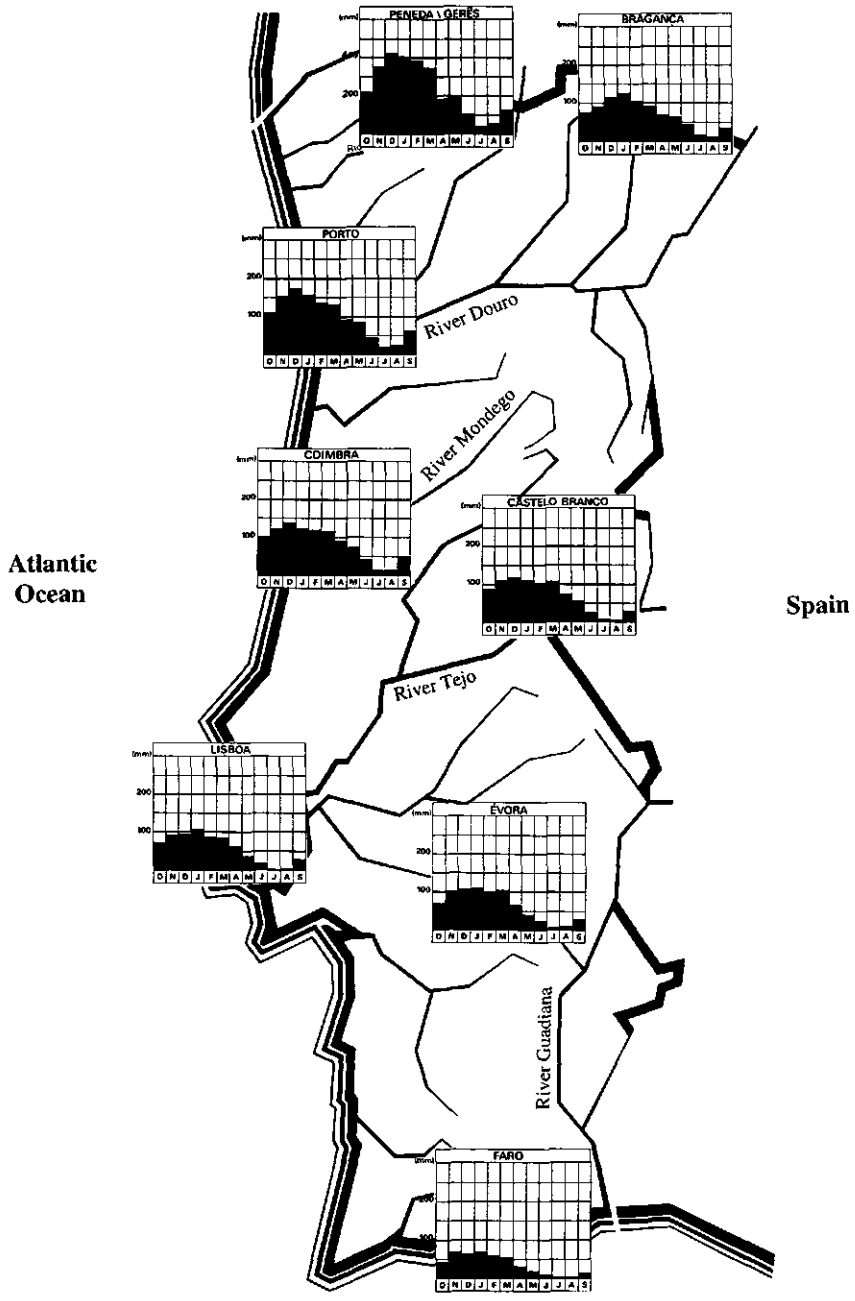

Figure 2.1 Example of spatial and temporal differences of precipitation in mainland Portugal, showing the monthly variation of precipitation at different locations (adapted from DGRN).

available for many hydrological studies and applications. This problem is caused by the difficulties inherent to the data collection over the time and space scale ranges associated with the variability of precipitation. Data collection over such ranges of scales is both technically difficult and expensive.

Some types of precipitation measurement are described below, which include gauge, radar, satellite and raindrop size.

Gauge measurement

The gauge measurement of precipitation is by far the method most commonly used. In this method, precipitation events are recorded by gauges at specific locations. Rainfall collected in gauges is referred to as *point-rainfall* to distinguish it from average figures of rainfall over large areas.

Gauges for measuring rainfall and snowfall are of two types: non-recording and recording. Non-recording gauges measure rainfall-depth accumulations over time. They do not provide information about the time of occurrence, duration, intensity and pattern of the precipitation. For this type of information a recording gauge is required.

There are two types of *non-recording* gauges: standard gauges and storage gauges (e.g. Shaw, 1983; Chow et al., 1988). *Standard* gauges are used for daily rainfall readings (or any other desirable time-interval readings). These gauges consist simply of a collector above a funnel leading to a receiver (a cylindrical container), and they have a calibrated measuring stick, which may be a part of the gauge. The measuring stick, when inserted, shows the equivalent rainfall depth. Rain gauges for locations where readings are only taken weekly or monthly are similar in design to the daily type, but have a larger capacity receiver. *Storage* gauges are used to measure rainfall over an entire season. Such measurements are usually done in remote, sparsely inhabited areas. The gauges consist of a collector above a funnel that leads into a storage area sufficiently large to contain the seasonal rainfall volume.

The three major types of *recording* rain gauges are the weighing type, the float type, and the tipping-bucket type (e.g. Chow et al., 1988; Singh, 1992; Smith, 1993). They yield either a continuous record of cumulative rainfall depth over time, on a moving chart (i.e. a mass curve of rainfall-depth versus time), or an indication of the time of occurrence of sequential rainfall-depth increments, through a tipping-bucket. Recording gauges can have temporal resolutions of less than one minute.

Weighing-type rain gauges record continuously the accumulated precipitation over time by means of a spring mechanism or a system of balance weights. The record in a chart, of a mass curve, can be translated into an intensity-time graph by calculating the ratios of accumulated precipitation to time for whatever time-step is desired. This type of gauge is useful for recording snow, hail, and mixtures of snow and rain.

A schematic representation of a *float-and-syphon* recording rain gauge is shown in Figure 2.2. This type of gauge has a chamber containing a float that rises vertically as the water level in

the chamber rises; the vertical movement of the float causes a pen to move on a chart. A device for syphoning the water out of the gauge into a receiver-collector is used so that the total amount of rain falling can be collected.

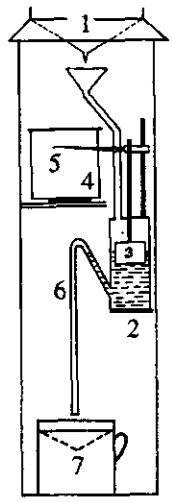

1 - Metal funnel with limiting ring
2 - Measuring vessel
3 - Float
4 - Drum
5 - Pen
6 - Syphon
7 - Collecting jar

Figure 2.2 Schematic representation of a float-and-syphon recording rain gauge.

Tipping-bucket gauges sense each consecutive rainfall accumulation when it reaches a prescribed amount. A tipping-bucket rain gauge operates by means of a pair of buckets (reservoirs), having a certain depth capacity. Figure 2.3 shows a scheme of the way such gauges operate (in Figure 2.3 reservoirs *A* and *B* designate the buckets). The rainfall fills first one bucket, which overbalances, directing the flow of water into the second bucket. The motion of the tipping-buckets is transmitted to the recording device and provides a measure of the rainfall intensity. Tipping-bucket gauges do not have a well-defined temporal resolution.
Recording and non-recording rain gauges can differ in relation to the collecting area, height, wind shields, etc. (see e.g. Sevruk and Klemm, 1989; Sevruk, 1993c). Recording rain gauges are often equipped with telemetry to allow real-time transmission and utilization of the information for water management.

Gauges can be used to measure *snowfall*, when appropriate modifications are made. Usually, these involve providing a melting agent so that the snow can be converted into measurable water (see e.g. Viessman and Lewis, 1996).

There are several factors that may affect the accuracy of gauge measurements of precipitation (e.g. Dingman, 1993, Jones, 1997; Rodda, 1997; Yang et al., 1998). Some errors that must be considered include: (a) systematic errors caused by the measuring device; (b) human errors; (c) numerical errors in the processing of raw data. Systematic errors may be related to: the gauge orifice size and orientation; orifice height; wind shielding (i.e. distance from obstructions); splash; evaporation losses prior to measurement; losses due to 'wetting'; and

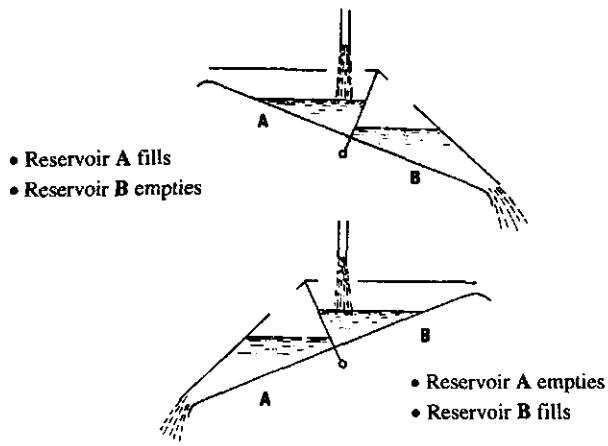

Figure 2.3 Schematic representation of a tipping-bucket recording rain gauge.

other instrument errors due to malfunctions (e.g. interruption of registration, damage of the clock mechanism). Human errors include observation errors and administration errors. Other errors may be due to differences in the observation time, and low-intensity rains, for example. The inherent potential inaccuracy of the measurements should be kept in mind when using precipitation data.

Precipitation amounts sometimes vary considerably within short distances. Under windy conditions, rain gauge measurements may be affected by disturbance of the wind pattern around the gauge; this usually causes low readings (e.g. Dingman, 1993; Sevruk, 1993c; Viessman and Lewis, 1996; Jones, 1997). The magnitude of the error depends on the type of rain gauge, climatic conditions at the gauge site (wind speed, type of precipitation — rain or snow —, and temperature), and its degree of exposure (e.g. Sevruk and Klemm, 1989; Sokollek et al., 1989). The magnitude of wind-speed and turbulence increases with the distance from the ground. Measurement errors (i.e. collection deficiencies) for snow are typically much larger than for rain (e.g. Larson and Peck, 1974; Smith, 1993). Gauge collection deficiencies of wind-driven rain are difficult to estimate because of local variations of rainfall inclination in relation to the topography. Local variation in rain-flux above the ground may be the result of a redistribution of falling drops due to local wind-flow deformations. Theses are induced by local topography and surface roughness elements (e.g. Sharon, 1980; Sharon and Arazi, 1993). A non-uniform distribution of rainfall, over a hill-slope area, can be explained by geometric relationships between the direction and inclination of incoming rainfall, varying local aspect and slope inclination (Sharon, 1980; Sharon et al., 1988; Lima, 1990).

Unfortunately, there are no international standard for the height of the rain gauges, or other gauge characteristics (see e.g. Sevruk, 1989). Therefore, whereas some gauges face the

problem just described (caused by turbulence), others face the opposite problem of rain splashing up and into the gauge, from the ground surface.

Although in some parts of the world rain gauges have been in use for over two millennia, extensive coverage has been available for only one or two centuries, at most. As with other hydrological data, coverage is poorest in arid, semi-arid, tropical and highland regions, as well as over the oceans. Nevertheless, rain gauges still yield the most accessible and most reliable data at ground point-scale. Until the late 1940s rain gauge networks were practically the only means of obtaining measurements of the areal distribution of rainfall. This method presents problems in gathering and processing data from many points; it is also expensive to invest in a high gauge-density. Large-scale rain fields are, therefore, difficult to derive from point gauge measurements, many of which are made at non-representative sites. In addition, for many studies and applications, data recorded daily, hourly, or even over shorter time-intervals, are necessary, although data on time scales of less than a month are difficult to obtain.

Radar measurement

Radar can be used to observe the location and movement of areal precipitation. Estimates of rainfall rate, over areas within the range of the radar, can be obtained with certain types of equipment. It is thus possible to sample a large area from one station. This method of rain measurement provides high spatial and temporal resolutions (see e.g. Almeida-Teixeira et al., 1994). However, the physics of the radar measurements and the processing of data affect the inferred statistics of rainfall (see e.g. Krajewski et al., 1996).

Radar stands for *radio detecting and ranging* and utilizes the propagation and reflection of electromagnetic waves (e.g. Eagleson, 1970; Singh, 1992; Smith, 1993). A (radar) transmitter produces impulses of energy that are radiated by a narrow-beam antenna. The same antenna intercepts echoes of the impulses, from targets in the range of the beam. The azimuth of a target is determined by the direction of the beam; the time between emitting a pulse and receiving its echo from that target determines its range (e.g. Eagleson, 1970). Scanning with the antenna gives the polar coordinates of all reflecting targets in the range of the radiation emitted.

Weather radars depend on the reflection of the waves from the droplets of water in the air (within the storm). The rainfall intensity, for a storm, can be determined from the corresponding reflectivity values. The degree of reflection is related to the density of the droplets and, therefore, to the rainfall intensity (e.g. Eagleson, 1970; Smith, 1993). The relation, however, is not unique. In addition to other factors, there are systematic deviations introduced by the climatology of precipitation in different parts of the world, and by different synoptic precipitation types (e.g. Eagleson, 1970; Smith, 1993; Almeida-Teixeira et al., 1994). The accuracy of radar measurements should be determined through comparison with recording rain gauges. This requires the presence of such a gauge or network inside the storm and within the radar range. Moreover, the gauge data must be of good quality (e.g. Almeida-Teixeira et al., 1994).

The development of weather radars has increased the understanding of the vertical structure of precipitation in cold clouds. Some cloud features play an important role in the development of procedures for estimating rainfall from radar and satellite sensors (e.g. Smith, 1993; Jones, 1997).

Satellite measurement

Currently, satellites are not capable of measuring precipitation directly. Nevertheless, they provide useful information about rainfall, in particular over uninhabited regions such as oceans. The basic information for estimating rainfall from satellites is provided by infrared images (e.g. Smith, 1993; Jones, 1997). They are composed of measurements of radiant energy originating from the atmosphere, land, or water. Measurements of infrared energy can be converted to temperature of the medium. These measurements are designated by brightness temperatures, and can be used to infer cloud-top heights, once a temperature lapse rate is given (see e.g. Smith, 1993, Jones, 1997). Low brightness temperatures indicate high cloud-tops, which implies large thickness and, therefore, high probability of rainfall. High brightness temperatures indicate low cloud-tops (or no clouds) and low probability of rainfall.

The lack of well-established direct physical relationships between cloud properties and rainfall is one of the major problems for satellite measurements. Satellite methods for estimating rainfall are being developed (see e.g. Bell and Kundu, 1996; Tsonis et al., 1996; Jones, 1997); they may help to rectify some of the current problems inherent to the gauge-measurement of rainfall.

Raindrop-size measurements

Several methods and devices have been developed for measuring raindrop size. By exposing a pan of oil to rainfall (*oil method*), one can count and size individual drops using a microscope. This method is based on the premise that water-drops, suspended in a viscous fluid less dense than water, assume a near-perfect shape, owing to surface tension forces (Eigel and Moore, 1983). Similar methods use liquid sensitive paper (*stain method*) or a tray with flour (*flour method*). With these methods small drops might be deflected away from the target and the large drops might break up on impact.

Momentum methods that include pressure transducers and piezoelectric sensors have also been successfully used to measure raindrop size and energy. Accurate drop-size analysis requires several sophisticated measuring aids, including photo-imaging, laser light diffraction, linear diode and phase-Doppler (Ferrazza et al., 1992). Automated devices include the *distrometer* and the *raindrop camera*. With these techniques it is possible to characterize raindrops and obtain information such as drop-diameter average, drop-size distribution and velocity profiles. Drop-size distribution is typically specified by a function representing the density of drops as a function of drop diameter (e.g. Smith, 1993). A number of important variables related to rainfall can be computed from these observations, including rainfall rate, rainfall energy flux (i.e. kinetic energy per unit time), and radar reflectivity factor.

There is a need to improve methods that combine satellite, radar, and ground measurements with statistical theory, to produce large-scale precipitation fields and to create better archives of already existing data (see e.g. NRC, 1991).

It is important to assess the *homogeneity* of precipitation records, both in spatial and temporal studies of this process (see e.g. Sevruk, 1993a). The main sources of data inhomogeneity are: (a) changes of the accuracy of the measurements; (b) changes of temporal and/or spatial sampling and/or data processing; and (c) microclimatic changes of the local sampling environment. Some methods were developed for detecting inhomogeneity in climatic records in the absence of information about the history of the observations (e.g. Witter, 1984; Dahmen and Hall, 1990). Knowledge of this history is very important. For gauge-measured precipitation, it should contain information about: the type of instruments used, their elevation above ground and exposure; the local surroundings; observation schedules; and maintenance procedures (see e.g. Sevruk, 1993b). Without such information, many cases of inhomogeneity in climatic data cannot be identified or corrected.

2.4 Some 'traditional' approaches to the study of temporal rainfall

The study of precipitation, and the requirements of hydrological and engineering applications, have led to many different approaches to analyzing and modelling temporal rainfall, and to the development of various design procedures. A review of some of these approaches and procedures, and brief explanations about their structure are given below. The inclusion of this review in this introductory chapter, about rainfall studies in hydrology, aims at pointing out various advantages and drawbacks found by the researchers in relation to the different approaches and methods. This review also shows that the scientific community is very active in trying to find and investigate new 'tracks' that may increase the understanding of the complex non-linear process of precipitation.

The approaches to the study of rainfall that are reviewed below are labelled 'traditional' to distinguish them from the more recently proposed approach based on *scale-invariance*. This 'alternative' approach is investigated in this work, and is discussed in Chapters 3 and 5.

2.4.1 Analysis techniques

Time series

Hydrological processes, such as precipitation, evolve on a *continuous* time-scale. However, for practical purposes, most hydrological processes are defined in *discrete* time (see e.g. Wu, 1973; Salas, 1993). A discrete time-series may be obtained by sampling the continuous process at discrete points in time; or by integrating the process over successive time-intervals (such a time series, of one hydrological variable at a given site, is called a *single time-series*). In

general, a time series $x(t)$ over a finite period of time T is not capable of characterizing the entire random process unless T is extended to infinity. One should consider the statistical analysis of a time series as being an approach to studying the statistical properties and probability structures of random processes (Wu, 1973).

Two features of hydrological time-series that are relevant for precipitation are *intermittency* and *stationarity* (e.g. Salas et al., 1980; Salas, 1993). Hydrological time-series are intermittent if throughout the record there are periods during which the process has a constant value of zero. For example, the precipitation observed in a (continuously) recording gauge is an intermittent continuous time-series. A discrete precipitation time-series, obtained from integrating an intermittent continuous precipitation time-series, can be intermittent when the time interval of integration is relatively small. Depending on the location, monthly and annual rainfall time-series are usually non-intermittent.

A hydrological process is stationary if its statistical characteristics (e.g. mean, variance) do not vary in time. Consequently, the time series is free of trends, shifts, or periodicity. Otherwise, the time series is non-stationary. In general, hydrological time-series defined on an annual time-scale are stationary. This assumption may be invalid as a result of large-scale climatic variability, or natural and human-induced changes (see e.g. Weatherhead et al., 1998). Hydrological time-series defined over time scales smaller than a year (e.g. monthly series) are typically periodic and, thus, non-stationary within yearly climatic fluctuations (the annual cycle).

Time-series analysis includes the estimation of a number of statistical properties (see e.g. Box and Jenkins, 1976; Salas, 1993). In hydrology, this analysis is used for building mathematical models to generate synthetic hydrological records, to forecast hydrological events, and to improve hydrological records (e.g. filling in missing data). Moreover, it is used in the detection and estimation of trends, shifts, seasonality, and non-normality in hydrological records.

Spectral analysis

Spectral methods are also known as Fourier transform methods (see e.g. Wu, 1973; Box and Jenkins, 1976; Press et al., 1989; Hastings and Sugihara, 1993). The idea behind these methods is that a physical process can be described either in the time domain (by the values of some quantity as a function of time) or in the frequency domain (where the process is specified by giving its amplitude as a function of frequency). The two representations are linked by means of the Fourier transform equations. The Fourier transform can be an efficient computational tool for accomplishing certain manipulations of the data. The related *power spectrum*, which can be defined as the distribution of variance or power across wavelength or frequency, can be itself of intrinsic interest (see e.g. Press et al., 1989).

Spectral analysis is one approach to the study of the statistical properties of time series. It provides a useful exploratory analysis tool for examining time-series data. Spectral analysis can provide an intuitive frequency-based description of the time series and indicate interesting features such as long memory, presence of high frequency variation and cyclical behaviour

(e.g. McLeod and Hipel, 1995). This type of analysis is useful to detect periodicity of short-interval precipitation sequences at a point (Wu, 1973). If a process contains periodic terms, the frequencies of these terms exhibit a number of high and sharp peaks in the spectrum. This indicates that a significant amount of variance is contained in these frequencies (Wu, 1973; Press et al., 1989). Spectral analysis can handle the transformation of the time series either with a power transformation, to stabilize the variance, or by filtering, to remove non-stationary features. Spectral analysis methods possess a certain degree of robustness because the normal distribution does not need to be assumed (e.g. McLeod and Hipel, 1995).

Rainfall frequency analysis

Frequency analysis relates the magnitude of (extreme) events to their frequency of occurrence using probability distributions. Rainfall frequency analysis is extensively used, mostly for design purposes of engineering works. It also plays an important role in problems related to hazards associated with extremely large rainfall events (the magnitude of an extreme event is inversely related to its frequency of occurrence). Rainfall frequency analysis is a means to compute the amount of rain falling over a given area in a certain time interval, with a given probability of occurrence. However, in most practical situations, the data available are insufficient to define precisely the frequency of occurrence of certain rainfall events. This type of analysis does not deal directly with temporal patterns associated with rainfall depths of a given duration and frequency.

Many types of standard theoretical statistical distributions are used for frequency analysis (see e.g. Haan, 1977; Chow et al., 1988; Singh, 1992; Stedinger et al., 1993; Viessman and Lewis, 1996). Among them one can mention the normal, log-normal, Gumbel, and log-Pearson type 3 distributions. The reliability of the results of frequency analysis depends on how well the assumed probabilistic model applies to a given data set.

2.4.2 Hydrologic design procedures

Probable maximum precipitation

Because of the high risk to lives and property below major hydraulic structures (e.g. spillways on large dams), their design includes provisions for a flood caused by a combination of the most severe meteorological and hydrological conditions. Thus it is necessary to determine precipitation values with very low probability of being exceeded. This need motivated the idea and definition of *probable maximum precipitation* (see e.g. Chow et al., 1988; Smith, 1993). It implies the existence of an upper boundary on rainfall amounts. This limit is theoretically the greatest depth of precipitation for a given duration of the event that is physically possible over a given storm area of a particular geographical location, at a certain time of the year. Such a storm would result from the most critical meteorological conditions considered probable. The question remains of whether there is indeed an upper limit on rainfall amounts. Another (troublesome) problem, given this possibility, is determining this upper boundary.

Intensity-duration-frequency curves

For short duration storms over small areas, the most convenient method of determining storm depth is to acquire the rainfall *intensity-duration-frequency curves* for the locale. These curves are a typical application of rainfall empirical frequency distribution analysis. For design purposes, intensity-duration-frequency curves allow the calculation of the rainfall-intensity for a given probability of exceedance and rainfall duration.

For design applications it is often necessary to specify a temporal pattern associated with rainfall depths; this is generally done for a given rainfall duration and frequency. The time sequence of precipitation (hyetographs) in typical storms can be determined by analysis of storm events observed (e.g. Huff and Changnon, 1964; Huff, 1967; Pilgrim and Cordery, 1975). If one follows procedures available, design hyetographs can be developed from intensity-duration-frequency curves (see e.g. Chow et al., 1988; Smith, 1993).

2.4.3 Modelling approaches

Rainfall is the product of complex atmospheric processes evolving continuously over space and time. Rainfall modelling, based on mathematical deterministic descriptions of the underlying processes, is extremely complicated. Mainly for operational purposes, rainfall is modelled as a stochastic process. In rainfall modelling it is an important issue to couple the statistical structure of the process to the physics and dynamics of rainfall. Many rainfall models have problems in handling the great spatial and temporal variability present in this process.

Three general classes of *statistical models* of rainfall can be distinguished, according to their representation of rainfall in space and time: *spatial models*, which represent the spatial distribution of accumulated rainfall over a certain time interval; *temporal models*, which represent rainfall accumulations at a point over time; and *space-time models*, which represent both the spatial and temporal evolution of rainfall (see e.g. Smith, 1993).

The rainfall process observed with high temporal resolution (e.g. hourly or daily) is characterized by intermittency. Thus, the two following processes are important: the rainfall occurrence process; and the process of the non-zero rainfall-amounts. These two processes can be modelled simultaneously (as a compound process) or separately (and then superimposed).

Existing *temporal* rainfall models can be classified in relation to the modelling of rainfall occurrences in three main categories (Foufoula-Georgiou and Georgakakos, 1991): the *wet-dry spell* approach; the *discrete time-series* approach; and the *point-process* approach. Some of these models are reviewed briefly below.

Wet-dry spell approach

In the *wet-dry spell* approach, the time-axis is split up into intervals called *wet periods* and *dry periods*. A rain *event* is an interval in which it rains continuously (it is an uninterrupted sequence of wet periods). The definition of event is associated with a rainfall threshold value

which defines *wet*. In this approach, the process of rainfall occurrences is specified by the probability laws of the length of the wet periods (storm duration), and the length of the dry periods (time between storms or inter-event time).

Several distributions have been used for the length of the wet and dry periods, e.g. the exponential distribution (e.g. Green, 1964), the discrete negative binomial distribution (e.g. Galloy et al., 1981). For the wet period length, the Weibull distribution has also been used to model short time-increment rainfall occurrences (e.g. Todorovic and Yevjevich, 1969; Eagleson, 1978). Among other studies using the wet-dry spell approach one can cite, for example, Roldán and Woolhiser (1982), Small and Morgan (1986), Bogardi et al. (1988); these studies used different probability distributions for the length of the wet and dry periods.

The wet-dry spell model is known as an *alternating renewal model*. The term *renewal* comes from the (implied) independence of the length of the dry and wet periods, whereas the term *alternating* is used to indicate that a wet/dry transition is always followed by a dry/wet transition (meaning that there is no transition to the same state). The varying duration of the events requires that the cumulative rainfall-amounts corresponding to each event should be conditioned by the duration of the event. The identification and fitting of conditional probability distributions to rainfall amounts may be a problem, especially in the case of short records and for events with extreme (long) durations (Foufoula-Georgiou and Georgakakos, 1991). An additional question or problem is the redistribution of a total storm rainfall within the wet period, therefore recreating 'internal' storm characteristics.

Discrete time-series approach

This modelling approach sees rainfall occurrences (e.g. daily or hourly) as a binary series of zeros and ones (zero corresponding to a dry occurrence, and one to a wet occurrence), and does not group them into periods.

The simplest probabilistic model for such a binary series is the *Bernoulli process* (characterized by its independent structure), followed (in simplicity) by Markov chain models (with a dependence structure). *Markov chain* models of the first and second order have been extensively used to model daily rainfall. Markov chains can be homogeneous (i.e. with constant parameters), and non-homogeneous (i.e. with time-varying parameters). Among the many existing works using Markov chains Gabriel and Neumann (1957, 1962), Caskey (1963), Weiss (1964), Hopkins and Robillard (1964), Feyerhem and Bark (1967), Smith and Schreiber (1973), Chin (1977), Woolhiser and Pegram (1979), and Stern and Coe (1984) can be mentioned.

Markov chain models provide simple mathematical representations of daily rainfall occurrences. Nevertheless, unless one uses a very high order Markov model (which has the disadvantage of involving a lot of parameters), these models cannot describe the long-term persistence (i.e. long wet and dry spells) and the effect of clustering (i.e. higher likelihood of having an event due to a previous event) present in short time-increment rainfall occurrences (Foufoula-Georgiou and Georgakakos, 1991).

A more general class of binary discrete time-series models is the class of *discrete autoregressive moving average* (DARMA) models (e.g. Buishand, 1978; Chang et al., 1984). DARMA models are considered an improvement on Markov chains, in the sense that they can accommodate longer term persistence better than a higher-order Markov chain. The lack of a physical motivation for the model structure is pointed out as one of the disadvantages of DARMA models (see e.g. Foufoula-Georgiou and Georgakakos, 1991).

Point-process approach

A *point-process* is a stochastic process describing the occurrence (position) of discrete *events* on the time-axis (see e.g. Cox and Isham, 1980). The process is called a ***marked*** point-process when an intensity is attached to each occurrence. In a *continuous-time* point-process the events may occur anywhere on the time-axis. In a *discrete-time* point-process the occurrence of events is governed by equally spaced increments (for example, one day apart). Because rainfall may be considered as a continuous time-process recorded over discrete time-intervals, both continuous and discrete point-processes are used in research (see e.g. Foufoula-Georgiou and Lettenmaier, 1986). An overview of the existing models can be found, for example, in Waymire and Gupta (1981a, 1981b, 1981c) and in Foufoula-Georgiou and Georgakakos (1991). A brief overview of some point-process models are given below.

The simplest continuous-time point-process is the *Poisson process*, which has extensively been used to model rainfall occurrences (e.g. Todorovic and Yevjevich, 1969; Gupta and Duckstein, 1975; Rodríguez-Iturbe et al., 1984). In a Poisson process the times between events are independent and exponentially distributed; and the number of events in a time interval is independent and Poisson distributed. In this process the *marks* associated with each event can be of two types: instantaneous random rainfall-amounts (*Poisson white noise* model) or rectangular pulses (*Poisson rectangular pulses* model). The pulses are characterized by random intensity and duration, and are independent of each other. These models have a scale-dependent structure.

Another type of point-process model is the *Neyman-Scott cluster* model. A Neyman-Scott process is a two-level process. The rainfall generating mechanisms occur according to a Poisson process. Each mechanism gives rise to a group, or cluster, of rainfall events (which can be assumed to be Poisson or geometrically distributed). Within each cluster, the occurrence of events is completely specified by the distribution of the number of events and the distribution of their positions relative to the cluster centre. If the rainfall burst is described by an instantaneously random rainfall-depth, the resulting rainfall process is known as the *Neyman-Scott white noise*. If the rainfall process is described by a rectangular pulse, it is called the *Neyman-Scott rectangular pulse*. Among the many existing works using Neyman-Scott models one can mention Kavvas and Delleur (1981), Rodríguez-Iturbe et al. (1984), Valdes et al. (1985), Foufoula-Georgiou and Guttorp (1986), Rodríguez-Iturbe et al. (1987a), Obeysekera et al. (1987). A disadvantage of these types of models is their scale-dependency.

Rodríguez-Iturbe et al. (1987a) introduced another model, with the same type of structure of the Neyman-Scott model: the *Bartlett-Lewis rectangular pulse* model. The rectangular pulse is characterized by random intensity and duration. The Bartlett-Lewis and the Neyman-Scott processes differ only in the way in which the cells are positioned within a cluster (see also Rodríguez-Iturbe et al., 1987b). In the Neyman-Scott process the position of the cells is determined from the storm origin according to an exponential distribution; and in the Bartlett-Lewis process the intervals between successive cells are exponentially distributed. The number of cells within a cluster was studied both with a Poisson and a geometric distribution. A modified version of the model was developed by Rodríguez-Iturbe et al. (1988), which allows storms to have different characteristics; this is achieved by randomizing several parameters of the distribution of the number of cells per storm, cell positions, and cell durations. These modifications improved the representation of the extreme events.

Smith and Karr (1983) introduced a point-process model of a different structure: the *doubly stochastic Poisson* process (also known as the *Cox* process). This process has a rate of occurrence that alternates between two states, one zero and the other positive. There are no events occurring during periods when the intensity is zero. During periods with positive intensity, events occur according to a Poisson process. The sequence of states (zero and positive) form a Markov chain. This model is a renewal process (the inter-arrival times are independent) and was called the *Renewal Cox* process with a Markovian intensity.

The construction of discrete-time point-process models was proposed by Foufoula-Georgiou and Lettenmaier (1987). They introduced a *Markov Renewal* model for the description of daily rainfall occurrences. In this model the sequence of times between events is formed by sampling from two geometric distributions according to transition probabilities specified by a Markov chain. This Markov Renewal process is a clustered process.

The selection of a distribution function and the specification of their dependency (the temporal correlation of the temporal amounts) is important to model precipitation amounts associated with rainfall occurrences (see e.g. Woolhiser and Roldán, 1982). Several probability distributions have been proposed for the non-zero interval (daily or hourly) rainfall-amounts. Among these distributions one can mention the exponential distribution (e.g. Todorovic and Woolhiser, 1974; Woolhiser et al., 1975; Richardson, 1981, 1982), the mixed exponential distribution (e.g. Smith and Schreiber, 1974; Woolhiser and Pegram, 1979; Richardson, 1982; Woolhiser and Roldán, 1982), the gamma distribution (e.g. Ison et al., 1971; Buishand, 1977; Carey and Haan, 1978; Richardson, 1982), the kappa or generalized beta distribution (e.g. Mielke, 1973; Mielke and Johnson, 1974), and the generalized Pareto distribution (e.g. Monfort and Witter, 1986). Similarly, different assumptions (varying with the time scale of the model) have been made on temporal correlation of precipitation amounts. Several studies have examined the simultaneous modelling of daily rainfall occurrences and amounts via multiple-state Markov chain models (e.g. Khanal and Hamrick, 1974; Haan et al., 1976; Carey and Haan, 1978).

Chapter 3

Theory of fractals and multifractals and its application to rainfall

3.1 Introduction

This Chapter gives an introductory review of the fractal and multifractal theories. The main theme of these theories is the property of *scale-invariance*. The term *scale-invariance* (or *scaling*) is used to indicate that certain features of a system are independent of scale. This scale-invariance holds over a broad range of scales. Thus, scaling theories apply to processes and systems without a characteristic scale. Scale-invariance leads to a class of scaling *rules* (power laws) characterized by scaling *exponents*. Statistical properties of scale-invariant systems at different scales are related by a scale-changing operation that involves only scale ratios. Scaling theories are developed in a non-dimensional framework, because one looks for features that are independent of the physical size of the object of study.

In this Chapter special attention is given to methods of the *fractal* and *multifractal* theories that are relevant for the analysis of the temporal structure of rainfall. For more complete descriptions and/or discussions of the different topics the reader should consult other works; many references are given throughout the text.

Section 3.2 gives an introduction to fractals. It discusses: general properties and different types of fractals; the notion of fractal dimension; and a fractal analysis method ('box-counting'). Section 3.3 deals with different elements of the theory of multifractals. It discusses general properties of multifractals as well as the statistical characterization of multifractal processes through the probability distributions and statistical moments. Moreover, the concept of 'multifractal phase transitions' is reviewed. A universality class of multifractal models based on Lévy random variables is discussed in Section 3.4. Section 3.5 is dedicated to the description of some multifractal analysis techniques: the 'functional box-counting' method, the 'probability distribution/multiple scaling' method, and the 'trace moment' and 'double trace moment' methods. Finally, Section 3.6 gives an overview of the fractal and multifractal studies of rainfall.

Some theoretical topics that are not dealt with in the review of the multifractal theory in Chapter 3 are given in Appendices. Appendix I discusses the role of Lévy variables in 'universal' multifractals. Appendix II shows the relation between the multifractal ('turbulence') formalism used in this dissertation and the 'strange attractor' formalism.

3.2 Fractals

Recently, there has been increasing interest in the mathematical description of sets with a *fractal* structure as observed in many natural phenomena. The word *fractal* (from the Latin *fractus*, meaning broken, irregular) was introduced by Mandelbrot (1975, 1977) to indicate objects that are too irregular to fit into a traditional geometric framework.

Classical geometry is used to describe the structure of regular physical objects; these objects are usually of a 'simple' geometrical character. Fractal geometry (Mandelbrot, 1977; 1982) is an extension of classical geometry and concerns the description, classification, and analysis of sub-sets of metric spaces that are (typically) geometrically 'complicated.' Thus, fractal geometry provides a general framework for characterizing sets of points which in space have a form different from such structures as smooth lines or surfaces. Generally, the 'complicated' structure and organization of a fractal set does not make it possible to specify directly where each point in it lies. Alternatively, the set may be defined by some (recursive) 'relation' between the 'structures' observed in the set at various levels of resolution (e.g. Barnsley, 1993). This 'relation' is formulated quantitatively by the concept of *fractal dimension*. It describes the scaling behaviour of the geometry of fractal structures. Fractal theory deals with *simple scaling* since there is only one scaling index involved in this description.

3.2.1 Some general properties and types of fractals

Scale-invariance/scaling property and scaling regions

Fractals can be defined as geometric objects that exhibit scale-invariance. Scale-invariant patterns or objects contain no natural internal measures of size and, thus, their form is the same at all scales. Similarly, scale-invariant processes and systems (at least for a large range of scales) do not have a characteristic scale. One can think of a scale-invariant process as one in which the same type of elementary process acts at each relevant scale. Over a range of scales the statistics will exhibit *power-law* (scaling) behaviour characterized by scaling exponents (i.e. these statistical exponents are independent of scale). Thus, the statistics on large and small scales are related by a scale-changing operation that involves only scale ratios. If the operation is a simple magnification the system is statistically isotropic (*self-similar*). A geometric object is called *self-similar* if it is the 'union' of rescaled copies of itself; the rescaling should be isotropic or uniform in all directions (e.g. Hastings and Sugihara, 1993).

The expectation is that with fractal geometry one may quantify the structure of complex patterns, identify characteristic scales and scaling behaviour, and describe the underlying dynamics giving rise to those patterns. Fractal geometry is also expected to contribute to identify processes, with relevant dynamics occurring at a variety of (spatial and/or temporal) scales. One expects that changes in the dynamics are reflected in corresponding changes in patterns and, thus, in the fractal exponents quantifying those patterns.

If several scaling regions are present in a system, one expect that the scaling exponents are constant within each scaling region, but that they may differ from region to region. The existence of multiple scaling regions is visualized by a graphical representation of the data. It may lead to jumps at the break-points separating scaling regions. If there are more than one scaling region, linear regression fittings of log-transformed data yield different slopes in adjacent regions (e.g. Hastings and Sugihara, 1993). Thus, fractal methods have the potential to objectively identify the range of scaling regions in the underlying structure of geometric patterns by the shift in the fractal exponents where the break-points of the different scales occur.

Types of fractals

In general, a set is called *fractal* if it has the following properties (Falconer, 1990):

(i) the set has a fine structure; it has detail that remains present at arbitrarily small scales;

(ii) the set is too irregular to be described both locally and globally in a traditional geometric framework;

(iii) the set has some form of self-similarity (it is made up of parts that resemble the whole in some way);

(iv) the *fractal dimension* of the set (see Section 3.2.2, below) is larger than its topological dimension (the topological dimension of a set is always an integer);

(v) the set is defined in a very simple way (e.g. recursively).

One can distinguish between *deterministic* and *random* fractals (e.g. Tél, 1988; Falconer, 1990; Hastings and Sugihara, 1993). Deterministic fractals are the class of fractals that are constructed by deterministic rules. They are classified as one-scale fractals and multi-scale fractals. Random fractals are generated by non-deterministic rules. Four examples of types of fractals are given below:

- *one-scale deterministic fractals*

The construction of one-scale deterministic fractals starts by dividing a single object, defined in $\mathbb{R}^n$, into N identical pieces; each new piece is a copy of the original object reduced by the same factor $r<1$ (see e.g. Tél, 1988). In the next step of the construction, the procedure is repeated yielding N newly created pieces, which are arranged inside a piece originating from the previous step exactly in the same way as these parts are arranged inside the original object.

The fractal is obtained by repeating this rule indefinitely. The fractal can then be divided into N identical parts, each being rescaled versions, by a factor r, of the complete set.

A classical example of a fractal set of this type in $\mathbb{R}$ is the middle-third Cantor set (Figure 3.1(a)). The initiator of the construction of this set is the unit interval $[0, 1]$. The generator divides the interval into three equal parts and deletes the middle part leaving its end-points; the generator is then applied again to each of the two parts, and so on. Figure 3.1(a) shows the construction of the three first generation-steps. After an infinite number of generations, an infinite set of points remains scattered over the interval. Many other sets may be constructed using some recursive procedure (see e.g. Mandelbrot, 1982; Barnsley, 1993).

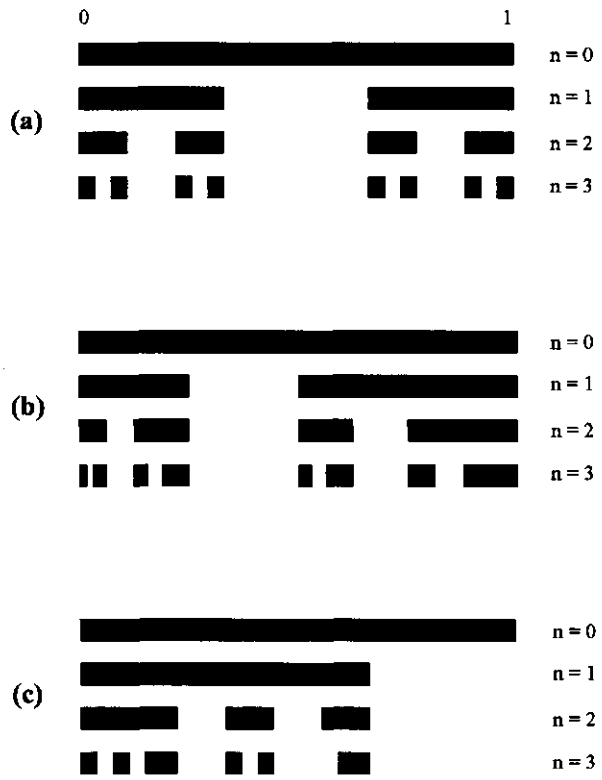

Figure 3.1 Examples of the construction of different fractal sets, for the first three steps of recursive procedures: (a) the middle-third Cantor set (one-scale deterministic fractal); (b) a two-scale Cantor set with reducing factors $r_1 = 0.25$ (left) and $r_2 = 0.5$ (right) (multiple-scale deterministic fractal); (c) a random version of the Cantor set, where each interval is divided into three equal parts from which some are selected at random to be withdrawn (random fractal).

- *multi-scale deterministic fractals*

In the construction of multi-scale fractals the starting object is divided into N parts which are not all identical. These parts are copies of the original object reduced by certain factors $r_j<1$, with j=1,N (all r_j cannot be identical). The procedure is then repeated many times, in a similar way. The resulting fractal can be divided into N parts, each being rescaled versions of the complete fractal.

The two-scale Cantor set is an example of this type of fractals. The initiator of the construction of this set is also the unit interval [0, 1]. The example shown in Figure 3.1(b) has a generator that replaces (initially) the unit interval by two intervals, kept at its end-points, of length r_1 and r_2, with $r_1+r_2<1$; the reducing factor for the left interval is $r_1=0.25$ and for the right interval is $r_2=0.5$. At the next stage of the construction the same process is applied to each of these two new intervals. The procedure is then repeated indefinitely.

- *random fractals*

An example of a random fractal is the random analogue of the middle-third Cantor sets (described earlier). The middle-third Cantor set construction can be randomized in several ways (see e.g. Falconer, 1990). In the example illustrated in Figure 3.1(c) each interval is divided into three equal parts from which some are selected at random to be withdrawn. Another possibility for the randomization would be the replacement of each interval by two sub-intervals of random lengths. Random fractals should display randomness at each stage of their construction. Therefore, they do not have the self-similarity of their non-random counterparts. The non-uniform appearance of random fractals is often closer to natural phenomena (e.g. coastlines, topographical surfaces, clouds). To describe fractal constructions involving infinitely many random steps one must use probability theory (Falconer, 1990).

- *fractals extracted from nature*

An example of a fractal set extracted from nature is given in Figure 3.2(b). This set corresponds to the daily rainfall occurrences, in a particular location, observed during a period of 32 days (see Figure 3.2(a)). The rainfall occurrences are defined with the help of a threshold of 0.1 mm/day, which establishes here the distinction between *wet* and *dry* days. An uninterrupted sequence of wet days is called a *rainy period*. Rainy periods can be used to define fractal objects or sets embedded in the 1-dimensional space of time. In Figure 3.2(b) the 32-day period is mapped in the interval [0, 1], and the (fractal) set of interest is formed by the rainy periods in that interval (i.e. only wet sub-intervals count).

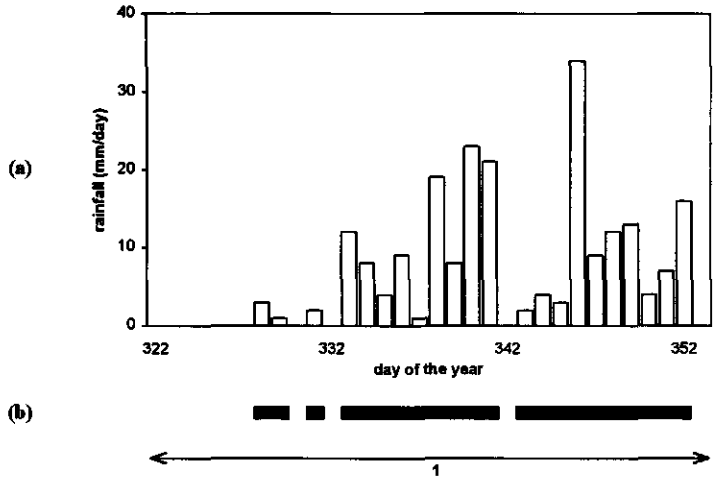

Figure 3.2 Example of a fractal set extracted from rainfall: (a) daily rainfall observed during a period of 32 days; (b) the 32-day period is mapped in the interval [0,1], and the (fractal) set of interest (embedded in the 1-dimensional space of time) is formed by the rainy periods in that interval.

3.2.2 Fractal dimension and codimension

Standard mathematical tools, based on differentiability and continuity of analytical functions, do not apply to the characterization of fractal forms (see Section 3.2.1). Fractal geometry uses for this purpose the notion of *fractal dimension* (e.g. Mandelbrot, 1967, 1977, 1982; Feder, 1988; Falconer, 1990; Barnsley, 1993; Hastings and Sugihara, 1993). One is familiar with the idea that a dimension contains information about the geometric properties of a set; for example, a straight line is a 1-dimensional object, a surface is a 2-dimensional one, and so on. Similarly, fractal dimensions characterize 'quantitatively' fractal objects and sets. The notion of fractal dimension is the main 'tool' of fractal geometry.

In defining (fractal) dimension the idea of *measurement at scale* δ is fundamental. For each scale δ, a set A is *measured* or characterized in a way that ignores irregularities (i.e. details, variability) on smaller scales (i.e. scales of size less than δ). Even at the finest resolution available (imposed by technical limitations, for example), the process might not be truly homogeneous.

The scaling behaviour that is found in the measurements for $\delta \rightarrow 0$ is the key to the notion of dimension. Let a geometric object defined in a 1-dimensional space have a *size* L. It is more convenient to use the quotient $\lambda = L/\delta$ instead of the *length* δ of the scale of homogeneity.

Length is related to a metric in the particular study and can, of course, have different meanings. The parameter λ is called a *scale ratio*. For example in Figure 3.2 is λ=32.

The previous examples dealt with sets of points on the real line. An arbitrary set A of points is considered now in a D-dimensional space. Let N_λ be the number of non-overlapping *cubes* of side λ^{-1} necessary to cover a bounded part of the dimensional space containing the set A of interest (*cube* is, of course, an interval in $\mathbb{R}^1$ and a square in $\mathbb{R}^2$). The number N_λ satisfies the (power-law) relation

$$N_\lambda \approx \lambda^D \tag{3.1}$$

meaning that N_λ is proportional to λ^D in the limit $\lambda \to \infty$.

Let $N_{\lambda,A}$ be the number of non-overlapping *cubes* of side λ^{-1} necessary to cover the set A. The number $N_{\lambda,A}$ satisfies the relation

$$N_{\lambda,A} \approx \lambda^{D_A} \tag{3.2}$$

where D_A is the (*fractal*) *dimension* of the set A. Set A is a *fractal* if D_A is a non-integer number.

The number of *cubes* of side λ^{-1} that contain an element of the set A is an indicator of how spread-out, or irregular, the set A is when examined at that scale. The dimension reflects how rapidly the irregularities develop as $\lambda^{-1} \to 0$ (e.g. Falconer, 1990). Very roughly, the dimension of a set tells how densely the set occupies the metric space in which it lies; thus, it tells how much space a set 'fills'. More generally, it tells how frequent a phenomenon is. It can be interpreted as a measure for the sparseness of the set. The fractal dimension is a specific form of characterizing a set. It does not give full information about the 'structure' of the set.

One can also define the *fractal codimension* of a set A of points as

$$c = D - D_A \tag{3.3}$$

where D_A is the fractal dimension of the set A, and D is the dimension of the space containing the set A. In a purely geometric framework, the dimension D equals the Euclidean dimension (d=1,2,3) of the geometric entity in which a fractal set A is embedded (d should be the smallest possible Euclidean dimension).

With Eqs. (3.1) and (3.2) one arrives at a 'probabilistic' definition of a fractal object based on the codimension (e.g. Lovejoy and Schertzer, 1992). A *cube* of side λ^{-1} has the probability $Pr=N_{\lambda,A}/N_\lambda$ of intersecting the set A. This probability scales as

$$\frac{N_{\lambda,A}}{N_\lambda} \approx \frac{\lambda^{D_A}}{\lambda_D} = \lambda^{D_A - D} = \lambda^{-c} \tag{3.4}$$

With Eq. (3.4) one can relate the codimension to the fraction of the space of observation occupied by the fractal set A of dimension D_A. This shows the importance of the notion of codimension.

Generalizations of the concepts of fractal dimension and scale-invariance beyond the geometry of the physical space are possible and lead to a definition of codimension different from the definition given in Eq. (3.3). Such generalizations are necessary to deal with (non-linear) processes rather than with (geometric) sets. This will be discussed later in this Chapter. The notion of codimension, with its probabilistic interpretation (Eq. (3.4)), provides a framework for characterizing fractals (and multifractals) making use of familiar (probabilistic) concepts.

3.2.3 Fractal analysis with the box-counting method

There are various techniques for studying the scaling of fractal sets and of linear stochastic processes that are characterized by a single scaling exponent. These methods include the *box-counting* method, *correlation dimensions*, *area-perimeter* relations, *area-distribution* exponents, *structure functions* and *power spectra*, among others (see e.g. Feder, 1988; Falconer, 1990; Barnsley, 1993; Hastings and Sugihara, 1993). Here only the box-counting method is described. Spectral analysis is discussed in Section 3.3.1.

The *box-counting* method uses directly the definition given above in Eq. (3.2) to estimate the fractal (box) dimension D_A of a set A. When Eq. (3.2) was introduced, the set A was defined as a non-empty bounded sub-set of $\mathbb{R}^n$, and $N_{\lambda,A}$ was defined as the number of non-overlapping *cubes* of side λ^{-1} needed to cover the set A. These *cubes* are also called *boxes*. In practical applications of the box-counting method, the D-dimensional space of the observations is covered with gradually-decreasing (it is common that the size is decreased gradually by a factor of two), non-overlapping *boxes* of side λ^{-1}. For every grid-size, the number of *boxes* that contain at least one point of the set being analyzed are 'counted' (hence the name *box-counting*). If the set exhibits scale-invariance, it can be characterized by Eq. (3.2). This means that plots of $\log(N_{\lambda,A})$ against $\log(\lambda)$ should yield a linear relation indicating the scaling in the form of the power law (Eq. (3.2)). The fractal dimension D_A can be estimated from the slope of the regression line fitted to the data.

An example of application of the box-counting method is given in Figure 3.3 for the set shown in Figure 3.2(b). The set was defined for daily rainfall occurrences observed during a 32-days period; this period was mapped in the interval $[0, 1]$. In Figure 3.3 this set was covered systematically with *boxes* of different sizes; counting the number of *boxes* of side λ^{-1} needed to cover the set gives the number $N_{\lambda,A}$ in Eq. (3.2). The number of such *boxes* increases with decreasing size of the *boxes* (Figure 3.3(a)). One can determine the fractal dimension of the set by finding the slope of the plot of $\log(N_{\lambda,A})$ as a function of $\log(\lambda)$; the fractal dimension is the value of the slope. Figure 3.3(b) shows the box-counting plot for the set in Figure 3.2(b). The plot can be divided in two sections: one on the left, with slope equal to 1,

and another on the right, with slope of approximately 0.83. The slope of the section on the right yields an estimate for the fractal dimension of the set defined in Figure 3.2. The section with slope 1 is a typical example of a practical problem of application of the box-counting method to rainfall occurrences. The slope equal to 1 is a trivial result and corresponds to 'saturation.' This is a consequence of all the *boxes* larger than a given scale being 'non-empty.' In general, this can occur if one uses *boxes* that are not sufficiently small with respect to the size of the set that is being studied (i.e. in relation to the highest resolution of the grid). For rainfall, 'saturation' is present whenever the size of the *boxes* is such that at least one rainfall occurrence is observed in each of the *boxes* (corresponding to a certain time interval).

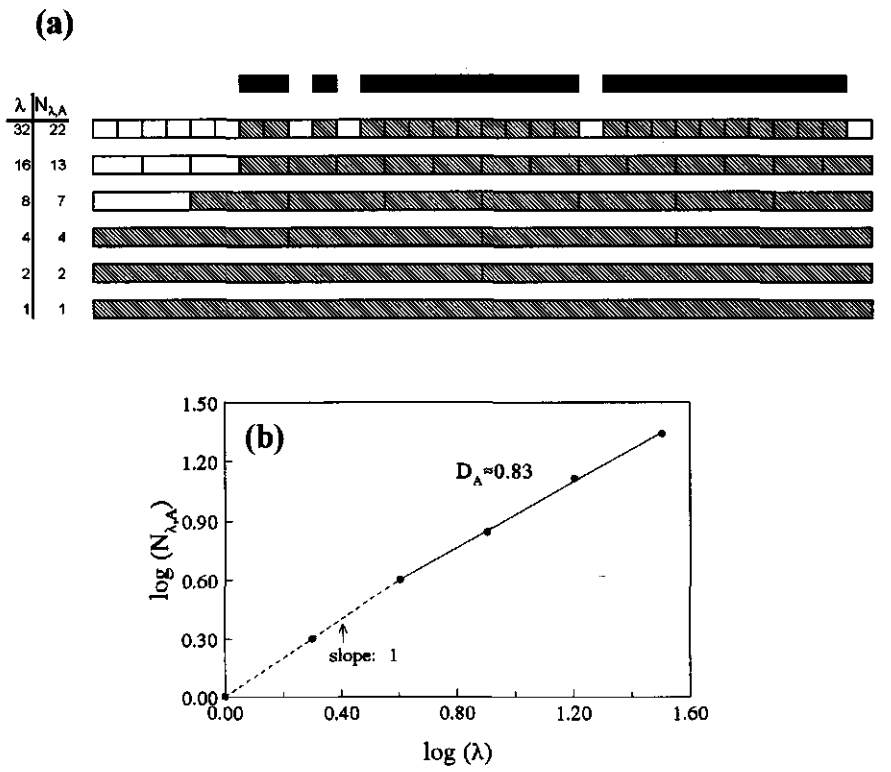

Figure 3.3 Example of application of the box-counting method to estimating the fractal dimension of a set embedded in a 1-dimensional space: (a) the process of *box-counting*; (b) log-log plot of the number of *boxes* of side λ^{-1} needed to cover the set in Figure 3.3(a) against λ. The solid line in the log-log plot is a fit of $N_{\lambda,A} = a\lambda^{D_A}$ to the observations, where a is a constant. The line is chosen such that it fits the points with large λ. The fractal dimension is $D_A \approx 0.83$.

3.3 Multifractals

The geometry of fractal structures can be characterized by a scaling index (the fractal dimension). Frequently in nature, such structures are the (geometric) 'support' of physical or other quantities, to which a more 'refined' scaling index can be assigned. This is generally the case with geophysical processes and systems that themselves cannot be studied as sets. The underlying phenomena are characterized by different levels of intensity and one can rarely reduce it to the oversimplified binary question of occurrence or non-occurrence. Giving again the example of rainfall, one obtains much more information about the (rainfall) process if one studies both the occurrence of rainy periods (which were given earlier as an example of a fractal set embedded in the 1-dimensional space of time) and the rainfall rate (see Figure 3.2(a), for example). The monofractal approach studies rainfall occurrences only, disregarding that rainfall is a highly non-linear process exhibiting a large variability over a wide range of time and space scales.

Multifractal theory offers a framework for studying non-linear processes exhibiting different levels of intensity. This theory deals with the distribution of physical or other quantities (measures) on a geometric support and can handle large-scale variability. The multifractal theory resulted from the need for a generalization of the scaling properties of physical processes: instead of dealing with simple scaling, associated with the (mono) fractal theory/geometry, it deals with *multiple scaling*. The term *multifractals* was introduced by Frisch and Parisi (1985) referring to (fractal) measures characterized by an infinite set of scaling indices or fractal dimensions (this was recognized first by: Hentschel and Procaccia, 1983; Grassberger, 1983; Schertzer and Lovejoy, 1983, 1984).

In this work, the multifractal theory is discussed using the *turbulence* formalism (see below for more details). In parallel, in literature there is also the *strange attractor* formalism that has been introduced by, among other, Hentschel and Procaccia (1983), Grassberger (1983), and Halsey et al. (1986). The *strange attractor* formalism was developed for dealing with multifractal probability measures in low-dimensional phase-spaces. The relation between the *strange attractor* notation and the *turbulence* notation is discussed in e.g. Schertzer and Lovejoy (1989, 1993), Schmitt (1993); see also Appendix II.

3.3.1 General properties and classification of multifractals

Multiscaling

Many geophysical processes are highly intermittent (*intermittency* expresses that the process does not 'fill' all the volume of the space available to it) and characterized by different levels of intensity (see e.g. Schertzer and Lovejoy, 1985; Ladoy et al., 1991; Davis et al., 1994). Often, increasingly intense levels are distributed over increasingly sparse fractal sets, each characterized by a different fractal dimension. Thus, these processes have different scaling

behaviour for the weak and strong intensities. These processes cannot be described statistically by a unique scaling exponent (the simple scaling of the monofractal case). The *multiple scaling* (or *multifractality*) implies that these processes are described by an infinite hierarchy of scaling exponents (a scaling exponent function).

For rainfall, this can be checked in Figure 3.2(a): for increasing values of the intensity-threshold the corresponding fractal dimension decreases (the fractal dimension traduces the sparseness of the set associated with a given intensity, see Section 3.2.2). A single fractal dimension is not sufficient to describe the process. Infinite fractal dimensions (described by a dimension function) are necessary to quantify how the various intensity levels of the process are distributed over a given space of observation. Thus, the codimension c (Eq. (3.3)) is non-unique. The process is *multifractal*.

Scale-invariance

One can use standard *spectral* methods and analysis (see Section 2.4) to test for scale-invariance. The most familiar consequence of scaling is the power-law behaviour that is expected in the energy (power) spectra of scaling processes (e.g. Mandelbrot, 1982; Schertzer and Lovejoy, 1985, 1987; Ladoy et al., 1991; Lovejoy and Schertzer, 1995a):

$$E(\omega) \approx \omega^{-\beta} \tag{3.5}$$

where ω is the wave-number, $E(\omega)$ is the energy, and β is the spectral exponent. This type of behaviour is expected to occur over a range of wave-numbers and might not be observed for small samples. The energy spectrum is only second-order statistics (i.e. the spectrum is related to the Fourier transform of the autocorrelation function) and, thus, is not particularly robust. When applied to highly intermittent data, large samples may be needed to obtain good estimates of the ensemble average spectra (see e.g. Lovejoy and Schertzer, 1991). For (mono-dimensional) fractals, one expects that the scaling of the second-order moments (characterized by the spectral exponents) provides almost complete information about its scaling properties. For multifractals such information may not be sufficient.

Variability

Geophysical processes display typically non-linear variability (see e.g. Ladoy et al., 1991; Schertzer and Lovejoy, 1993; Davis et al., 1994). A fundamental characteristic of such variability is the very large range of associated scales: from very large scales down to very small scales. The latter correspond to the 'inner' scales of the various processes. At these very small scales the processes are homogeneous (i.e. no more variability occurs; the intensity is constant on these scales). In practice, these processes are observed in some experimental discrete way, and the scale of observation (or scale of measurement) is generally larger than their innermost scale. Thus the observations are averages of the densities of the processes over the resolution of the measuring devices. Figure 3.4 illustrates that the intensity range depends

on the resolution level of the observation of a continuous process. The (associated) notion of 'observables' is not trivial (e.g. Schertzer and Lovejoy, 1989, 1991b) because the observation of processes 'misses' the scale of the smallest detail (i.e. the 'inner' scale of the process or the true scale of homogeneity). The details on these small scales may be very important because of the singular statistics of the small-scale limit behaviour (see below).

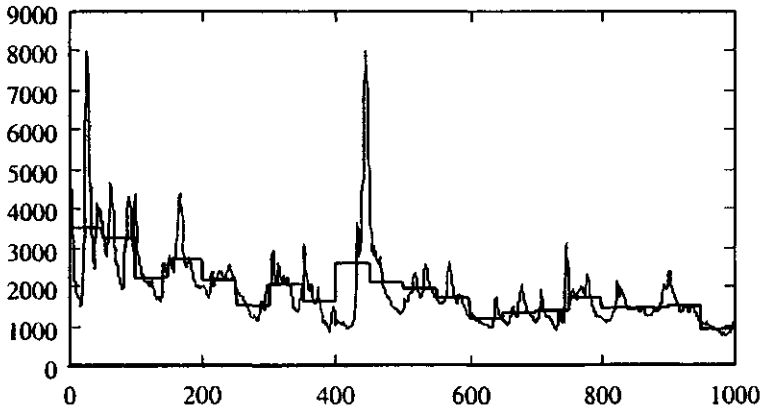

Figure 3.4 Illustration of the relation between the range of intensities and the level of temporal resolution of the observation of a continuous process (Torfs, 1998).

Common assumptions in traditional approaches to the study of geophysical processes are that the measurements of the underlying phenomena can be described by functions; i.e. one accepts a 'theoretical' representation of a certain continuous type. One furthermore assumes that such continuous representation is the limit of the representation of discrete observations when the resolution (scale of observation) goes to zero. This approach tends to make use of (mathematical) regularity constraints (smoothness) which contrasts with the strong variability present on scales smaller than the scale of the observation. Thus, the study of processes that exhibit non-linear variability should be conducted in a framework that uses (mathematical) measures and not functional analysis (see e.g. Schertzer and Lovejoy, 1989; Lovejoy and Schertzer, 1991). The use of functions rather than measures is purely a mathematical idealization.

In the study of 'irregular' structures it is not possible to use Lebesgue measures (see e.g. Falconer, 1990; Barnsley, 1993) because they are regular measures (with respect to the usual line, surface, volume measures). They are defined for integer dimension d. Instead, the (non-integer) D-dimensional Hausdorff measure (e.g. Schertzer and Lovejoy, 1987; 1989; 1993) should be used. The D-dimensional Hausdorff measure of a set A defined in the space X

is denoted by $\int_A d^D x$. The Hausdorff dimension D_A of the set A is defined by the divergence rule

$$\int_A d^D x = \infty, \quad D < D_A \tag{3.6a}$$

$$\int_A d^D x = 0, \quad D > D_A \tag{3.6b}$$

The transition at $D=D_A$, from infinity to zero, defines the Hausdorff dimension of the set A. An important property of Hausdorff measures is related to the simple scaling relation associated with any dilation of scale ratio λ ($A \rightarrow \lambda A$):

$$\int_{\lambda A} d^D x = \lambda^D \int_A d^D x \tag{3.7}$$

The singular nature of the small-scale limit

Let one observe by one variable the intensity (or density) ε^* of a multifractal process in the embedding space X of dimension D. In practice, this intensity is measured at some finite level of resolution λ (see Section 3.2.2), and is constant on *cubes* of side λ^{-1} (centred at some x). On a space of dimension D one can define a number λ^D of such (non-overlapping) *cubes*. Thus, at resolution level λ, there are intensities $\varepsilon_{\lambda,i}{}^*(x_i)$, with $i=1,\lambda^D$. For the sake of simplicity, hereafter the centring of the *cubes* is omitted.

One can obtain the corresponding *non-dimensional* intensities $\varepsilon_{\lambda,i}$ by dividing $\varepsilon_{\lambda,i}{}^*$ by the ensemble average intensity of the process $\langle \varepsilon_\lambda{}^* \rangle$, which is estimated as

$$\langle \varepsilon_\lambda{}^* \rangle = \frac{\sum_{i=1}^{\lambda^D} (\varepsilon_{\lambda,i}{}^*)}{\lambda^D} \tag{3.8}$$

where the angular brackets mean ensemble average. Thus, the non-dimensional intensities are

$$\varepsilon_{\lambda,i} = \frac{\varepsilon_{\lambda,i}{}^*}{\langle \varepsilon_\lambda{}^* \rangle}, \qquad i = 1,\lambda^D \tag{3.9}$$

Hence $\langle \varepsilon_\lambda \rangle = 1$, independent of scale. The index i is dropped below.

The multifractal framework used in this study assumes that the intensity ε_λ of a process displays a behaviour approximated by (e.g. Frisch and Parisi, 1985; Halsey et al., 1986; Schertzer and Lovejoy, 1987)

$$\varepsilon_\lambda \approx \lambda^\gamma \tag{3.10}$$

where: λ is the scale ratio, defined as the quotient between the largest scale of interest and the homogeneity scale; and γ is a parameter that characterizes (qualitatively) the intensity ε_λ and is independent of the level of resolution λ. The '$\approx$' sign in Eq. (3.10) 'absorbs' factors slowly varying with λ (e.g. log's) and normalization constants.

In Eq. (3.10) the exponent γ is referred to as *singularity* or *order of singularity* (with respect to a range of γ-values). These singularities would correspond from (very) small up to (very) high intensity levels of the process. Thus, the exponent γ is a measure of the 'strength' of the intensity ε_λ observed on a scale of resolution λ. The resolution-independent characterization of the intensity provided by the parameter γ is important because the process is studied at different scales. Figure 3.5 gives a schematic illustration of the relation between the order of singularity γ of the intensities ε_λ and the scale ratio λ.

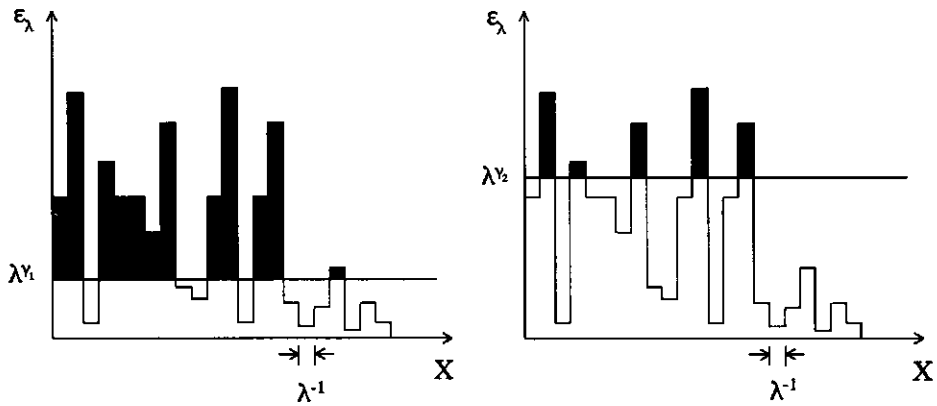

Figure 3.5 Schematic illustration of the relation between the orders of singularity γ of the intensities ε_λ of a multifractal process in the embedding space X and the scale ratio λ, defined as the quotient between the largest scale of interest and the homogeneity scale. The singularities γ_1 and γ_2 express two levels of intensity of the process (adapted from Lovejoy and Schertzer, 1992).

The term *singularity* is linked to the very singular nature of the multifractal behaviour $\varepsilon_\lambda \approx \lambda^\gamma$ (Eq. (3.10)) at the small-scale limit $\lambda \to \infty$: for all singularities $\gamma > 0$, $\varepsilon_\lambda \to \infty$ as $\lambda \to \infty$ (e.g. Schertzer and Lovejoy, 1987; 1989; 1993). In a strict sense, the expression singularity applies to the exponent γ when $\gamma > 0$; when $\gamma < 0$, the point is a *regularity* rather than a singularity (e.g. Schertzer and Lovejoy, 1987, 1989, 1993; Lovejoy and Schertzer, 1990a). In practice, both exponents $\gamma > 0$ and $\gamma < 0$ are called singularities.

A consequence of the singular behaviour when $\lambda \to \infty$ is that one cannot consider a limit in the sense of functions (e.g. Schertzer and Lovejoy, 1989, 1993). Singularities will prevent convergence in the usual sense. The limit of the densities ε is singular, and it is only implicitly defined by the more regular limit of the fluxes over the different sets as $\lambda \to \infty$ (Schertzer and

Lovejoy, 1987, 1989); the fluxes are integrals over the densities ε. The notion of flux means here *flux through a scale* (see Schertzer and Lovejoy, 1989).

The (total) flux, $\Pi_\lambda(A)$, over a set A of dimension D, defined in the space X at resolution level λ is given by

$$\prod_{\lambda}(A) = \int_{A} \varepsilon_\lambda \, d^D x \tag{3.11}$$

The fluxes have the regular limit (e.g. Schertzer and Lovejoy, 1993)

$$\prod_{\infty}(A) = \lim_{\lambda\to\infty} \prod_{\lambda}(A) = \lim_{\lambda\to\infty} \int_{A} \varepsilon_\lambda \, d^D x \tag{3.12}$$

Cascade-type behaviour

Different multifractal processes exhibit a behaviour analogous to the cascade-type behaviour that is typically observed in turbulence. Thus, the general properties of multifractals are often introduced with the phenomenology of (scalar) cascades (e.g. Schertzer and Lovejoy, 1987, 1988, 1989; Siebesma, 1989; Lovejoy and Schertzer, 1990a, 1990b). The cascade phenomenology of turbulence is used to investigate and simulate intermittency and scale-invariance. This phenomenology is based on the tendency of the 'activity' of turbulence to becomes more and more locally concentrated as the scales become smaller. This yields more and more inhomogeneity as the scales become smaller. The 'activity' of turbulence can be estimated by the rate at which energy is transferred to smaller scales. The cascade phenomenology has the following three properties: i) scale-invariance; ii) conservation of fluxes from large to small scales, i.e. its ensemble average $\langle\varepsilon\rangle$ is independent of scale, and is a basic cascade quantity; and iii) localized dynamics in Fourier space (the dynamics involve interactions primarily between neighbouring scales). In real flow, viscosity will break the scaling at a small 'viscous'-scale (e.g. Lovejoy and Schertzer, 1990b); in the atmosphere this scale is typically of 1 mm.

In dynamical cascade models, 'structures' at neighbouring scales modulate each other in a multiplicative way, simulating the breaking of *eddies* (and the consequent transfer of energy to smaller scales) due to non-linear interactions and internal instability (see e.g. Schertzer and Lovejoy, 1987; Lovejoy and Schertzer, 1990a; Wilson et al., 1991). Although the term *eddy* is related to turbulence, it is used here in a broader sense. In these (multiplicative) models, the fraction of the energy flux ('activity') from a parent structure to an offspring is determined in a scale-invariant way (see e.g. Schertzer and Lovejoy, 1987; Over and Gupta, 1994, 1996). Moreover, in phenomenological models of turbulence successive steps define independently the fraction of the energy flux distributed over smaller scales.

For discrete cascade models (i.e. cascade models where the scales are discretized), one usually uses an elementary constant ratio of scales λ_0 (larger than 1, very often equal to 2). On the

largest scale of characteristic length L (λ=1), the (initial) non-dimensional energy is uniform: ε_1=1. During the process of developing a cascade, this large 'structure' is broken up into smaller and smaller 'sub-structures' of characteristic length δ. A random factor determines the fraction of the rate of energy transferred from one large 'structure' to one of its *offsprings*. The mechanism of flux redistribution is repeated at each cascade step. After n steps of the cascade (i.e. after n iterations of the multiplicative process), in a space of dimension D, there is a number λ^D of 'sub-structures' of characteristic length $\delta_n=L/\lambda_0^n$ (the total ratio of scales is $\lambda=L/\delta_n$) and energy flux density ε_n (i.e. $\varepsilon_{n,i}$, with i=1,λ^D). These densities (or, in general terms, the value of the field) satisfy the relation $\varepsilon_n=\mu\varepsilon\ \varepsilon_{n-1}$, where $\mu\varepsilon$ is a random variable.

Next, two rather simple (phenomenological) models of turbulence will be described. The inclusion of the description of these models in this work is justified by their importance in the development of multifractal theory.

- *the* **β-*model*** *(a monofractal model)*

The simplest cascade model is known as the β-*model* (e.g. Novikov and Stewart, 1964; Mandelbrot, 1974; Frisch et al., 1978). This model takes into account the intermittency of turbulence by assuming that *eddies* are either *dead* (inactive) or *alive* (active). In the model the energy-rate at a position defined at a given resolution λ may have two values, either 0 or λ^c, with probabilities

$$\Pr(\mu\varepsilon = \lambda^c) = \lambda^{-c} \qquad \text{(alive)} \tag{3.13a}$$

$$\Pr(\mu\varepsilon = 0) = 1 - \lambda^{-c} \qquad \text{(dead)} \tag{3.13b}$$

where ε is the energy at the higher scale, $\mu\varepsilon$ is the fraction of the energy transferred to smaller scales, λ is the scale ratio and c is the codimension of the *alive eddies* (thus, of the 'support' of the process). The corresponding dimension is equal to D-c, where D is the dimension of the embedding space. The random variable $\mu\varepsilon=\lambda^c$ (>1; corresponds to a *boost*) should respect conservation of the ensemble average, so that $\langle\mu\varepsilon\rangle$=1 (at all levels of the cascade).

At each step in the cascade the fraction of the *alive eddies* decreases by λ_0^{-c}; their energy flux density must then increase by $1/(\lambda_0^{-c})$ to assure conservation (for the average). After n steps the dichotomy is amplified by the total scale ratio λ_0^n. As a consequence, either the density diverges (with an order of singularity c), or is 'calmed' down to zero.

- *the* **α-*model*** *(an explicit multifractal model)*

The need for a more realistic alternative to the *dead/alive* dichotomy resulted in the α-*model* (Schertzer and Lovejoy, 1983). The model is obtained by introducing a random two-state multiplicative factor. Instead of allowing *eddies* to be either *dead* or *alive*, this model allows

them to be either *more active* (yielding *strong sub-eddies*) or *less active* (yielding *weak sub-eddies*), according to the following Bernoulli process with binomial distribution:

$$\Pr(\mu\varepsilon = \lambda^{\gamma^+}) = \lambda^{-c} \qquad \text{(more active; strong sub-eddy)} \tag{3.14a}$$

$$\Pr(\mu\varepsilon = \lambda^{\gamma^-}) = 1 - \lambda^{-c} \qquad \text{(less active; weak sub-eddy)} \tag{3.14b}$$

In Eq. (3.14a), parameters γ^+, γ^- and c (the parameter c is the codimension of the support of the process) are usually constrained so that the ensemble average is conserved, $\langle\mu\varepsilon\rangle=1$. This implies that

$$\lambda^{\gamma^+}\lambda^{-c} + \lambda^{\gamma^-}(1-\lambda^{-c}) = 1 \tag{3.15}$$

The conservation requirement implies that $\lambda^{\gamma^+}>1$ (i.e. $\gamma^+>0$, corresponds to a *boost*) and $\lambda^{\gamma^-}<1$ (i.e. $\gamma^-<0$, corresponds to a *decrease*). Figure 3.6 illustrates one cascade-step of the α-model, with representation of *sub-eddies* with singularities γ^- and γ^+. The (*dead/alive*) β-model is recovered from the α-model with $\gamma^-=-\infty$ and $\gamma^+=c$.

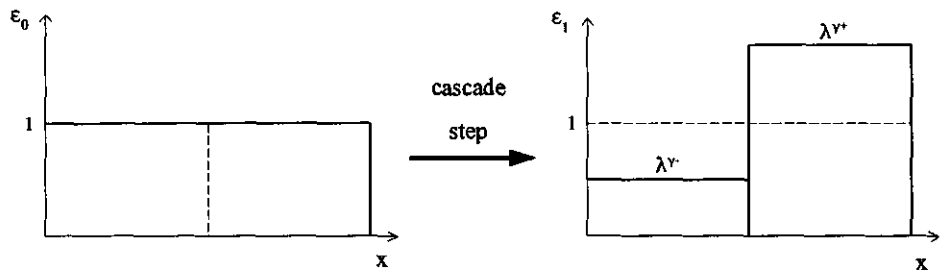

Figure 3.6 Illustration of one cascade step of the α-model. On the left-hand side, the model starts from an uniform (unit) flux density; on right-hand side, and after one cascade step, the model yields a *weak sub-eddy*, related to the singularity $\gamma^-<0$, and a *strong sub-eddy*, related to the singularity $\gamma^+>0$ (adapted from Schertzer and Lovejoy, 1993).

The cascade step-by-step succession of parameters γ^- and γ^+ leads to a (full) hierarchy of intensity levels and, hence, to a hierarchy of dimensions characterizing the sets associated with these different intensities. In this model the values of the parameter γ (i.e. of the singularities) are bounded (e.g. Schertzer and Lovejoy, 1993). After n steps of the cascade, the probability density of the resulting process or field with density ε_n is given by (e.g. Schertzer and Lovejoy, 1987; Lovejoy and Schertzer, 1990b)

$$\Pr(\varepsilon_n \geq (\lambda_0{}^n)^\gamma) \approx f(\gamma)\,(\lambda_0{}^n)^{-c_n(\gamma)} \tag{3.16}$$

which associates specific codimensions with every order of singularity γ. In Eq. (3.16) $f(\gamma)$ is a multiplicative factor that depends on the number of *occurrences* containing the singularity γ. In Eq. (3.16) the '$\approx$' sign 'absorbs' factors slowly varying with λ (e.g. log's). Let the total scale ratio of the n steps (from the outer-scale to the smallest scale) λ_0^n be replaced by λ. For $\lambda \to \infty$ (i.e. for $n \gg 1$), is $c_n(\gamma) \approx c(\gamma)$ which is a function independent of n. Thus, one obtains

$$\Pr(\varepsilon_\lambda \geq \lambda^\gamma) \approx f(\gamma)\,\lambda^{-c(\gamma)}; \qquad \frac{dc}{d\gamma} > 0 \tag{3.17}$$

which is a fundamental multifractal relation for cascades (Schertzer and Lovejoy, 1987). In this equation, ε_λ is the intensity (or density) resulting from developing a cascade down to a scale of resolution λ, and $c(\gamma)$ is a function characterizing the distribution of the singularities γ of the intensities of a process (thus, it is a codimension function).

There are many other phenomenological models in literature. These include the 'pulse-in-pulse' model (Novikov and Stewart, 1964); the 'log-normal' model (Kolmogorov, 1962; Obukhov, 1962); the 'weighted curdling' model (Mandelbrot, 1974); the 'random β-model' (Benzi et al., 1984); and the 'continuous' and 'universal' cascade model (Schertzer and Lovejoy, 1987). These models support the theory that scale-invariant multiplicative processes generally yield multifractals. The model by Schertzer and Lovejoy explores the existence of certain (stable attractive) multifractal generators and argues that the generated multifractals are 'universal' in the sense that these multifractals are characterized by only a few parameters. This model will be discussed in Section 3.4.

The type of phenomenological models mentioned above were classified by Siebesma (1989) as 'non-interacting' cascade models, in contrast with the multifractal cascade model 'with interactions' proposed by this author. In his cascade model the fragmentation of an *eddy* depends on the 'activity' of the neighbouring 'regimes'; this involves the local boundary conditions of each *eddy*.

Divergence of moments

The strong intermittency in multifractals is associated with the phenomenon of divergence of moments. *Divergence of moments* means that $\langle \varepsilon_\lambda^q \rangle \to \infty$ for all $q > q_D$, where ε_λ is the usual intensity of the process on a scale of resolution λ, q is the order of the statistical moment and q_D is the critical order for divergence. This behaviour is a direct result of the singular small-scale cascade limit (see above). Empirical moments, which are averages of empirical values, are always finite: the divergence of moments means in this case that the empirical moments increase without limit as the sample size increases. This statistical behaviour occurs because the sum of independent contributions is determined by the largest of the contributions (i.e. rare events will have dominant contributions); see e.g. Schertzer and Lovejoy (1993). Empirically, it implies the existence of 'outliers,' even in very large experimental samples.

There is equivalence between the divergence of moments (for $q>q_D$) and the algebraic fall-off of the probability distribution for extreme events (e.g. Feller, 1971; Mandelbrot, 1974; Schertzer and Lovejoy, 1985; Lovejoy and Schertzer, 1985b). The tail of the probability law determines the relative frequency of extreme behaviour (see e.g. Mandelbrot, 1982). The slope of this tail is the critical order for divergence of statistical moments, q_D:

$$\Pr(\varepsilon_\lambda > s) \approx s^{-q_D} \tag{3.18}$$

where s is a sufficiently large intensity-threshold. The smaller the exponent q_D, the more extreme is the fluctuation of the process.

Classification of multifractals

Different types of cascades (for example, with different conservation 'rules') and of statistical behaviours have led to a *classification* of multifractals. Some classes are described below.

- *bare and dressed*

The *bare* and *dressed* classification is related to the nature of the multifractal (cascade) process (e.g. Schertzer and Lovejoy, 1987; 1989; 1992; 1993; Lovejoy and Schertzer, 1990b). *Bare* quantities and properties of the cascade are those obtained theoretically after a finite number of cascade steps. They result from a *fine-grained* process (i.e. the cascade is developed from a large scale down to a certain small scale). Therefore, they are not affected by non-linear interactions on scales smaller than the observation-scale because the process (i.e. the cascade) is 'truncated' at this scale.

In contrast, *dressed* quantities and properties are associated with *coarse-grained* processes. *Dressed* processes are those obtained experimentally from a physical process by taking (temporal or spatial) averages at a certain resolution scale (i.e. the observation scale). Because of observational limitations this scale is often larger than the 'inner' scale of the process. This 'inner' scale corresponds to the 'true' homogeneity-scale (i.e. in the sense that it is a physical scale); it is the lower-limit scale for the occurrence of variability (i.e. on even smaller scales the process is 'truly' homogeneous or smooth, no more variability occurs). The integration of the small-scale variability on the observation scale 'smoothes out' some singularities of the physical process. Nevertheless, the smaller details of the process and, thus, the effect of all interactions, are included in the evaluation of the *dressed* quantities. The observed process is *dressed* by the small-scale 'activity'. In contrast, the theoretical process is a *bare* process (i.e. a 'truncated' process that results from developing a cascade from a larger scale down the observation-scale); it is *bare* in the sense that it is 'stripped' of the small-scale 'activity.'

In *dressed* multifractals, all scale interactions and variability on scales between the scale of observation and the innermost scale of the process are *hidden* from direct observation. Nevertheless, this *hidden* small-scale variability has an important contribution to the ('violent') variability of *dressed* processes. This is explained by the multiplicative nature of the processes,

3.3.2 Statistical description of multifractal processes

The properties of a random variable can be equivalently specified with its probability distribution or (all) its statistical moments. For a non-negative random variable x, these two representations are linked by a Mellin transform, M (e.g. Hochstadt, 1971):

$$\langle x^{q-1} \rangle = M(p) = \int_0^\infty x^{q-1} p(x)\, dx \tag{3.19}$$

where p means probability density and q is the order of the statistical moment. There is also an inverse Mellin transform:

$$p(x) = M^{-1}(\langle x^{q-1} \rangle) = \frac{1}{2i\pi} \int_{b-i\infty}^{b+i\infty} \langle x^{q-1} \rangle\, x^{-q}\, dq \tag{3.20}$$

where b is a constant and i is the imaginary $(-1)^{1/2}$.

Anticipating that a similar duality (between probabilities and moments) exists in the statistics of multifractal processes, they can be studied either with the probability distributions or the statistical moments of the intensity of the process (see e.g. Schertzer and Lovejoy, 1987).

Scaling functions associated with different statistical descriptions

Characterization of a process exhibiting infinite number of levels of intensity involves not one but an (infinite) hierarchy of fractal dimensions. Each dimension characterizes the set associated with a particular order of singularity γ of the process intensity on different scales. It is thus natural to define the fractal dimension D as a function of the singularity γ, which is called a *fractal dimension function*, $D(\gamma)$. Correspondingly there is a fractal *codimension function* $c(\gamma)$, associating a fractal codimension with the sets defined for each singularity γ. This corresponds to generalizing the definition of codimension given in Eq. (3.3). Thus, is

$$c(\gamma) = D - D(\gamma) \tag{3.21}$$

where D is the fractal dimension of the space that embeds or 'supports' the process (i.e. of the geometric 'support' of the process), and $D(\gamma)$ is the fractal dimension of the 'support' of singularities whose order is greater than γ. The dimension D can be non-integer, which means that the 'support' of the process can be a fractal itself.

In terms of *probabilities*, the general statistical characterization of multifractals arises directly from multiplicative cascade processes (Schertzer and Lovejoy, 1987; Lovejoy and Schertzer, 1990a; see also Section 3.3.1). For a range of scales without a characteristic scale, the following relation holds:

$$\Pr(\varepsilon_\lambda \geq \lambda^\gamma) \approx \lambda^{-c(\gamma)} \tag{3.22}$$

This relation holds for proportionality constants varying slowly with λ and depending weakly on γ (e.g. Schertzer and Lovejoy, 1989; Lovejoy and Schertzer, 1991). In Eq. (3.22), ε_λ is the non-dimensional intensity that is observed at resolution level λ, and stands implicitly for all $\varepsilon_{\lambda,i}$, with $i=1,\lambda^D$, observed on cubes of side λ^{-1}; γ is the order of singularity of ε_λ; and $c(\gamma)$ is the associated codimension. At resolution λ the fraction of the probability space with singularities greater than or equal to γ is given by the probability distribution of Eq. (3.22). The codimension function is thus the exponent describing the scaling of the probability distribution of the process intensity. It is a resolution-independent function. The function $c(\gamma)$ gives a statistical exponent for each intensity level of the process (thus, for each order of singularity γ). It indicates how the histograms change with resolution.

The definition of the codimension function implies that $c(\gamma)$ is an increasing function of γ; further, it must be concave. A sketch of a typical codimension function is in Figure 3.8(a).

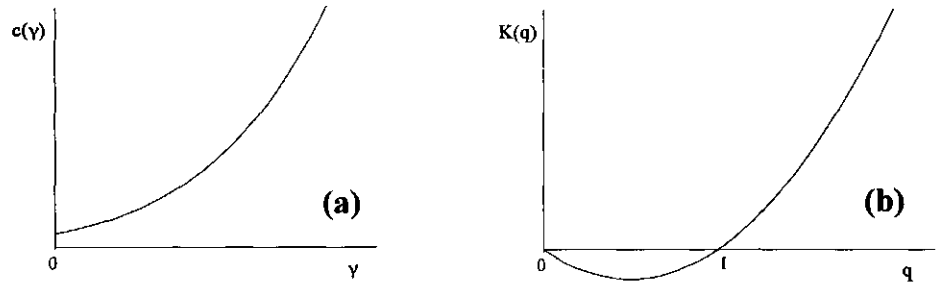

Figure 3.8 Examples of multifractal scaling exponent functions: (a) the codimension function, $c(\gamma)$; and (b) the moments scaling function, $K(q)$.

Another (equivalent) way to describe multifractals is through the *statistical moments* of the intensity ε_λ. For a range of scales without a characteristic scale, the following relation holds (e.g. Schertzer and Lovejoy, 1987; Lovejoy and Schertzer, 1990a):

$$\langle \varepsilon_\lambda{}^q \rangle \approx \lambda^{K(q)} \tag{3.23}$$

where q is the order of the statistical moments, $\langle \varepsilon_\lambda{}^q \rangle$ is the average q^{th} moment of the intensities at resolution level λ (i.e. of all the $\varepsilon_{\lambda,i}$, with $i=1,\lambda^D$), and $K(q)$ is the *moments scaling exponent function*. The function $K(q)$ is also a concave function of the type sketched in Figure 3.8(b). If the multifractal is space filling trivially $K(0)=0$; and, via the conservation condition $\langle \varepsilon_\lambda \rangle=1$, also $K(1)=0$. In the other case with $K(0)=-c$, c is the codimension of the 'support' of the process (thus, it relates to the 'zeros' of the process).

The dual Legendre transforms

For large scale ratios, the duality expressed in Eqs. (3.19) and (3.20) reduces to a particular simple form for the multifractal scaling exponents functions $c(\gamma)$, in Eq. (3.22), and $K(q)$, in Eq. (3.23) (see the explanations given in e.g. Lovejoy and Schertzer, 1990b; Schertzer and Lovejoy, 1993). The relation between these exponent functions, associated with the scaling of the probability distributions and statistical moments, is a type of *Legendre transform* (Frisch and Parisi, 1985) by which the function $K(q)$ is obtained from the function $c(\gamma)$:

$$K(q) = \max_{\gamma} \{q\gamma - c(\gamma)\} \tag{3.24}$$

This relation was obtained from Eq. (3.19). The relation of Eq. (3.24) can be inverted to obtain $c(\gamma)$ from $K(q)$. Using the inverse Mellin transform in Eq. (3.20), one obtains the relation

$$c(\gamma) = \max_{q} \{\gamma q - K(q)\} \tag{3.25}$$

which is called an inverse Legendre transform; nevertheless, the transformation in Eq. (3.25) is just another Legendre transform (e.g. Schertzer and Lovejoy, 1993). This shows the complete equivalence of a description in terms of moments and in terms of probabilities.

The Legendre transforms arise because, in the limit $\lambda \to \infty$, for each moment q there is a corresponding singularity γ_q that dominates the average. The singularity γ_q is the singularity that maximizes $(q\gamma\text{-}c(\gamma))$, and is given by the solution of $c'(\gamma_q)=q$. Similarly, the value of the moment that maximizes $(\gamma q\text{-}K(q))$ is q_γ, and is given by the solution of $K'(q_\gamma)=\gamma$.

Graphically, the Legendre transform in Eq. (3.24) is the maximum distance between the line $q\gamma$ and the curve $c(\gamma)$. An illustration of this is given in Figure 3.9(a). For the (inverse) Legendre transform in Eq. (3.25) it is the distance between the line γq and the curve $K(q)$ (see Figure 3.9(b)). The Legendre transformations relate points of the function $c(\gamma)$ to tangents of the function $K(q)$ and vice-versa.

The one-to-one correspondence between moments and orders of singularities is, thus,

$$q = c'(\gamma) \tag{3.26}$$

$$\gamma = K'(q) \tag{3.27}$$

If the singularities γ are bounded by a value γ_{max} (for example, in microcanonical multifractals, described earlier; or because of finite sampling, see below), the Legendre transform of $c(\gamma)$ takes place for only a finite range of γ-values. This leads to a linear behaviour of the moments scaling function $K(q)$ for moments $q>q_{max}$. The critical moment is $q_{max}=c'(\gamma_{max})$. For this range of values the function $K(q)$ is obtained by

$$K(q) = q\gamma_{max} - c(\gamma_{max}) \tag{3.28}$$

Figure 3.10 gives a graphical illustration of this behaviour (see e.g. Schertzer and Lovejoy, 1993; Tessier et al., 1994).

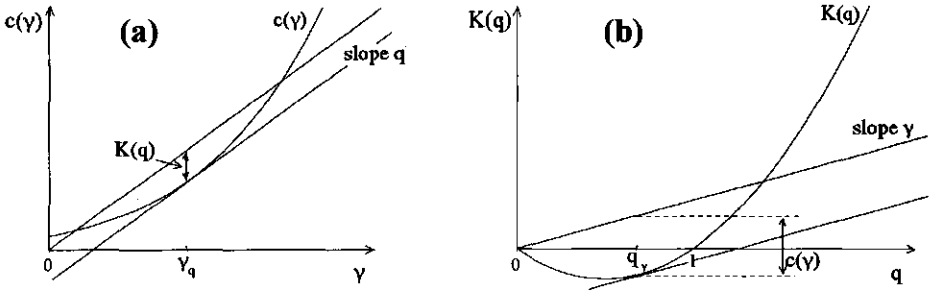

Figure 3.9 Illustration of the (dual) Legendre transforms relating graphically the scaling functions associated with the probability distributions, $c(\gamma)$, and with the statistical moments, $K(q)$: (a) obtaining $K(q)$ from $c(\gamma)$; and (b) obtaining $c(\gamma)$ from $K(q)$ (adapted from Tessier et al., 1993).

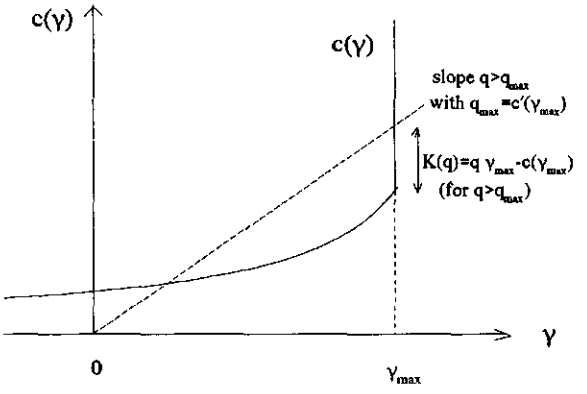

Figure 3.10 Illustration of the graphical construction of the Legendre transform to derive the moments scaling function $K(q)$, for $q>q_{max}$, from a bounded codimension function $c(\gamma)$ (adapted from Schertzer and Lovejoy, 1993).

Other properties of the scaling exponent functions

The function $c(\gamma)$ has several properties that can be illustrated graphically (e.g. Schertzer and Lovejoy, 1989; Lovejoy and Schertzer, 1990a). From Eqs. (3.23) and (3.24), with $q=1$, one obtains $\langle \varepsilon_\lambda \rangle \sim \lambda^{\gamma_1 - c(\gamma_1)}$, where γ_1 is the singularity corresponding to the mean of the process. The last relation yields $\gamma_1 = c(\gamma_1)$ for $\langle \varepsilon_\lambda \rangle = 1$, thus, if conservation is respected, the singularity γ_1

equals the codimension associated with this value of γ. Using Eq. (3.26), one furthermore concludes that $c'(\gamma_1)=1$. Moreover, Eq. (3.27) shows that the singularity γ_1 is also the local trend of the moments scaling function $K(q)$ near the mean (for $q=1$). The singularity γ_1 will be denoted further by C_1 in agreement with the notation used in literature.

Thus, summarizing the above, for *conserved* processes the codimension function satisfies the fixed point relation $C_1=c(C_1)$ and is tangent to the bisectrix (i.e. the line $\gamma=c(\gamma)$) in that point (see Figure 3.11(a)). That is,

$$c(C_1) = C_1 \qquad \text{and} \qquad c'(C_1) = 1 \tag{3.29}$$

Therefore, C_1 is the codimension of the mean of the process. If a process is embedded on a space of dimension D, and the condition $D \geq C_1$ is not satisfied, the mean of the process will be too sparse to be observed (e.g. Lovejoy and Schertzer, 1992).

For *non-conserved* processes, (non-conserved) densities are obtained from the conserved density ε_λ by multiplying it by λ^{-H}, where the parameter H is a measure for the degree of non-conservation (e.g. Lovejoy and Schertzer, 1992). For conserved processes $H=0$. Whenever $\varepsilon_\lambda=\lambda^\gamma$ the non-conserved density equals $\lambda^{\gamma-H}$ (i.e. there is a translation of singularities by $-H$). Thus, the codimension function for the non-conserved case suffers a shift of H in relation to the conserved case. Thus

$$c(C_1 - H) = C_1 \qquad \text{and} \qquad c'(C_1 - H) = 1 \tag{3.30}$$

This is illustrated in Figure 3.11(b).

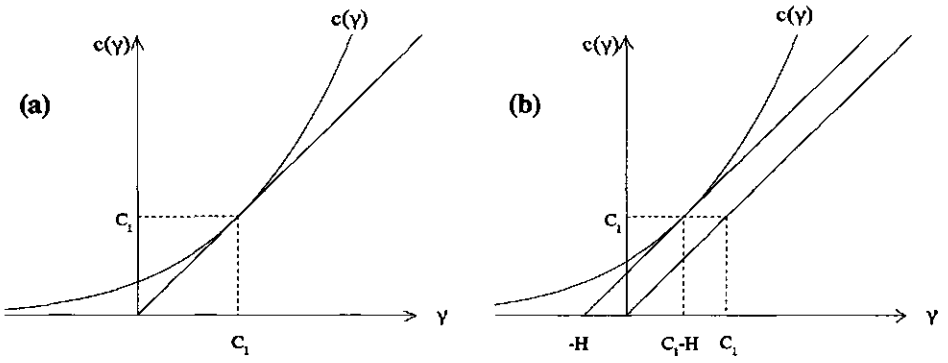

Figure 3.11 Illustration of some properties of the codimension function, $c(\gamma)$: (a) for conserved processes is $c(C_1)=C_1$ and $c'(C_1)=1$; and (b) for non-conserved processes is $c(C_1-H)=C_1$ and $c'(C_1-H)=1$ (adapted from Lovejoy and Schertzer, 1992).

A codimension function $C(q)$, 'dual' to $c(\gamma)$, has been defined (Hentschel and Procaccia, 1983; Grassberger, 1983; Schertzer and Lovejoy, 1984):

$$C(q) = \frac{K(q)}{q-1} \tag{3.31}$$

where $K(q)$ is the moments scaling exponent function and q is the order of the statistical moments. The graphical construction in Figure 3.12 shows that $C(q)$ is the slope of the chord between the points $(1,0)$ and $(q,K(q))$ (e.g. Schertzer and Lovejoy, 1993). Therefore, due to the convexity of $K(q)$, the function $C(q)$ must be increasing. This function satisfies the relation $C_1=C(1)$, which is obtained, for $q=1$, by applying the l'Hôpital rule to Eq. (3.31) and using Eq. (3.27).

The codimension function $C(q)$ relates to a dimension function $D(q)$ by (e.g. Schertzer and Lovejoy, 1993)

$$D(q) = D - C(q) \tag{3.32}$$

The fact that $C(q)$ is an increasing function implies that $D(q)$ is a strictly decreasing function.

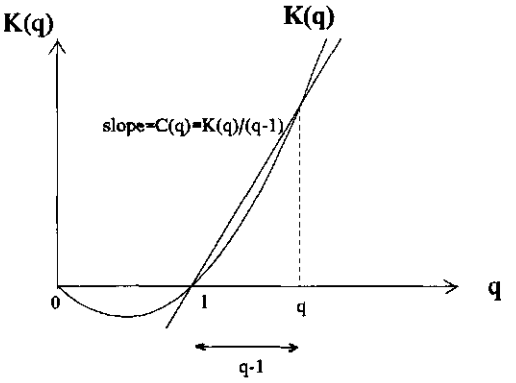

Figure 3.12 Illustration of the relation between the scaling exponent functions $K(q)$ and $C(q)$ (adapted from Schertzer and Lovejoy, 1993).

Limitations imposed by finite sampling

The *size* of experimental samples is known to be a limiting factor for the statistical characterization of processes. For multifractal processes, the sample size can be related to critical values of the empirical scaling exponent functions, at $c(\gamma_s)$ and $K(q_s)$, beyond which values statistical estimates are not considered reliable. The subscript s is used to indicate that quantities (or features) are affected by sample size limitations.

The probability space is formed by the total number of D-dimensional samples observed in the physical space. The codimension function $c(\gamma)$ is a measure of the fraction of the probability space occupied by singularities of order equal or superior to γ. This function is increasing (see Section 3.3.2): the largest (and most extreme) singularities are the rarest. Consequently, one expects that such singularities are only present in some (large) samples. The empirical codimension function is thus limited by the finite size of the sample used in the analysis (Schertzer and Lovejoy, 1989; Lavallée et al., 1991a); the function $c(\gamma)$ is bounded from above. Increasing the number of samples will increase the probability space and, thus, the chance of encountering extreme (i.e. of large singularities) and rare events that are almost surely missed on a finite sample. It will also improve the precision of the determination of the entire empirical codimension function.

The maximum value of the singularity γ_s (or γ_{max}) observed at least once in N_s independent samples of volume λ^{-D} (with λ^D *boxes* in each sample) relates to the codimension $c(\gamma_s)$ according to Eq. (3.22), so

$$\Pr(\varepsilon_\lambda = \lambda^{\gamma_s}) = \frac{1}{N_s \lambda^D} \approx \lambda^{-c(\gamma_s)} \quad \rightarrow \quad N_s \lambda^D \lambda^{-c(\gamma_s)} \approx 1 \tag{3.33}$$

To quantify the extent to which the probability space is explored, Lavallée et al. (1991a) introduced the definition of *sampling dimension* D_s, for N_s samples:

$$\lambda^{D_s} = N_s \quad \rightarrow \quad D_s = \frac{\log(N_s)}{\log(\lambda)} \tag{3.34}$$

where the scale ratio λ is the ratio of the smallest and largest scale used. The sampling dimension can be used to determine the highest order of singularity γ_s that is likely observed in N_s independent samples. Substituting Eq. (3.34) in Eq. (3.33) one obtains the maximum reliable estimate of the codimension of the rarest singularity likely to be observed at least once in the N_s samples:

$$c(\gamma_s) \approx D + D_s \tag{3.35}$$

Figure 3.13 illustrates how the value of γ_s can be obtained from the codimension $c(\gamma_s)$ of magnitude $D+D_s$.

The value of $D+D_s$, in the right-hand side of Eq. (3.35), corresponds to the (overall) *effective dimension* (e.g. Schertzer and Lovejoy, 1993; Tessier et al., 1994). Thus, the dimension function $D(\gamma)$ is

$$D(\gamma) = D + D_s - c(\gamma) \tag{3.36}$$

Limitations imposed by sample size also affect the estimates of statistical moments. Using Eq. (3.26), one obtains the moment $q_s=c'(\gamma_s)$ which is thus the dual moment of the highest-order singularity that can be estimated reliably from a finite sample.

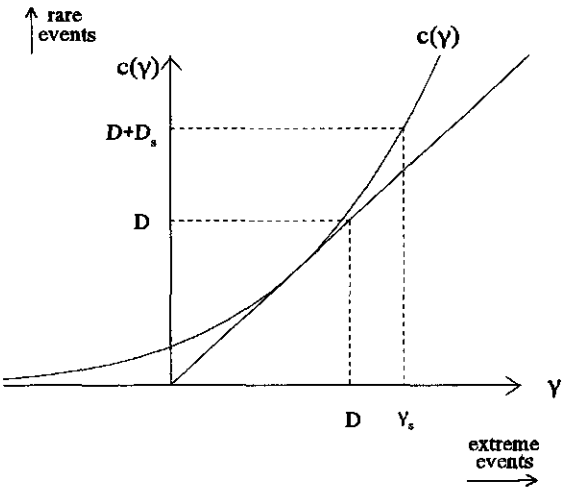

Figure 3.13 Illustration of how the notion of effective dimension $D+D_s$ relates to the maximum values of the codimension, $c(\gamma_s)$, and singularity, γ_s, that are estimated reliably from a finite sample (adapted from Lavallée et al., 1991a).

3.3.3 Multifractal phase transitions

Various analogies have been established between thermodynamic variables of equilibrium systems and multifractal exponents of dissipative non-equilibrium systems. They have led to the investigation of the analogues of (thermodynamical) *phase transitions* in multifractals (e.g. Schuster, 1988; Tél, 1988; Schertzer and Lovejoy, 1989, 1991b, 1993; Schertzer et al., 1993; Schmitt, 1993; Schertzer and Lovejoy, 1994). The purpose is to determine qualitatively different regimes in multifractals and the transitions from one regime to another. Such study is important for characterizing multifractal processes.

Formal analogy between flux dynamics and thermodynamics

Both in thermodynamics and in flux dynamics there are *Legendre transform pairs*. In *thermodynamics*, a Legendre transform relates the free energy F to the corresponding entropy S. In *flux dynamics*, the (multifractal) moments scaling exponent function $K(q)$ and codimension function $c(\gamma)$ are Legendre transform pairs defined in Eqs. (3.24) and (3.25). It follows from this analogy that one can associate the moment of order q with the inverse temperature β (i.e. $\beta=1/T$, where T is the temperature), and the function $K(q)$ with the Massieu potential $\Sigma(\beta)$. Furthermore, there are analogies between the order of singularity γ and the energy E, and between the function $c(\gamma)$ and the entropy. Therefore, one can establish the following *formal analogies* between the multifractal and standard thermodynamic descriptions:

i) the probability description $(\gamma, c(\gamma))$ is the multifractal analogue of the (energy, entropy) description; and ii) the moment description $(q, K(q))$ is the analogue of the (inverse temperature, Massieu potential) description. These analogies are summarized in Table 3.1.

Table 3.1 Formal analogies between flux dynamics and thermodynamics. The symbols are explained in the text.

Flux dynamics	*Thermodynamics*
Probability space	Phase space
γ	$-E$
$c(\gamma)$	$-S(E)$
q	$\beta=1/T$
$K(q)=-c(\gamma)+q\gamma$	$\Sigma(\beta)=S(E)-\beta E$
$C(q)=K(q)/(q-1)$	$F(\beta)=-\Sigma(\beta)/\beta$

Multifractal phase transitions and the statistical thermodynamic analogues

In standard thermodynamics, *phase transitions* refer to discontinuities of the free energy and thermodynamic potential. If one follows the analogies indicated above, discontinuities in the derivatives of the function $K(q)$ correspond to discontinuities in the derivatives of thermodynamic potentials. Hence, discontinuities in the derivatives of the function $K(q)$ are also called (multifractal) phase transitions. Discontinuities in the first derivative of the function $K(q)$ are called *first-order multifractal phase transitions* and discontinuities in the second derivative of $K(q)$ are called *second-order multifractal phase transitions*. In the framework of stochastic multifractals, (multifractal) phase transitions occur because of two different statistical mechanisms. First-order phase transitions are associated with *divergence of moments*, and second-order phase transitions arise from *finite sampling* (i.e. bounded singularities). The critical exponents associated with the divergence of moments are the moment q_D and the singularity γ_D; and with finite sampling limitations are the moment q_s and the singularity γ_s. These exponents are discussed further below.

Second-order multifractal phase transitions

Finite sampling of a process restricts the observation of the probability space and, thus, the chance of encountering extreme and rare events that are almost surely missed on a finite sample (see Section 3.3.2). Therefore, it imposes limitations to the magnitude of the maximum observable order of singularity γ_s (or γ_{max}) of the intensity of a process. Consequently, the

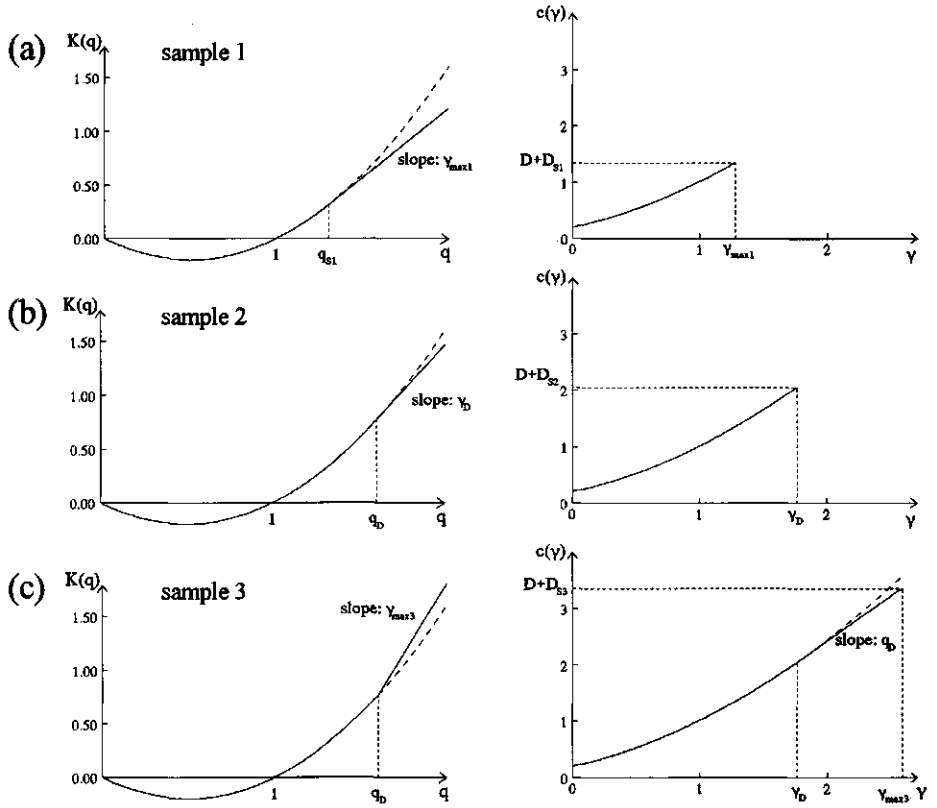

	Sample 1	Sample 2	Sample 3
size of sample	N_{s1}	N_{s2}	N_{s3}
sampling dimension	D_{s1}	D_{s2}	D_{s3}
effective dimension	$D+D_{s1}=1.35$	$D+D_{s2}=2.05$	$D+D_{s3}=3.36$
max. singularity	$\gamma_{max1}=\gamma_{s1}=1.28$	$\gamma_{max2}=\gamma_{s2}=\gamma_D=1.76$	$\gamma_{max3}=2.58$
critical moment	$q_{s1}=1.3$	$q_{s2}=q_D=1.6$	$q_D=1.6$
order of multifractal phase transition	$\gamma_{max1}<\gamma_D$ **second order**	$\gamma_{max2}=\gamma_D$	$\gamma_{max3}>\gamma_D$ **first order**
behaviour of the empirical $K(q)$	$q\le q_{s1}$: non-linear $q>q_{s1}$: linear, slope γ_{max1}	$q\le q_D$: non-linear $q>q_D$: linear, slope $\gamma_{max2}=\gamma_D$	$q\le q_D$: non-linear $q>q_D$: linear, slope γ_{max3}
behaviour of the empirical $c(\gamma)$	non-linear, for $\gamma\le\gamma_{max1}$	non-linear, for $\gamma\le\gamma_{max2}$	$\gamma\le\gamma_D$: non-linear $\gamma_D<\gamma\le\gamma_{max3}$: linear, slope q_D

Figure 3.14 Illustration of the behaviour displayed by the empirical scaling exponent functions $K(q)$ and $c(\gamma)$ that characterize a (*dressed*) process observed in a D-dimensional space by 3 finite samples of increasing size $N_{s1}<N_{s2}<N_{s3}$. These functions are represented with solid lines. The dashed lines represent the theoretical scaling functions expected to characterize a *bare* process with the same degree of multifractality and singularity of the mean.

corresponding codimension function is bounded from above. However, the same does not occur with the moments scaling function characterizing the same process.

The existence of an upper boundary for observable singularities leads to a second-order phase transition (i.e. the first derivative of the moments scaling function is continuous, only the second derivative is discontinuous). The Legendre transform of $c(\gamma)$ for only a finite range of γ-values (for singularities $\gamma \le \gamma_s$) yields a (spurious) linear estimate of the empirical moments scaling exponent function $K(q)$, for moments $q > q_s$ (see Section 3.3.2). The function $K(q)$ exhibits, in this case, both non-linear and linear behaviours. The critical moment $q_s = c'(\gamma_s)$ (see Eq. (3.26)) is the moment dual to the singularity γ_s (in Eq. (3.35)) The subscript s is used to indicate variables that are affected by limitations inherent to finite sampling.

The behaviour of the scaling functions $K(q)$ and $c(\gamma)$ described above is illustrated in Figure 3.14(a). Figure 3.14 shows the empirical scaling exponent functions $K(q)$ and $c(\gamma)$ (solid lines) that characterize a multifractal process observed in a D-dimensional space by 3 finite samples of increasing size: $N_{s1} < N_{s2} < N_{s3}$. Figure 3.14 includes a Table that summarizes the characterization of the three cases analyzed. Let the *samples 1, 2,* and *3* have sampling dimensions $D_{s1} < D_{s2} < D_{s3}$, and the corresponding maximum observable singularities be $\gamma_{max1} < \gamma_{max2} < \gamma_{max3}$. The dashed functions represented in Figure 3.14 indicate the theoretical (non-linear) characterization of a *bare* process (obtained by a large number of 'realizations'): $c_b(\gamma)$ and $K_b(q)$. The subscript b is used here to indicate variables related to theoretical *bare* processes. Empirical and theoretical functions coincide below the critical exponents.

The behaviour of the empirical scaling functions for *sample 1* (in Figure 3.14(a)) indicates a second-order phase transition: after the critical moment q_{s1} the corresponding moments scaling function follows a linear behaviour of slope γ_{max1} (or γ_{s1}). For moments $q \le q_{s1}$, the moments scaling function coincides with the (theoretical) non-linear function $K_b(q)$. This critical moment q_{s1} is dual to the singularity γ_{max1}.

The moments scaling exponent function for a dressed process observed by a finite sample can be described in the following way:

$$K(q) = \begin{cases} K_b(q), & q \le q_s \\ \gamma_s (q - q_s) + K_b(q_s), & q > q_s \end{cases} \tag{3.37}$$

where $\gamma_s = \gamma_{max}$ is the (critical) maximum singularity in the sample that is observed reliably. For moments $q > q_s$, the statistics are then 'dominated' by the largest of the contributions. The behaviour described by Eq. (3.37) is valid for experimental samples with singularities γ_{max} that are smaller than the critical singularity γ_D associated with divergence of moments (see below, and also Section 3.3.2).

First-order multifractal phase transitions

The statistical behaviour called first-order multifractal phase transition occurs typically in (multifractal) processes that are observed (by spatial or temporal averaging) on scales larger than the 'inner'-scale of those processes. These are *dressed* processes ('dressed' by the small-scale 'activity'), whereas theoretical processes are *bare* processes (in the sense that they are 'stripped' of the small-scale 'activity'; see Section 3.3.1). A fundamental difference in their behaviour is that while all the moments of *bare* processes are finite, sufficiently high-order moments of *dressed* processes will diverge (see also Section 3.3.1). This divergence is a consequence of the (more) violent variability of *dressed* processes: on a same scale, the singularities of a *dressed* process are expected to be much larger than the singularities that result from a *bare* model, for the same probability of occurrence. This behaviour may be observed only when the *dressing* takes place over a few orders of magnitude. The higher intensities of *dressed* processes bring about divergence of all statistical moments above a critical order q_D (i.e. $K(q)=\infty$ for $q>q_D$). Up to this critical order, the characterization of *dressed* processes is not expected to be statistically different from that of *bare* processes. Hence, the moments scaling function of *dressed* multifractals would be expected to behaves as

$$K(q)=\begin{cases} K_b(q), & q \le q_D \\ \infty, & q > q_D \end{cases} \tag{3.38}$$

Nevertheless, for finite samples, the moments scaling function of *dressed* processes exhibit a different behaviour. When the observations of *dressed* processes are limited to a finite number N_s of samples there is a maximum observable singularity γ_{max}, which is given by the solution of $c(\gamma_{max})=D+D_s$ (Eq. (3.35)). Hence, because the Legendre transform of the codimension function $c(\gamma)$ is determined with the restriction $\gamma \le \gamma_{max}$ (see Section 3.3.2), the corresponding function $K(q)$ displays a linear behaviour for moments larger than a critical value. Two different cases can be distinguished: $\gamma_{max} \le \gamma_D$ and $\gamma_{max} > \gamma_D$, where $\gamma_D=K'(q_D)=D$ is the singularity that is related to the critical order moment q_D for divergence of moments (see Sections 3.3.1 and 3.3.2). The first case was discussed above, and it leads to second order multifractal phase transitions. For the second case, the moments scaling function behaves as

$$K(q)=\begin{cases} K_b(q), & q \le q_D \\ \gamma_{max}(q-q_D)+K_b(q_D), & q > q_D \end{cases} \tag{3.39}$$

The slope of the linear section of the moments scaling function in Eq. (3.39), for moments $q>q_D$, is the value of the singularity γ_{max}; the intercept is $-c(\gamma_{max})$. This behaviour is illustrated in Figure 3.14 for *samples 2* and *3*.

The singularity γ_{max} is expected to increase with the sampling dimension D_s, i.e. with the number of samples by which a process is observed. For *dressed* processes, this implies that

when the number of samples N_s increases, the slope of the moments function for $q>q_D$ increases. In the limit, $N_s\to\infty$ and $\gamma_{max}\to\infty$. Hence, for moments $q>q_D$, the corresponding empirical moments function $K(q)\to\infty$. For a number of samples N_s large but finite, a first-order phase transition (i.e. a discontinuity in the first derivative of the moments scaling function $K(q)$) is observed for high-order moments $q>q_D$. For small samples (i.e. whenever $D+D_s<c(\gamma_D)$) this transition will be missed. In the schematic representation of the behaviour displayed by the moments scaling function $K(q)$ shown in Figure 3.14, the straight sections of the moments functions of slopes $\gamma_{max1}<\gamma_D<\gamma_{max3}<\gamma_\infty$ indicate the behaviour for increasing sample-sizes, $N_{s1}<N_{s2}<N_{s3}<N_{s\infty}$ (it is $N_{s\infty}=\infty$).

There is equivalence between divergence of moments and algebraic fall-off of the probability distributions (for sufficiently large thresholds; see Section 3.3.2). The slope of the algebraic tail of the probability distribution for extreme and rare (*dressed*) events is the critical order for divergence of statistical moments, q_D (see Eq. (3.18)).

The codimensions of the singularities $\gamma\le\gamma_D$, of a *dressed* process ($c(\gamma)$) and of a *bare* process ($c_b(\gamma)$), coincide (see Figure 3.14). However, for $\gamma>\gamma_D$ the maximization of the probability implies to minimize the codimension. Because the only constraint is the convexity of the codimension function, the empirical codimension function $c(\gamma)$ follows a straight line behaviour (tangent to the non-linear codimension function at γ_D). The slope of the empirical function is the critical order of divergence of statistical moments, q_D ($c'(\gamma_D)=q_D$).

Thus, the codimension function of a *dressed* multifractal process behaves as

$$c(\gamma)=\begin{cases} c_b(\gamma), & \gamma\le\gamma_D \\ q_D(\gamma-\gamma_D)+c_b(\gamma_D), & \gamma>\gamma_D \end{cases} \tag{3.40}$$

Figure 3.14 illustrates schematically the behaviour of the codimension function that characterize a *dressed* process observed by three samples of increasing size. For the smaller *samples 1* and *2*, the empirical codimension functions are non-linear, and coincide with the codimension function of the *bare* process. Nonetheless, their upper boundary is different, accordingly to the corresponding effective dimensions of these samples. The linearity in the codimension function due to the divergence of moments of order q_D cannot be observed for these cases. The singular statistics of a *dressed* process will be present only when the sample size is sufficiently large; that is, when the effective dimension $D+D_s\ge c(\gamma_D)$ or, equivalently, when the singularity $\gamma_{max}>\gamma_D$. This is verified by *sample 3* (see Figure 3.14(c)).

It is discussed in Section 3.5.3, below, that the critical moment q_D is the solution of $K(q_D)=(q_D-1)D$ (Eq. (3.63)). Graphically, this has two consequences (see e.g. Schertzer and Lovejoy, 1993). One can be checked in Figure 3.14(b) and (c), for the moments scaling function: the line of slope D that contains the point $(1,0)$ contains also the point $(q_D,K(q_D))$. The other arises from rewriting the previous expression as

$$D = q_D D - K(q_D) = q_D(D - \gamma_D) + c(\gamma_D) \tag{3.41}$$

Thus, for $\gamma > \gamma_D$ (see Eq. (3.40), the critical tangent of slope q_D followed by the codimension function of a *dressed* process (see Figure 3.14(c)) contains the point (D,D).

3.4 A multifractal model: 'Universal' multifractals

The statistics of multifractal processes are characterized by the corresponding scaling exponent functions $c(\gamma)$ and $K(q)$. The description of these functions by models is therefore important. In multifractals, there is only a convexity constraint on the scaling exponent functions $c(\gamma)$ and $K(q)$ (at least up to critical orders of singularity γ and moment q, for *dressed* processes; see Section 3.3.3). Thus, an infinite number of parameters would be required to determine, or describe, a multifractal process (i.e. to specify its scaling behaviour). A simplifying approach to this problem is the concept of 'universality,' which is well known in physics. 'Universality' is the presence in different processes of the same structural dynamic behaviour, which can be quantified with a few (relevant) parameters (i.e. many details of the dynamics turn out to be unimportant).

The 'universality' of multiplicative random processes has been discussed from different points of view (e.g. Mandelbrot, 1974; Schertzer and Lovejoy, 1987; Mandelbrot, 1989; Lovejoy and Schertzer, 1990a; Mandelbrot, 1991; Schertzer and Lovejoy, 1991b, 1993; Gupta and Waymire, 1993; Schertzer et al., 1995; Schertzer and Lovejoy, 1997; Gupta and Waymire, 1997). The alternative proposed by Schertzer and Lovejoy (1987), for continuous processes, explores the existence of certain (stable attractive) generators that lead to different classes of multifractals having distinct (qualitative) behaviour. These classes are 'universal' in the sense that under repeated iteration, the generator may converge to a well-defined limit which depends on relatively few of its characteristics. Moreover, these generators yield ('universal') equations for the exponent functions describing the scaling behaviour of (*bare*) multifractal processes. The scaling functions are parametrized by only three parameters.

Continuous cascades and 'universal' generators

Discrete (multiplicative) cascades (see Section 3.3.1), constructed using arbitrary and fixed (integer) scale ratios for each step of the process, are not realistic for many physical processes. More realistic continuous cascades must have an infinite number of cascade steps over a wide range of scales. Such processes can be obtained from a discrete model (determined by a finite number of discrete steps over the given ratio of scales) by introducing more and more intermediate steps (i.e. by 'densifying' the cascade process) up to an infinity of infinitesimal ones. For multiplicative cascades, this yields stable and attractive processes exhibiting 'universal' behaviour (see e.g. Schertzer and Lovejoy, 1987, 1989; Lovejoy and Schertzer, 1990a).

Let a multifractal process be obtained in such a way that the density ε_λ of the process, on a scale of resolution λ, is

$$\varepsilon_\lambda \approx e^{\Gamma_\lambda} \tag{3.42}$$

where Γ_λ is called the generator of the process (see e.g. Schertzer and Lovejoy, 1987; 1989; Wilson et al., 1991).

The modelling of the multiplicative nature of multifractal (cascade) processes leads to the operation of multiplying densities with densities (see Section 3.3.1). This operation corresponds simply to adding generators to generators of the type $\Gamma_\lambda \approx \ln(\varepsilon_\lambda)$ (in Eq. (3.42)). Thus, these generators can be studied in a framework of additive processes (see e.g. Schertzer and Lovejoy, 1993).

One can rewrite the relation $\langle(\varepsilon_\lambda)^q\rangle \approx \lambda^{K(q)}$ (Eq. (3.23)):

$$\langle e^{q\Gamma_\lambda}\rangle \approx e^{K_\lambda(q)} \approx e^{K(q)\ln(\lambda)} \tag{3.43}$$

which means that $K_\lambda(q) \approx \ln(\lambda)K(q)$ is the second Laplace characteristic function of the generator Γ_λ (i.e. the logarithm of the first Laplace characteristic function, which is $\lambda^{K(q)}$).

The (*bare*) generator Γ_λ of a scale-invariant multiplicative cascade process must satisfy the following basic properties (Schertzer and Lovejoy, 1987, 1989):

i) the (finite-resolution) generator is a random noise process restricted to the range $[1, \lambda]$; this ensures that the process will be smooth on scales smaller than λ^{-1};

ii) the second characteristic function $K_\lambda(q)$ of the generator Γ_λ has a logarithmic behaviour with scale ($\lambda \to \infty$) in order to assure multiple scaling;

iii) the probability distribution of positive fluctuations of the generator Γ_λ must fall-off more quickly than exponentially, in order to have some finite moments $q \geq 0$;

iv) the generator must be normalized so that $K_\lambda(1)=0$ (i.e. $\langle\varepsilon_\lambda\rangle=1$), to assure (canonical) conservation of the flux.

Properties i) and ii) require that the spectrum of the generator is proportional to the inverse of the wave-number: $E_\Gamma(\omega) \approx \omega^{-1}$. Such noises are called $1/f$ noises or *pink* noises.

A generator that respects the above properties and is also stable and attractive under addition is the (stable) extremal Lévy noise (e.g. Schertzer and Lovejoy, 1987, 1989; Wilson et al., 1991; see also Appendix I). The term extremal means with maximal asymmetry. The Lévy noise has a $1/f$ spectrum and is characterized by a *Lévy index* α. This index α equals the order of divergence of the statistical moments of the generator. So it is

$$\Pr(-\Gamma \geq s) \approx s^{-\alpha}, \text{ for } s \gg 1 \quad \Rightarrow \quad \langle(-\Gamma)^q\rangle \geq \infty, \text{ for } q > \alpha \tag{3.44}$$

where $0<\alpha<2$. In Eq. (3.44) s is an intensity threshold.

Extremal Lévy noise is a generalization of the Gaussian case. The Gaussian case corresponds to the case $\alpha=2$, for which there is no order of divergence. By applying the 'generalized central limit theorem' to the addition of random variables with infinite variance (see Appendix I), Lévy distributions are obtained as limiting distributions for (normalized) sums of independent and identically distributed random variables of infinite variance. It is due to this 'attractive' property that they form the basis of the 'universality' classes for multiplicative processes (discussed below).

'Universal' scaling exponent functions

Generators satisfying Eq. (3.44) yield 'universal' expressions (Schertzer and Lovejoy, 1987, 1989; Lovejoy and Schertzer, 1990a) for the multifractal exponent functions describing the scaling of the probability distributions ($c(\gamma)$ in Eq. (3.22)) and of the statistical moments ($K(q)$ in Eq. (3.23)). These expressions are derived by applying the (generalized) central limit theorem for the addition of random variables to the generator of the cascade (see Schertzer and Lovejoy, 1987, 1989). The 'universal' relation for the moment scaling function $K(q)$ is obtained respecting conservation of the moment of order 1 (i.e. $K(1)=0$). The (dual) expression for $c(\gamma)$ is obtained with the help of Legendre transforms.

The 'universal' expressions, holding for *bare* cascades and quantities and for the limit $\lambda\rightarrow\infty$, are

$$c(\gamma - H) = \begin{cases} C_1\left(\dfrac{\gamma}{C_1\alpha'} + \dfrac{1}{\alpha}\right)^{\alpha'} & \text{for } \alpha \neq 1 \\ C_1 \exp\left(\dfrac{\gamma}{C_1} - 1\right) & \text{for } \alpha = 1 \end{cases} \tag{3.45}$$

$$K(q) - qH = \begin{cases} \dfrac{C_1}{\alpha - 1}(q^{\alpha} - q) & \text{for } \alpha \neq 1 \\ C_1\, q \ln(q) & \text{for } \alpha = 1 \end{cases} \tag{3.46}$$

for $q(=dc/d\gamma) \geq 0$ in Eq. (3.46), and where the parameter α lies within the interval [0,2], and the parameter α' satisfies

$$\frac{1}{\alpha} + \frac{1}{\alpha'} = 1 \qquad \text{for } \alpha \neq 1 \tag{3.47}$$

In Eqs. (3.45) and (3.46) H, C_1, and α are the fundamental parameters needed to characterize the scaling functions and, therefore, the statistical properties of multifractal processes. They are called *'universal' multifractal parameters*:

— H characterizes the *deviation from conservation* (that is: $\langle\varepsilon_\lambda\rangle=\lambda^{\gamma H}$). The parameter H is sometimes known theoretically for different processes, although usually it must be determined experimentally. For conserved processes is $H=0$, and the functions in Eqs. (3.45) and (3.46) reduce to two-parameter functions.

— C_1 describes the sparseness or inhomogeneity (i.e. the distance from homogeneity) of the mean of the process. This parameter is the *codimension of the singularity of the mean*: $C_1=c(C_1\text{-}H)$ (see Section 3.3.2). In conserved processes the parameter C_1 is, simultaneously, the order of singularity and the codimension of the mean of the process: $C_1=c(C_1)$. Thus, a process with $C_1=0$ is homogeneous. The parameter C_1 is related to the coefficient of the canonical Lévy measure (see e.g. Schertzer and Lovejoy, 1989; Wilson et al., 1991; Schertzer and Lovejoy, 1993).

— α represents the *degree of multifractality* (i.e. the deviation from monofractality), and it is a parameter fundamental to the classification of multifractal processes. The parameter α is also the Lévy index (e.g. Schertzer and Lovejoy, 1987, 1989, 1992, 1993; Lovejoy and Schertzer, 1990b, 1992; see also Appendix I).

Figure 3.15 shows 'universal' scaling exponent functions for values of the parameter α between 0 and 2. Figure 3.15(a) shows codimension functions $c(\gamma)$, and Figure 3.15(b) shows moments scaling exponent functions $K(q)$.

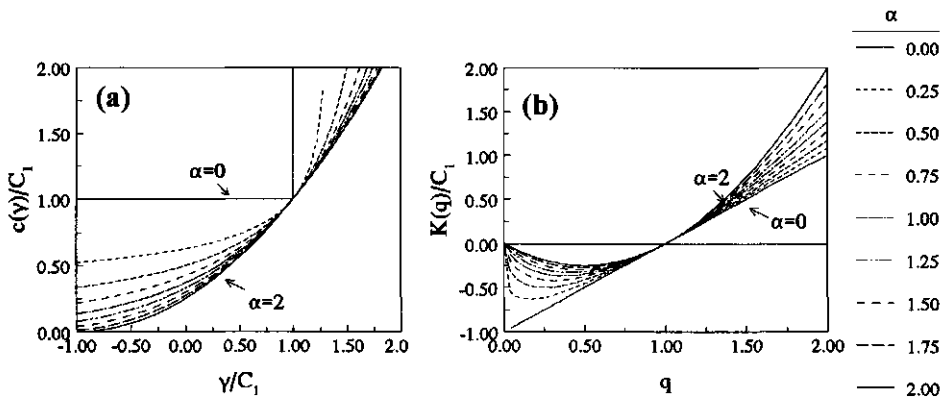

Figure 3.15 'Universal' scaling exponent functions for various values of the parameter α between 0 and 2 (see legend): (a) codimension functions, $c(\gamma)/C_1$; (b) moments scaling functions, $K(q)/C_1$ (adapted from Lovejoy and Schertzer, 1990b).

Since the function $c(\gamma)$ is concave with fixed point C_1 (see Eq. (3.29)), it is possible to define the degree of multifractality α by the (local) rate of change of slope at C_1, given by the radius of curvature, R_c, of the function $c(\gamma)$ (Eq. (3.45)) at $\gamma=C_1$ (e.g. Lovejoy and Schertzer, 1992; Schertzer and Lovejoy, 1993; Tessier et al, 1993):

$$R_c(C_1) = \left[\frac{(1+c'(\gamma))^{3/2}}{c''(\gamma)} \right]_{\gamma=C_1} = 2^{3/2} C_1 \alpha \tag{3.48}$$

One can also establish the corresponding radius of curvature of the function $K(q)$ near the moment $q=1$ (Schertzer et al., 1991).

In 'universal' multifractals this 'local' (i.e. around the average) description of the (*bare*) multifractal behaviour, obtained in terms of α, is sufficient to characterize the functions $c(\gamma)$ and $K(q)$ over the whole range of singularities γ and moments q. For *dressed* processes, observed by finite samples, this 'universal' characterization is valid up to critical orders of singularities and moments associated with multifractal phase transitions (see Section 3.3.3). The estimation of the multifractal parameters H, C_1 and α from empirical data is discussed in Section 3.5.5.

'Universality' classes

'Universality' classes (e.g. Schertzer et al., 1988; Schertzer and Lovejoy, 1989; Lovejoy and Schertzer, 1990a, 1990b, 1991; Schertzer and Lovejoy, 1991b) are defined according to the magnitude of the parameter α: $\alpha=2$, $1<\alpha<2$, $\alpha=1$, $0<\alpha<1$ and $\alpha=0$. The first three cases are classified as *unconditionally hard* multifractals; that is, integration over an observational set with dimension D will yield divergence of statistical moments for sufficiently large (always finite) q_D, regardless of the value of D. For these classes: the upper boundary $\alpha=2$ corresponds to the log-normal (Gaussian) case; the case $1<\alpha<2$ corresponds to (log) Lévy processes with unbounded singularities; and $\alpha=1$ corresponds to log-Cauchy multifractals. The case $0<\alpha<1$ corresponds to (log) Lévy processes with bounded singularities; integration of such multifractals over an observational set with sufficiently large dimension D may yield *soft* behaviour, which leads to a classification of these multifractals as *conditionally hard*. The lower boundary $\alpha=0$ corresponds to the *monofractal* case of the β-model (see Section 3.3.1), whose singularities all have the same fractal dimension.

'Universality' and multifractal phase transitions

In practice, the multifractal 'universal' parameters C_1 and α can be used to estimate the *critical moments* associated with multifractal phase transitions: q_s, for second-order transitions; and q_D, for first-order transitions (see Section 3.3.3).

The critical moment q_s can be obtained with the expression (Lavallée et al., 1991a)

$$q_s = \left[\frac{dc(\gamma)}{d\gamma} \right]_{\gamma=\gamma_s} = \left[\frac{D+D_s}{C_1} \right]^{1/\alpha} \tag{3.49}$$

This expression is obtained with Eqs. (3.26), (3.35), and (3.45). Equation (3.49) is valid only for moments $q_s<q_D$ (e.g. Tessier et al., 1993).

To estimate the critical order for divergence of moments, q_D, the following relation can be used:

$$\frac{C_1}{\alpha - 1}\frac{q_D{}^{\alpha} - q_D}{q_D - 1} = D \tag{3.50}$$

This relation is obtained with Eq. (3.63) (see Section 3.5.3, below) and the 'universal' expression for $K(q)$, in Eq. (3.46).

3.5 Multifractal analysis techniques

Multifractals cannot be studied directly with monofractal analysis methods (see Section 3.2.3). Moreover, extension of these methods to multifractals has its restrictions. Monofractal techniques applied to multifractals can lead to incorrect conclusions, some of which concern (method-induced) breaks in the scaling (e.g. Lovejoy and Schertzer, 1992). The analysis of processes with monofractal methods, developed to study the geometric properties of topological sets, has to be preceded by the definition of the sets that are associated with intensity levels of the processes. Those sets can be obtained by introducing a family of thresholds to the intensity data. The analysis is based on the study of those sets.

'New' multifractal analysis methods study the processes at different levels of resolution. This involves the 'definition' of the processes at a series of lower-scale resolutions, starting from the observational-scale resolution. It implies to average out the processes (i.e. the experimental data), observed at a certain scale, on larger scales (i.e. the intensities themselves are blurred). These methods allow one to determine directly the exponent functions associated with the scaling of the probability distributions and statistical moments that characterize the multifractal processes (see Section 3.3.2).

An important issue in the multifractal analysis of processes is that the information available about the process is discrete. The experimental measuring devices integrate the underlying phenomena over their own scale resolution, which may be more coarse than that of the process itself. The properties observed depend on the scale resolution of the measuring device (see Sections 3.3.1 and 3.3.3).

Some multifractal analysis techniques are described below: 'functional box-counting,' 'probability distribution/multiple scaling,' 'trace moments,' and 'double trace moments.' The estimation of the 'universal' multifractal parameters (see Section 3.4) is discussed at the end of this Section.

3.5.1 Functional box-counting method

Certain scaling processes need not one but an infinity of fractal dimensions to describe their structure. For that purpose Lovejoy et al. (1987) introduced a method to estimate directly those multiple dimensions. The 'functional box-counting' method is an 'extension' of the (monofractal) box-counting method to characterize multifractals (see Section 3.2.3). The objective of the method is to obtain a functional version of the fractal dimension D.

This method of analysis starts with the definition of 'appropriate' finite-resolution topological sets (associated with certain intensity levels of the processes), with the help of intensity thresholds. Figure 3.16 illustrates this procedure, for a number of intensity thresholds applied to the daily rainfall sequence shown in Figure 3.2(a). In the functional box-counting method the geometric properties of each of the resulting sets are characterized by a scaling exponent, i.e. a fractal dimension. The procedure is as follows. Each set is covered with non-overlapping *boxes* of increasing size, which constitutes the standard box-counting procedure. The systematic study of the properties of sets as functions of scale and threshold T_{hr} allows one to determine the dimension function $D(T_{hr})$. By relating thresholds to orders of singularity γ, one obtains (indirectly) the codimension function $c(\gamma)$ (Eq. (3.22)). This can be done with the approximation $T_{hr} \approx \lambda^{\gamma}$, where λ is the resolution scale ratio (Gabriel et al., 1988).

Figure 3.16 Illustration of the definition of sets associated with intensity thresholds. The example uses the daily rainfall sequence shown in Figure 3.2(a), for a 32-day period; this period is mapped in the interval [0, 1]. As the threshold increases the corresponding set is increasingly sparser, thus, characterized by a decreasing fractal dimension.

The functional box-counting method has the advantage that it avoids the use of statistical moments. However, the method has some drawbacks: i) it is not easy to relate thresholds to orders of singularity; ii) the method has the tendency to 'saturate' in certain situations (all the

boxes larger than a given size are 'filled'; see Section 3.2.3), which is a behaviour that can lead to spurious breaks in the scaling; and iii) the method is an 'all-or-nothing' estimator, so it does not consider whether a given *box* is filled by more than one element. The indirect procedure of studying the sets associated with thresholds, rather than the densities themselves, makes this method less satisfactory than other methods, such as the ones described below.

3.5.2 Probability distribution/multiple scaling method

The 'probability distribution/multiple scaling' (PDMS) method (Schertzer and Lovejoy, 1989; Lovejoy and Schertzer, 1990a; Lavallée et al., 1991a) is a multifractal technique developed to estimate directly the exponent function describing the multiple scaling of the probability distributions of processes. This function is the codimension function $c(\gamma)$ in Eq. (3.22). In this technique the histograms are examined over a range of scales rather than at single scales. The PDMS method avoids the use of Legendre transforms and their implicit assumption of convergence of all statistical moments. The method is based on the equation

$$\Pr(\varepsilon_\lambda \geq \lambda^\gamma) = F\,\lambda^{-c(\gamma)} \tag{3.51}$$

where F is a pre-factor 'absorbing' proportionality constants depending weakly on γ (i.e. smaller than algebraic) and slowly varying with λ (see Section 3.3.1). The method assumes that the probability distributions in Eq. (3.51) are either from a single sample or from several independent samples observed in a space of dimension D (e.g. Lovejoy and Schertzer, 1990a).

To calculate the probability distributions in Eq. (3.51), the relevant region of the D-dimensional space is 'covered' with $N_\lambda=\lambda^D$ non-overlapping *boxes* of volume λ^{-D}. The number of *boxes* with intensity ε_λ verifying the inequality

$$\frac{\log(\varepsilon_\lambda)}{\log(\lambda)} \geq \gamma \tag{3.52}$$

is $N_\lambda(\gamma)$. So Eq. (3.51) is approximated by the relation

$$\Pr(\varepsilon_\lambda \geq \lambda^\gamma) \approx \frac{N_\lambda(\gamma)}{N_\lambda} = F\,\lambda^{-c(\gamma)} \tag{3.53}$$

The operation is repeated for different values of the singularity γ, and for decreasing values of the scale ratio λ. To obtain the empirical codimension function $c(\gamma)$ one determines the absolute value of the slopes of plots of $\log(N_\lambda(\gamma)/N_\lambda)$ against $\log(\lambda)$ for particular values of the singularity γ. This method has the advantage that it takes readily into account the slowly varying pre-factor F, as $\log(F)$ is simply the intercept at $\log(\lambda)=0$. Some limitations in estimating and characterizing the function $c(\gamma)$ over the whole range of singularities γ are discussed in Sections 3.3.2, 3.3.3, and 3.4.

Although the PDMS method may seem a variation of the functional box-counting method (Section 3.5.1), the fundamental difference between the two methods is that in the PDMS method the intensity data, themselves, are averaged out on the different scales that are investigated. The functional box-counting method deals instead with the (topological) sets associated with different intensity-thresholds. In addition, while the functional box-counting uses fixed arbitrarily-defined intensity-thresholds, the PDMS method studies intensity levels depending directly on the order of singularity γ and on the scale ratio λ, i.e. $\varepsilon_\lambda \approx \lambda^\gamma$ (Eq. (3.10)).

3.5.3 Trace moment method

The 'trace moment' (TM) method (Schertzer and Lovejoy, 1987) allows the determination of the moments scaling exponent function, $K(q)$ in Eq. (3.23), and, therefore, of the dual codimension function, $C(q)$ in Eq. (3.31).

One is interested in investigating the scaling of the (usual) moments of order q of the (conserved) density ε_λ on different scales of resolution λ. The multifractal singular behaviour of the small-scale limit $\lambda \to \infty$ (see Section 3.3.1) leads to $\langle \varepsilon_\lambda{}^q \rangle = \lambda^{K(q)} \to \infty$ for all moments $q>1$, because $K(q)>0$ for $q>1$ (see Section 3.3.2). To deal with this type of behaviour, the scaling of the moments are studied using the fluxes (integrals) of the densities instead of the densities themselves (the advantages are discussed briefly in Section 3.3.1).

Let a cascade process be observed by an arbitrary sub-set A, of dimension D, defined on a space X. At resolution level λ, the flux over the set A is $\prod_\lambda(A) = \int_A \varepsilon_\lambda \, d^D x$ (see Eq. (3.11)), where ε_λ is the usual density on that scale. Microcanonical conservation implies that $\Pi_\lambda(A)$ is constant independent of the choice of λ (see Section 3.3.1) whereas, for canonical cascades, $\Pi_\lambda(A)$ remains random, with only the ensemble average $\langle \Pi_\lambda(A) \rangle$ being constant. This last class of multifractals is considered here.

The ensemble average of the q^{th}-moment of the flux is defined as

$$\left\langle \left(\prod_\lambda (A) \right)^q \right\rangle = \left\langle \left(\int_A \varepsilon_\lambda \, d^D x \right)^q \right\rangle \tag{3.54}$$

This formula cannot be used for non-integer q because fractional moments are not defined. Therefore, the trace moment of the flux over the set A is introduced, being the (ensemble) average of these quantities

$$Tr_\lambda [\varepsilon_\lambda{}^q] = \left\langle \int_A (\varepsilon_\lambda)^q \, d^{qD} x \right\rangle \tag{3.55}$$

which is called the q^{th}-order *trace moment*, at resolution λ.

The integral in Eq. (3.55) is related to the one in Eq. (3.54) as follows. Because the integral of Eq. (3.54) can be rewritten as

$$\left(\int_A \varepsilon_\lambda d^D x\right)^q = \int_A \int_A \ldots \int_A \varepsilon_\lambda(x_1)\ \varepsilon_\lambda(x_2)\ldots\ \varepsilon_\lambda(x_q)\ d^D x_1\ d^D x_2 \ldots\ d^D x_q \tag{3.56}$$

the integral in Eq. (3.55) reduces this integration to a path integral in the qD-dimensional space, with the path coinciding with the diagonal (trace) over the geometrical structure A^q (i.e. $x_1=x_2=\ldots.=x_q$); one therefore sums over the $\varepsilon_\lambda{}^q(x)$.

The use of trace moments instead of the usual moments has the advantage that it is defined for all moments q including the cases that q is non-integer. The usual moments can only be expanded as multiple integrals for positive integer moments. In practical applications, the trace moments can be estimated by the statistical moments of the densities ε, integrated over *boxes* of volume λ^{-D}.

At resolution level λ an observational set A, of dimension D, can be partitioned in λ^D sub-sets (or 'sub-structures') A_λ (i.e. $A_{\lambda,i}$, $i=1,\lambda^D$), defined by means of a covering of A with non-overlapping *boxes* of side λ^{-1}. The flux over an observational set $A_{\lambda,i}$ is

$$\prod_{\lambda'}(A_{\lambda,i}) = \int_{A_{\lambda,i}} \varepsilon_{\lambda'}\, d^D x \tag{3.57}$$

where $\lambda<\lambda'$, and $\varepsilon_{\lambda'}$ stands for all the intensities at scale resolution λ' that 'contribute' to the intensities $\varepsilon_{\lambda,i}$ that are associated with $A_{\lambda,i}$. The scale ratio λ' is defined here as the ratio of the outer (larger) scale of interest to the smallest known scale of homogeneity.

At resolution λ, the q^{th}-order trace moment is defined by first summing the flux $[\Pi_{\lambda'}(A_{\lambda,i})]^q$ over all the λ^D sub-sets $A_{\lambda,i}$ needed to cover the set A. Next the (ensemble) average is taken over all the 'realizations.' One can write the trace as a sum over *boxes* of side λ^{-1} yielding

$$\int_A (\varepsilon_\lambda)^q\ d^{qD}x \approx \sum_{i=1}^{\lambda^D} (\varepsilon_{\lambda,i})^q\ \lambda^{-qD} \tag{3.58}$$

so that using Eqs. (3.23) and (3.31) one obtains

$$Tr_\lambda[\varepsilon_\lambda{}^q] \approx \lambda^D \lambda^{K(q)} \lambda^{-qD} = \lambda^{K(q)-(q-1)D} = \lambda^{(q-1)(C(q)-D)} \tag{3.59}$$

The q^{th}-order trace moment defined in Eq. (3.59) shows that statistical (ensemble) averages depend not only on the scale, but also on the dimension of the support over which they are averaged.

In practice, for the set A of dimension D, the intensities $\varepsilon_{\lambda,i}$ that are associated with the sub-sets $A_{\lambda,i}$ (with $i=1,\lambda^D$) are obtained from the (contributing) intensities $\varepsilon_{\lambda'(i,j)}$ (with $j=1,(\lambda'/\lambda)^D$) by

averaging them out on the larger scale. Figure 3.17 illustrates schematically, for a 1-dimensional volume, one step in the computation of the intensities $\varepsilon_{\lambda,i}$ at resolution level λ starting from the intensities $\varepsilon_{\lambda'}$ at resolution level λ' (i.e. the observation scale). Each one of the λ^D sub-sets $A_{\lambda,i}$, of the set A of dimension D, is centred at some point x_i defined on a space X, with $i=1,\lambda^D$. The centring and the index i of the sub-sets $A_{\lambda,i}(x_i)$ are omitted in the text.

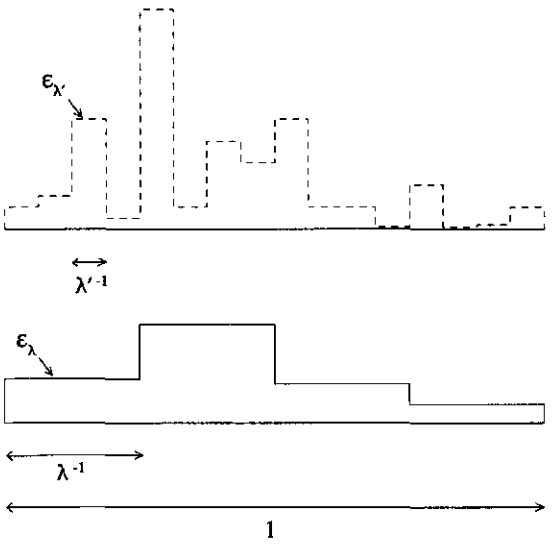

Figure 3.17 Illustration of the computation of the intensities ε_λ on a scale of resolution λ with the intensities $\varepsilon_{\lambda'}$ on the ('inner') scale of resolution λ', for a set $A=[0,1]\in \mathbb{R}$. The example is for a 1-dimensional volume.

At resolution level λ, the (average) intensities ε_λ defined above are raised to powers q. The determination of the trace moments, at various resolution levels λ, implies to average over all the λ^D sub-sets A_λ of the set A. The estimation of the ensemble average is based on the assumption of a sum of independent empirical samples (assumed themselves to contain many independent 'realizations'). Over the scaling range of the process, the function $K(q)$ is estimated from the slopes of plots of $\log(Tr_\lambda[\varepsilon_\lambda{}^q])$ against $\log(\lambda)$ for particular values of the moment q.

Because the density ε_λ is positive, the trace moments are bounds on the usual moments (e.g. Schertzer and Lovejoy, 1993):

$$\left\langle \left(\prod_{\lambda} (A) \right)^q \right\rangle \geq Tr_\lambda[\varepsilon_\lambda{}^q] \qquad \text{for } q > 1 \tag{3.60a}$$

$$\left\langle \left(\prod_{\lambda} (A) \right)^{q} \right\rangle \leq Tr_{\lambda}[\varepsilon_{\lambda}{}^{q}] \qquad \text{for } q < 1 \tag{3.60b}$$

These relations have two important consequences, with respect to the behaviour expressed in Eq. (3.59). In this Equation, if $C(q) > D$, is for all $q < 1$

$$\lim_{\lambda \to \infty} Tr_{\lambda}[\varepsilon_{\lambda}{}^{q}] \to 0 \quad \Rightarrow \quad \left\langle \left(\prod_{\infty} (A) \right)^{q} \right\rangle = 0 \tag{3.61}$$

Due to the monotonicity of the function $C(q)$ (Eq. (3.31) the condition $C(q) > D$ for $q < 1$ is equivalent to $C_1 > D$ (Schertzer and Lovejoy, 1993). Thus, if $C_1 > D$, the mean of the process is too sparse to be observed in the space D. In such a case it is impossible to normalize the process so that the mean is finite. For the other case $C_1 < D$, the trace moments diverge for $q < 1$; however, this does not affect the convergence of the (*dressed*) moments (see Eq. (3.60a)). For $q > 1$ (and for $C(q) > D$), another important consequence of the relation in Eq. (3.60a) is that

$$\lim_{\lambda \to \infty} Tr_{\lambda}[\varepsilon_{\lambda}{}^{q}] = \infty \quad \Rightarrow \quad \left\langle \left(\prod_{\infty} (A) \right)^{q} \right\rangle \to \infty \tag{3.62}$$

i.e. divergence of the trace moments implies divergence of the corresponding (*dressed*) moments. This divergence occurs when the exponents $C(q)-D > 0$ or $K(q)-(q-1)D > 0$ (i.e. the exponents in Eq. (3.59) must be positive). Thus, the critical moment q_D for divergence of moments of *dressed* quantities is defined by

$$C(q_D) = D \qquad \text{or} \qquad K(q_D) = (q_D - 1)D \tag{3.63}$$

and verifies, in the limit $\lambda \to \infty$,

$$\left\langle \left(\prod_{\infty} (A) \right)^{q} \right\rangle \to \infty, \qquad \text{for } q > q_D \tag{3.64}$$

3.5.4 Double trace moment method

The 'double trace moment' (DTM) method (Lavallée et al., 1991b; Lavallée, 1991) is a generalization of the 'trace moment' (TM) method (Schertzer and Lovejoy, 1987; see previous Section). It was developed specifically to estimate directly the 'universal' multifractal parameters H, C_1 and α (see Section 3.4). This application is also discussed in Section 3.5.5, below. The DTM method assumes that multifractals belong to 'universality' classes. This is in contrast to the methods described above where no assumption is made about the type of

multifractal that is being analyzed. Similarly to the TM method, the DTM method allows also the determination of the scaling exponent functions $K(q)$, in Eq. (3.23), and $C(q)$, in Eq. (3.31).

Compared to the TM method, the DTM technique introduces a *second* (double) *moment* in the analysis of the data. This second moment η is chosen within an interval of $\mathbb{R}^+$. The basic idea behind this procedure is to generalize the application of statistical methods to other (normalized) 'versions' of the multifractal process. This aims at increasing the dynamic range of the process that can be analyzed. The procedure acts on the intensity $\varepsilon_{\lambda'}$ associated with the finest (known) resolution λ' of the process (see e.g. Figure 3.17), being the scale ratio λ' defined here as the ratio of the outer (larger) scale of interest to the smallest scale of homogeneity. It starts by taking the η^{th}-power of the intensity $\varepsilon_{\lambda'}$ and then normalizing it with the ensemble average $\langle \varepsilon_{\lambda'}{}^{\eta} \rangle$:

$$\varepsilon_{\lambda'}{}^{(\eta)} = \frac{\varepsilon_{\lambda'}{}^{\eta}}{\langle \varepsilon_{\lambda'}{}^{\eta} \rangle} \tag{3.65}$$

where the intensity $\varepsilon_{\lambda'}{}^{(\eta)}$ is the η-renormalized 'version' of the intensity $\varepsilon_{\lambda'}$.

Let $A_{\lambda,i}$ ($i=1,\lambda^D$) be sub-sets, at resolution λ, of the set A of dimension D (see Section 3.5.3). For each sub-set $A_{\lambda,i}$, the η-power renormalization (Eq. (3.65)) transforms the flux Π (in Eq. (3.57)) into a 'η-flux' $\Pi^{(\eta)}$:

$$\prod_{\lambda'}{}^{(\eta)}(A_{\lambda,i}) = \int_{A_{\lambda,i}} \varepsilon_{\lambda'}{}^{(\eta)} \, d^D x \tag{3.66}$$

where $\lambda<\lambda'$, and $\varepsilon_{\lambda'}{}^{(\eta)}$ stands for all the η-renormalized intensities $\varepsilon_{\lambda'}$, at scale resolution λ', that contribute to the (renormalized) intensity that is associated with $A_{\lambda,i}$ (see Section 3.5.3).

At resolution λ, the q^{th}-order *double trace moment* is defined as

$$Tr_{\lambda}[\varepsilon_{\lambda}{}^{(\eta)q}] \approx \lambda^{K(q,\eta)-(q-1)D} \tag{3.67}$$

where $K(q,\eta)$ is a (*double*) moments scaling exponent function (see Section 3.5.3). This function reduces to the usual $K(q)$ function when $\eta=1$.

In practice, the double trace moments analysis consists of studying the scaling behaviour of various q^{th}-moments of η-power renormalized versions of a multifractal process, at decreasing values of the scale ratio $\lambda \leq \lambda'$. One can obtain the function $K(q,\eta)$ by determining the slope of plots of $\log(Tr_{\lambda}[\varepsilon_{\lambda}{}^{(\eta)q}])$ against $\log(\lambda)$ for various moments q and η.

The idea of renormalizing the multifractal process with η-moments can also be used to study the scaling of the probability distributions (Schertzer and Lovejoy, 1993). The codimension function of a η-power renormalized process is $c(\gamma,\eta)$. Different η-moments yield different codimension functions. This results from the existing duality between the statistical moments and the probability distributions of multifractal processes (see Section 3.3.2).

Some transformations from single to double trace moments (e.g. Schertzer and Lovejoy, 1993) can be summarized as follows (the superscript * is associated here with double trace moment variables):

$$\gamma \quad \rightarrow \quad \gamma^* = \eta\gamma - K(\eta) \tag{3.68}$$

$$c(\gamma) \quad \rightarrow \quad c^*(\gamma^*) = c(\gamma,\eta) = c(\gamma) \tag{3.69}$$

$$q \quad \rightarrow \quad q^* = q/\eta \tag{3.70}$$

$$K(q) \quad \rightarrow \quad K^*(q^*) = K(q,\eta) = K(\eta q^*) - q^* K(\eta) \tag{3.71}$$

For 'universal' multifractals, one obtains the transformations and functions that follow. Being the first derivative of the 'universal' function $K(q)$ (in Eq. (3.46))

$$K'(q) = \frac{dK(q)}{dq} = \frac{C_1}{\alpha - 1}(\alpha q^{\alpha-1} - 1) \tag{3.72}$$

the transformation of the parameter C_1, from single to double trace moments, is

$$C_1 = \left[\frac{dK(q)}{dq}\right]_{q=1} \rightarrow \quad C_1^* = \left[\frac{dK^*(q^*)}{dq^*}\right]_{q^*=1} = C_1\eta^\alpha \tag{3.73}$$

This transformation is obtained with Eq. (3.72) and the transformations indicated in Eqs. (3.70) and (3.71).

Moreover, the function $K^*(q^*)=K(q,\eta)$ in Eq. (3.71) is related to the function $K(q)$ by

$$K(q,\eta) = \eta^\alpha K(q) \tag{3.74}$$

The function $K(q,1)$, obtained with double trace moments for $\eta=1$, and the function $K(q)$, obtained with trace moments, are the same. So, one can obtain the 'universal' form of the function $K(q,\eta)$ by substituting in Eq. (3.74) the 'universal' form of the function $K(q,1)$ (in Eq. (3.46), with $H=0$):

$$K(q,\eta) = \begin{cases} \dfrac{C_1}{\alpha-1}\eta^\alpha(q^\alpha - q) & \text{for } \alpha \neq 1 \\ C_1\,\eta\, q \ln(q) & \text{for } \alpha = 1 \end{cases} \tag{3.75}$$

with $0 \leq \alpha \leq 2$, and $q>0$ for $\alpha \neq 2$.

The direct determination of the 'universal' multifractal parameters is discussed in Section 3.5.5 (see also e.g. Lavallée et al., 1992; Schmitt et al., 1992a, 1992b, 1993; Tessier et al., 1993).

3.5.5 Estimating the 'universal' multifractal parameters

Characterization of 'universal' multifractal processes is simplified greatly if one uses the three-parameter (H, C_1 and α) analytical exponent expressions defined in Eqs. (3.45) and (3.46) to describe the scaling of the probability distributions and of the moments. There are different possibilities to estimate the 'universal' parameters from empirical data. The parameters can be estimated: i) from the empirical scaling exponent functions, with non-linear regression; ii) based on geometrical properties of the codimension function, $c(\gamma)$; iii) using the empirical and theoretical moments scaling functions, $K(q)$; and iv) directly with the double trace moments method. Parameter H can be also estimated from the slope of the energy spectrum of the process.

- *non-linear fitting of the empirical scaling functions (estimating H, C_1 and α)*

One can estimate the 'universal' multifractal parameters (H, C_1 and α) by fitting directly the empirical scaling exponent functions with the 'universal' expressions in Eqs. (3.45) and (3.46). Nevertheless, non-linear curve-fitting algorithms (e.g. the Levenberg-Marquant algorithm, see e.g. Press et al., 1989) fail frequently in converging to a solution. Factors that contribute to this are the high correlation between the parameters α and C_1 and, often, the small range of singularities γ or moments q that is appropriate to use in the regression. The 'universal' form of the scaling functions will hold only for a finite range of singularities and moments of empirical processes, which must be determined in advance (see Sections 3.3.2, 3.3.3, and 3.4). The critical values are associated with multifractal phase transitions. The approach based on non-linear regression leads usually to poor estimates of the parameters.

- *geometrical properties of the codimension function (estimating H, C_1 and α)*

The codimension function $c(\gamma)$ can be parametrized empirically with parameters C_t and γ_t (Schertzer and Lovejoy, 1989; Lovejoy and Schertzer, 1990a):

$$c(\gamma) = C_t\left(\frac{\gamma+\gamma_t}{C_t\alpha'}+\frac{1}{\alpha}\right)^{\alpha'} \qquad \text{for } \alpha \neq 1 \tag{3.76}$$

see Eqs. (3.45) and (3.47). The same parametrization can be used for the case $\alpha=1$.

The above parametrization of $c(\gamma)$ is useful in graphical parameter estimates, because it enables the convenient exploitation of the special properties of the codimension function (see Section 3.3.2). The function $c(\gamma)$ has the special point satisfying $c(C_1)=C_1$ and $c'(C_1)=1$ for conserved multifractals (Eq. (3.29)), or satisfying $c(C_1\text{-}H)=C_1$ and $c'(C_1\text{-}H)=1$ for non-conserved multifractals (Eq. (3.30)); see Figure 3.11. One is interested in these properties for estimating the parameters because they are independent of the parameter α. With the parametrization in Eq. (3.76) (where the subscript t indicates tangent), the properties can be expressed as

$$c(C_t - \gamma_t) = C_t \qquad \text{and} \qquad c'(C_t - \gamma_t) = 1 \tag{3.77}$$

This implies that a line with slope 1 will be tangent to $c(\gamma)$ at the point $c(\gamma) = C_t$ and will intercept the γ-axis at the point $\gamma = -\gamma_t$.

Another convenient order of singularity is $\gamma_0 = -C_1\alpha'/\alpha$ (Schertzer and Lovejoy, 1989). This singularity is either: for $\alpha > 1$, the lower boundary of fractal singularities ($c(\gamma)=0$, i.e. singularities occupying all the space of observation); or, for $\alpha < 1$, the upper boundary of singularities ($c(\gamma)=\infty$, i.e. 'unreachable' singularities). The singularity γ_0 is then also the slope of the tangent at the origin of $K(q)$ ($\gamma_0 = K'(0)$; for $\alpha > 1$) or of the asymptote ($\gamma_0 = K'(\infty)$; for $\alpha < 1$).

Rewriting Eq. (3.45), for $\gamma \geq \gamma_0$ when $1 < \alpha \leq 2$, and $\gamma < \gamma_0$ when $0 \leq \alpha < 1$, yields

$$c(\gamma) = c_0 \left(1 - \frac{\gamma}{\gamma_0}\right)^{\alpha'} \qquad \text{for } \alpha \neq 1 \tag{3.78}$$

where $c_0 = c(0)$ (the graphical estimate of this value is also simple). The parameter α can be estimated with Eq. (3.78). This way of estimating the parameters depends on the values of the curve $c(\gamma)$ in the statistically well defined region near $\gamma = 0$, rather than on the large γ-regime (which corresponds to extremely low probabilities) or on the small (negative) γ-regime (which could be easily contaminated by noise).

- *empirical and theoretical moments scaling functions (estimating C_1 and α)*

From the 'universal' form of the function $K(q)$ expressed in Eq. (3.46) it is possible to obtain two relations, each depending on only one of the parameters C_1 and α. This involves studying the first derivative of the function $K(q)$ at the points $q=1$ and $q=q_{min}$, with $K'(q_{min})=0$. Evaluating Eq. (3.72) at the point $q=1$ gives

$$\left[\frac{dK(q)}{dq}\right]_{q=1} = C_1 \tag{3.79}$$

So, the parameter C_1 is the slope of the tangent to $K(q)$ at $q=1$, and can be estimated from the empirical function. The other point, the minimum of the function $K(q)$ (at $q=q_{min}$), is at

$$q_{min} = \left[\frac{1}{\alpha}\right]^{\frac{1}{\alpha-1}} \qquad \text{for } \alpha \neq \{0,1\} \tag{3.80}$$

Thus, the position of the minimum of the empirical function $K(q)$ allows one to determine the parameter α with Eq. (3.80).

- *double trace moments method (estimating C_1 and α.)*

The double trace moments technique (Lavallée et al., 1991b; see Section 3.5.4) can be used to determine directly the 'universal' parameters α and C_1.

The main feature of the relation $K(q,\eta)=\eta^{\alpha}K(q)$ (in Eq. (3.74)) is that it factors into the product of two functions, one for each of the independent variables η and q. This allows one to estimate the multifractal parameter α by determining the slope of plots of $\log(|K(q,\eta)|)$ against $\log(\eta)$ for fixed moments q (different from the special values of 0 and 1). Parameter C_1 can be estimated with the help of the intercept. Using different values of the moment q increases the statistical reliability of the parameters α and C_1, and it allows for a systematic verification of Eq. (3.74). The estimation of the parameter C_1 is affected by the accuracy of the estimate of α.

Equation (3.74) is valid only when the statistical moments converge (let the moment q_D be the critical order) and the sample is sufficiently large to estimate accurately the scaling exponents (the critical moment is $q_s=c'(\gamma_s)$) (see Sections 3.3.2, 3.3.3 and 3.4). These critical moments are associated with multifractal phase transitions. Whenever $\max(q\eta,q) > \min(q_s,q_D)$, in Eq. (3.74), the *dressed* function $K(q,\eta)$ becomes independent of η. This leads to a break in the linearity observed in plots of $\log(|K(q,\eta)|)$ versus $\log(\eta)$, and yields a characteristic 'S'-shape for this plot. Breaks in the linearity of these plots occur not only for sufficiently large η-moments (q_s and q_D are critical values) but also for sufficiently small η-moments (for $\min(q,q\eta)<q_{min}$).

Knowledge of the critical moments q_s and q_D is important because they define one of the boundaries of the range of values of η-moments that provide reliable statistical estimates of the multifractal parameters. However, the 'universal' parameters themselves can be used to estimate the moments q_s (Eq. (3.49)) and q_D (Eq. (3.50)). Thus, an iterative procedure is required that involves different phases: i) estimating the critical moments; ii) verifying the range of moments (respecting the moments q_s and q_D) used to estimate the 'universal' parameters; and iii) estimating again (and more reliably) the parameters.

The break in the linear behaviour of the DTM plot for low values of η-moments occurs because in this range, where extremely low values of the intensity are analyzed, it is expected that at some point the signal of the intensity will be overcome by noise (the noise level is, of course, characteristic of the measuring device). In such case, there is a characteristic codimension characterizing the noise and also a corresponding critical order of singularity γ_{min} and moment q_{min}. The noise can be space-filling. This qualitative change in statistical behaviour is another example of a multifractal phase transition (e.g. Schertzer and Lovejoy, 1993; Tessier et al., 1994). Thus, at both large and small η-moments, sample limitations may lead to scaling problems for the extreme moments. In fact, in this analysis one should consider the product of the moments q and η, instead of η-moments alone.

- *power spectrum (estimating H)*

In the characterization of a multifractal process, the parameter H is the degree of non-conservation of the process. The estimation of the parameter H uses the scaling exponent of the energy spectrum of the process. If the energy spectrum of the intensities ε_λ is of the form $\omega^{-\beta}$, as expressed in Eq. (3.5), the expectation is that the absolute value of the spectral exponent β will be related to the parameter H and the moments scaling exponent by (e.g. Schertzer and Lovejoy, 1993)

$$\beta = 1 - K(2) + 2H \tag{3.81}$$

The spectral exponent is related to a single value of the function $K(q)$, which is for the moment 2 because spectra are second-order statistics. The energy (power) spectrum is obtained from the Fourier transform of the autocorrelation function, which is a second-order moment (see Section 2.4, and 3.3.1).

Parameter H can be obtained with Eq. (3.81), using either the empirical or theoretical estimate of $K(2)$. The theoretical value of $K(2)$ can be obtained with Eq. (3.46), after determining parameters C_1 and α, yielding the expression

$$H = \frac{\beta - 1 + K(2)}{2} = \frac{\beta - 1}{2} + \frac{C_1(2^\alpha - 2)}{2(\alpha - 1)} \tag{3.82}$$

For a conserved process, the spectrum is always less steep than a $1/f$ noise, which is characterized by a spectrum of the type $E(\omega)=\omega^{-1}$ (see Section 3.4). For processes having spectra with absolute slope $\beta>1$, see e.g. Schertzer and Lovejoy (1993), Schmitt (1993).

3.6 Overview of scale-invariant approaches to the study of rainfall

Rainfall is a highly non-linear process which exhibits extreme variability over a wide range of time and space scales. Its study has been an active area of research (for a review see Chapter 2). In studying rainfall one can distinguish between *deterministic* and *stochastic* approaches. The deterministic approach is linked to the description of the physical phenomena, whereas the stochastic one stresses the statistical aspects. These approaches have usually been used as alternatives. Each has advantages (and disadvantages) in relation to the other. However, neither of these approaches offers a completely satisfactory framework for rainfall studies. Ideally, the deterministic approach should involve the integration of the non-linear partial differential equations that describe the dynamics of rainfall. However, the exact equations that govern such dynamics are not known. To overcome this problem deterministic rainfall models make use of parametrizations of the underlying processes. Nevertheless, the

validity of these parametrizations is often questioned. To these problems one can add the difficulties of handling the marked non-linearity of these processes and the meagre knowledge one has about the initial and boundary conditions. These difficulties have sometimes favoured the stochastic approach for studying rain, although this approach has serious limitations if one wishes to tackle the fundamental problem of the extreme non-linear variability exhibited by the rainfall process.

The models that have been developed to study rainfall contain different numbers of parameters, and have different degrees of complexity. The simpler models require fewer parameters but their ability to describe the rainfall process is limited. The more complex models require the estimation of many parameters and are sometimes difficult to apply. Moreover, these models can not normally be used for conditions different from the one for which they were validated. These conditions include the scale of the model.

About studying rainfall in a scale-invariant framework

Rainfall studies based on *scaling* (or *scale-invariance*) are only of recent date. Scaling is a well-known concept in physics. It is based on the invariance of properties across scales. Thus, scaling relates to the absence of a characteristic scale or length in, for example, processes or equations. An example of such an equation is the Navier-Stokes equation, which is the basic equation of fluid dynamics and, thus, also of meteorology. Scaling is expected to hold from some large (*outer* or upper) scale down to a small (*inner* or lower) scale. These critical scales are basic *length*-scales.

Under the umbrella of scaling, different hypotheses have been investigated in relation to rain modelling. One of them — a multifractal approach — was developed by Schertzer and Lovejoy (1987, 1988, 1989), who modelled the variability of rainfall by a (multiplicative) cascade process. Cascade models, which are used to describe turbulence, assume a multiplicative energy-transfer process from larger to smaller scales (e.g. Kolmogorov, 1962; Obukhov, 1962; Novikov and Stewart, 1964; Mandelbrot, 1974; Over and Gupta, 1994). This type of behaviour is also expected for the flux of water in the atmosphere. The rainfall process must have mechanisms (analogous to the turbulence mechanism) that are responsible for the concentration of energy and moisture into smaller and smaller regions of the atmosphere. Empirical observations of the variability of rainfall are in favour of this cascade type of behaviour in the atmosphere (e.g. Schertzer and Lovejoy, 1987; Gupta and Waymire, 1993; Lovejoy and Schertzer, 1995a). Because the lifetime of atmospheric processes, including storms, depends on their spatial scale, the actual cascade related to rain is expected to be a space/time process (e.g. Schertzer and Lovejoy, 1995a; Over and Gupta, 1996; Marsan et al., 1996).

The scaling approach to the study of atmospheric fields was motivated by the lack of knowledge of certain atmospheric processes (for example, the full non-linear partial differential equations governing the atmosphere are not known). For scale-invariant studies of

atmospheric fields, see e.g. Lovejoy (1981, 1982, 1983), Schertzer and Lovejoy (1983), Lovejoy and Mandelbrot (1985), Lovejoy and Schertzer (1985a, 1985b), Schertzer and Lovejoy (1987), Lovejoy and Schertzer (1990a, 1990b, 1991). Cascade models have proved to be of value in describing atmospheric processes. Atmospheric fields have multifractal structures over a considerable part of their dynamic range and over meteorologically significant space-time scales in which the dynamics of the atmosphere takes place. These structures extend from thousands of kilometres to 1 mm in space, coupled with time scales ranging from geological scales to milliseconds (Lovejoy and Schertzer, 1991). Such ranges involve scale ratios of at least 10^9.

The relation between scale-invariance and non-linear atmospheric dynamics is difficult to derive theoretically from first principles. Therefore, many researchers give special attention to the empirical characterization of both scaling and the mechanisms that impose bounds on this scaling (e.g. Lovejoy and Schertzer, 1991). The (non-linear) coupling between different meteorological processes has the consequence that the presence of a basic length-scale in one process is also likely to be manifested in the others (e.g. Schertzer and Lovejoy, 1985). In principle, scaling can be broken by the boundary conditions if they have well-defined length-scales. In the atmosphere, for example, the scaling property is broken by the finite size of the earth; and, due to viscosity, the scaling range has its lower limit at about 1 mm.

Some scale-invariant studies of rain

The innovative element of the approach that uses the cascade phenomenology of turbulence to study rain is that it gives a physical basis to the stochastic modelling. Thus, it aims to combine the different advantages of the stochastic and deterministic models.

Early tests of multifractal theories used radar volume scans of rain from the McGill University radar weather observatory (e.g. Schertzer and Lovejoy, 1985; 1987). The radar volume scans were made every 5 minutes, at 200 ranges and 375 azimuthal and 13 elevation angles. This type of data covers a wide range of scales in space-time. The data analysis showed that the scaling property present was extremely accurate; it clarified the multifractal nature of rain.

Other multifractal studies that have been dedicated to rain include, among others, the study of cloud radiance (e.g. Gabriel et al., 1988; Lovejoy and Schertzer, 1990a; Tessier et al., 1993; Lovejoy et al., 1993), satellite data (e.g. Lovejoy and Schertzer, 1991; Schertzer and Lovejoy, 1995b), lidar reflectivities from raindrops (e.g. Lovejoy and Schertzer, 1991, Schertzer and Lovejoy, 1993), blotting paper traces of raindrop impacts (e.g. Lovejoy and Schertzer, 1990c; 1991), stereo photography of rain drops and snow flakes (Desaulniers-Soucy et al., 1995).

For rain gauge data, both temporal and spatial scale-invariant studies have been reported. Such an approach to the study of the temporal structure of rainfall started by using (mono) fractal theory (e.g. Tessier et al., 1988; Hubert and Carbonnel, 1989, 1991; Olsson et al., 1992). Fractal studies of the distribution of rainfall in space, using gauge data, can also be found in e.g. Hubert and Carbonnel (1988).

The approach to the study of point-rainfall based on multifractal theory has been also reported in some studies. Temporal rainfall studies are reported by e.g. Ladoy et al. (1991), Hubert (1992), Tessier et al. (1992), Ladoy et al. (1993), Tessier et al. (1993), Hubert et Carbonnel (1993), Hubert et al. (1993), Lima et al. (1993, 1994), Olsson and Niemczynowicz (1994), Hubert (1995), Tessier et al. (1995), Lima and Bogardi (1995), Lima et al. (1995), Olsson (1995, 1996), Svensson et al. (1996), Harris et al. (1996), Bendjoudi et al. (1997). Rain gauge data have also been used to conduct multifractal spatial studies of rainfall, see e.g. Tessier et al. (1992, 1993, 1994), Olsson and Niemczynowicz (1996).

The studies of rain referred to above were conducted in a framework that uses the multifractal formalism that is discussed in Chapter 3. Other scale-invariant and multifractal studies of rain have been developed in different frameworks (see e.g. Waymire, 1985; Rodríguez-Iturbe et al., 1989; Gupta and Waymire, 1991, 1993). For recent works see e.g. Perica and Foufoula-Georgiou (1996a, 1996b), Burlando and Rosso (1996), Gupta et al. (1996), Over and Gupta (1996), Cârsteanu and Foufoula-Georgiou (1996), Koutsoyiannis and Pachakis (1996), Onof et al. (1996), Menabde et al. (1997).

Generally, the scientific community agrees that more research is needed to get a better understanding of the variability exhibited in rainfall. An important contribution to the solution of this problem is being given by multifractal studies of rain. The invariance of properties and multifractality of the rainfall process over a range of scales is leading to a better understanding of strongly irregular fluctuations of rainfall that could not be grasped from other descriptions of the complex dynamics of this process. The expectation is that multifractal theory and models can be used as a tool to characterize this process and to produce high-resolution synthetic rainfall. Multifractal models, such as the ones based on Lévy random variables (see Section 3.4), may be used for this goal.

The multifractal approach to the study of rainfall has still not been fully explored. This work aims to give a contribution to the current research on this application by investigating the multifractal behaviour present in the temporal structure of rainfall observed at different locations in Europe. This study is conducted in Chapter 5. For details about the data see Chapter 4.

Chapter 4
The rainfall data

4.1 Introduction

This Chapter presents the data used in the multifractal study of the temporal structure of rainfall, in Chapter 5. The point-rainfall data are from four locations in Europe (Figure 4.1): (1) Vale Formoso, Portugal; (2) Nancy, France; (3) Assink, The Netherlands; and (4) Coimbra, Portugal.

Figure 4.1 Location map of the rainfall measuring sites: 1 - Vale Formoso, Portugal; 2 - Nancy, France; 3 - Assink, The Netherlands; and 4 - Coimbra, Portugal.

The data sets differ with respect to climatic origin, type of device used in the measurements, resolution of the data, and length of the records. Information about the different rainfall data sets is given in Sections 4.2 to 4.5. It also includes details about the location and a general description of the measuring sites, and some preliminary analyses of the rainfall data (annual and monthly variability, and monthly average pattern, for example). Attention is paid to features of the rainfall data that are considered relevant for interpreting some results of the multifractal analysis in Chapter 5.

4.2 Data from Vale Formoso, Portugal

General description of the measuring site

The rainfall data were recorded in Vale Formoso, in the southern part of Lower Alentejo Province, in Portugal. The location of Vale Formoso is shown on the maps in Figure 4.1 and Figure 4.2. The coordinates of the measuring site are 37°45′ N and 7°33′ W.

Vale Formoso is located on the river Guadiana catchment area. The area has a rolling topography. It has both gentle and steep slope angles, the latter due to outcrops of the bedrock.

There is a wet season in winter and a dry season in summer. The climate of the region is Mediterranean and semi-arid. Mean annual rainfall is around 500 mm. Mean potential evaporation is around 1600 mm yearly. The average annual temperature is around 16°C.

Two storm types are characteristic of this semi-arid area: convective storms and frontal storms. Convective storms are frequent during the summer season and the early and mid autumn; they are characterized by their high localization and intensity, and their brief duration. Frontal storms occur principally in the winter season; they are known for their low to medium rainfall-intensity and their long duration, lasting several hours or even days. In Vale Formoso, high-intensity rainfall events are accompanied generally by strong winds, which sometimes affect the quality of high-intensity rainfall data.

In Vale Formoso, rainfall was measured at the three sites shown in Figure 4.2 as Locations *I*, *II*, and *III*. Locations *I* and *II* are in the Erosion Experimental Station of Vale Formoso (*Estação Experimental de Erosão de Vale Formoso*). Location *III* is in the Vale Formoso climatological station of the Portuguese Institute of Meteorology (*Instituto de Meteorologia* — IM). The Experimental Station was established in 1960 by the *Direcção Geral de Hidráulica e Engenharia Agrícola* (DGHEA) of the Portuguese Ministry of Agriculture. The climatological station is operated since the early 1930s.

The Erosion Experimental Station of Vale Formoso is presently the only research centre of this type in Portugal. Its location in Lower Alentejo Province is explained by the serious soil erosion problems (and consequent desertification) that exist in this region of Portugal (e.g. Ferreira et al., 1984; Tomás, 1992; Roxo et al., 1996). The purpose of the research that

led to the establishment of this experimental station was to verify the applicability to the local conditions of the Universal Soil Loss Equation (e.g. Ferreira et al., 1984). This model (Wischmeier, 1976; Wischmeier and Smith, 1978) was developed to determine long-term soil loss from agricultural lands. Moreover, the purpose was also to develop guidelines for the most suitable agricultural practices for the local conditions. The data collection programme of the Experimental Station includes measurements of the following: runoff and soil loss from experimental plots; rainfall; evaporation; humidity; temperature; wind. It also includes records of agricultural practices, and of crop and soil conditions. The record length and measurement resolution vary greatly. The experimental plots are represented in Figure 4.2.

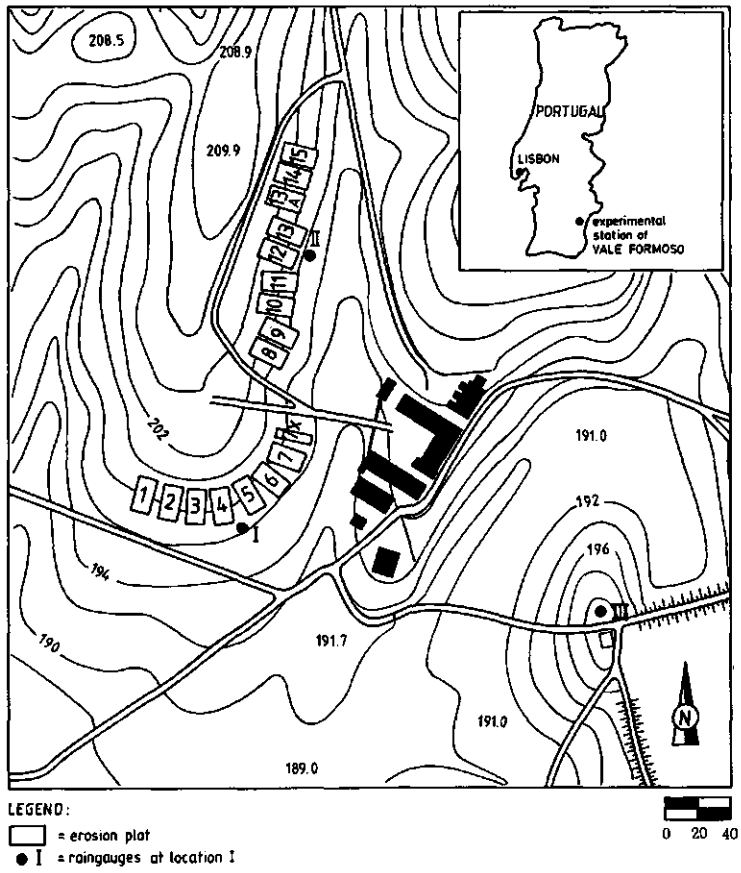

Figure 4.2 Map of the Erosion Experimental Station of Vale Formoso showing the soil erosion plots and sets of rain gauges (at Locations *I* and *II*); the climatological station from the IM is at Location *III*.

Measurement methods and instrumentation

In the Experimental Station of Vale Formoso, rainfall is measured at two locations approximately 120 m apart (Locations *I* and *II*, in Figure 4.2):

— At Location *I* the measuring devices are (Photo 4.1):
- one recording and one non-recording gauge with horizontal openings;
- three non-recording gauges with inclined openings, respectively, at 10, 16 and 22%, and oriented to the South;
- one recording and one non-recording gauge with openings inclined 30%, and oriented to South West.

— At Location *II* the rainfall measuring devices are:
- one recording and one non-recording gauge with horizontal openings.
- three non-recording gauges with inclined openings, respectively, at 10, 16 and 22%, and oriented to the East.

The rainfall data analyzed in Section 5.3 are from: the recording and non-recording gauges with horizontal openings, in Location *I*; and the non-recording gauge with horizontal opening (from the climatological station of the IM), in Location *III* (see Figure 4.2). These two measuring sites are approximately 220 m apart. The altitude is approximately 196 m at Location *I*, and 190 m at Location *III*.

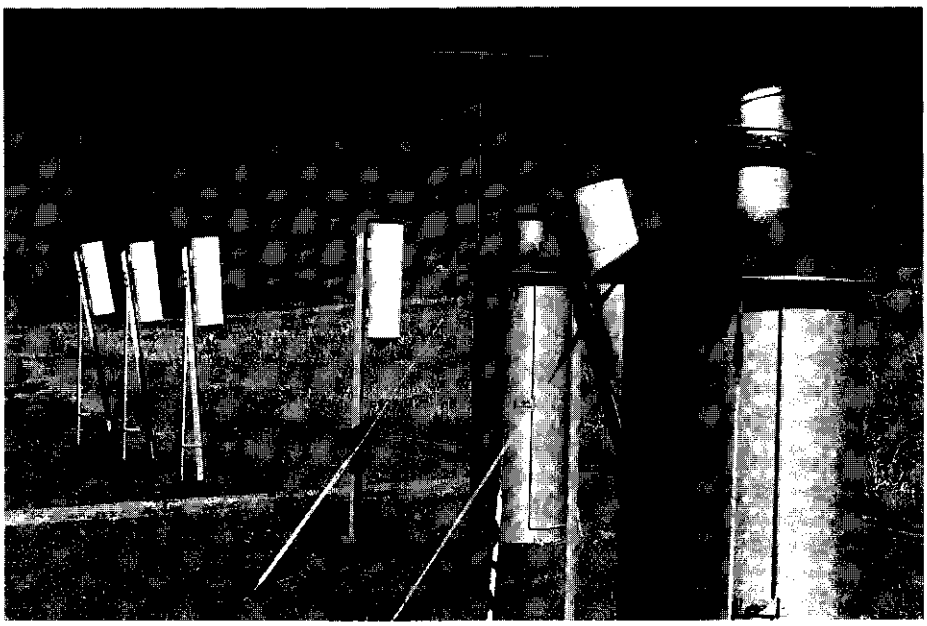

Photo 4.1 General view of rain gauges (at Location *I*) in the Erosion Experimental Station of Vale Formoso (Portugal).

The rain gauges are of the type 20-14-G (according to the classification by Sevruk and Klemm, 1989), with a horizontal opening of 200 cm^2 at 1.5 m height. The continuously recording rain gauges are of the float-and-syphon type. Figure 2.2 shows this type of gauge (see Section 2.3). The non-recording rain gauges are observed daily. The resolution of their measurements is 0.1 mm of rainfall. Any trace of rain below 0.1 mm is neglected by the observer and days are considered dry (zero-rainfall days).

Rainfall time-series

The rainfall data analyzed in this study consist of different time resolutions over different periods:

- *Monthly rainfall* data are available for the period from 1932 to 1990. Records before 1960 are only available from the climatological station (of the IM). Monthly data are obtained by aggregating daily rainfall during monthly periods.
- *Daily rainfall* data are available for the period from 1960 to 1991.
- *High-resolution rainfall* data (i.e. with time resolution higher than 1 day) are available for the period from 1963/64 to 1985/86 (hereafter, this period is referred to as the period from 1963 to 1985). The data were obtained from the observation graphs of the continuously recording rain gauge with horizontal opening, in Location *I*. The graphs contain a continuous record of accumulated rainfall over time. An example of this type of pluviographs is shown in Figure 4.3.

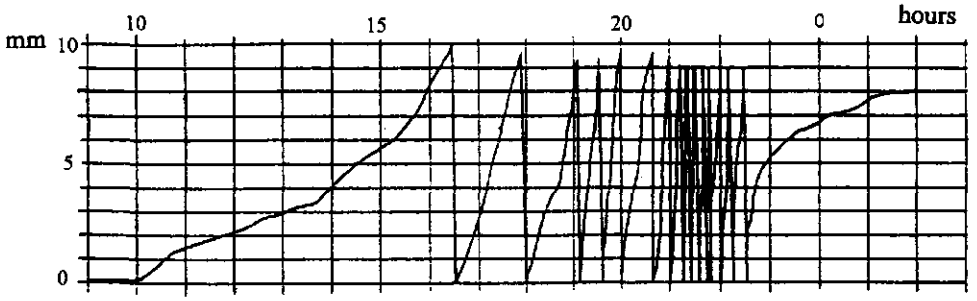

Figure 4.3 Example of a pluviograph from a continuously recording rain gauge of the float-and-syphon type.

The pluviographs from 1963 to 1985 (i.e. over a period of 23 years) were processed with a digitizing bench. The digitization is accurate to within 1 minute in time and 0.1 mm of rainfall depth. The digitization followed a technique that yields *break-point* data (Bärring, 1993). The digitization was based on the identification of segments of the pluviographs associated with

periods of constant rainfall intensity. The time interval between two consecutive digitized points is, therefore, not necessarily constant. Thus, the data do not have well-defined temporal and dynamic resolutions. This digitization approach is considered more adequate and flexible to 'describe' the rainfall process than the approach based on a fixed time-resolution (Bärring, 1993).

During digitization and owing to the scale of the pluviographs, it was sometimes difficult to distinguish between rain-free periods and periods of very low rainfall-intensities. This may have led to over or underestimates of rainfall duration. Another potential problem is associated with the very high intensities, either because of device limitations or/and because of the time resolution of the digitization (i.e. 1 minute). In addition, there may be device limitations. For example, there may be delays in the rise of the float with respect to the rise of the water in the gauge reservoir (because of internal friction of the device components, for example). Moreover, some digitized data-points had different rainfall-depth accumulations over time and the same time t. In practice, this has led to an arbitrary (yet necessary) distribution of rainfall by the neighbouring 1-minute intervals. Such procedure can affect the correctness of the data from very steep segments of the pluviographs, corresponding to very high rainfall-intensities on time intervals of less than 1 minute.

Other problems affecting the quality of the data are errors in measuring wind-driven rain, which are partly due to the location of the measuring site (Location *I*, see Figure 4.2). Rain gauges at Location *I* underestimate systematically high rainfall-intensities. Evidence of the underestimation of rainfall totals at Location *I* was obtained by comparing the rainfall measured with non-recording gauges at Location *I* and Location *II*. This underestimation of high rainfall-intensity periods was also observed by comparing the rising limbs of the pluviographs from the recording gauges at Location *I* and *II*. The non-availability of data, from the gauge at Location *II*, in digital form, made it impossible to analyze quantitatively the differences observed. One expects these differences to be explained by deficiencies in the collection of wind-driven rainfall (see Section 2.3). The hill-slope where the rain gauges are installed (Location *I*) is directly exposed to the prevailing direction of strong winds accompanying high-intensity rainfall events.

The reconstruction of (pseudo) time series from the digitized data was done in the usual way. Accumulated rainfall depth at any time t was estimated by interpolating between two digitized points and assuming constant rainfall intensity in the corresponding time-interval. Time series of different resolutions were obtained by aggregating the rainfall on time intervals of different lengths. One expects that the rainfall measuring device and data processing procedure have led to inaccuracies in representing the very low and very high rainfall-intensities. This introduced an unquantifiable bias in the data. Because the multifractal characterization of a process requires the investigation of a large dynamic range, it is to be expected that 'problems' of the data will introduce difficulties into the multifractal analysis.

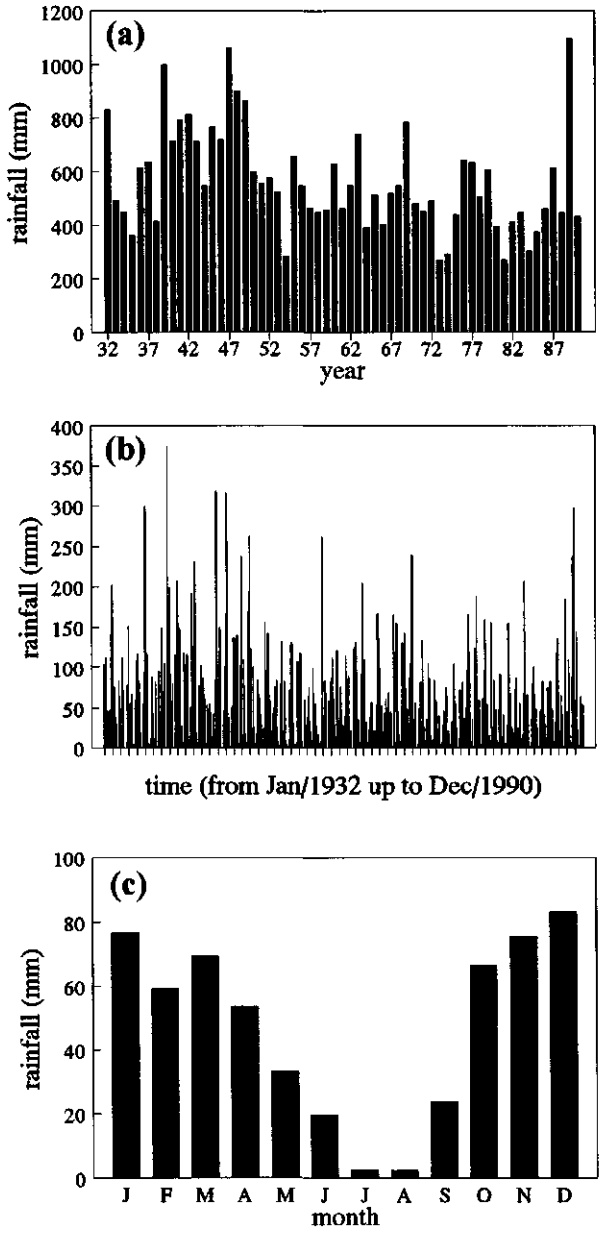

Figure 4.4 Rainfall (in mm) in Vale Formoso, for the years 1932 to 1990: (a) annual rainfall; (b) monthly rainfall; and (c) monthly average rainfall.

A preliminary analysis of the data

This preliminary investigation of the rainfall uses monthly data for the period from 1932 to 1990. Figure 4.4(a) shows the annual rainfall variability observed in this period. The mean is 565.9 mm; the coefficient of variation is 0.34. In this 59-year period the wettest year was recorded in 1989, with 1097.1 mm, and the driest year in 1973, with 269.0 mm. For the same period, Figure 4.4(b) shows the monthly rainfall and Figure 4.4(c) shows the monthly average rainfall. For the monthly rainfall, the mean is 47.2 mm; the coefficient of variation is 1.15. The plot in Figure 4.4(b) illustrates the great variability of rainfall in time, even at large time scales. The wettest month during the period from 1932 to 1990 was October 1939, with 374.8 mm. Of the 708 months that constitute this sample, 14.3% of the months had zero-rainfall, and 17.1% had less than 1.0 mm of rainfall. On average, the wettest month was December, with 83.1 mm of rainfall, and the driest months were July and August, with less than 3 mm of rainfall each (Figure 4.4(c)).

4.3 Data from Assink, The Netherlands

General description of the measuring site

The rainfall data were recorded in the Assink meteorological station, located in the Hupselse Beek catchment (see e.g. SGHB, 1971). This station is known also as the Hupsel meteorological station. The Hupselse Beek catchment is situated in the East of The Netherlands, between the villages of Eibergen and Groenlo, and the Dutch/German border. The rivulet Hupselse Beek is the upper reach of the Leerinkbeek, which is a tributary of the river Berkel. The area of the Hupselse Beek catchment is approximately 6.5 km^2. The landscape is undulating. The altitude varies between 24 and 33 m above mean sea level. The average slope of the land is 0.8 % from east to west. Within the catchment, the Hupselse Beek is 4 km long and flows through a wide valley. The coordinates of the outlet of the catchment are 52°04′ N and 6°38′ E. There is no village in the catchment. Land use is predominantly agricultural.

The location of the Assink meteorological station is shown on the map of The Netherlands in Figure 4.5. This Figure also shows a map of the Hupselse Beek catchment, which has been used as an experimental site for the study of rainfall-runoff processes and groundwater flow (see e.g. Warmerdam et al., 1997). The rainfall measurements are part of the hydrological monitoring programme of this catchment. The research started in 1968. The hydrological data collected in the Hupselse catchment include: precipitation; runoff; groundwater level; soil moisture content; temperature; relative humidity; radiation; wind; and evaporation.

The climate in the Netherlands is maritime and influenced mainly by western winds. However, towards the East, the continental character increases with lower winter temperatures and higher summer temperatures. The yearly rainfall distribution and the occurrence of thunder and

storms are also influenced. Mean annual rainfall is around 760 mm. Mean evaporation (from a free water surface) is around 660 mm yearly. The average annual temperature is around 10°C. These data are 30-year averages from the nearby meteorological station of Winterswijk (SGHB, 1972), situated 10 Km south-east of the Hupsel area.

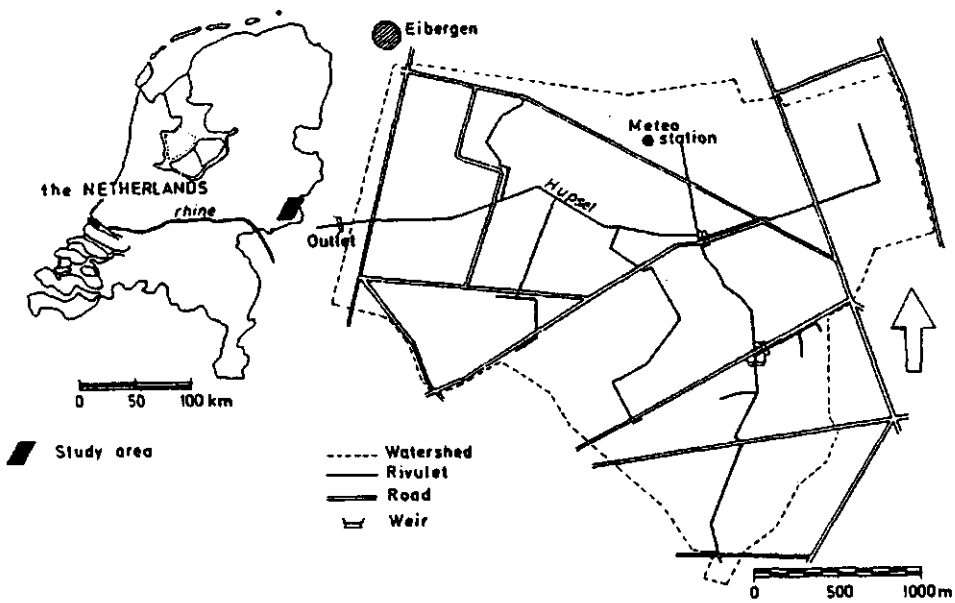

Figure 4.5 Map of The Netherlands situating the Hupselse Beek catchment, and a blow up of the catchment area locating the Assink meteorological station.

Measurement methods and instrumentation

Photo 4.2 shows a view of the meteorological station of Assink. The equipment of this station consists of recording and non-recording rain gauges installed at ground level and at the Dutch standard height of 40 cm above ground level. The station also has a snow gauge.

The rainfall data used in this study were measured with a recording gauge of the float type (see Section 2.3). This is called a Recover rain gauge (*Regenmeter Colenbrander Verstraate*; see e.g. Colenbrander and Verstraate, 1967; SGHB, 1971; Seyhan, 1977). It is shown in Figure 4.6 and Photo 4.3. The gauge is installed at ground level. The collection funnel of the gauge has an area of 2460 cm^2. During the winter season, this collection funnel is substituted by another one with a larger diameter and 40 cm high, for the collection of snow. In addition,

the gauge is equipped with a heating device for melting the snow. This allows one to obtain a reasonable estimate of precipitation (i.e. of both liquid and solid forms of precipitation) over time, which is not possible with the conventional gauges for the measurement of rainfall only. For simplicity, the term rainfall is used below referring to precipitation. The reservoir of the gauge has a large volume (of approximately 150 mm), and is emptied only after a number of months.

The level of the float of the measuring device is recorded at 15-minute intervals. Accumulation of rainfall-depth over time, corresponding to a rise of the float from a level i to a level $i+1$, is obtained by using an appropriate calibration coefficient. The resolution is 0.12 mm of rainfall. The record is automatic, with the help of a data logger.

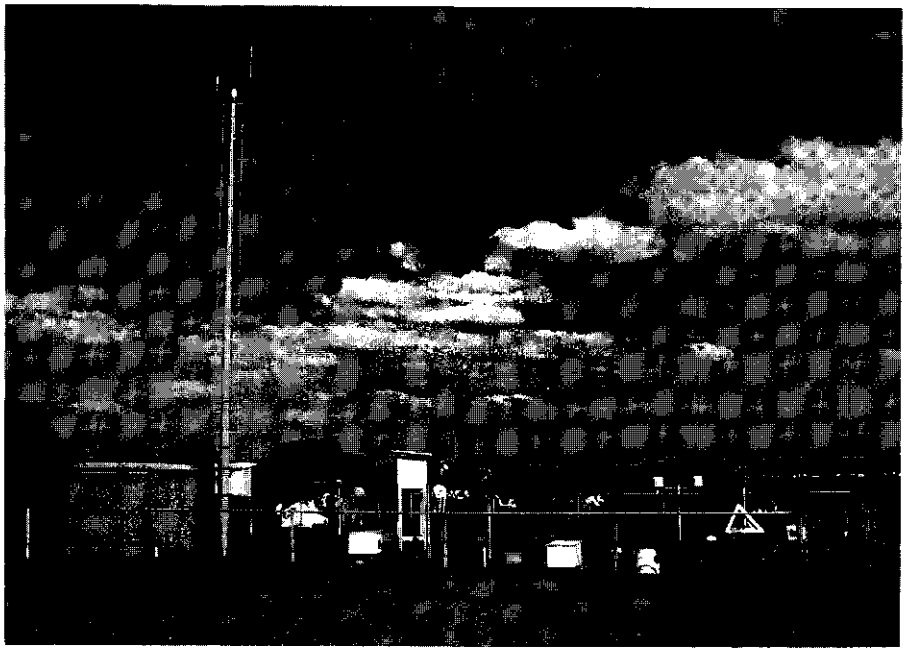

Photo 4.2 View of the meteorological station of Assink (Hupsel, The Netherlands).

Rainfall time-series

The Recover rain gauge yields 15-minute rainfall data. Aggregation of the data on larger time-intervals allows one to obtain time series with lower resolutions. The study in Section 5.4 investigates hourly rainfall, obtained in this way, for the period from 1976 to 1986. This was the resolution of the rainfall data that was available for this study.

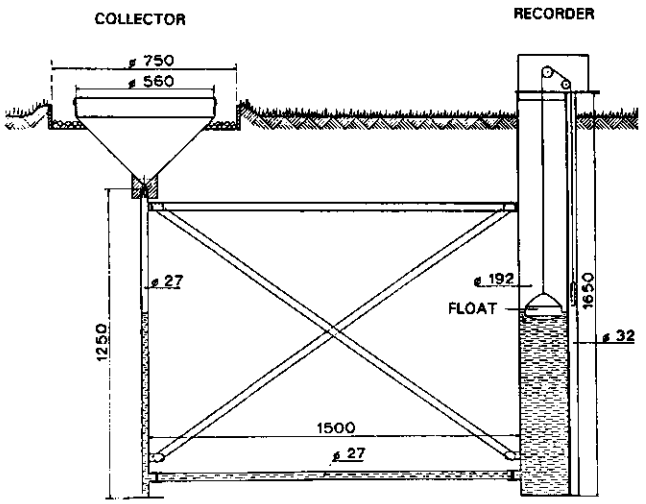

Figure 4.6 Schematic representation of the Recover rain gauge.

Photo 4.3 Recover rain gauge in the Assink meteorological station (Hupsel, The Netherlands).

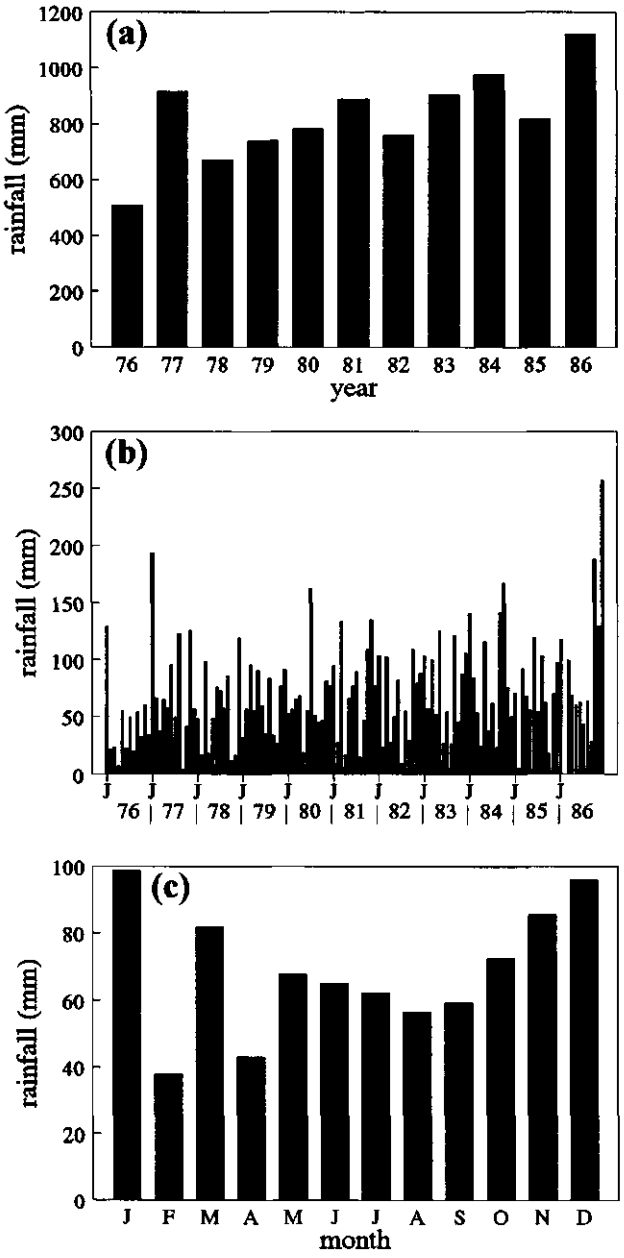

Figure 4.7 Rainfall (in mm) in Assink, The Netherlands, for the years 1976 to 1986: (a) annual rainfall; (b) monthly rainfall; and (c) monthly average rainfall.

A preliminary analysis of the data

The rainfall recorded in Assink, from 1976 to 1986, is shown in Figure 4.7. Figure 4.7(a) shows the annual rainfall. The mean is 826.0 mm; the coefficient of variation is 0.20. In this 11-year period the wettest year was recorded in 1986, with 1120.9 mm, and the driest year in 1976, with 509.6 mm. Figure 4.7(b) shows the monthly rainfall, and Figure 4.7(c) shows the monthly average rainfall. For the monthly rainfall, the mean is 68.8 mm; and the coefficient of variation is 0.62. The wettest month during the period from 1976 to 1986 was December 1986, with 257.0 mm, and the driest month was February 1986, with 0.2 mm. On average, for this period, the wettest month was January, with 98.7 mm of rainfall, and the driest month was February, with 37.8 mm of rainfall.

4.4 Data from Nancy, France

The rainfall data were recorded in the Nancy Region, in France. The location of the measuring site is shown roughly on the map in Figure 4.1. The coordinates of Nancy are approximately 48°42′ N and 6°12′ E.

The data collecting programme included measurements in 15 locations in the Nancy Region. Section 5.5 deals with the analysis of the rainfall data from one of the measuring stations (station 9). The rainfall data available cover a period of 4 years, from January 1988 to December 1991. There were no reports of interruptions in the precipitation records.

Measurement methods and instrumentation

The rainfall was measured with a tipping-bucket recording rain gauge. For details about this type of gauge see Section 2.3. The records of the device identify the time t when the buckets tip. This happens whenever the reservoirs (buckets) of the gauge are filled. The records are accurate to within 1 second in time; and they have a fixed rainfall-depth resolution of 0.2 mm (it corresponds to the capacity of the buckets). Thus, one would expect the records to indicate that 0.2 mm of rain fell in a certain time-interval, from recorded time t_i to recorded time t_{i+1} (hereafter called *sampling*-interval). Nevertheless, some records showed a different behaviour. For some high rainfall-intensity periods, the records indicate that more than one bucket were filled in a certain interval of time; i.e. they indicate the number of times the buckets tipped since the last record of time. In such cases, the *sampling*-intervals exceeded largely the time resolution of the records. Although it was not possible to verify how the rain gauge performs under high intensity rainfall, one may expect that the device has some limitations in relation to this range of rainfall dynamics.

The rainfall data from tipping-bucket gauges appear in the form of step-mass curves. In the present case, each step-increment represents 0.2 mm of rainfall, or multiples of this value whenever several depth increments are registered in the same *sampling*-interval. Rainfall

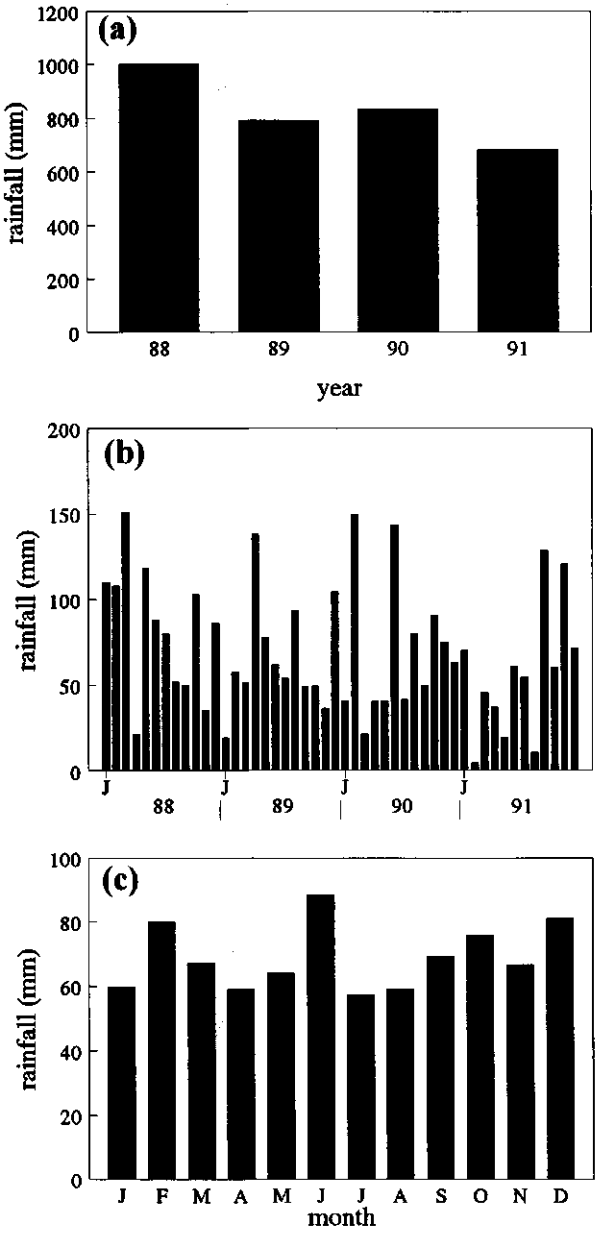

Figure 4.8 Rainfall (in mm) in Nancy, France, for the years 1988 to 1991: (a) annual rainfall; (b) monthly rainfall; and (c) monthly average rainfall.

intensities can be obtained by dividing the rainfall depth by the time elapsed between two successive step-increments. It is not possible to obtain more refined information about the rainfall process from tipping-bucket data, owing to the characteristics of the sampling mechanism of the rain gauge. In particular, it is not possible to distinguish rainless periods from tipping-bucket rain gauge records.

Rainfall time-series

The usual way to process rainfall data from a tipping-bucket rain gauge is to reconstruct (pseudo) time-series from the records. To obtain accumulated rainfall-depth over time at any time t, one interpolates between the records and assumes uniform rainfall-intensity during the time intervals recorded. This procedure affects the representation of the rainfall process by the data. The importance of these 'distortions' increases with the increasing depth capacity of the gauge buckets. The data-processing method attenuates rainfall-intensity 'peaks' and overestimates clearly the length of periods with low intensity rainfall. These 'manipulations' of the data are expected to affect the multifractal analysis of rainfall, in Section 5.5. The choice of the resolution of the time-series that is analyzed in Section 5.5 is discussed in the beginning of that Section.

A preliminary analysis of the data

Figure 4.8(a) shows the annual rainfall in Nancy, for the years 1988 to 1991. The average annual rainfall is 827.8 mm. In this 4-year period the wettest year was 1988, with 1002.6 mm, and the driest year was 1991, with 683.0 mm. For the same period, Figure 4.8(b) shows the monthly rainfall, and Figure 4.8(c) shows the monthly average rainfall. For the monthly rainfall the mean is 69.0 mm; the coefficient of variation is 0.55. During this 4-year period the wettest month was March 1988, with 151.0 mm of rainfall, and the driest month was February 1991, with 4.8 mm of rainfall. On average, the wettest month was June, with 88.4 mm of rainfall, and the driest month was July, with 57.4 mm of rainfall.

4.5 Data from Coimbra, Portugal

General description of the measuring site

The rainfall data were recorded in the climatological station of Coimbra, in the Beira Litoral Province, in Portugal. The station is from the Portuguese Institute of Meteorology (IM), and is situated in the city of Coimbra. The location of the measuring station is shown roughly on the map of Europe in Figure 4.1. The coordinates of the site are approximately 40°12' N and 8°25' W. The altitude is 141 m. Coimbra is located on the river Mondego catchment area.

There is a wet season in winter and a dry season in summer. The climate of the region can be classified as maritime. Mean annual rainfall is around 990 mm. The average annual temperature is around 13°C.

Measurement methods and instrumentation

The rainfall data used in this study were measured with a non-recording rain gauge of the type 20-14-G (according to the classification by Sevruk and Klemm, 1989). It has a horizontal opening of 200 cm^2 at 1.5 m height. The gauge was observed daily. The resolution of the measurements is 0.1 mm of rainfall. Any trace of rain below 0.1 mm is neglected by the observer and days are considered dry (zero-rainfall days).

Rainfall time-series

The time series available for this study is an aggregation of daily rainfall during monthly periods. The time span of the record is 90 years, from 1901 to 1990. There are no reports of missing data in this rainfall record.

A preliminary analysis of the data

The rainfall recorded in Coimbra for the years 1901 to 1990 is shown in Figure 4.9. Figure 4.9(a) shows the annual rainfall. The mean is 989.3 mm; the coefficient of variation is 0.22. In this 90-year period the wettest year was recorded in 1960, with 1674.2 mm, and the driest year in 1953, with 522.2 mm. Figure 4.9(b) shows the monthly rainfall, and Figure 4.9(c) shows the monthly average rainfall. For the monthly rainfall, the mean is 82.4 mm; and the coefficient of variation is 0.90. The wettest month during the period from 1901 to 1990 was November 1963, with 467.4 mm, and the driest months registered zero-rainfall amounts (i.e. less than 0.1 mm of rainfall). Of the 1080 months that constitute this sample, 9 months had zero-rainfall (roughly 0.8% of the sample). On average, for this period, the wettest month was December, with 138.1 mm of rainfall; and the driest months were August, with 14.2 mm of rainfall, and July, with 14.3 mm of rainfall (Figure 4.9(c)).

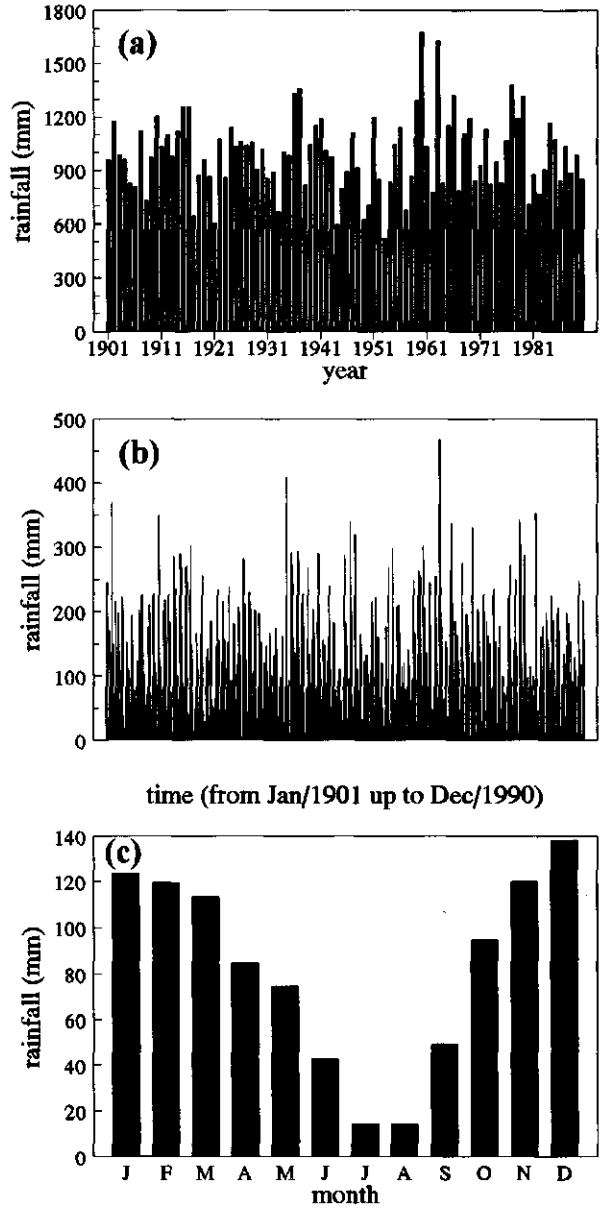

Figure 4.9 Rainfall (in mm) in Coimbra, for the years 1901 to 1990: (a) annual rainfall; (b) monthly rainfall; and (c) monthly average rainfall.

Chapter 5
Scale-invariant analysis of the rainfall data

5.1 Introduction

This Chapter deals with the investigation of the scale-invariant and multifractal behaviour present in the temporal structure of rainfall. The main motivation to use this approach to the study of rainfall, and a review of the studies dedicated to this topic can be found in Section 3.6.

The purpose of this study is to contribute to the understanding of the dynamics of rainfall and to the clarification of some aspects related to the use of multifractal theory to studying this process. Rainfall data sets from four different locations in Europe are analyzed (see Chapter 4). The study investigates different scaling regimes and the effect of the different types of acquisition of the point-rainfall data (e.g. different data resolutions, different types of measuring devices, different sample sizes) on the multifractal analysis. Special attention is given to small-scale behaviour and to scale-shifts transferring the results obtained at one (low-resolution) time-scale to another (high-resolution) scale.

Section 5.2 gives an overview of the Sections dealing with rainfall analysis; it also discusses some practical aspects of the fractal and multifractal analysis of the temporal structure of rainfall. Sections 5.3 to 5.6 give the results and interpretation of the analysis of the different rainfall data sets described in Chapter 4. Section 5.3 deals with the analysis of the data from Vale Formoso (Portugal), consisting of different time resolutions (monthly, daily and higher time-resolutions) over periods of time varying between 23 and 59 years. In Section 5.4, 11 years of hourly rainfall from Assink (The Netherlands) are analyzed. Section 5.5 deals with the analysis of 4 years of tipping-bucket rainfall data from Nancy (France). Analysis of 90 years of monthly rainfall from Coimbra (Portugal) is conducted in Section 5.6. Chapter 5 ends with a final discussion of the results of the multifractal analysis of the temporal structure of rainfall (in Section 5.7).

The study of the temporal structure of rainfall starts with a fractal approach (using the box-counting technique) and it proceeds by showing the multifractal structure of the process

(using the functional box-counting technique). The scale-invariance of rainfall is also investigated with spectral analysis. The multifractality of the process is investigated through the probability distributions and moments of the rainfall intensity on different scales. The empirical multifractal exponent functions that describe the scaling of the probability distributions and of the moments of the rainfall intensity are estimated. Multifractal phase transitions are studied empirically. The description of the multifractal behaviour of the temporal rainfall (i.e. of the statistics of rainfall) by the 'universal' multifractal model is investigated; the agreement between the empirical and theoretical scaling exponent functions is analyzed. The data from Vale Formoso are used to conduct a systematic empirical study of multifractal phase transitions, with the purpose to derive a phase-diagram (see Section 5.3.4). These data are also used to investigate the presence of 'seasonal' variation of the multifractal behaviour exhibited by the temporal structure of rainfall (see Section 5.3.5).

5.2 Methods of analysis

This Section gives an overview of the methodology that is used in the rainfall analyses presented in this Chapter. It also discusses some practical aspects of using fractal and multifractal techniques (see Chapter 3) to study point-rainfall data. In the next Sections, results and interpretation of the rainfall analyses are given without major details about the techniques that are used.

There is a contrast between the theory (see Chapter 3), which deals with multifractal processes and data without zero values or scale-dependent measurement effects, and the application of the multifractal theory to rainfall, which suffers from both problems. These aspects will be discussed in the next Sections.

Non-dimensional variables

The variables involved in the multifractal analysis of the temporal structure of rainfall are time and rainfall intensity. They have to be considered in a *non-dimensional* framework.

To non-dimensionalize time, one assumes that the duration of the longest period of interest is equal to 1. If this period has a duration T, then the magnitude of any time interval τ should be divided by T. Any time scale corresponding to τ can then be characterized by a scale ratio λ, with $1/\lambda=\tau/T$ (see Sections 3.2.2 and 3.3.1).

To non-dimensionalize the rainfall intensity on a time scale of resolution λ, the intensity can be divided by the ensemble average intensity of the process. For rainfall, this means the climatological average rainfall. Nevertheless, in practice, one generally uses the sample average-intensity corresponding to the longest period of observation, T (see e.g. Lovejoy and Schertzer, 1991). At resolution λ, let the rainfall intensity on a time interval i be $R_{\lambda,i}$, with $i=1,\lambda$, and the average rainfall-intensity be

$$\langle R_\lambda \rangle = \frac{\sum_{i=1}^{\lambda} R_{\lambda,i}}{\lambda},$$

independent of scale. So, the corresponding non-dimensional intensity on any time interval i is $\varepsilon_{\lambda,i}=R_{\lambda,i}/\langle R_\lambda \rangle$. In this way, at resolution level λ, is $\langle \varepsilon_\lambda \rangle=1$, where the angular brackets $\langle\ \rangle$ mean (ensemble) average (see Section 3.3.1). Below, the index i is dropped.

The fractal character of rainfall occurrences studied with the box-counting method

The *box-counting* method (see Section 3.2.3) can be used to test the scale-invariant temporal structure of rainfall. This type of analysis is based on the occurrence and non-occurrence of the rainfall process. The binary question (i.e. the definition of rainfall occurrence) is generally associated with a rainfall-intensity threshold. The method allows one to estimate the fractal dimension of the geometric structure that is the 'support' of the rainfall process. This 'support' can be regarded as a fractal object embedded in the 1-dimensional space of time and is defined as the set of rainy periods observed in a particular location. Its fractal dimension is between 0 and 1 (see Section 3.2.2). The fractal dimension evaluates, thus, the sparseness of rainfall occurrences within the time domain. Below, the application of the box-counting method to rainfall is based on a zero-rainfall threshold definition of rainfall occurrences.

The box-counting method has its limitations when it is applied to rainfall occurrences. The scaling range may be bounded from above as well as from below because of methodological and technical restrictions. A practical problem is the tendency of the box-counting method to 'saturate' in certain conditions; this yields box-counting log-log plots of slope -1.

The multifractality of the rainfall process observed with the functional box-counting method

The rainfall process is characterized by different levels of intensity. Thus, mono-fractal studies of rainfall are not satisfactory for many hydrological applications. Moreover, different applications use different magnitudes of the rainfall threshold to define a period as *wet*. In many studies of non-linear rainfall-induced hydrological processes (e.g. infiltration, runoff, soil erosion) these thresholds are fixed arbitrarily. The choice of the magnitude of the threshold is difficult because of the non-trivial relation between the threshold and the scales involved in the various studies. Therefore, it is important to characterize rainfall in a more refined way, which involves studying the process at different intensity levels and scales. This is done using multifractal analysis techniques (see Section 3.5). The *functional box-counting* method (see Section 3.5.1) is used in this study to show that the sets formed by rainfall occurrences embedded in the 1-dimensional space of time, defined for different rainfall-intensity thresholds, are characterized by different fractal dimensions; thus, it shows that temporal rainfall is a multifractal process.

The agreement between the theoretical and empirical multifractal scaling exponent functions is discussed. In the presence of phase transitions, the theoretical and empirical scaling functions are only expected to agree well until critical orders of singularity and moments. These critical exponents are discussed for the different cases analyzed.

Below, the estimate of some parameters and critical exponents are based on the average value obtained from several analyses. To give some indication of the variation observed, this value is presented together with the value of one standard deviation (i.e. it is given the mean$\pm$standard deviation). The indication of the standard deviation is omitted whenever the number of cases analyzed is very small.

5.3 Analysis of rainfall from Vale Formoso

The rainfall data that are analyzed in this Section are from Vale Formoso (Portugal). These data consist of different time-resolutions (monthly, daily and higher time-resolutions) over periods of time varying between 23 and 59 years. The analyses of the different resolution data are presented in separate Sections. Details about the data are given in Section 4.2.

6.3.1 High-resolution rainfall

This Section deals with the analysis of 23 years of high-resolution rainfall data, from 1963 to 1985. The average annual rainfall in this period is 456.4 mm. The rainfall was measured with a recording gauge of the float-and-syphon type.

About the choice of the resolution of the (pseudo) time-series

The rainfall data were obtained by digitizing pluviographs containing the continuous records of accumulated rainfall over time (see Section 4.2). The digitization of the pluviographs leads to the definition of periods with constant rainfall-intensity. The time interval between two consecutive digitized points is, therefore, not necessarily constant. Thus, the digitized rainfall data do not have well-defined temporal and dynamic resolutions. Nevertheless, the analysis of rainfall time-series requires one to reconstruct such (pseudo) series from the digitized data by interpolating between two digitized points. The digitization is accurate to within 1 minute in time and 0.1 mm of rainfall depth.

Theoretically, the choice of the resolution of the time series would be only restricted by the time accuracy of the digitization. In practice, other factors must be also taken into consideration. Because of methodological and technical restrictions, the data resulting from the digitization of the pluviographs is affected by human bias. The correct identification and digitization of periods with constant rainfall-intensity depends on personal judgement and skill. Small-scale variability tends to be neglected during the digitization process, both because of

the amount of man-labour involved and of physical limitations related to the graphical scale of the pluviographs. Moreover, limitations of the measuring device itself (such as its ability to record the very high and very low rainfall-intensities) may also affect the correctness of the description of the 'true' rainfall process by the final 'product' (i.e. the digitized data). Whilst, an unquantifiable bias might have been introduced in the data which can affect the analysis of rainfall in different ways.

With the purpose to clarify some features of the data, some of which may have been introduced by the digitization, a simple preliminary analysis of the data was conducted. The digitized time-intervals (hereafter called *sampling-intervals*) that are expected to correspond to segments of the pluviograph with constant rainfall-intensity, were analyzed with respect to their *size* (i.e. duration) and intensity.

Table 5.1 shows some information about the sampling-intervals used to digitize the pluviographs from 1963 to 1985. The size of the sampling-intervals depends strongly on the rainfall intensity that was 'sampled' (i.e. digitized). Thus, the digitization might have introduced intensity-dependent characteristic scales in the data. The average size of the sampling-intervals smaller than 30 minutes is roughly 10 minutes (9.79±0.21 minutes); this scale is thus 'characteristic' for the higher rainfall-intensities in the data. For the lowest (digitized) intensities, the sampling-intervals are always less than 6 hours. If there were rainfall events with longer durations and with very low intensities, they were assimilated to rainless intervals. Thus, the definition of *rainless* period is related to restrictions of the measuring device itself in recording rainfall below a certain intensity level, and of the digitization methodology in interpreting the pluviographs. The average size of the sampling-intervals between 3 hours and 6 hours, for the range of smaller rainfall-intensities, is around 4 hours (4.06±0.26 hours).

Table 5.1 Data about the digitization of the pluviographs with the record of accumulated rainfall over time, from 1963 to 1985. The records are from Vale Formoso.

duration of the sampling-interval, Δt	contribution to total digitized rainy-periods (%)	average duration of the sampling-interval (min)	average rainfall intensity sampled (mm/h)
$0 < \Delta t \leq 30$ min	41.8	9.79±0.21	5.435±3.635
30 min $< \Delta t \leq 1$ h	15.9	42.21±7.79	0.594±0.114
1 h $< \Delta t \leq 2$ h	16.5	84.96±15.97	0.174±0.000
2 h $< \Delta t \leq 3$ h	10.1	146.86±3.15	0.086±0.046
3 h $< \Delta t \leq 6$ h	15.7	243.66±15.69	0.046±0.020

Results of this analysis suggest that there are limitations in relation to the (maximum) 'detail' of the information about the rainfall process that it is possible to extract from the digitized rainfall data. Time scales smaller than a characteristic scale are not expected to contain, on average, more information about the rainfall intensity on those scales than the characteristic scale itself. Such information is just obtained by dividing up sampling-intervals into even smaller intervals. Therefore, below these critical scales, the variability of rainfall was certainly not well captured, nor is it well represented by the data. For the periods with the highest intensities one expects that this problem is present at scales of around 10 minutes. For the lowest intensities, the expectation is that the problem is present even at time scales larger than 4 hours.

In the data, about 58% of the total (digitized) time associated with rainy periods was digitized with sampling-intervals of less than 1 hour, with an average of 12.42±2.42 minutes. This motivated the choice of 15 minutes to be the resolution of the rainfall (pseudo) time-series that is analyzed in this Section. Below this scale, the variability of the process should be studied reliably only with better quality data. Scaling problems are still expected to occur during the analysis, particularly for the low intensities. These problems are expected in the form of intensity-dependent breaks in the scaling. Empirical observations support that such characteristic scales are artificial, in the sense that they are not related to the rainfall process itself. They might result from technical limitations of the rainfall measuring device and digitization of the pluviographs. Analysis of a higher resolution 2-minute rainfall time-series (also given in this Section) shows that these scaling problems are aggravated with decreasing resolution of the time series.

The fractal and multifractal structure of rainfall

The box-counting plot obtained with the 2-minute rainfall from 1963 to 1985 is shown in Figure 5.1. The plot displays time scales from 2 minutes up to 1 year. Thus, it accumulates the statistics over 23 years. The absolute value of the slope of the log-log plot over a range of scales gives an estimate of the fractal dimension of the set of rainy periods observed in the 1-dimensional space of time. Rainfall occurrences are defined here for 2 minutes, and include all the events in the digitized data. Thus, the definition of rainfall occurrences is affected by the resolution of the measurements.

One can distinguish three (straight) sections in the log-log plot in Figure 5.1. Linear regressions were fitted to each of these sections, with slopes of absolute values 0.90, 0.50 and 1 (from left to right in Figure 5.1). The slope of -0.90 was determined for scales from 2 minutes up to 128 minutes (left); the slope of -0.50 is for scales from 128 minutes up to 11.4 days (middle); and the slope of -1 is for scales larger than 3 months (right). The slope of the middle section of the plot yields the estimate of the fractal dimension of the geometric 'support' of rainfall occurrences $D \approx 0.5$; this 'support' is defined in the 1-dimensional space of time. The upper and lower limits of the scaling range can not be determined precisely because scales

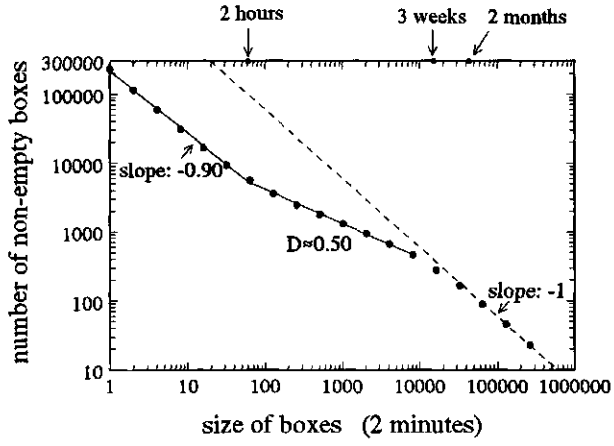

Figure 5.1 Box-counting log-log plot obtained with 2-minute rainfall from Vale Formoso, from 1963 to 1985. A box of unit-size corresponds to 2 minutes. The plot displays time scales from 2 minutes up to 1 year.

larger than about one-and-a-half months and smaller than about 2 hours are not properly investigated with the box-counting method. There are problems of 'saturation' affecting the left and right sections of the box-counting plot in Figure 5.1. For the larger scales, 'saturation' is trivial and it yields the slope -1. The type of 'saturation' that can be observed for very small time-scales (below a critical scale) indicates that the set of rainy periods described by the data almost 'fills up' the observational space of time (i.e. there are almost no zero-rainfall periods). This behaviour is expected to be the result of the measuring device inability to properly capture and register the intermittency and variability of the rainfall process at small scales. To this problem add the restrictive technique used to digitize the pluviographs (see above). Some authors (e.g. Olsson et al., 1992) relate the observation of such a critical scale in the box-counting plots to an average duration of the rainfall events.

In Figure 5.1, the critical scale for 'saturation' at small time-scales can be associated with the average duration of the sampling-intervals used in the digitization. This supports empirically the explanation given here for the type of behaviour (i.e. breaks in the scaling) observed for the data from Vale Formoso. Such behaviour is not attributed to any intrinsic characteristic of the rain process itself (at least on this range of scales). Instead, in this case, it should result from the need to define rainfall occurrences based on intensity thresholds. Thus, it must be a consequence of the resolution of the measuring device, and the digitization technique. The 'support' of the rainfall process observed is the result of the integration of the process on a certain (observation) scale and of the 'assimilation' to zero-values of very low rainfall-intensities.

Figure 5.2 shows the functional box-counting plot, for three intensity thresholds, obtained with the 2-minute rainfall from 1963 to 1985. The intensity thresholds are, for the lines from top to bottom, 0, 1, and 10 mm/hour. Similar to Figure 5.1, different sections can be distinguished in Figure 5.2. The absolute value of the slope of the regression lines fitted to the middle sections of the plot decreases for increasing magnitudes of the threshold; these values are (from top to bottom, in Figure 5.2) 0.50, 0.44, and 0.19. This illustrates that the rainfall process cannot be fully described by a single fractal dimension because the process is characterized by an (infinite) hierarchy of dimensions: each fractal dimension corresponds to a different rainfall-intensity level. This behaviour indicates that the rainfall process has a multifractal structure.

The absolute values of the slope of the regression lines fitted to the left-hand side sections of the plot in Figure 5.2 are (from top to bottom) 0.90, 0.74, and 0.54. This means that in the rainfall structure the more intense events are the rarest. At small time-scales, the scale corresponding to the 'break' in the log-log plot varies with the magnitude of the threshold value. For increasingly larger intensity-thresholds, the critical scale moves toward smaller and smaller time-scales. Such behaviour is consistent with the ('average') size of the sampling-intervals used to digitize segments of the pluviographs of different rainfall intensities (see Table 5.1). Therefore, the intermittency of rainfall might not be properly described by the digitized data at scales smaller than the scales corresponding to these sampling-intervals. Thus, the expectation is that the 'breaks' in the scaling (power-law) behaviour are intensity-dependent: the critical scale changes with the intensity level that is being studied (see Figure 5.2).

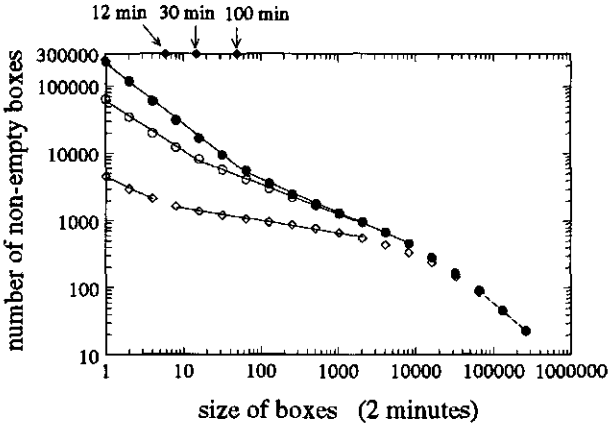

Figure 5.2 Functional box-counting log-log plot obtained with 2-minute rainfall from Vale Formoso, from 1963 to 1985. A box of unit-size corresponds to 2 minutes. The plot displays time scales from 2 minutes up to 1 year. The rainfall threshold values are, for the lines from top to bottom, 0, 1, and 10 mm/hour.

Investigating scale-invariance with energy spectra

The energy spectrum obtained for the 2-minute rainfall from 1963 to 1978 is shown in Figure 5.3. The spectrum has been smoothed for high frequencies (this procedure is also used below for the other spectra). The spectrum in Figure 5.3 shows scale-invariant (power-law) behaviour over a range of scales. For the lowest frequencies, a spectrum peak occurs at approximately $\omega \approx 0.00011\ h^{-1}$, which corresponds to the annual cycle frequency observed for the rainfall process. The annual frequency spectral peak seems to emerge in the spectra, with power-law behaviour holding on both sides of this frequency. This scaling behaviour holds up to a critical scale observed at the highest frequencies (i.e. small time-scales). Thus, two different parts can be distinguished in the plot: above and below time scales corresponding to a frequency of about $\omega \approx 0.6\ h^{-1}$ (≈100 minutes). This spectral 'break' agrees with the critical scale observed in the box-counting plot in Figure 5.1. Power laws were fitted to the two sections of the energy spectrum with linear regressions of $\log(E(\omega))$ versus $\log(\omega)$. The spectral slope is -0.15, for time scales larger than 2 hours; for smaller time-scales, the spectral slope is -0.73.

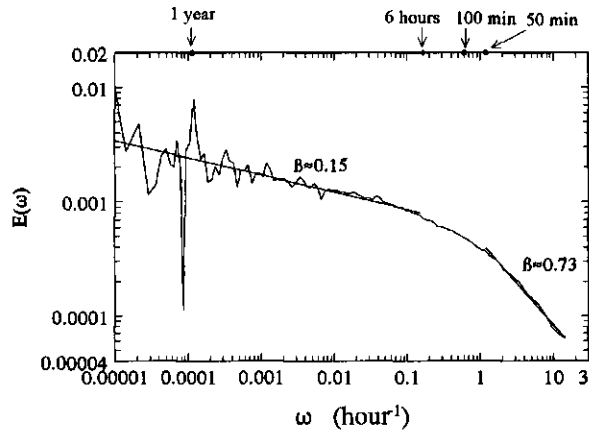

Figure 5.3 Energy spectrum obtained for 2-minute rainfall from Vale Formoso, from 1963 to 1978.

Figure 5.4 shows examples of the spectra obtained for different η-power renormalized versions of the rainfall data. This renormalization followed the principle discussed in the Double Trace Moment technique (see Section 3.5.4). Figure 5.4(a) shows the spectrum for $\eta=0.3$, and Figure 5.4(b) shows the spectrum for $\eta=3$. Small moments η highlight the contributions of small singularities of the rainfall intensity, and large moments η highlight those of the strong singularities. In the plots in Figure 5.4, the spectral break does not occur at a fixed scale. The break moves toward the lowest frequencies for $\eta<1$ and toward the highest

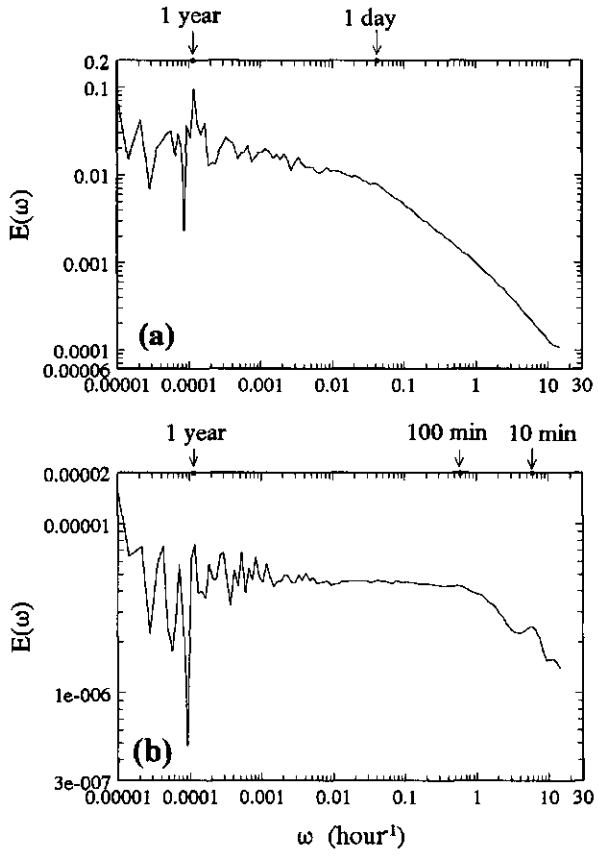

Figure 5.4 Energy spectra obtained for 2-minute rainfall from Vale Formoso, from 1963 to 1978: (a) for the data renormalized with $\eta=0.3$; and (b) for the data renormalized with $\eta=3$.

frequencies for $\eta>1$. This is also observed in the spectra of the different η-renormalized versions of 15-minute rainfall, from 1963 to 1985, that are shown in Figure 5.5. In this Figure, and for scales larger than about 6 hours, the spectral slope for $\eta=1$ is also -0.15.

A fundamental break, indicating the transition between two different scaling regimes (i.e. governed by different dynamics), is expected to occur always at the same critical scale, regardless of the type of renormalized data (i.e. of the intensity of the process) that are being analyzed. The type of behaviour observed, that depends on the intensity of the process, supports that the break in the scaling is related to the dynamic range covered by the rainfall measuring device and/or captured by the technique used to digitize the pluviographs. Preliminary analysis of the digitized data from the continuously recording rain gauge used at

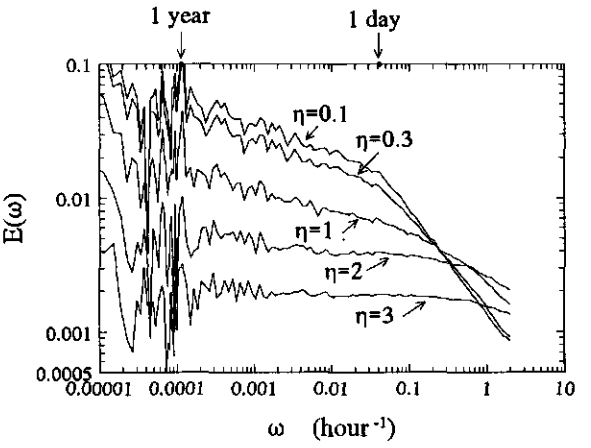

Figure 5.5 Energy spectra obtained for η-renormalized versions of 15-minute rainfall from Vale Formoso, from 1963 to 1985.

Vale Formoso (see above) showed that the 'sampling' (i.e. the data digitization criteria) was different for different rainfall-intensities. It can explain why the results show some kind of dependency on the dynamic range of the rainfall data. These 'problems' are expected to affect the description of the rainfall process beyond certain time scales, and to introduce artificial breaks in the scaling. In the spectra obtained for η-renormalized versions of the 2-minute rainfall, as one increases the η-moment a characteristic frequency 'emerges' in the high frequency range. Figure 5.4(b) shows this for $\eta=3$, with the spectral 'peak' occurring at approximately $\omega=6\ h^{-1}$. This frequency corresponds to 10 minutes, which is exactly the average duration of the sampling-intervals used to digitize the higher rainfall-intensity records in the pluviographs. This spectral 'peak' is also observed, already for $\eta=1$, in the spectrum of the 2-minute rainfall from 1963, shown in Figure 5.6. It occurs at the frequency of $\omega\approx8.4\ h^{-1}$, which corresponds to about 7 minutes. The individual investigation of the yearly rainfall from 1963 to 1985 showed that the pluviographs from 1963 were digitized with the smallest sampling-intervals. Moreover, for 1963, the 'average' sampling-interval associated with the highest rainfall-intensities in the data agrees with the (spurious) critical frequency observed in the spectrum. The spectral slope for the 2-minute rainfall in 1963 is -0.06. This spectrum does not exhibit the 'break' observed earlier for the high frequencies. In the other spectra of individual years this 'break' was also not always present or it occurred shifted to a different frequency. This observation also supports the hypothesis that the scaling-break at small time-scales is not fundamental in nature; thus, it is an artificial break. Several authors observed a break in the scaling, at about 16 days, in the spectra of rainfall (e.g. Ladoy et al., 1993; Fraedrich and Larnder, 1993; Tessier et al., 1996). These authors associated this critical scale with synoptic phenomena. Such a critical scale was not observed in the spectra of the rainfall

from Vale Formoso (see Figure 5.3, Figure 5.5 and Figure 5.6). Thus, from these spectra, it is not possible to determine precisely the upper limit of the scale-invariant regime of the rainfall process observed at Vale Formoso.

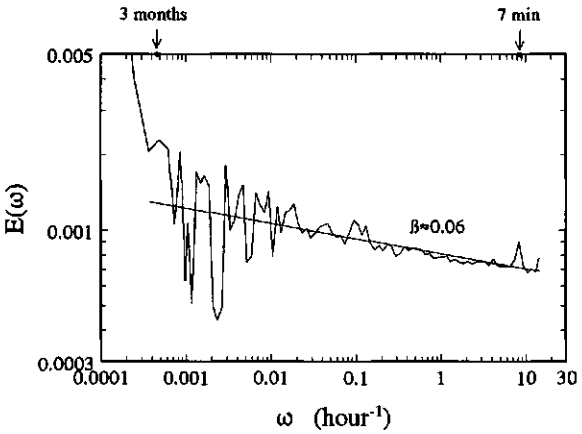

Figure 5.6 Energy spectrum obtained for the 2-minute rainfall from Vale Formoso, from 1963.

Scaling of the probability distributions

Figure 5.7 shows the log-log plot of the probability of exceeding rainfall-intensity levels of singularity γ, observed on scales of resolution λ, against the scale ratio λ. The data are 15-minute rainfall from 1963 to 1985. The probability plot in Figure 5.7 is for rainfall on time scales from 15 minutes (λ=16384) up to about 5.7 months (λ=1). Thus, the plot includes the statistics of 49 'samples' of 5.7 months. The orders of singularity γ of the rainfall intensity ε_λ plotted in Figure 5.7 are indicated in the legend.

For some values of the orders of singularity γ, the scaling of the probabilities is well respected over the range of time scales from 15 minutes up to at least one-and-a-half months (the points follow closely a straight line). In particular for the small singularities, a smaller scaling range is observed. Both for the low and high values of the singularities, the behaviour of the probability plot deviates from the expected power-law at a time scale of around one hour. This scaling 'problem' found in the probability plot (Figure 5.7) was also observed earlier (see Figure 5.1, Figure 5.2, and Figure 5.3), and it occurs at approximately the same critical time-scale. The 'bends' in the plot in Figure 5.7 are in the upward direction for the low intensities and in the downward direction for the high intensities, with respect to the power-law behaviour observed at larger scales. If one expects that the same scaling behaviour is maintained down to scales smaller than the 'critical' scale of 1 hour, the direction of the 'bends' of the probability plots suggests that, in this data set, the lower rainfall-intensities are overestimated and the higher intensities are underestimated.

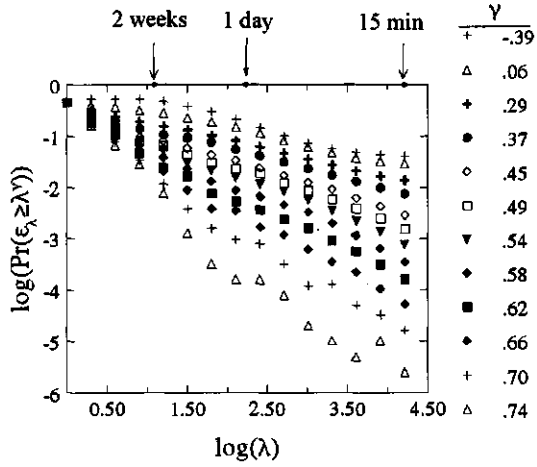

Figure 5.7 Log-log plot of the probability of exceeding rainfall-intensity levels of singularity γ, observed on scales from 15 minutes (λ=16384) up to 5.7 months (λ=1), against the scale ratio λ. The data are 15-minute rainfall from Vale Formoso, from 1963 to 1985. The legend indicates the order of singularity γ of the rainfall intensity ε_λ.

Analysis of the probability plot in Figure 5.7 suggests the presence of a critical scale in the structure of temporal rainfall; i.e. the existence of another scaling regime occurring on scales larger than about two weeks. Different scaling regimes and critical scales in the temporal structure of rainfall have been reported by several authors (e.g. Ladoy et al., 1993; Fraedrich and Larnder, 1993; Tessier et al., 1996). The different findings reported might be associated with differences in climatic regimes.

Scaling of the moments

Figure 5.8 shows the log-log plot of the average q^{th} moments of the rainfall intensity ε_λ on time scales from 15 minutes (λ=16384) up to 5.7 months (λ=1), against the scale ratio λ. The data are 15-minute rainfall from 1963 to 1985. Thus, the plot in Figure 5.8 includes the statistics of 49 'samples' of 5.7 months. Figure 5.8(a) shows moments larger than 1, and Figure 5.8(b) moments smaller than 1. The q-moments plotted in Figure 5.8 are indicated in the legend. Large moments highlight strong singularities (i.e. high rainfall-intensities), and small moments highlight small singularities (i.e. small rainfall-intensities) of the process.

The scaling of the moments of the rainfall intensity is good (the points follow closely a straight line) for the range of scales from 15 minutes up to about one-and-a-half weeks, even though this occurs only for a range of q-moments. Particularly for the small moments, the behaviour deviates from the expected power law at a time scale of around 30 minutes to one hour.

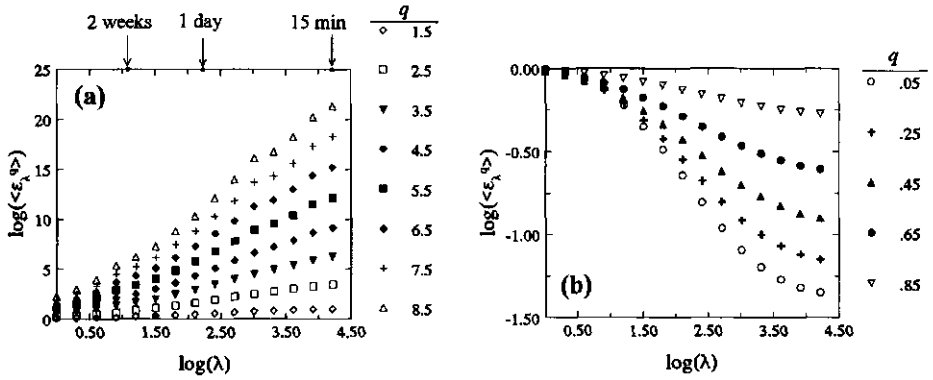

Figure 5.8 Log-log plot of the average q^{th} moments of the rainfall intensity ε_λ on time scales between 15 minutes (λ=16384) and 5.7 months (λ=1), against the scale ratio λ: (a) for moments larger than 1; and (b) for moments smaller than 1. The data are 15-minute rainfall from Vale Formoso, from 1963 to 1985.

The plots in Figure 5.8 'bend' in the downward and upward direction relatively to the power-law behaviour observed for the larger scales and up to about one-and-a-half weeks. This suggests that, in this rainfall data set, the higher intensities are underestimated and the lower intensities are overestimated. The behaviour in Figure 5.8, and the associated critical scales (for the 'break' in the scaling), are consistent with the previous analyses. One observes once more a shift of the critical scale with the intensity of the process. The dependency of the critical scale on the intensity level of the process was already illustrated earlier with the functional box-counting analysis (see Figure 5.2) and the spectra of η-renormalized versions of the 2-minute rainfall (see Figure 5.3 and Figure 5.4). The behaviour observed supports the possibility of intensity-dependent measurement-problems. Such problems are expected to be caused both by the type of rainfall measuring device that was used, and the data processing method that was employed.

The overestimation of a range of (low) intensities is consistent with what is known about the measuring device and the method used to process the data (this is discussed above, and in Section 4.2). The very low rainfall-intensities are outside of the dynamic range that is covered accurately by the rain gauge. One expects these intensities to be present (artificially) in the data (i.e. in the pseudo time-series), as a result of the methodology used to digitize the pluviographs and to reconstruct the time series. There are probably two explanations for the underestimate of the high rainfall intensities. For large scales, it can be explained by undersampling; some high-order singularities (i.e. high rainfall-intensities are not observed because of the finite size of the sample. Another explanation might be the digitization procedure used to obtain the

rainfall data. Moreover, the location and exposure of the rain gauge might also contribute to underestimate high rainfall-intensity 'peaks' (see Section 5.2).

Some rainfall intensities being not represented correctly by the data affect the analysis of the corresponding q-moments. These limitations are expected to be present only for a limited range of rainfall intensities.

The empirical scaling exponent functions

The multiscaling behaviour observed for the probability distributions (in Figure 5.7) and for the moments (in Figure 5.8) can be described by multifractal exponent functions: the codimension function $c(\gamma)$ and the moments scaling function $K(q)$. These functions, obtained with the 15-minute rainfall from Vale Formoso (from 1963 to 1985), were determined for the range of scales extending from 15 minutes up to 10.7 days. Some of the scaling problems observed at the smaller time-scales are expected to affect the estimate of the empirical scaling functions. The analysis of the very low singularities and moments (i.e. associated with the low-intensity rainfall events), over the range of time scales mentioned above, is expected to lead to scaling exponents that are smaller (in absolute value) than the exponents that would be determined for scales larger than 1 to 2 hours. Moreover, there will be some uncertainty in the estimate of the empirical function $c(\gamma)$ over a range of values. This uncertainty is expected because the plots in Figure 5.7 do not follow closely a straight line for the extreme high singularities.

Empirical codimension function

The empirical codimension function $c(\gamma)$ is plotted in Figure 5.9 (dotted line). The function consists of both non-linear and linear sections. It is bounded from above by $(\gamma_{max}, c(\gamma_{max}))$, because of the finite size of the sample. The codimension of the maximum order of singularity γ_{max} that is likely to be observed (reliably) in a finite sample corresponds to the effective dimension $D+D_s$ (in Eq. (3.35)), where D_s is the sampling dimension (see Section 3.3.2).

The empirical function $c(\gamma)$ takes approximately the value 0.36 for roughly $\gamma<0.3$. Thus, the codimension function has a minimum value ($c_{min}\approx 0.36$). This behaviour is also expected to lead to linearity in the empirical function $K(q)$, over the corresponding (small) moments (see Section 3.3.2). The minimum codimension in Figure 5.9 is associated with the singularity of the smallest rainfall-intensity that was 'captured' (reliably) by the observation of the process; it is $c_{min}=c(\gamma_{min})$. Thus, the critical singularity γ_{min} is around 0.3. The minimum value of the codimension c_{min} gives an estimate of the fractal dimension of the geometric 'support' (defined in the 1-dimensional space of time) where the rainfall is integrated by the observation scheme of the process; so $D=1-c_{min}\approx 0.64$. This value is larger than the fractal dimension $D\approx 0.50$ obtained by box-counting analysis over the range of scales from about 2 hours up to 11.4 days (see Figure 5.1). This result can be explained because the study of the scaling of the probabilities, over a range of scales starting from 15 minutes, introduced underestimates of the codimension (see Figure 5.7), which yields a larger D. On the other hand, during digitization,

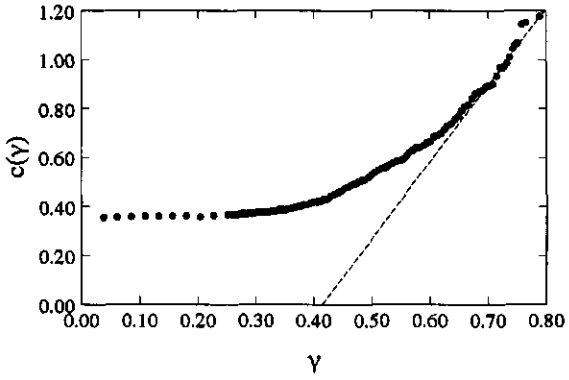

Figure 5.9 Empirical codimension function (dotted line) determined with 15-minute rainfall from Vale Formoso (from 1963 to 1985), for the range of scales from 15 minutes up to 10.7 days.

the assimilation to zero-values of very low rainfall-intensities could have sometimes led to a underestimate of the 'true' fractal dimension that characterizes rainfall occurrences in Vale Formoso.

The codimension function exhibits linear behaviour for orders of singularity γ larger than around 0.68. The statistical behaviour that leads to the linear section in the function $c(\gamma)$ (Figure 5.9), for large singularities (for $\gamma>\gamma_D$), is empirical evidence of a first-order multifractal phase transition. This type of phase transition is associated with the divergence of moments larger than a critical order $q_D=c'(\gamma_D)$. The slope of the regression line fitted to the linear section of the empirical function $c(\gamma)$ gives an estimate of $q_D\approx3.1$, and the intercept an estimate of $K(q_D)\approx1.3$. The estimate of the dual critical singularity for divergence of moments is thus $\gamma_D\approx0.68$.

The intersection of the line $c(\gamma)=\gamma$ with the linear asymptote to the function $c(\gamma)$ for large singularities (Figure 5.9), gives an estimate of the fractal dimension D; it is 0.61. This estimate falls between the two other estimates of D, above.

To investigate further the special statistical behaviour exhibited by the empirical function $c(\gamma)$, one can also study the probability distributions of the rainfall intensity on different scales. Some of these histograms are shown in Figure 5.10; from top to bottom, the histograms are for rainfall on 15 minutes, 30 minutes, and 1 hour (the histograms were offset vertically so as not to overlap). The histograms exhibit algebraic tails which indicate divergence of moments of order equal to the absolute value of the slope of these tails. Estimates of these slopes are (also from top to bottom, in Figure 5.10) 3.08, 3.06, and 3.17. Analysis of the histograms confirms the estimate of $q_D\approx3.1$. The behaviours of the histograms for the highest rainfall-intensities (which deviate from the expected power behaviour of the tails) are believed to result from undersampling.

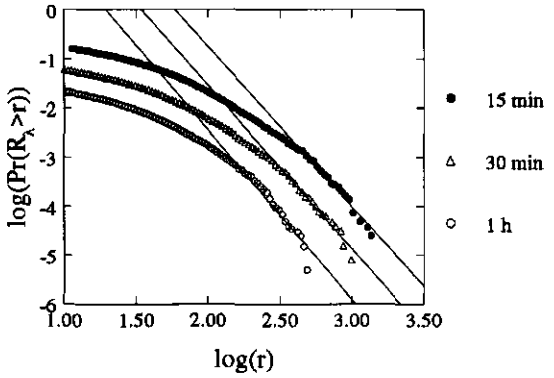

Figure 5.10 Histograms of rainfall on time scales (from top to bottom) of 15 minutes, 30 minutes, and 1 hour (the histograms were offset vertically so as not to overlap). The absolute slopes of the algebraic tails of the histograms are (also from top to bottom) 3.08, 3.06, and 3.17. The histograms were obtained with 15-minute rainfall from Vale Formoso, from 1963 to 1985.

Empirical moments scaling function

The empirical moments scaling function $K(q)$ is plotted in Figure 5.11 (dotted line). The plot on the right-hand side of Figure 5.11 shows a detail of the function $K(q)$ for moments $q<1$. The empirical function $K(q)$ consists of both non-linear and linear sections. It exhibits a linear behaviour for moments larger than around 3.1. This linear behaviour is also empirical evidence of a multifractal phase transition. The linear behaviour exhibited by the function $c(\gamma)$ (in Figure 5.9) for high orders of singularity γ, and the algebraic tails of the histograms of rainfall on various scales (in Figure 5.10) indicate that this is a first-order phase transition.

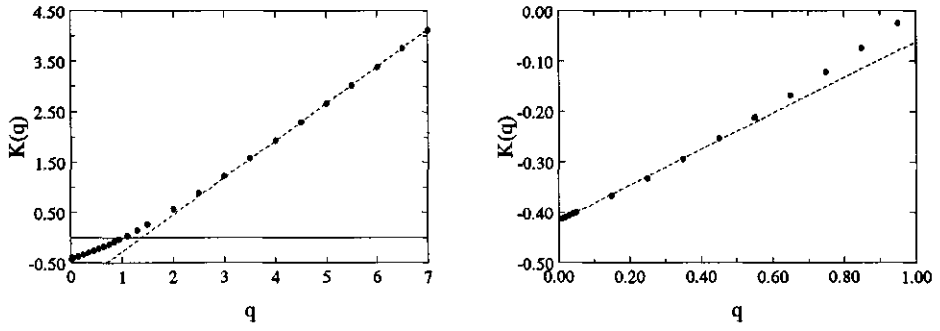

Figure 5.11 Empirical moments scaling function (dotted line) determined with 15-minute rainfall from Vale Formoso (from 1963 to 1985), for the range of scales from 15 minutes up to 10.7 days. The plot on the right-hand side shows a detail of the function $K(q)$ for $q<1$.

The slope of the linear section of the empirical function $K(q)$ (exhibited, in this case, for moments $q>q_D$) gives an estimate of the maximum order of singularity γ_{max} that is present in this finite sample. The absolute value of the intercept gives an estimate for the codimension of that singularity, $c(\gamma_{max})$. From Figure 5.11, the estimates are $\gamma_{max}\approx 0.74$, and $c(\gamma_{max})\approx 1.02$. Both values agree well with the corresponding estimates from the empirical function $c(\gamma)$ (Figure 5.9). The value of γ_{max} is larger than the critical singularity determined above (it was $\gamma_D\approx 0.68$), which supports that the phase transition is of the first order.

The values of q_D and $K(q_D)$ estimated from the empirical function $c(\gamma)$ agree with the behaviour exhibited by the empirical function $K(q)$. This function yields $K(3.1)=1.30$; moreover, the (dual) determination of the critical singularity $\gamma_D=K'(q_D)=K'(3.1)\approx 0.68$ agrees with the previous estimate from the function $c(\gamma)$. The value of the dimension D that satisfies the relation $D=K(q_D)/(q_D-1)$ (in Eq. (3.63)) is 0.62, for $q_D=3.1$ and the empirical $K(q_D)\approx 1.30$. This estimate of D agrees with the previous estimates.

The empirical function $K(q)$, in Figure 5.11, also exhibits linear behaviour for moments smaller than a critical order of around 0.5. The slope of this linear section of the function is 0.36 (an estimate of γ_{min}) and the intercept is -0.42 (an estimate of $-c(\gamma_{min})$). These estimates were obtained from the regression (dashed) line fitted to the data that are shown on the right-hand side plot in Figure 5.11. The discontinuity in the function $K(q)$ at small moments is also associated with a type of phase transition, and it arises from the Legendre transform relation between the functions $c(\gamma)$ and $K(q)$. If there is a restriction on the available orders of singularity γ, the Legendre transform between $c(\gamma)$ and $K(q)$ will take place over a finite range of γ's. This leads to linear behaviour in the function $K(q)$ over a range of q-moments, which is observed in this case for moments q smaller than approximately $q_{min}\approx 0.5$. The dual critical singularity is γ_{min}, which represents the lower limit of the range of γ-values that are present in the rainfall data. This singularity γ_{min} is explained by the 'assimilation' of very low rainfall-intensities to zero values (yielding rain-free periods). It results from the limitations of the measuring device and method used to digitize the pluviographs. Thus, the minimum codimension $c(\gamma_{min})\approx 0.42$ (estimated from the empirical function $K(q)$ in Figure 5.11) is related to the observed (geometric) 'support' of rainfall (defined in the 1-dimensional space of time). The corresponding estimate for its fractal dimension is $D\approx 0.58$. The values obtained here for γ_{min} and $c(\gamma_{min})$ are slightly larger than the values obtained from the analysis of the function $c(\gamma)$. Such estimates, relying on the study of small singularities and moments, may be affected by the scaling problems ('bends') observed in the probability and moments plots in Figure 5.7 and Figure 5.8.

'Universal' multifractals

The description of the statistics of the temporal rainfall by the 'universal' multifractal model (see Section 3.4) is investigated. The parameters of this model are C_1, α, and H. Different methods can be used to estimate these parameters (see Section 3.5.5). These methods include

the Double Trace Moment (DTM) technique (see Section 3.5.4), which was developed to estimate directly these parameters.

The DTM plot of $\log(|K(q,\eta)|)$ versus $\log(\eta)$ is shown in Figure 5.12 for some of the q-moments investigated for testing the scaling (see legend). The study of different q-moments increases the reliability of the estimates of the multifractal parameters. The lines in Figure 5.12 being parallel confirms the scaling and 'universal' multifractal behaviour of the rainfall process over the range of scales from 15 minutes up to 10.7 days. The breaks in the scaling that yield the characteristic 'S'-shape of the DTM plot occur at critical orders of moments: at q_{min} and q_{max}. These critical moments limit the range that can be used to estimate the parameters. Examples of the estimation of the moments q_{min} and q_{max} from the plots in Figure 5.12 are given in Table 5.2: the moment q_{min} is around 0.6 and the moment q_{max} is around 3.1. These estimates agree with the critical values obtained earlier. In this case it is, thus, $q_{max}=q_D$.

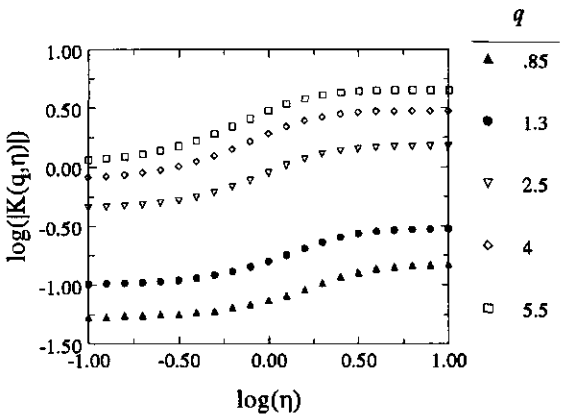

Figure 5.12 DTM plot of $\log(|K(q,\eta)|)$ versus $\log(\eta)$ estimated for the range of scales from 15 minutes up to 10.7 days with 15-minute rainfall from Vale Formoso (from 1963 to 1985). The legend indicates the q-moments plotted.

Estimation of the 'universal' multifractal parameters

The DTM estimates of the 'universal' multifractal parameters are $\alpha=0.49\pm0.04$ and $C_1=0.51\pm0.02$ (the study is based on the investigation of the scaling of 11 q-moments, within the range from 0.55 up to 3). Thus, the process belongs to the 'universality' class with $0<\alpha<1$ (see Section 3.4).

Another estimate of the parameter C_1 can be obtained from the empirical moment scaling function $K(q)$ (Figure 5.11), with the relation $K'(1)=C_1$. An approximation is $K'(1)\approx[K(1.1)-K(0.95)]/0.15=(0.051+0.025)/0.15=0.51$, which confirms the value obtained with the DTM technique.

Table 5.2 Estimation of the critical moments (q_{min} and q_{max}) associated with the breaks in the scaling of plots of $\log(|K(q,\eta)|)$ versus $\log(\eta)$, in Figure 5.12, from the curves obtained for q-moments of order 0.85 and 1.3.

type of scaling-break at η	q	$\log(\eta)$	η	$q\eta=q_{critical}$
q_{min}	0.85	-0.15	0.70	0.60
q_{min}	1.3	-0.30	0.50	0.65
q_{max}	0.85	0.55	3.55	3.00
q_{max}	1.3	0.40	2.51	3.26

The multifractal parameter H can be estimated with the relation $H=(\beta-1+K(2))/2$ (Eq. (3.81)), where $-\beta$ is the slope of the energy spectrum plotted in log-log axis. From the spectra in Figure 5.3 and Figure 5.5, the estimate is $\beta\approx0.15$. The empirical $K(2)=0.568$ yields the estimate of $H\approx-0.14$. One obtains roughly the same estimate of H (in Eq. (3.82)) with the theoretical value $K(2)=0.592$: $H\approx-0.13$.

The value of H estimated from the geometrical properties of the function $c(\gamma)$ (it is $c'(C_1-H)=1$ and $c(C_1-H)=C_1$, in Eq. (3.30)) supports that the parameter H is approximately zero. The previous estimates of H can be affected by uncertainties in estimating the spectral slope β. Thus, one expects the parameter H to be rather small. The estimate of the parameter C_1 also from the empirical function $c(\gamma)$ is slightly lower than the other estimates of it; it is approximately 0.45.

Agreement between the theoretical and empirical scaling functions

The empirical and theoretical scaling functions obtained for this case are represented in Figure 5.13. Figure 5.13(a) shows the empirical (dotted line) and theoretical (solid line) codimension functions. Figure 5.13(b) shows the empirical (dotted line) and theoretical (solid line) moments scaling functions. The agreement between the empirical and theoretical scaling exponent functions is good only for a range of values (see also Figure 5.9 and Figure 5.11). This range is limited by the critical exponents (orders of singularity and moments) associated with the multifractal phase transition discussed above.

In the presence of a first-order phase transition, the theoretical and empirical codimension functions are only expected to agree well until an order of singularity γ_D; this is observed in Figure 5.13. The critical singularity that is associated with the critical order for divergence of moments $q_D=3.1$ is $\gamma_D=K'(q_D)\approx0.68$, estimated from the empirical function $K(q)$ in Figure 5.11. The value of γ_D that is estimated from the 'universal' multifractal function with parameters $C_1=0.49$ and $\alpha=0.51$ (Eq. (3.72)) is 0.72. Figure 5.13(a) shows that the empirical codimensions of singularities $\gamma>\gamma_D$ are smaller than the theoretical estimates. Thus, their

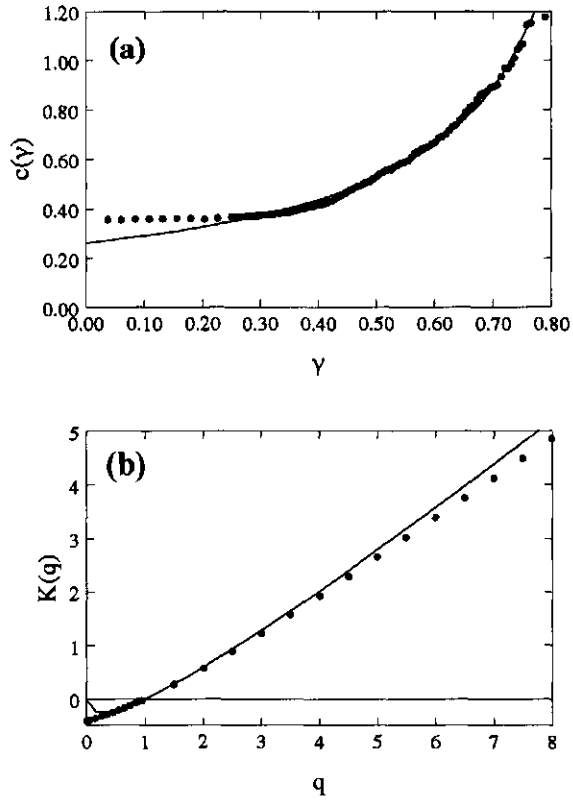

Figure 5.13 Empirical multifractal scaling exponent functions (dotted line) plotted with the 'universal' multifractal function (solid line) with parameters α=0.49, C_1=0.51 and H=-0.02: (a) codimension function; and (b) moments function. The empirical functions were determined with 15-minute rainfall from Vale Formoso (from 1963 to 1985), for the range of scales from 15 minutes up to 10.7 days.

probability of occurrence (in Eq. (3.22)) is larger than that predicted by the theoretical model, which corresponds to a *bare* multiplicative cascade process. This discrepancy can be explained by the different way that is used to obtain the two processes (empirical and theoretical): (*bare*) theoretical processes are fine-grained; and (*dressed*) empirical processes are coarse-grained (see Section 3.3.1). These differences result from the finite resolution of the measuring devices and the consequent integration of the ('true', fully developed) process on the scale of observation. Finite sampling from a process (each sample with a finite scale ratio) imposes an upper boundary on the orders of singularity γ that might be observed. Thus, the linear behaviour of the function $c(\gamma)$ for singularities $\gamma>\gamma_D$ is only observed for sufficiently large samples since those high singularities are almost surely not present in small samples (in small samples is $\gamma_s<\gamma_D$, with $c(\gamma_{max})=c(\gamma_s)\approx D+D_s$).

For small orders of singularity, the disparity between the theoretical and empirical codimension functions can also be explained. It occurs approximately for $\gamma<0.3$ (see Figure 5.13(a)), which is very close to the singularity γ_{min} estimated from the empirical codimension function. This function takes a constant value ($c(\gamma)\approx 0.36$) for roughly $\gamma<0.30$. The derivative of the $c(\gamma)$ at the critical point yields an estimate of $q_{min}\approx 0.45$. Until this critical γ-value, (small) singularities are observed (in the data) less often than it is described by a multiplicative *bare* cascade process (represented in Figure 5.13(a) with a solid line). For orders of singularity smaller than γ_{min}, the empirical function $c(\gamma)$ is affected by the integration of the process on certain scales, and 'assimilation' to zero-values of very small rainfall-intensities. This is caused by technical restrictions of the measuring device and digitization method.

The theoretical and empirical functions $K(q)$, in Figure 5.13(b), show good agreement for q-moments lying within the interval from around 0.6 up to 3.1. This interval corresponds to the dynamic range of the process where one expects that the statistics are well described by 'universal' multifractals. The critical exponents agree with the DTM plots of $\log(|K(q,\eta)|)$ versus $\log(\eta)$ (see Figure 5.12 and Table 5.2). Outside this range Eq. (3.39) must be used.

Estimation of the critical moment q_{max} (q_s or q_D) with 'universal' multifractals

The critical moments q_s and q_D can be estimated with the 'universal' multifractals parameters. The critical moment q_s can be estimated by $q_s=[(D+D_s)/C_1]^{1/\alpha}$ (Eq. (3.49)), whenever is $q_s<q_D$. For the rainfall data analyzed in this Section, this expression yields $q_s\approx 4.1$, which is well above the critical moment associated with the linear section of the function $K(q)$ in Figure 5.11. This value of the moment q_s was obtained with $D+D_s\approx 1.02$, which was estimated from the analysis of the empirical function $K(q)$ (see above).

The effective dimension $D+D_s$ can also be estimated by using the notion of sampling dimension defined in Eq. (3.32). Thus, it is $D_s=\log(N_s)/\log(\lambda)=\log(49)/\log(1024)=0.56$. As a first approximation, one uses the fractal dimension (of the 'support' of the process) obtained with box-counting analysis over the range of scales from 2 hours up to 11.4 days; it is $D=0.50$. Thus, $c(\gamma_{max})=D+D_s=1.06$. This estimate agrees reasonably with the empirical function in Figure 5.9. According to this function, the maximum order of singularity estimated reliably from this sample is approximately 0.74.

With $C_1(q_D^{\alpha}-q_D)/[(\alpha-1)(q_D-1)]=D$ (Eq. (3.50)) one obtains an estimate of $q_D\approx 3$ by taking $D=1-c(\gamma_{min})=0.64$; the value of $c(\gamma_{min})$ was estimated directly from the empirical codimension function. This estimate of the moment q_D is in good agreement with the previous estimates. It also supports that the phase transition is of the first-order. The small discrepancy in the estimate of the critical moment is due to uncertainties in estimating the dimension D.

The 'universal' multifractal model was used successfully to describe the statistics of rainfall. Although there was good agreement between the empirical and theoretical behaviours for only a range of values, 'universal' multifractals estimated well the upper limit of this range, i.e. the

critical exponents observed for the large singularities and moments of the process. These exponents are associated with multifractal phase transitions of the first and second order. The behaviour observed for the small intensities of the rainfall requires more study, especially the relation of the data and analysis with the measuring device itself.

5.3.2 Daily rainfall

This Section deals with the analysis of 30 years of daily rainfall from Vale Formoso (Portugal), recorded from 1961 to 1990 (see Section 4.2). In this period, the average annual rainfall is 498.8 mm. The daily data are from a non-recording rain gauge. The resolution of the measurements is 0.1 mm of rainfall. This is, thus, the minimum daily rainfall depth recorded. Any trace of rain below 0.1 mm is neglected by the observer and days are considered dry (zero-rainfall days).

The fractal and multifractal structure of the daily rainfall

Figure 5.14 shows the box-counting log-log plot obtained for the daily rainfall. The plot displays time scales from 1 day up to 256 days (approximately 8.5 months). The statistics are thus for 41 'samples' of 256 days. It is possible to distinguish different sections in the plot in Figure 5.14. The fractal dimension that characterizes rainfall occurrences on a range of time scales from 1 day up to about 11 days is 0.56. This value is given by the absolute value of the slope of the regression line fitted to the left-hand side section of the plot in Figure 5.14. The result differs from the box-counting estimate of the fractal dimension obtained for the 2-minute rainfall (see Section 3.3.1), which was 0.50. The different rainfall thresholds (imposed by the resolution of the records) that are used in the two analyses may contribute to this difference. The resolution is 0.1 mm/min for the recording rain gauge, and is 0.1 mm/day for the non-recording gauge. For time scales larger than 128 days (roughly 4.2 months), the right-hand side section of the plot has a slope of -1 (dashed line). This is caused by 'saturation.' The slope of the regression line fitted to the range of time scales from about 11 days up to about 4 months (128 days), in the middle section of the box-counting plot, is -0.80. This range of scales can be affected by the 'saturation' observed at scales larger than about 4 months. The result may also indicate a different scaling regime. The behaviour observed at different intensity levels of the daily rainfall is shown in the functional box-counting log-log plot in Figure 5.15. The corresponding rainfall thresholds are, for the lines from top to bottom, 0, 1, 5, 8, and 10 mm/day. For increasing values of the threshold the corresponding fractal dimension decreases; the absolute values of the slopes of the plots in Figure 5.15 are smaller. For the range of scales from 1 day up to about 11 days, the estimate for the fractal dimension of the (geometric) 'support' of daily rainfall is: 0.56 for 0 mm/day, 0.49 for 1 mm/day, 0.33 for 5 mm/day, 0.26 for 8 mm/day, and 0.22 for 10 mm/day. For the same thresholds, the absolute values of the slopes of the regression lines fitted to the range of scales from 11 days up to 128 days are: 0.80 for 0.1 mm/day, 0.76 for 1 mm/day, 0.64 for

5 mm/day, 0.53 for 8 mm/day, and 0.51 for 10 mm/day. The intersection of the regression lines from the left and middle sections of the plot in Figure 5.15 shows that the critical scale separating these two sections remains at the same scale for the different thresholds (at about 11 days). This observation suggests that different scaling regimes might govern time scales above and below this critical scale. The plot in Figure 5.15 shows 'saturation' (see right-hand side section of the plot) for all the rainfall thresholds investigated, but the critical time-scale is different from threshold to threshold. The critical scale increases with increasing threshold which indicates that the rainfall events are more and more sparse as the intensity level increases.

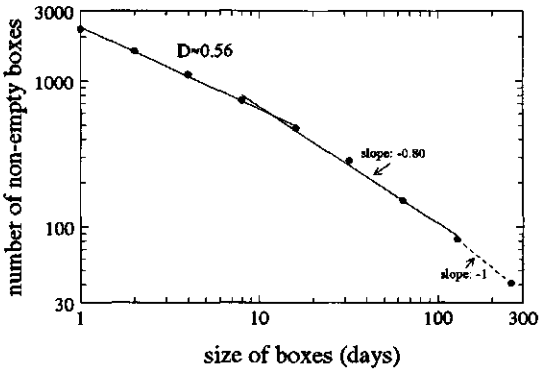

Figure 5.14 Box-counting log-log plot obtained with daily rainfall from Vale Formoso, from 1961 to 1990. The plot displays time scales from 1 day up to 256 days.

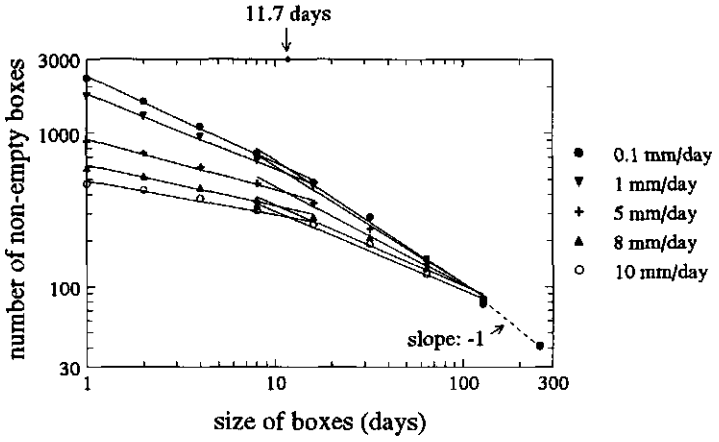

Figure 5.15 Functional box-counting log-log plot obtained with daily rainfall from Vale Formoso, from 1961 to 1990. The plot displays time scales from 1 day up to 256 days. The threshold values of the daily rainfall are, for the lines from top to bottom, 0.1, 1, 5, 8, and 10 mm/day.

Investigating scale-invariance with spectral analysis

The energy spectrum of the daily rainfall is plotted in Figure 5.16. The spectrum was smoothed for the high frequencies. In Figure 5.16, the spectral peak at $\omega \approx 0.0027$ day^{-1} corresponds to the annual cycle frequency. The other (smaller) peak in the higher frequency range (at $\omega \approx 0.0055$ day^{-1}) corresponds to a half-annual frequency.

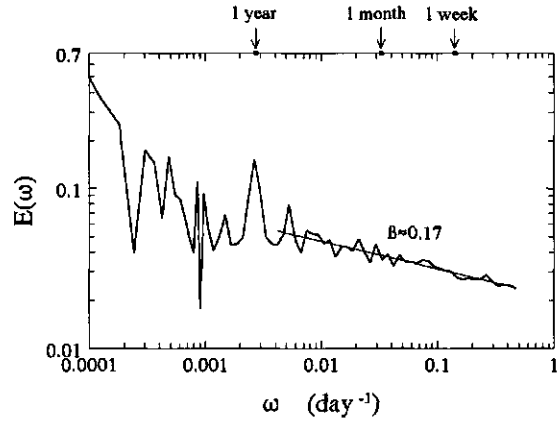

Figure 5.16 Energy spectrum obtained for daily rainfall from Vale Formoso, from 1961 to 1990.

The spectrum exhibits a power-law behaviour that extends from 1 day up to at least 8 months. A linear fit to this section of the spectrum yields an estimate for the spectral slope of -0.17. It is not possible to conclude about the upper limit of the scaling range. The behaviour suggests that the scaling behaviour extends to even larger scales, although a different (flat-power) behaviour might be present for the low frequency range. The analysis of the low frequency range should be approached with care because the estimates are based on a small number of long-period cycles. It would be necessary to analyze a larger sample to confirm this spectral break.

For rainfall in Europe, Fraedrich and Larnder (1993) reported a flat spectral plateau ($E(\omega) \approx \omega^0$), for time scales from about 3 years down to 3 days. Such type of spectral plateau is not seen in Figure 5.16, at least for this range of scales. The scaling regime associated with the range of scales characterized by such spectral plateau is expected to govern inter- and intra-seasonal variability (Fraedrich and Larnder, 1993). The critical scale (of about 3 days) that was observed in the spectra investigated by Fraedrich and Larnder (1993) is associated by the authors with the duration of synoptic events (see also e.g. Ladoy et al., 1991; Tessier et al., 1993). A similar critical scale at about 3 days was reported by Olsson (1995). The critical scale was observed at around 2 weeks by Ladoy et al. (1993) and Tessier et al. (1995), among others.

Scaling of the probability distributions

Figure 5.17 shows the log-log plot of the probability of exceeding rainfall intensity levels of singularity γ, observed on time scales of resolution λ, against the scale ratio λ. Figure 5.17 is for rainfall on time scales from 1 day (λ=256) up to 256 days (λ=1). The orders of singularity γ of the rainfall intensity ε_λ that are plotted in Figure 5.17 are indicated in the legend. This Figure includes the statistics of 41 'samples' of 256 days. In Figure 5.17, scaling is maintained from 1 day up to about 1 to 2 weeks.

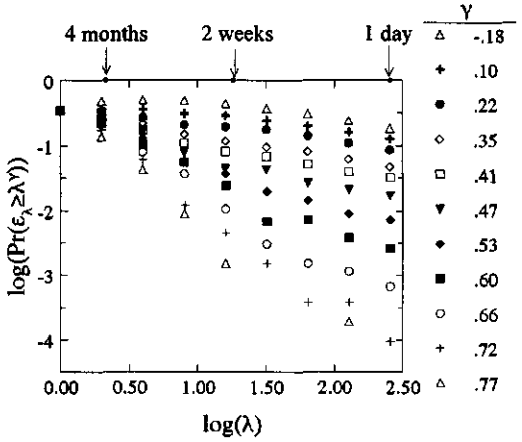

Figure 5.17 Log-log plot of the probability of exceeding rainfall intensity levels of singularity γ, observed on scales from 1 day (λ=256) up to 256 days (λ=1), against the scale ratio λ. The data are daily rainfall from Vale Formoso, from 1961 to 1990. The legend indicates the order of singularity γ of the rainfall intensity ε_λ.

Scaling of the moments

Figure 5.18 shows the log-log plot of the average q^{th} moments of the rainfall intensity ε_λ on time scales from 1 day (λ=256) up to 256 days (λ=1), against the scale ratio λ. Figure 5.18(a) shows moments larger than 1, and Figure 5.18(b) shows moments smaller than 1 (see legend).

The plot in Figure 5.18 suggests that two different scaling regimes hold above and below a critical scale at about one-and-a-half weeks. This range of scales spans less than one order of magnitude. Its analysis must be approached with care. Analysis of the scaling of moments larger than 1 suggests that the second scaling regime is maintained for time scales up to more than 8 months.

The rainfall threshold of 0.1 mm/day that was imposed at the smallest observation-scale (i.e. one day) by the rainfall measuring technique, introduced in the data a minimum 'observable' intensity. Thus, the orders of singularity of the process that are possible to study are bounded from below. They are also bounded from above because of the finite size of the

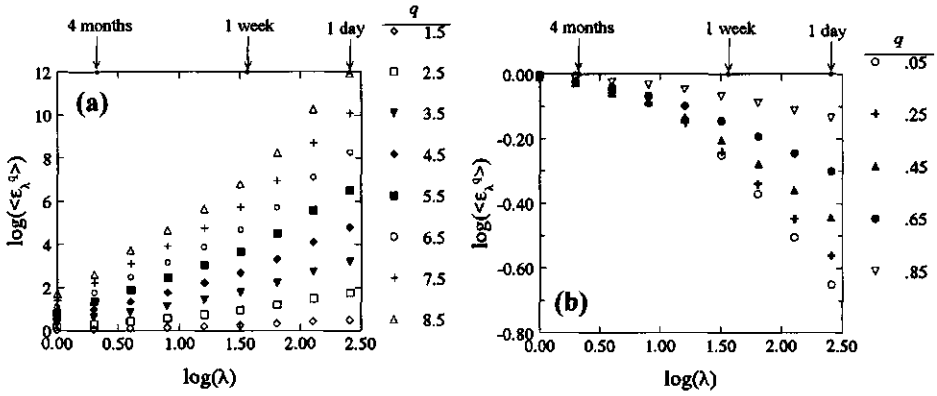

Figure 5.18 Log-log plot of the average q^{th} moments of rainfall intensity ε_λ on time scales between 1 day (λ=256) and 256 days (λ=1), against the scale ratio λ: (a) for moments larger than 1; and (b) for moments smaller than 1. The data are daily rainfall from Vale Formoso, from 1961 to 1991.

sample. This affects particularly the scaling of the very small moments q (corresponding to very low rainfall-intensities). Because it is convenient to study scale resolutions that are equal to powers of 2, the investigation of two scaling regimes in the temporal structure of rainfall will consider the critical scale at 8 days. Thus, the behaviour observed at scales smaller and larger than 8 days will be studied. The scaling of the moments smaller than 1 has determined the upper limit of the range of scales that will be analyzed, which is 128 days. Nevertheless, the invariance of properties is believed to occur on even larger scales.

Analysis of rainfall on the range of scales from 1 up to 8 days

The empirical scaling exponent functions

The exponent scaling functions that describe the multifractal temporal structure of rainfall on the range of scales from 1 up to 8 days are derived below (this scaling regime is expected to be maintained up to about 11 days, see Figure 5.17 and Figure 5.18). One should approach this analysis with caution because of the small range of time scales investigated in this analysis.

Empirical codimension function

The empirical codimension function, $c(\gamma)$, that describes the scaling of the probability distributions of the rainfall intensity is shown in Figure 5.19. For singularities γ smaller than around 0.45 the function displays a linear (flat) behaviour, which indicates the presence in the data of a minimum (observable) singularity γ_{min}. The codimension of this singularity is $c(\gamma_{min})$ $\approx$0.35. This leads to the estimate $D\approx$0.65, D being the fractal dimension of the (geometric)

'support' of the observed rainfall process, defined on the time domain. This value is larger than the (monofractal) box-counting estimate of the fractal dimension ($D \approx 0.56$), but it agrees with values of D estimated using high-resolution rainfall (see Section 5.3.1).

The empirical codimension is rather poorly estimated for $\gamma > 0.65$. It is not possible to analyze the behaviour of the function beyond this value.

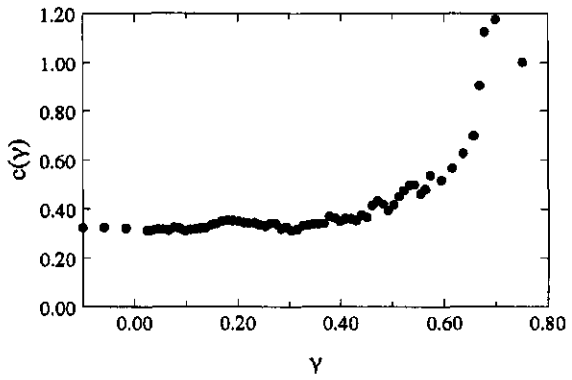

Figure 5.19 Empirical codimension function that describes the scaling of the probability distributions of rainfall intensity on scales between 1 day and 8 days. The study used daily rainfall from Vale Formoso, from 1961 to 1990.

Empirical moments scaling function

The empirical function, $K(q)$, that describes the scaling of the moments of the rainfall intensity on time scales from 1 day up to 8 days is plotted in Figure 5.20 (dotted line). The function consists of both non-linear and linear sections. The function $K(q)$ is linear for moments larger than around 3.5. The slope of this linear section is an estimate of $\gamma_{max}=0.86$. The absolute value of the intercept gives an estimate of $c(\gamma_{max})=1.5$. One expects that the discrepancy between these estimates and the empirical function $c(\gamma)$ results from the small range of scales used to estimate the empirical functions.

Examples of histograms of rainfall on different scales are shown in Figure 5.21; from top to bottom, the scales are 1, 2, 4, and 8 days (in Figure 5.21, the histograms were offset vertically so as not to overlap). The histograms exhibit algebraic tails which indicates divergence of statistical moments. The critical order for divergence of moments is given by the slope of the algebraic tails. The absolute values of the slopes of the regression lines fitted to the tails of the histograms are (from top to bottom) 3.7, 3.6, 3.7, and 3.6. The value of the moment q_D is estimated as 3.65. It agrees with the behaviour of the function $K(q)$. The multifractal phase transition present in the statistics of rainfall is believed to be of the first-order, although the

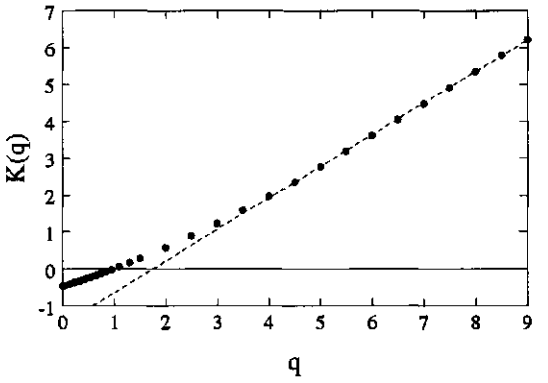

Figure 5.20 Empirical moments scaling function (dotted line) determined with daily rainfall from Vale Formoso (from 1961 to 1990), for the range of scales from 1 day up to 8 days.

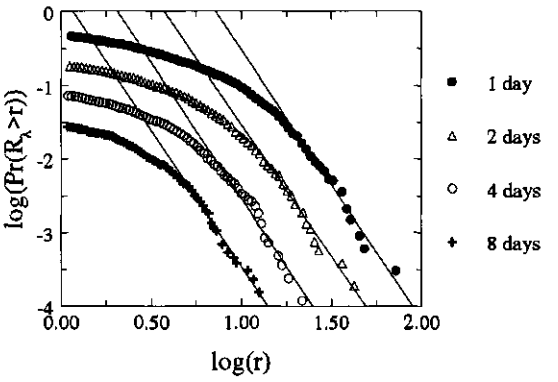

Figure 5.21 Histograms of rainfall on time scales (from top to bottom) of 1 day, 2 days, 4 days, and 8 days (the histograms were offset vertically so as not to overlap). The absolute values of the slopes of the algebraic tails of the histograms are (also from top to bottom) 3.7, 3.6, 3.7, and 3.6. The histograms were obtained with daily rainfall from Vale Formoso, from 1961 to 1990.

estimate of the codimension function (in Figure 5.19) does not exhibit clearly linear behaviour for the large singularities. Using Eq. (3.41), one estimates $D=K(q_D)/(q_D-1)\approx 0.64$ from the empirical function $K(q)$.

The empirical function $K(q)$, in Figure 5.20, also exhibits linear behaviour for moments smaller than a critical order of around 0.7 (q_{min}). The slope of this linear section is 0.44 (an estimate of γ_{min}), with intercept at -0.46 (an estimate of $-c(\gamma_{min})$). The value of γ_{min} agrees well with the estimates from the empirical codimension function. The value of $c(\gamma_{min})$ is larger than

the value that is observed by inspection of the empirical function $c(\gamma)$. It leads to $D=1-c(\gamma_{min})\approx 0.54$. This value agrees reasonably with the estimate of the box-counting dimension D for scales between 1 and 8 days. The linear behaviour of the function $K(q)$ for small moments ($q<q_{min}$) is also a type of multifractal phase transition. It results from limitations of the measuring technique, which introduced a minimum (non-zero) observable singularity of the rainfall intensity.

'Universal' multifractals

The 'universal' parameters that characterize the multifractal behaviour described by the scaling exponent functions in Figure 5.19 and Figure 5.20 were estimated with the Double Trace Moment (DTM) method. The DTM plot of $\log(|K(q,\eta)|)$ versus $\log(\eta)$ is shown in Figure 5.22 for some of the different values of the moment q that were used to test the scaling (see legend).

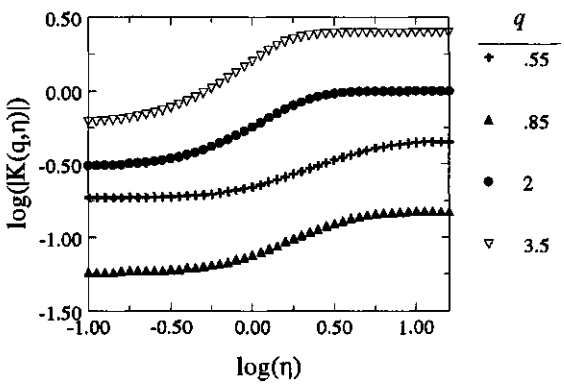

Figure 5.22 DTM plot of $\log(|K(q,\eta)|)$ versus $\log(\eta)$, estimated for the range of scales from 1 day up to 8 days. The data are daily rainfall from Vale Formoso, from 1961 to 1990. The legend indicates the q-moments plotted.

The lines in Figure 5.22 are parallel, which confirms the scaling and 'universal' multifractal behaviour of the rainfall process over the range of scales from 1 day up to 8 days. The study of different q-moments increases the reliability of the estimates of the multifractal parameters. In Figure 5.22, the scaling breaks down for critical orders of moments: at q_{min} and q_{max} (where $q_{max}=\min(q_s, q_D)$). Analysis yielded the 'universal' parameters $C_1=0.51\pm0.03$ and $\alpha=0.48\pm0.08$ (the averages are for 9 q-values). This result confirms that the rainfall process belongs to the 'universality' class with $0<\alpha<1$. The multifractal parameters estimated here with daily rainfall agree very well with the estimates obtained with 15-minute rainfall, for the range of scales from 15 minutes up to 10.7 days (see Section 5.3.1). This result is rather promising with respect to shifts in the scale. This finding is favourable for the transfer of

information across scales, i.e. it is useful if one wishes to determine the statistics of rainfall on small time-scales from daily data.

One can estimate the value of C_1 from the first derivative of the function $K(q)$ at q=1. An approximation is $K'(1)=[K(1.1)-K(0.95)]/0.15=(0.052+0.026)/0.15=0.52$, which confirms the DTM result.

The other multifractal parameter, H, can be estimated with Eq (3.81). The absolute value of the slope of the energy spectrum (Figure 5.16) is $\beta=0.17$ and the empirical $K(2)$ is 0.57; thus, the estimate of H is -0.13. With the 'universal' parameters C_1 and α, the estimate of the parameter H is -0.12 (using Eq. (3.82)).

Agreement between the theoretical and empirical scaling exponent functions

The theoretical 'universal' scaling functions, with the parameters estimated above, are shown in Figure 5.23 and Figure 5.24. Figure 5.23 shows the theoretical codimension function (solid line) plotted with the empirical codimension function (dotted line). Figure 5.24 shows the theoretical moments scaling function (solid line) plotted with the empirical moments function (dotted line).

The empirical and theoretical codimension functions in Figure 5.23 show agreement only for a very limited range of values. For the small singularities, the disparity between the two functions could be explained by a minimum reliably observed rainfall intensity in the data. For the large singularities, this discrepancy could be caused by a poor estimate of the multifractal parameters, or of the empirical function.

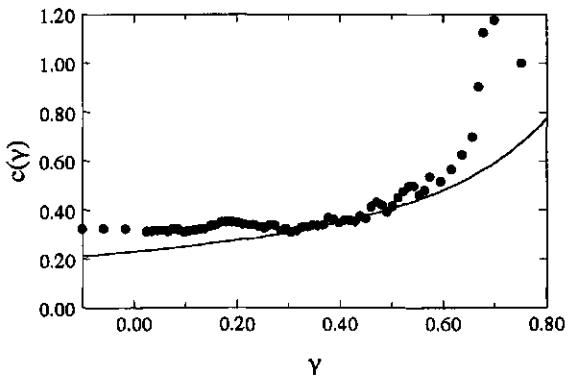

Figure 5.23 Empirical codimension function (dotted line) that describes the scaling of the probability distributions of rainfall intensity on scales between 1 day and 8 days, plotted with the 'universal' codimension function (solid line) with parameters $\alpha=0.48$ and $C_1=0.51$, $H=-0.12$. The study used daily rainfall from Vale Formoso (from 1961 to 1990).

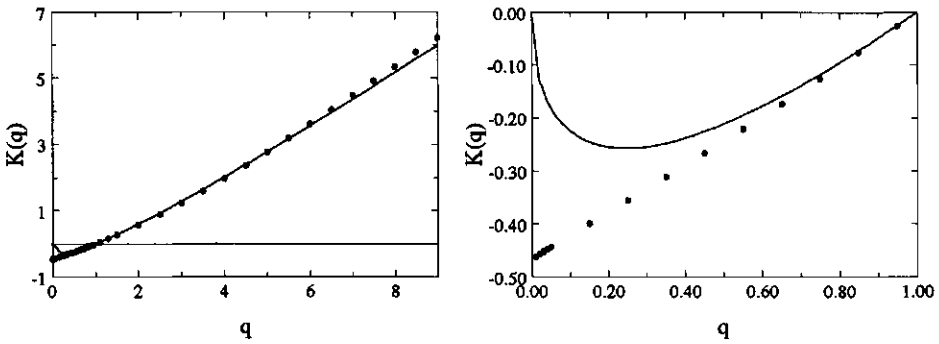

Figure 5.24 Empirical moments scaling function (dotted line) plotted with the 'universal' moments scaling function (solid line) with parameters α=0.48 and C_1=0.51. The plot on the right-hand side shows a detail of the function for moments $q<1$. The empirical function was determined with daily rainfall from Vale Formoso (from 1961 to 1990), for the range of scales from 1 day up to 8 days.

The empirical and theoretical moments scaling functions in Figure 5.24 agree well only for a finite range of moments q (see also Figure 5.20). The limits are the critical values of the order of moments discussed above. The upper limit is approximately of order 3.5~4. For moments larger than this critical order, the empirical function is linear. Such (special) statistical behaviour is associated with a multifractal phase transition. For the estimate q_D=3.65, the value of the dual critical singularity is $\gamma_D=K'(q_D)\approx 0.74$, estimated from the theoretical function $K(q)$ (Eq. (3.72)); and is 0.75, estimated from the empirical function. It is not possible to verify the correctness of these estimates of γ_D from the empirical codimension function $c(\gamma)$, in Figure 5.23.

There is also disparity between the empirical and theoretical functions $K(q)$ for moments smaller than a critical value $q_{min}\approx 0.7$. This critical moment is associated with a special linear behaviour of the empirical moments scaling function for $q<q_{min}$. This qualitative change in statistical behaviour is another example of a multifractal phase transition.

Estimation of the critical moment q_{max} (q_s or q_D) with 'universal' multifractals

The value of the critical moment q_D can also be estimated with Eq. (3.50); for D=0.65, is $q_D\approx 3.4$. This value agrees with other previous estimates of q_D. Small differences in the estimates of this critical moment can be explained by uncertainties in estimating D.

An estimate of the moment q_s can be obtained with Eq. (3.49). It is $q_s\approx 9.5$ for $c(\gamma_{max})$=1.5, estimated from the empirical moments function. This estimate is much larger than the critical moment observed in the function $K(q)$ and the estimate of the critical order for divergence of moments from the histograms (in Figure 5.21). This supports that the multifractal phase transition is of the first-order.

Analysis of rainfall on the range of scales from 8 days up to 4.3 months

The empirical scaling exponent functions

The exponent scaling functions that describe the multifractal behaviour in the temporal structure of rainfall (see Figure 5.17 and Figure 5.18) on the range of scales from 8 up to 128 days (approximately 4.3 months) are derived below.

Empirical codimension function

The empirical codimension function, $c(\gamma)$, that describes the scaling of the probability distributions of rainfall intensity on time scales from 8 days up to 128 days (see Figure 5.17) is shown in Figure 5.25 (dotted line). The function consists of both linear and non-linear sections.

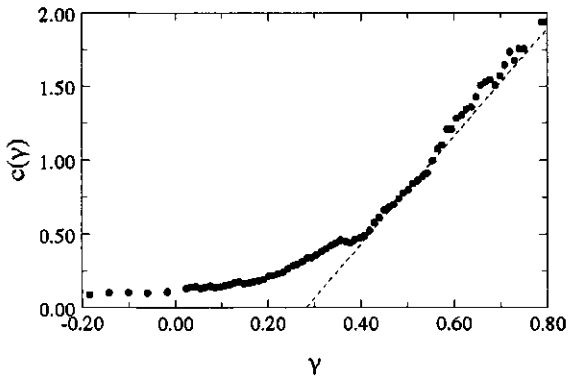

Figure 5.25 Empirical codimension function (dotted line) that describes the scaling of the probability distributions of rainfall intensity on scales between 8 and 128 days. The data are daily rainfall from Vale Formoso, from 1961 to 1990.

The empirical codimension function is 'flat' for orders of singularity γ smaller than around 0.05. This critical value corresponds to the singularity γ_{min}. The codimension of this singularity, $c(\gamma_{min})$, is estimated to be between 0.15 and 0.2. This value agrees reasonably with the monofractal analysis discussed earlier: the box-counting dimension was $D \approx 0.80$ (it is $D = 1 - c(\gamma_{min})$).

For orders of singularity larger than around 0.45, the codimension function also displays a linear behaviour. This type of behaviour is empirical evidence of a first-order multifractal phase transition. The slope of the linear fit to this section of the codimension function gives the estimate $q_D \approx 3.65$ and the intercept the estimate $K(q_D) \approx 1.03$. The intersection of this line with $c(\gamma)=\gamma$ gives an estimate of the fractal dimension D=0.39. This value is much smaller than that suggested by the box-counting plot in Figure 5.14. This result is consistent with the idea that,

over the range of scales of interest here, the box-counting estimate is affected by the 'saturation' observed on larger scales.

Another estimate of the critical order for divergence of moments can be obtained by studying the histograms of the rainfall intensity on different scales. Figure 5.26 shows (from top to bottom) histograms of the rainfall intensity on scales of 8, 16, and 32 days (in Figure 5.26, the histograms were offset vertically so as not to overlap). The histograms exhibit algebraic tails. The absolute values of the slopes of the regression lines fitted to the tails of the histograms are (also from top to bottom) 3.6, 3.5, and 3.6. These values agree with the previous estimates of the moment q_D obtained from the slope of the tail of histograms of rainfall on other scales. This result supports the estimate $q_D \approx 3.6$. Thus, it supports that the multifractal phase transition observed in the empirical scaling exponent functions is of the first-order.

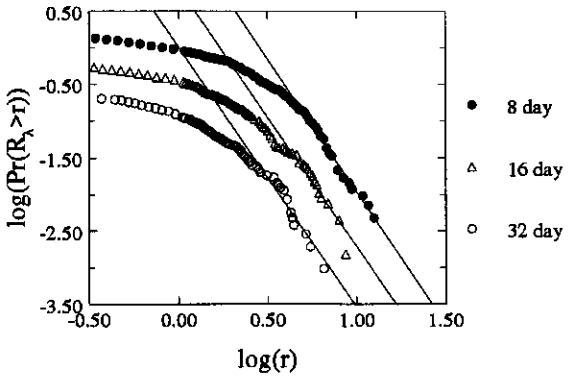

Figure 5.26 Histograms of rainfall on time scales (from top to bottom) of 8, 16, and 32 days (the histograms were offset vertically so as not to overlap). The absolute values of the slopes of the algebraic tails of the histograms are (also from top to bottom) 3.6, 3.5, and 3.6. The histograms were obtained with daily rainfall from Vale Formoso, from 1961 to 1990.

Empirical moments scaling function

The empirical moments scaling function, $K(q)$, that describes the scaling of the moments of the rainfall intensity on time scales between 8 days and 128 days is plotted in Figure 5.27 (dotted line). The empirical function $K(q)$ consists of both non-linear and linear sections.

The linear section is observed for moments larger than around 3.5. The slope of this section is an estimate of $\gamma_{max}=0.50$. The absolute value of the intercept gives an estimate of $c(\gamma_{max})=D+D_s \approx 0.80$. These values are smaller than it would be expected from inspection of the empirical codimension function in Figure 5.25. From the empirical moments scaling function, the estimate of the dual critical singularity for divergence of moments is $\gamma_D=K'(q_D)\approx 0.46$, which agrees with the behaviour observed in the empirical codimension function. The function $K(q)$ also yields the estimate $D\approx 0.39$ (using Eq. (3.41)).

The study of the empirical function $K(q)$ near $q=0$ yields the estimates $\gamma_{min}\approx 0.05$ and $c(\gamma_{min})=-K(0)\approx 0.20$. These values agree with the estimates of γ_{min} and $c(\gamma_{min})$ from the empirical codimension function.

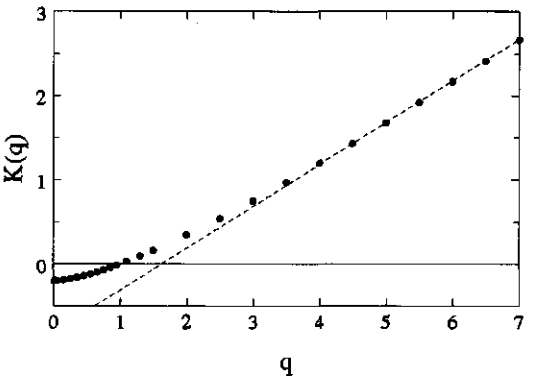

Figure 5.27 Empirical moments scaling function (dotted line) determined with daily rainfall from Vale Formoso (from 1961 to 1990), for the range of scales from 8 up to 128 days.

'Universal' multifractals

The 'universal' parameters that characterize the empirical scaling exponent functions in Figure 5.25 and Figure 5.27 were estimated with the Double Trace Moment (DTM) method. The DTM plot of $\log(|K(q,\eta)|)$ versus $\log(\eta)$ is shown in Figure 5.28 for some of the different values of the moment q that were used to test the scaling (see legend).

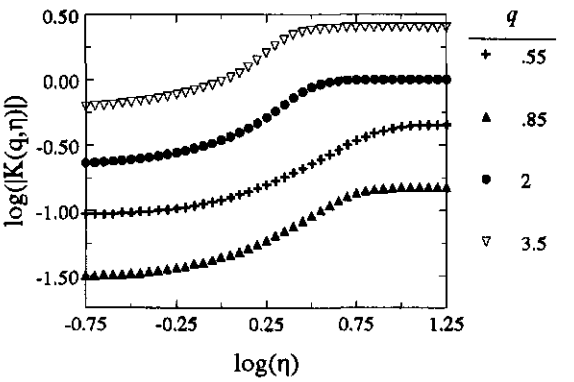

Figure 5.28 DTM plot of $\log(|K(q,\eta)|)$ versus $\log(\eta)$, estimated for the range of scales from 8 up to 128 days. The data are daily rainfall from Vale Formoso, from 1961 to 1990. The legend indicates the q-moments plotted.

DTM analysis yielded the 'universal' parameters C_1=0.30±0.02 and α=0.66±0.06 (the averages are for 12 q-values). These parameters describe the statistics of rainfall over the range of scales from 8 days up to 4.3 months. The rainfall process belongs to the 'universality' class with $0<\alpha<1$.

The multifractal parameter H is poorly estimated with Eqs. (3.81) and (3.82), if one uses the estimate of the spectral exponent β=0.17. The empirical $K(2)$=0.35 yields the estimate $H\approx$-0.24. With the 'universal' parameters the estimate is $H\approx$-0.23.

Analysis of the empirical codimension function suggests that the parameter H is smaller ($H\approx$-0.03). This result is obtained from the geometric properties of the codimension function $c(C_1\text{-}H)=C_1$ and $c'(C_1\text{-}H)=1$ (in Eq. (3.30)). These properties lead to an estimate of the parameter C_1 of approximately 0.3, which agrees with the DTM result.

The value of C_1 can also be estimated from the first derivative of the function $K(q)$ at q=1. An approximation is $K'(1)=[K(1.1)\text{-}K(0.95)]/0.15=(0.031+0.015)/0.15=0.31$, which confirms the DTM result.

Agreement between the theoretical and empirical scaling exponent functions

The theoretical 'universal' scaling functions with parameters α=0.66, C_1=0.30 and H=-0.03 are shown in Figure 5.29 and Figure 5.30. Figure 5.29 shows the theoretical codimension function (solid line) plotted with the empirical codimension function (dotted line); see also Figure 5.25. Figure 5.30 shows the theoretical moments scaling function (solid line) plotted with the empirical moments function (dotted line); see also Figure 5.27.

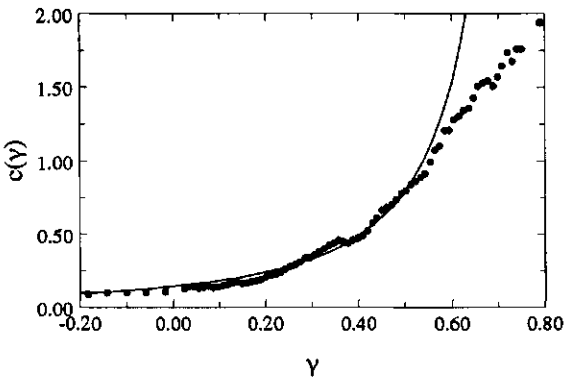

Figure 5.29 Empirical codimension function (dotted line) that describes the scaling of the probability distributions of rainfall intensity on scales between 8 and 128 days, plotted with the 'universal' codimension function (solid line) with parameters α=0.66, C_1=0.30, and H=-0.03. The data are daily rainfall from Vale Formoso, from 1961 to 1990.

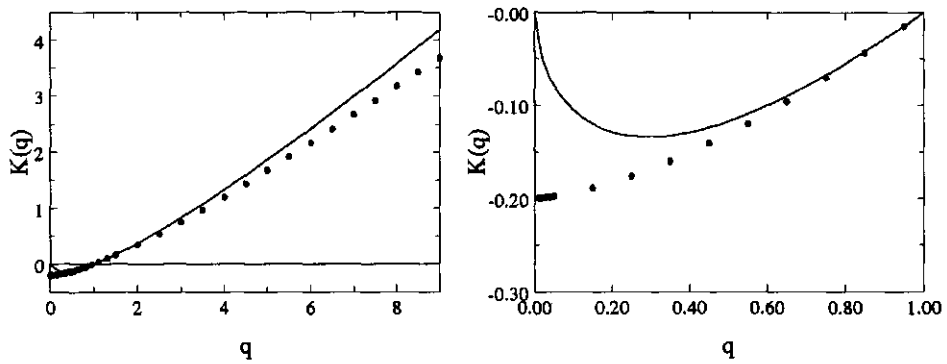

Figure 5.30 Empirical moments scaling function (dotted line) plotted with the 'universal' moments scaling function (solid line) with parameter values α=0.66 and C_1=0.30. The plot on the right-hand side shows a detail of the function for $q<1$. The empirical function was determined with daily rainfall from Vale Formoso (from 1961 to 1990), for the range of scales from 8 up to 128 days.

Estimation of the critical moment q_{max} (q_s or q_D) with 'universal' multifractals

The critical moments q_s and q_D can be estimated with 'universal' multifractals. To calculate the value of q_D using Eq. (3.50) it is necessary to know the dimension D. If one uses the estimate D=0.39, discussed above, the moment q_D is poorly estimated (≈2.4). The value of D that verifies Eq. (3.50) for q_D=3.6 is 0.43.

The empirical and theoretical scaling functions agree reasonably well for a range of values of the orders of singularity and moments. These critical values are discussed above. For large singularities and moments of the rainfall intensity, the disparity between the empirical and theoretical scaling functions is explained by a first-order phase transition. For moments smaller than 1, there is only agreement between the empirical and theoretical moments functions for moments larger than approximately 0.65.

The moment q_s can be estimated using Eq. (3.49). The estimate of the effective dimension obtained by analyzing the empirical moment function is 0.80. This leads to q_s≈4.4, which is larger than the critical moment observed. Because the value of the effective dimension estimated from the empirical function $K(q)$ seems to be underestimated, a even larger moment q_s would be obtained. This result supports that the multifractal phase transition is of the first-order (it is $q_s>q_D$).

The value of the dual critical singularity for divergence of moments can also be estimated with 'universal' multifractals. Using Eq. (3.72) one obtains $\gamma_D=K'(q_D)$≈0.51, which agrees well with the previous estimates.

5.3.3 Monthly rainfall

This Section deals with the analysis of 59 years of monthly rainfall from Vale Formoso (Portugal), recorded from 1932 to 1990 (see Section 4.2). In this period, the average annual rainfall is 565.9 mm. The data were obtained by aggregating daily rainfall (measured with a non-recording rain gauge) during monthly intervals. The temporal structure of rainfall on scales larger than 1 month is investigated with this longer monthly rainfall record.

The fractal structure of the monthly rainfall

The box-counting plot obtained with the monthly rainfall is shown in Figure 5.31. The plot displays time scales from 1 month up to 16 months. Thus, it accumulates the statistics over the 59 years, i.e. of 44 'samples' of 16 months. In this plot two linear sections can be distinguished: one with a slope of -0.89, for time scales from 1 month up to 4 months (on the left-hand side of the plot); and another with a slope of -1, for larger time-scales (on the right-hand side of the plot). The box-counting analysis of scales between 1 and 4 months may be affected by the 'saturation' observed for the larger scales. For climates that are not characterized by a well-defined dry season, the slope of the log-log box-counting plot for monthly rainfall is always -1 (i.e. it shows 'saturation' starting from scales of 1 month).

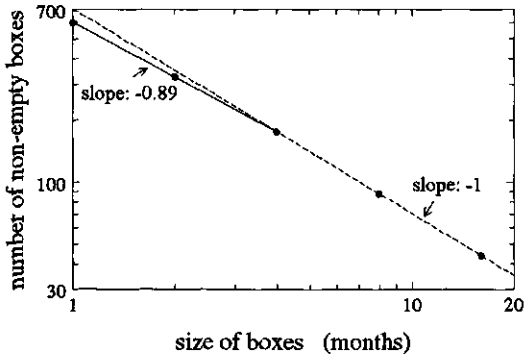

Figure 5.31 Box-counting log-log plot obtained with monthly rainfall from Vale Formoso, from 1932 to 1990. The plot displays time scales from 1 month up to 16 months.

Investigating scale-invariance with energy spectra

The energy spectrum for the monthly rainfall is given in Figure 5.32. The spectrum exhibits peaks at frequencies corresponding approximately to 1 year, 3.2 years, 6.6 years, and 8.5 years. Towards the low-frequency end, the spectrum starts rising with decreasing frequency, well outside the statistical fluctuations observed in the adjacent section exhibiting flat-power behaviour. This behaviour over the largest scales is expected to be related to climatic

fluctuations (Fraedrich and Larnder, 1993); it is expected to describe long-term variability. The presence of a (flat) spectrum plateau is observed now more clearly (in Figure 5.32) than when smaller samples were analyzed (see Figure 5.3, for 23 years, and Figure 5.16, for 30 years). This behaviour is not maintained for scales smaller than about 5 months. Linear regression of log(E(ω)) against log(ω), over this range of scales, yields an estimate for the spectral slope of -0.24.

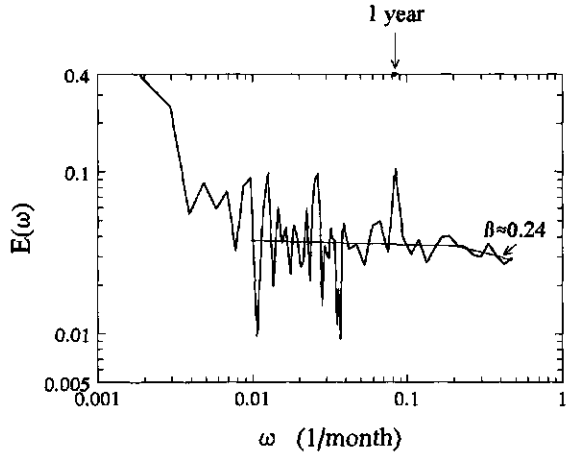

Figure 5.32 Energy spectrum obtained for monthly rainfall from Vale Formoso, from 1932 to 1990.

Scaling of the probability distributions

The log-log plot in Figure 5.33 shows the probability of exceeding rainfall intensity levels of singularity γ, observed on time scales from 1 month (λ=8) up to 8 months (λ=1), against the scale ratio λ. Figure 5.33 includes the statistics of 88 'samples' of 8 months. The legend indicates the orders of singularity γ of the rainfall intensity ε_λ that are plotted in Figure 5.33. The relatively small size of the sample hampers the study of this range of (larger) scales. Nevertheless, the plot in Figure 5.33 confirms that scaling is maintained over the range of scales from 1 month up to at least 4 months (see Section 5.3.2).

Scaling of the moments

Figure 5.34 shows the log-log plot of the average q^{th} moments of the rainfall intensity ε_λ on scales from 1 month (λ=8) up to 8 months (λ=1), against the scale ratio λ. Figure 5.34(a) shows moments larger than 1 and Figure 5.34(b) shows moments smaller than 1. The scaling behaviour seems to occur here from 1 month up to at least 8 months.

The topics of first-order and second-order phase transitions can be approached systematically by analyzing samples of different sizes, and different renormalized versions of the data with η-powers (see e.g. Schertzer and Lovejoy, 1993; Schmitt, 1993). This type of data renormalization is discussed in Section 3.5.4, and it is based on the technique of the Double Trace Moment method. By increasing the moment η one highlights increasingly intense events (i.e. of high order of singularity). Thus, by studying the statistical properties of the entire family of η-renormalized versions of the data as a function of the resolution of the process, a complete characterization of the scaling properties can be obtained. In this way, it is possible to determine a spectrum of values for the critical moments $q_D^{(\eta)}=q_{D,\eta}$ and $q_s^{(\eta)}=q_{s,\eta}$, which will depend non-linearly upon η. The critical moments $q_{D,\eta}$ are associated with first-order phase transitions, and the moments $q_{s,\eta}$ with second-order phase transitions (see Section 3.3.1). The moments $q_{D,\eta}$ and $q_{s,\eta}$ are obtained for the η-renormalized versions of the process in the same way the usual moments q_D and q_s are obtained for the original process (in this case it is η=1). The critical moments $q_{D,\eta}$ and $q_{s,\eta}$ plotted against the moment η, yield phase-transition lines on the plane (q,η). Such a plot is called a 'phase-diagram' on the (q,η) plane (Schertzer and Lovejoy, 1993). A phase-diagram can also be obtained on the plane (γ,η).

The purpose of the study conducted in this Section is to derive a phase-diagram on the plane (q,η). The study investigates the statistical behaviour of rainfall over the range of scales from 15 minutes up to 10.7 days; it uses 15-minute rainfall data from Vale Formoso, from 1963 to 1985 (see Sections 4.2 and 5.3.1).

Estimating the moment $q_{D,\eta}$ from the empirical codimension functions $c(\gamma,\eta)$

The empirical codimension functions $c(\gamma,\eta)$ obtained for a few η-renormalized versions of the (original) rainfall process are shown in Figure 5.41. The effect on the codimension function $c(\gamma,\eta)$ of varying η can be observed in Figure 5.41(a) for moments $\eta\leq 1$, and in Figure 5.41(b) for moments $\eta\geq 1$. As the order of the singularity decreases, the codimension $c(\gamma,\eta)$ tends to the same value ($c_{min}\approx 0.36$). As the value of the moment η increases, this behaviour is observed for smaller and smaller singularities; in Figure 5.41(b) this is observed outside the range of singularities that are plotted. Figure 5.41 also shows that the value of the order of singularity, and corresponding codimension, that satisfies the geometrical properties in Eq. (3.30) (i.e. the fixed point $c(C_1)=C_1$ and $c'(C_1)=1$) increases with η.

Estimating the moments $q_{D,\eta}$ or $q_{s,\eta}$ from the empirical moments scaling functions $K(q,\eta)$

The empirical moments scaling functions $K(q,\eta)$, obtained for a few η-renormalized versions of the data, are shown in Figure 5.42. The plot on the right-hand side shows a detail of the functions $K(q,\eta)$ for q-moments smaller than 1.

Figure 5.42 shows the effect on the function $K(q,\eta)$ of changing the value of the moment η. While the value of the singularity γ_{min} changes (γ_{min} is given by the slope of $K(q,\eta)$ as $q\rightarrow 0$), the value of $c(\gamma_{min},\eta)$ is constant. The slope of $K(q,\eta)$ as $q\rightarrow 1$ changes as a function of η; this

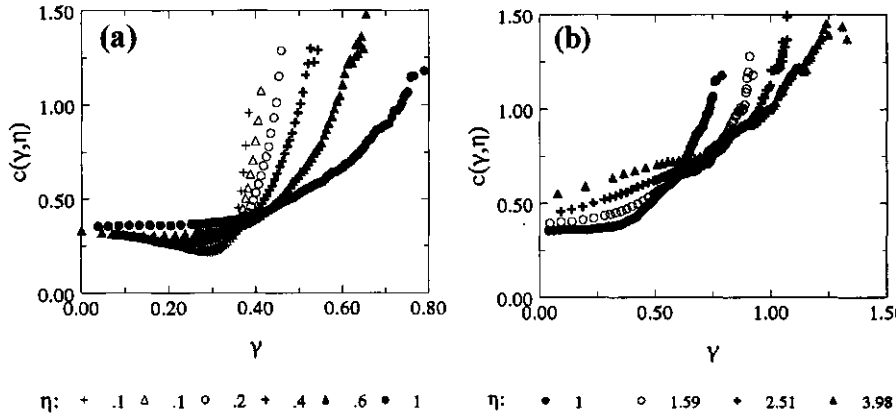

Figure 5.41 Empirical codimension functions $c(\gamma,\eta)$ that describe the scaling of the probability distributions of rainfall on time scales from 15 minutes up to 10.7 days. The functions were obtained for different η-renormalized versions of 15-minute rainfall from Vale Formoso, from 1963 to 1985. The functions represented are: (a) for $\eta \leq 1$; and (b) for $\eta \geq 1$. The legend indicates the value of the moment η.

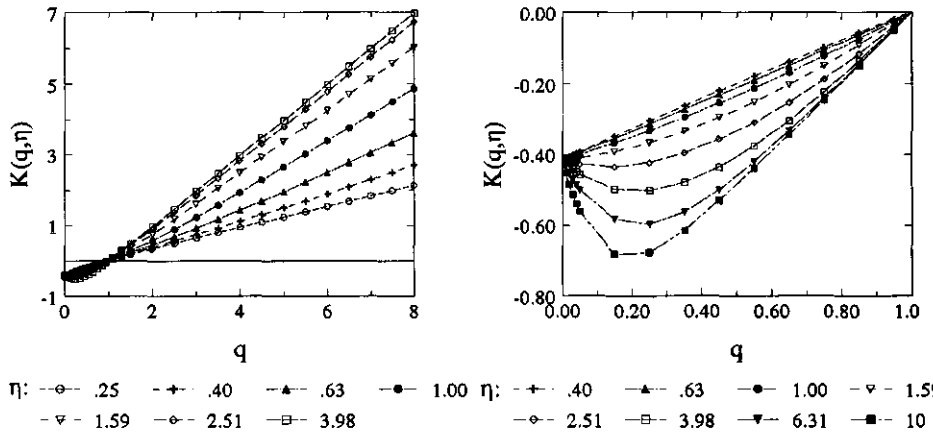

Figure 5.42 Empirical moments scaling functions $K(q,\eta)$ that describe the scaling of the moments of different η-renormalized versions of rainfall on time scales from 15 minutes up to 10.7 days. The data are 15-minute rainfall from Vale Formoso, from 1963 to 1985. The plot on the right hand side shows a detail of the functions for q-moments smaller than 1. The legend indicates the value of the moment η.

indicates (and confirms) that the codimension of the singularity of the mean of the process is a function of η.

The empirical functions $K(q,\eta)$ in Figure 5.42 consist of both non-linear and linear sections. The linear behaviour occurs for both large and small values of the moment q. For the smaller values of q, this behaviour is caused by the absence of weak orders of singularity in the data analyzed. It can be the result of a minimum (non-zero) detection limit of the measuring device (i.e. the measuring device cannot capture the complete dynamic range of the process). Otherwise, it would mean that such events are absent in the underlying multifractal process. The reason the function $K(q,\eta)$ becomes linear for large moments q can be explained with first-order or second-order phase transitions. The critical moments are different for different values of the moment η, and they are either $q_{D,\eta}$ or $q_{s,\eta}$.

Estimating the moment $q_{D,\eta}$ from the histograms of η-renormalized versions of the process

Moments $q_{D,\eta}$ can be estimated from the absolute values of the slopes of the algebraic tails of the probability distributions of the ('new') η-renormalized versions of the observed process (hereafter called η-histograms). To obtain the η-histograms at various levels of resolution, the rainfall data is renormalized at the highest resolution (i.e. 15 minutes) and averaged out on larger scales.

Figure 5.43 shows the histograms obtained after different η-renormalized 15-minute rainfall is averaged on 30-minute intervals. Figure 5.43(a) shows histograms for a few η-moments smaller than 1, and Figure 5.43(b) shows histograms for a few η-moments larger than 1. The slope of the algebraic tails of the histograms varies with the moment η. Slopes increase (decrease) with decreasing (increasing) magnitude of η.

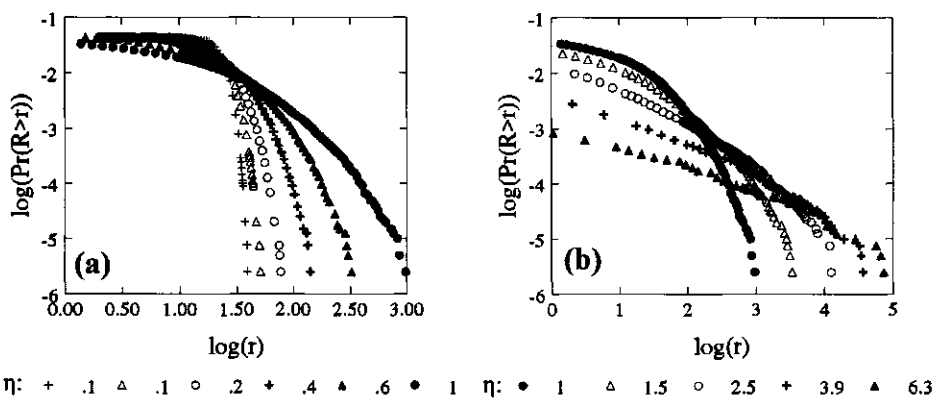

Figure 5.43 Histograms of η-renormalized rainfall on 30-minute intervals: (a) for $\eta \leq 1$; and (b) for $\eta \geq 1$. The data are 15-minute rainfall from Vale Formoso (from 1963 to 1985) averaged out on 30-minute intervals. The legend indicates the value of the moment η.

Figure 5.44 and Figure 5.45 show histograms of η-renormalized versions of rainfall on different scales. Figure 5.44 shows, for η=0.25, the histograms for scales of 16 hours, 32 hours, and 2.7 days. Figure 5.45 shows, for η=3.98, the histograms for 15 minutes, 30 minutes, 1 hour, 2 hours, and 4 hours. Figure 5.44 and Figure 5.45 show that the value of the critical moment $q_{D,\eta}$ is independent of the time scale; the slope of the algebraic tails of the histograms is roughly the same as the scale changes.

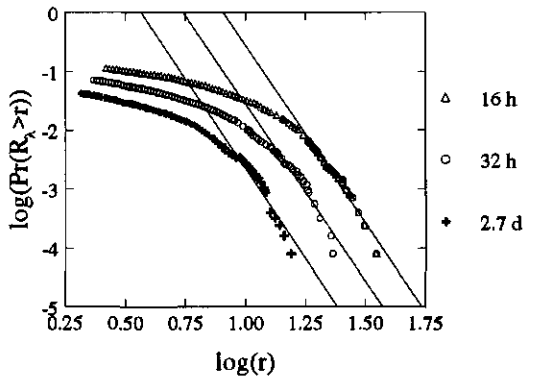

Figure 5.44 Histograms of η-renormalized rainfall on different scales, for η=0.25. The histograms are for 16 hours, 32 hours, and 2.7 days (the histograms were offset vertically so as not to overlap). The data are η-renormalized versions of 15-minute rainfall from Vale Formoso (from 1963 to 1985) averaged out on the different time-scales.

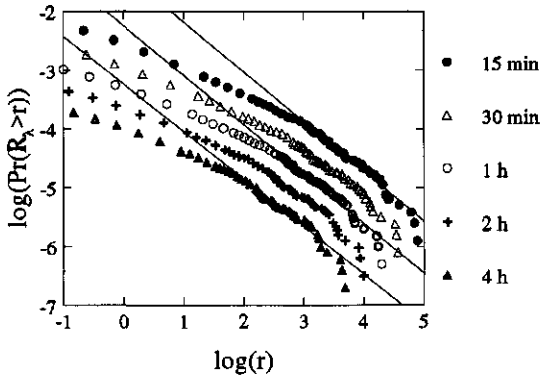

Figure 5.45 Histograms of η-renormalized rainfall on different scales, for η=3.98. The histograms are for 15 minutes, 30 minutes, 1 hour, 2 hours, and 4 hours (the histograms were offset vertically so as not to overlap). The data are η-renormalized versions of 15-minute rainfall from Vale Formoso (from 1963 to 1985) averaged out on the different time-scales.

In Figure 5.44, the absolute values of the slope of the regression lines fitted to the tails of the histograms are (from top to bottom) 6.1, 6.0, and 6.1. In Figure 5.45, the absolute values of the slope of the regression lines fitted to the tails of the histograms are between 0.85 (for 15-minute time-scales) and 0.81 (for 4-hour time scales). The behaviour exhibited by the last point of the tails of the histograms may be a consequence of the sample limitations that were discussed earlier (see Section 3.3.1).

Construction of the phase-diagram

In Figure 5.46, the phase-diagram plotted in the plane (η,q), 'summarizes' some statistical properties of the temporal rainfall process observed at Vale Formoso. The diagram is based on the study of rainfall in the 23 years' period (from 1963 to 1985), and in single years. It is constructed from the critical exponents associated with multifractal phase transitions of the first and second order. Therefore, two different types of statistical behaviour are represented: one for the moments $q_s^{(\eta)}$ (the behaviour is explained by a second-order phase transition), and another one for the moments $q_D^{(\eta)}$ (the behaviour is due to a first-order phase transition). For very large η-moments, one has the degeneracy phase; for moderate η-moments and for sufficiently large q-moments, one finds a transition from *soft* to *hard* phase; whereas for sufficiently low η-moments, one obtains transition to spurious scaling (see Schertzer and Lovejoy, 1993).

The critical exponents are important for the range of singularities γ, in $c(\gamma)$, and of moments q, in $K(q)$, where 'universal' multifractal behaviour is expected in the dynamics of rainfall.

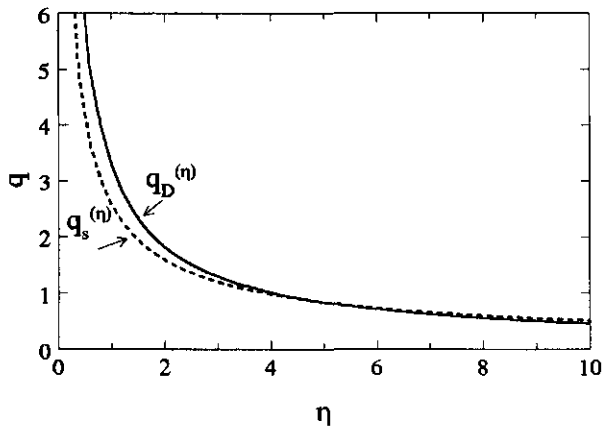

Figure 5.46 Multifractal phase-transition diagram on the plane (η,q) obtained with 15-minute rainfall data from Vale Formoso, Portugal. The line $q_D^{(\eta)}$ corresponds to first-order phase transitions and the line $q_s^{(\eta)}$ corresponds to second-order phase transitions.

5.3.5 Seasonal variation and multifractal rainfall

The previous analyses have not dealt with the investigation of any seasonal characteristic of temporal rainfall. However, this process exhibits often quite pronounced seasonal patterns. Such type of behaviour is observed in Vale Formoso (Portugal) with a wet season (in winter), and a marked dry season (in summer) lasting for several months (see Section 4.2). 'Local' analysis (i.e. in time) of point-rainfall may reveal to be of practical interest (e.g. to relate the rainfall process/events with other rainfall-induced process/events). The behaviour will then be dominated by the local presence and/or absence of certain singularities.

This Section deals with seasonal variations in the multifractal behaviour of rainfall. The study uses data from Vale Formoso (Portugal). It is based on the multifractal analysis of rainfall over four equally long periods defined within the year. With this choice of relatively long periods of 3 months, one expects to overcome the year-to-year variability observed in the rainfall process. The four trimesters of the year were defined from October to December, January to March, April to June, and July to September. The choice of these trimesters was based on the average wettest trimester, which was determined from monthly rainfall observed in the period from 1932 to 1990 (see Section 4.2). During this period, those trimesters contributed (on average) to the annual rainfall in the following way: 40% from October to December, 36% from January to March, 19% from April to June, and 5% from July to September.

The multifractal structure of rainfall, observed on the 3-month periods defined above, is studied in this Section with 15-minute rainfall data from Vale Formoso, from 1963 to 1985 (see Sections 4.2 and 5.3.1). The statistics are accumulated for the same (i.e. corresponding) period within the year, over the 23 years. The investigation of seasonal variations in the multifractal behaviour is conducted by comparing the multifractal exponent functions that describe the scaling of the probability distributions and moments of the rainfall intensity on each of the trimesters. The 'universal' parameters that characterize the multifractal temporal structure of rainfall on the different periods are also compared.

The normalization of the rainfall intensity on each of the trimesters was done with the 23-years average rainfall-intensity on the corresponding period. These intensities are shown in Table 5.3.

Table 5.3 Average rainfall-intensity observed during the four trimesters and the full annual period, from 1963 to 1985. The data are 15-minute rainfall from Vale Formoso.

	October to December	January to March	April to June	July to September	annual period
average rainfall-intensity (mm/h)	0.082	0.077	0.049	0.011	0.052

Box-counting analysis

Figure 5.47 shows the box-counting log-log plots for the rainfall observed, from 1963 to 1985, in each of the four trimesters: October to December, January to March, April to June, and July to September. For comparison, the box-counting plot obtained for the full annual period (i.e. from October to September) is shown also in Figure 5.47. This Figure shows scales ranging from 15 minutes (box-size 1) up to 85.3 days (box-size 8192). The rainfall threshold used in the box-counting analysis is the value imposed by the rainfall measuring device and data-processing techniques (see Sections 4.2 and 5.3.1).

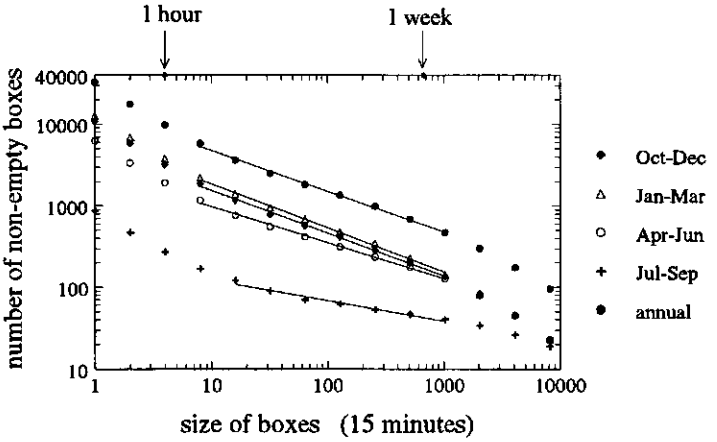

Figure 5.47 Box-counting log-log plots obtained with 15-minute rainfall from Vale Formoso (from 1963 to 1985), observed in the full annual period and in the four trimesters indicated in the legend. A box of unit size corresponds to 15 minutes. The slopes of the regression lines are (from top to bottom) 0.50, 0.53, 0.54, 0.44, and 0.25.

The behaviour displayed by the left-hand side sections of the plots in Figure 5.47 corresponds to the type of 'saturation' discussed in Section 5.3.1 (see also Figures 6.1 and 6.2). It affects scales from 15 minutes up to about 1 to 2 hours. The absolute values of the slopes of the regressions lines fitted to 15 minutes up to 1 hour are (for the periods represented from top to bottom, in Figure 5.47) 0.88, 0.88, 0.87, 0.85, and 0.84; these regression lines are not shown. These results suggest that the intermittency of rainfall is not well captured over this range of scales (e.g. by the measuring device and/or the digitization technique). Consequently, in the record, the rainfall appears less sparse (i.e. the fractal dimension is larger) than on larger scales. The straight lines shown in Figure 5.47 are fittings to the middle sections of the plots, over the range of scales from 2 hours (box-size 8) up to 10.7 days (box-size 1024). The absolute values of the slope of these lines yield estimates for the fractal dimension of the geometric set defined (in the 1-dimensional space of time) for rainfall occurrences on this range of scales. These

dimensions are (also from top to bottom in Figure 5.47) 0.50, 0.53, 0.54, 0.44, and 0.25. For the period from July to September, the regression was over the range of scales from 4 hours up to 10.7 days. In some of the cases analyzed the scale-invariance seems to extend to scales larger than one-and-a-half weeks. The fractal dimensions quantify the sparseness of the rainfall events on the various periods studied.

Scaling of the probabilities

Figure 5.48 shows log-log plots of the probability of exceeding rainfall intensity levels of singularity γ, observed on scales from 15 minutes ($\lambda = 8192$) up to 85.3 days ($\lambda = 1$), against the corresponding scale ratio λ. Figure 5.48(a) to Figure 5.48(d) are for rainfall in the following periods: (a) October to December, (b) January from March, (c) April to June, and (d) July to September.

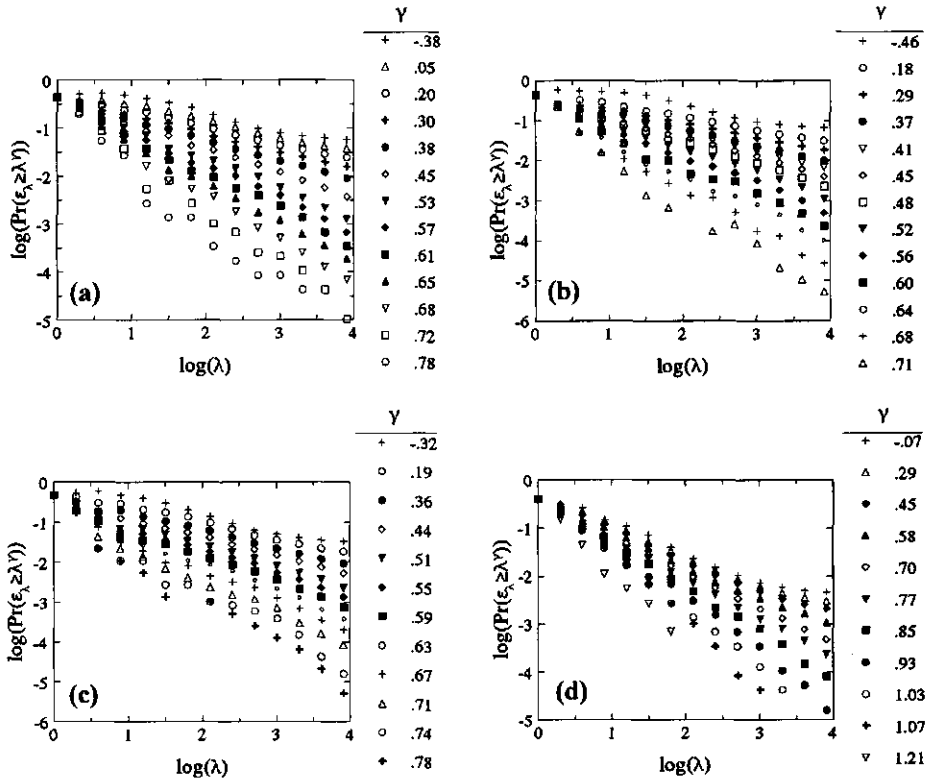

Figure 5.48 Log-log plots of the probability of exceeding rainfall intensity levels of singularity γ, observed on time scales from 15 minutes ($\lambda = 8192$) up to 85.3 days ($\lambda = 1$), against the scale ratio λ. The data are 15-minute rainfall, from Vale Formoso (from 1963 to 1985), in the periods from: (a) October to December; (b) January to March; (c) April to June; and (d) July to September. The legend indicates the order of singularity γ of the rainfall intensity ε_λ.

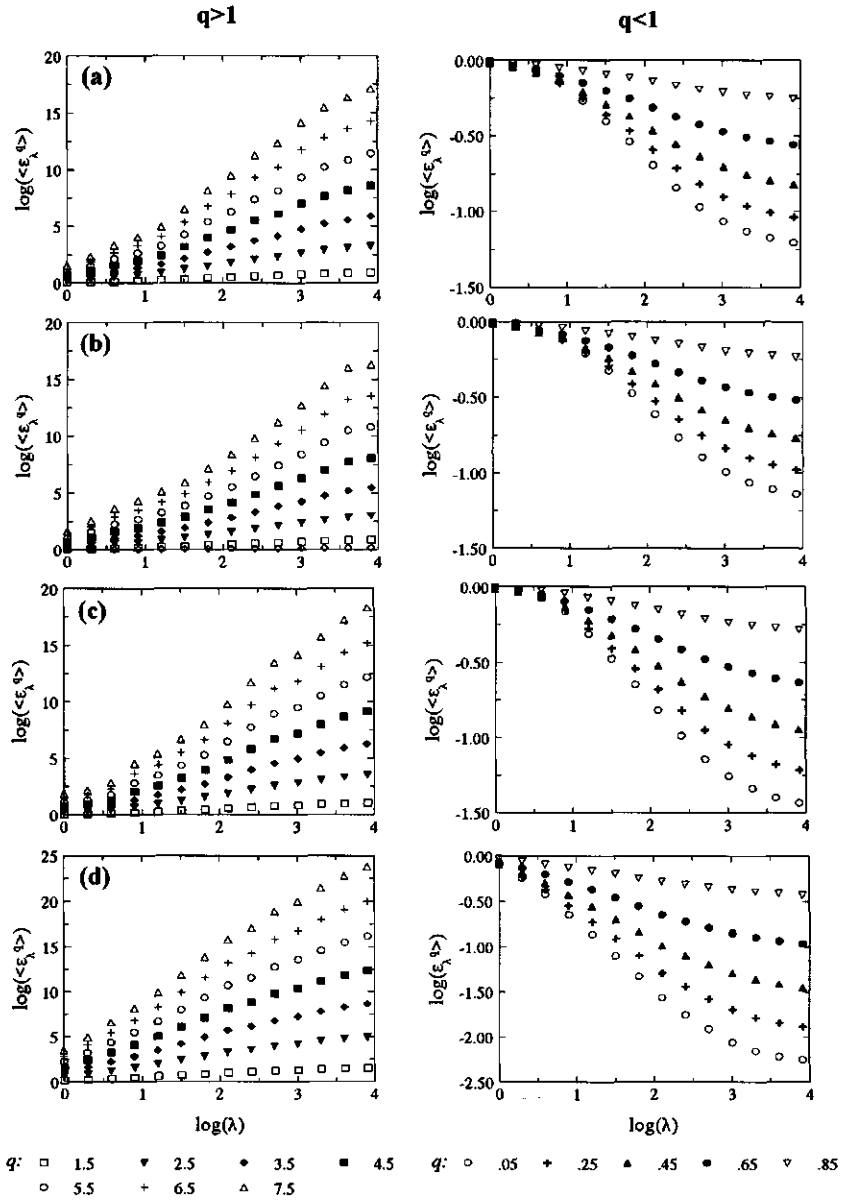

Figure 5.49 Log-log plot of the average q^{th} moments of the rainfall intensity ε_λ on time scales from 15 minutes (λ=8192) up to 85.3 days (λ=1), against the scale ratio λ. The data are 15-minute rainfall from Vale Formoso (from 1963 to 1985), in the periods from: (a) October to December; (b) January to March; (c) April to June; and (d) July to September. The plots on the left-hand side show the behaviour for moments larger than 1 and the plots on the right-hand side show the behaviour for moments smaller than 1 (see legend).

Scaling (power-law) behaviour is maintained over the range of scales from 15 minutes up to at least one-and-a-half weeks. Similarly to what was observed earlier (see Section 5.3.1), some deviations from the (expected) power-law behaviour can be observed for the very low rainfall-intensities (small singularities) and for the high rainfall-intensities (large singularities). One expects that the rainfall dynamics related to these ranges of rainfall intensities is not captured properly by the measuring device. Moreover, tone expects that those intensities are affected by the data digitization technique (this is discussed in Sections 4.2 and 5.3.1). Consequently, the scaling behaviour exhibited by the low rainfall-intensities on time scales smaller than about 2 hours may be affected by these data limitations. The scaling of the high rainfall-intensities is believed to be affected mainly by undersampling. These problems decrease the reliability of the estimates related to the low and high rainfall-intensities.

Scaling of the moments

Figure 5.49 shows log-log plots of the average q^{th} moments of the rainfall intensity ε_λ on scales from 15 minutes (λ=8192) up to 85.3 days (λ=1), against the corresponding scale ratio λ. Figure 5.49(a) is for rainfall from October to December, Figure 5.49(b) is for rainfall from January to March, Figure 5.49(c) is for rainfall from April to June, and Figure 5.49(d) is for rainfall from July to September. Scaling behaviour is maintained over the range of scales from 15 minutes up to at least one-and-a-half weeks, for a range of q-moments. At the very low and very high rainfall-intensities, the behaviour deviates from the expected power-law holding on the larger scales in the plot. It indicates the presence of critical (small) scales. The scaling 'problems' are expected to be caused by data limitations. Similar problems affect also the scaling of the probabilities (Figure 5.48), both for the low and high singularities γ (see also Section 5.3.1), up to scales of about 2 hours. One expects that the aggravation of the scaling problems observed for the rainfall from July to September (see Figure 5.48(d) and Figure 5.49(d)) is due to undersampling.

The number of (independent) samples of 85.3 days available for the study of the different trimesters is 23. The samples come from different years; therefore, they are surely independent. This may not be the case with the 98 samples of 85.3 days defined for the full annual period, because their total independence is not guaranteed. The process is analyzed in time without interruptions. Moreover, although the number of (independent) samples is presumably the same for all the four trimesters analyzed in this Section, the amount of 'information' that is analyzed effectively is affected by the number of zeros in the data. Thus, there are important differences between a 'wet' and a 'dry' period. In a 'dry' period there are several zero-rainfall samples and many 'rain-free' intervals from 15 minutes up to 10.7 days ('realizations').

Table 5.4 gives some information about the different cases analyzed in this Section (some of the values presented were obtained with box-counting analysis). Their effective dimensions are, thus, difficult to estimate.

Table 5.4 Some information about the rainfall samples analyzed. A 'realization' corresponds to the rainfall observed on scales from 15 minutes up to 10.7 days. Each sample includes 8 'realizations' and is 85.3 days long. The data are 15-minute rainfall from Vale Formoso, from 1963 to 1985.

	October to December	January to March	April to June	July to September	annual period
number of samples	23	23	23	23	98
number of realizations	184	184	184	184	784
number of rain-free samples	0	0	0	4	3
number of rain-free realizations	49	41	57	144	311
number of rainy realizations	135	143	127	40	473
% of rainy realizations	73	78	69	22	60
average rainfall-intensity (mm/h)	0.082	0.077	0.049	0.011	0.052

Multifractal scaling exponent functions

The empirical functions

Figure 5.50 shows the empirical exponent functions that describe the scaling of the probability distributions of the rainfall intensity on scales from 15 minutes up to 10.7 days, for the four sub-periods of the year and for the full annual period (see also Section 5.3.1). The functions are plotted in the same Figure to facilitate their comparison. In Figure 5.50 the dashed line is $c(\gamma)=\gamma$. The differences between the empirical scaling functions determined for the different periods are discussed below. The empirical codimension functions in Figure 5.50 show the effect of a lower 'cut-off' in the rainfall singularities present in the data. The functions are 'flat' for small singularities. It indicates the existence of a minimum codimension that can be explained (at least partly) by the observation scheme of the rainfall process. Some of the functions also show linear behaviour for the large singularities, which is empirical evidence of first-order multifractal phase transitions. This behaviour is clearly seen in the functions for the rainfall from October to December, January to March, and April to June. It is difficult to distinguish such behaviour in the empirical codimension function corresponding to the ('smallest') sample (i.e. from July to September). The behaviours of the codimension functions for the first two trimesters support the estimate of the critical order for divergence of moments $q_D \approx 3.1$ (see Section 5.3.1). The behaviour of the codimension function derived for the data from April to June gives an estimate of the critical moment of 2.3.

Figure 5.50 shows clearly the upper boundary of the codimension functions determined from finite samples. The codimension $c(\gamma_{max})$ obtained for the different cases is consistent with the differences in the (effective) size of the samples (see Table 5.4); the effective dimension

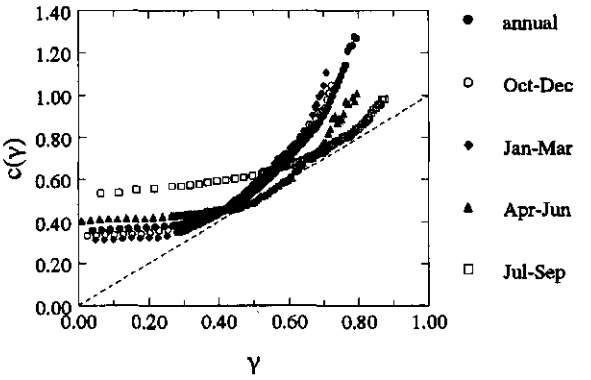

Figure 5.50 Empirical codimension functions that describe the multifractal behaviour of rainfall on the range of scales from 15 minutes up to 10.7 days. The data are 15-minute rainfall from Vale Formoso, from 1963 to 1985. The different functions are for the full annual period and for the sub-periods from October to December, January to March, April to June, and July to September. The straight dashed line is $c(\gamma)=\gamma$.

$c(\gamma_{max})$ (in Eq. (3.35)) is larger for the (effectively) largest samples. The singularities γ_{max} (i.e. the largest singularity estimated reliably from a finite sample) are larger, for example, for the samples from April to June, and from July to September, than for the 'ensemble' (i.e. for the full period). This is a consequence of determining 'locally' (i.e. in time) the statistics of rainfall. Table 5.3 indicates the average values that were used to normalize the rainfall intensity on the different periods studied.

Figure 5.51 shows the empirical exponent functions that describe the scaling of the moments of the rainfall intensity on scales from 15 minutes up to 10.7 days, observed in the four trimesters. These functions are plotted together with the function that characterizes rainfall on the full annual period. In Figure 5.51, the plot for the period from October to December is 'hidden' behind the plot corresponding to the full year. The empirical moments scaling functions for the different trimesters exhibit differences between them.

The functions in Figure 5.51 are non-linear for only a range of values. They exhibit linear behaviour for moments smaller than roughly 0.3. This behaviour indicates the presence of a minimum singularity γ_{min} and codimension $c(\gamma_{min})$. This is consistent with the lower bounded behaviour observed in the codimension functions, for the small singularities (see Figure 5.50).

For the large moments, linear behaviours are also observed in all the functions $K(q)$ in Figure 5.51. However, the critical moment is not always the same. This behaviour is discussed further below. For large moments q, the slopes of the linear asymptotes of the various functions $K(q)$ give estimates of the singularities γ_{max}, and the intercepts estimates of $-c(\gamma_{max})$. These values $(\gamma_{max}, c(\gamma_{max}))$, estimated from the empirical functions $K(q)$ in Figure 5.51, are

indicated in Table 5.5; they agree reasonably well with the empirical codimension functions in Figure 5.50. The function $K(q)$ determined for the rainfall from July to September shows the lowest intercept of the small-moments asymptote (thus, the largest $c(\gamma_{min})$) and the largest slope of the linear asymptote for the large moments (thus, the largest γ_{max}). These results agree with the corresponding codimension function in Figure 5.50.

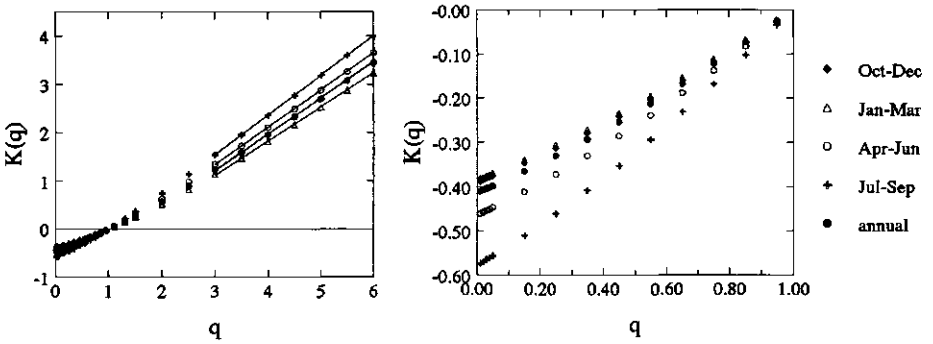

Figure 5.51 Empirical moments scaling functions that describe the multifractal behaviour of rainfall on the range of scales from 15 minutes up to 10.7 days. The data are 15-minute rainfall from Vale Formoso, from 1963 to 1985. The different functions are for the full annual period and for the sub-periods from October to December, January to March, April to June, and July to September. The plot on the right-hand side shows a detail of the functions $K(q)$ for moments q smaller than 1.

Table 5.5 Summary of estimates of the critical orders of singularities and codimensions obtained directly from the empirical moments scaling exponent functions (before and after rescaling the functions with respect to C_1). The data are 15-minute rainfall from Vale Formoso, from 1963 to 1985. The results are given separately for the different trimesters and for the full annual period.

	October to December		January to March		April to June		July to September		annual period (Oct-Sep)	
before after	before	after	before	after	before	after	before	after	before	after
γ_{min} γ_{min}/C_1	0.31	0.61	0.32	0.67	0.37	0.63	0.47	0.67	0.33	0.64
$c(\gamma_{min})$ $c(\gamma_{min})/C_1$	0.39	0.80	0.39	0.84	0.47	0.82	0.58	0.84	0.41	0.82
γ_{max} γ_{max}/C_1	0.76	1.54	0.71	1.54	0.77	1.35	0.82	1.19	0.75	1.48
$c(\gamma_{max})$ $c(\gamma_{max})/C_1$	1.10	2.17	1.05	2.21	1.00	1.72	0.93	1.34	1.07	2.04

There are discrepancies between the estimates of the (geometric) fractal dimension $D=1-c(\gamma_{min})$ (determined from the scaling functions $c(\gamma)$ and $K(q)$), and the estimate of D obtained from box-counting analysis (see Figure 5.47). The box-counting estimates lead to smaller values of D. The different estimates are expected to be affected by the scaling problems observed at the small singularities and by the (different) range of scales that was used for the box-counting estimates and for the other estimates.

'Universal' multifractals

Figure 5.52 shows, for a few q-moments, the DTM plots of $\log(|K(q,\eta)|)$ against $\log(\eta)$ for rainfall in the periods from: (a) October to December, (b) January to March, (c) April to June, and (d) July to September. The moments scaling functions were estimated for the range of scales from 15 minutes up to 10.7 days.

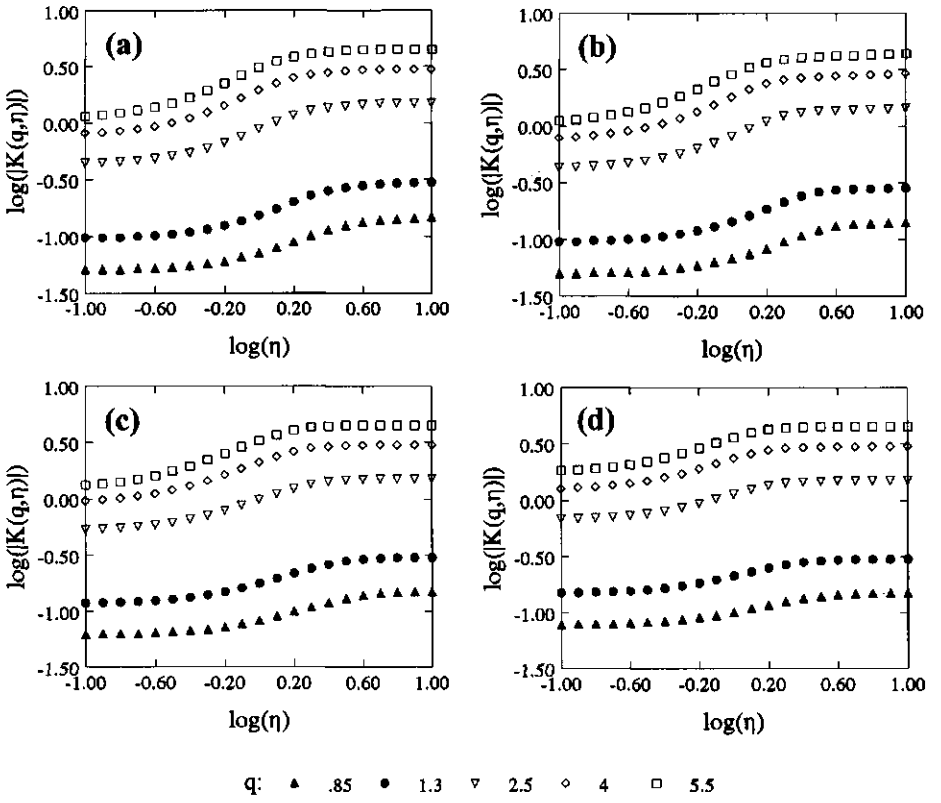

Figure 5.52 DTM plots of $\log(|K(q,\eta)|)$ versus $\log(\eta)$ estimated for rainfall on the range of scales from 15 minutes up to 10.7 days, for the periods from: (a) October to December; (b) January to March; (c) April to June; and (d) July to September. The data are 15-minute rainfall from Vale Formoso, from 1963 to 1985.

DTM analysis yields the estimates for the 'universal' multifractal parameters α and C_1 indicated in Table 5.6 (the estimates resulted from the analysis of 13 q-values). The values of C_1 agree well with the estimates obtained from the empirical moments scaling functions in Figure 5.51 (it is $K'(1)=C_1$; see Table 5.7). They also agree well with the estimates obtained from the empirical codimension functions in Figure 5.50. Figure 5.50 and Figure 5.51 show that the value of C_1 is larger for the summer period, with less rainfall. Because the parameter C_1 is the codimension of the mean singularity, this means a more sparse process. Analyses of the empirical functions $c(\gamma)$ show that the parameter H is nearly 0. Therefore, C_1 equals also the mean singularity. Thus, the larger value C_1 also indicates the greater intermittency and variability of the rainfall in this period. The higher rainfall intensities in Vale Formoso are known to be associated with the convective storms occurring in the end of the summer. These storms are responsible for enormous amounts of soil loss registered in this time of the year, in the region of Vale Formoso.

Table 5.6 DTM estimates of the 'universal' multifractal parameters C_1 and α that characterize the multifractal behaviour of rainfall on scales from 15 minutes up to 10.7 days for different periods defined within the year, over 23 years. The data are 15-minute rainfall from Vale Formoso, from 1963 to 1985.

Period	Average rainfall (mm/h)	C_1	α
October-December	0.082	0.49±0.02	0.52±0.05
January-March	0.077	0.46±0.02	0.52±0.05
April-June	0.049	0.57±0.02	0.40±0.04
July-September	0.011	0.69±0.02	0.31±0.04
annual period (Oct-Sep)	0.052	0.51±0.02	0.49±0.04

Table 5.7 Estimation of the multifractal parameter C_1 by an approximation to the derivative of the empirical function $K(q)$ at q=1. The functions were determined for the range of scales from 15 minutes up to 10.7 days. The data are 15-minute rainfall from Vale Formoso, from 1963 to 1985.

Period	$K(0.95)$	$K(1.1)$	$C_1=K'(1)\approx(K(1.1)-K(0.95))/2$
October to December	-0.024	0.050	0.49
January to March	-0.023	0.047	0.47
April to June	-0.028	0.058	0.57
July to September	-0.034	0.070	0.69
annual period (Oct-Sep)	-0.025	0.051	0.51

The periods studied in this Section were selected based on a seasonal pattern of rainfall. Therefore, there are obvious differences between the samples. The 'universal' multifractal parameters seem to be able to make a distinction between the different types of events and patterns of rainfall.

Rescaling the exponent functions

Figure 5.53 shows the rescaled empirical functions (dotted lines) $c(\gamma)/C_1$ against γ/C_1, for the different periods within the year and for the full year. The scaling functions are plotted in the same Figure to facilitate the comparison of results. In all the cases, the statistics are for 23 years. After rescaling, the codimension functions coincide (see also Figure 5.50). This indicates that the rainfall on the various periods studied belong to the same 'universality' class of multifractals.

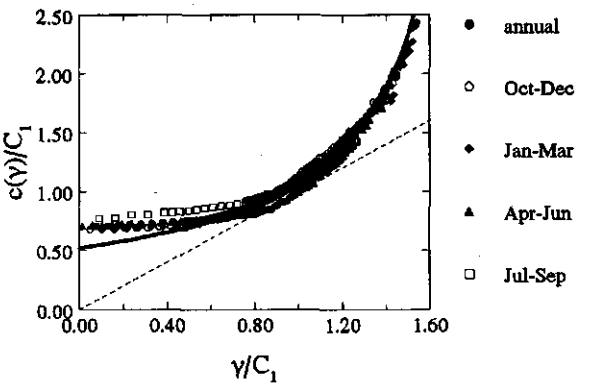

Figure 5.53 Empirical codimension functions (dotted lines) that describe the multifractal behaviour of rainfall on the range of scales from 15 minutes up to 10.7 days (for different sub-periods of the year and for the full year), plotted with the theoretical line with $\alpha=0.49$ (solid line). The data are 15-minute rainfall from Vale Formoso, from 1963 to 1985. The functions were rescaled with respect to C_1. The straight dashed line is $c(\gamma)=\gamma$.

One expects that the small differences between the empirical curves are explained by uncertainties in the estimates resulting from, for example, (statistical) undersampling. The 'universal' theoretical codimension function with parameter value $\alpha=0.49$ (obtained for the full annual period, see Section 5.3.1) is represented also in Figure 5.53 (solid line). There is good agreement between the empirical and theoretical curves for a finite range. The discrepancy at small and large γ-singularities was already discussed. For small γ, it is explained by 'noise' introduced by measurement limitations and the presence of zero-values in the data; whereas for large γ, it is caused by divergence of moments.

In Figure 5.54, and for the different periods that are being analyzed, the empirical (rescaled) functions $K(q)/C_1$ were plotted against the moment q. This Figure shows both the moments scaling functions corresponding to the different trimesters and the (ensemble) moments scaling function corresponding to the full year; the statistics are for 23 years. The moments scaling functions coincide for moments smaller than 2-3. There is only a small discrepancy for the very small moments. This range of small moments corresponds to the not well defined range of small rainfall-intensities that exhibit poor scaling (see Figure 5.49). The empirical moments scaling functions plotted in Figure 5.54 show linear behaviour for moments smaller than roughly 0.3. The slopes of these linear segments of the functions and their intercept are given in Table 5.5; the slope is an estimate of γ_{min}/C_1 and the intercept is an estimate of $-c(\gamma_{min})/C_1$.

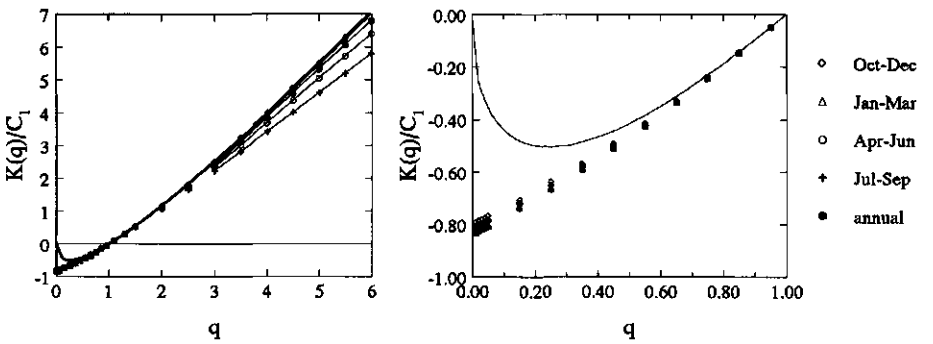

Figure 5.54 Empirical moments scaling functions (dotted lines) that describe the multifractal behaviour of rainfall on the range of scales from 15 minutes up to 10.7 days (for different sub-periods of the year and for the full year), plotted with the theoretical line with parameter α=0.49 (solid line). The data are 15-minute rainfall from Vale Formoso, from 1963 to 1985. The functions were rescaled with respect to C_1. The plot on the right-hand side shows a detail of these functions for moments q smaller than 1.

For the larger moments, the differences between the empirical moments scaling functions are expected to be caused by sample variations (e.g. the 'effective' sample size, the maximum rainfall-intensity observed in the different samples). For moments larger than a critical order (where the first or second derivative of the function $K(q)$ is discontinuous), the functions $K(q)$ are highly dominated by the largest singularity present in the corresponding samples. The selection of the sub-periods picked up characteristic 'wet' and 'dry' periods; this may explain why the functions for the 'wet' periods appear above the ensemble function although they were determined from smaller samples. The ensemble function was determined including all zero-rainfall periods; this lowers necessarily the average $\langle \varepsilon_\lambda{}^q \rangle$ in comparison to the value one would obtain for periods with less zero-rainfall intervals and the same γ_{max}. Table 5.5 gives, for the different cases, the 'new' estimates of the maximum (rescaled) order of singularity and codimension estimated reliably from the different samples: $(\gamma_{max}/C_1, c(\gamma_{max})/C_1)$. These

estimates were determined directly from the empirical (rescaled) moments functions (i.e. from the slope and intercept of the straight lines fitted to the linear sections of the empirical functions, for large moments).

For moments $q>1$, the critical moment associated with the linear behaviour of the moments scaling functions is the same for the ensemble function (determined for the full year) and the functions corresponding to the periods defined from October to December, and from January to March. The critical moment is $q_D \approx 3.1$ (see Section 5.3.1). The corresponding linear sections of the functions $K(q)$ intersect each other approximately at this value of q. This estimate of the critical order for divergence of moments agrees with the behaviour of the codimension functions in Figure 5.50, and the previous analyses in Section 5.3.1.

For the period from April to June, the critical moment associated with the discontinuity in the function $K(q)$, observed for large moments, is below the order 3. This result is consistent with the previous estimate of the moment q_D, for this case. The smaller order of q_D may indicate a more 'violent' behaviour of the rainfall in this period, or it may result from statistical uncertainty.

For the period from July to September, the critical moment in the function $K(q)$ is clearly lower than for the other cases, at around $q=2$. The function $c(\gamma)$ shows non-linear behaviour for the large singularities present in the sample.

The values of the critical moment q_s were estimated for the different cases using Eq. (3.49). The calculation used the DTM estimates of the multifractal parameters in Table 5.6, and the estimates of $c(\gamma_{max})$ in Table 5.5. The estimates of q_s were larger than 4 for the different cases; the exception was the estimate for the rainfall during the period from July to September, of $q_s \approx 2.6$. One expects that the type of special statistical behaviour observed for the data from July to September is a second-order phase transition (caused by the finite size of the sample), whereas the behaviour displayed by the scaling functions derived for the other periods corresponds to first-order phase transitions (explained by divergence of moments).

In Figure 5.54, the theoretical function for $\alpha=0.49$ is represented by a solid line (see Section 3.3.1). There is good agreement between the theoretical and empirical curves only for a range of values. For moments $q<1$, the critical moment is around 0.6 for all the cases analyzed. For moments $q>1$, the critical order of moments is different for the different functions (see also above).

The behaviour of the empirical scaling functions indicates that the process has the same type of dynamic behaviour throughout the year (i.e. belongs to the same multifractal class). Results show that annual rainfall patterns should be taken into account in simulations of the rainfall process involving large time-scales.

5.4 Analysis of rainfall from Assink

This Section deals with the analysis of 11 years of hourly precipitation from Assink (The Netherlands), recorded from 1976 to 1986. In this period, the average annual precipitation was 826.0 mm. The data are from a recording gauge of the float type with a fixed time-resolution of 15 minutes (details about the data are given in Section 4.3). This study uses hourly precipitation, which resulted from the aggregation of 15-minute data during 1-hour intervals. The data include the measurement of rain and snow. The term rainfall is used in the text to refer to precipitation (rainfall and snowfall).

The fractal structure of rainfall

Figure 5.55 shows the box-counting plot obtained with the hourly rainfall, for time scales from 1 hour up to 2.84 months. The plot accumulates the statistics over the 11 years covered by the data. Rainfall occurrences on the range of scales from 1 hour up to about 4.5 days are characterized by a fractal dimension 0.56. This value is estimated from the absolute value of the slope of the regression (heavy) line fitted to the left-hand side section of the plot. Analysis of larger time scales is affected by 'saturation.' The regression (dashed) line fitted to the right-hand side section of the plot has slope -1.

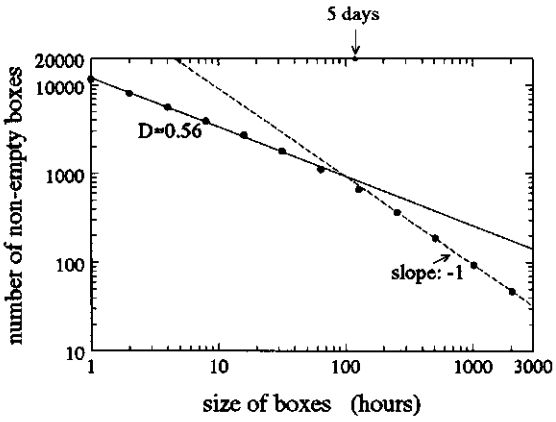

Figure 5.55 Box-counting plot obtained with hourly rainfall from Assink, from 1976 to 1986. The plot displays time scales from 1 hour up to 2.84 months.

Investigating scale-invariance with spectral analysis

The energy spectrum for the hourly rainfall is plotted in Figure 5.56. The spectrum has been smoothed for the high frequencies. It exhibits different power-law behaviour over two spectral regions. The critical scale value is roughly one week. For the higher frequency range the spectral exponent is approximately 0.23.

The spectrum does not display a clear peak corresponding to the annual cycle frequency ($\omega \approx 0.00011\ h^{-1}$). Such behaviour is observed in the spectra obtained for rainfall from Vale Formoso, which exhibit very strong signals for the annual cycle (see, for example, Figure 5.3). Instead, for the Assink data, one observes several spectral peaks, similar in magnitude; the frequencies correspond to roughly 1 year, 8.3 months, 5.9 months, and 3.8 months. This absence of a strong cyclic signal may be explained by the more regular distribution of rainfall amounts in Assink (see Figure 5.7), which is in strong contrast with the marked rainfall seasonal pattern observed in Vale Formoso (see Figure 4.4).

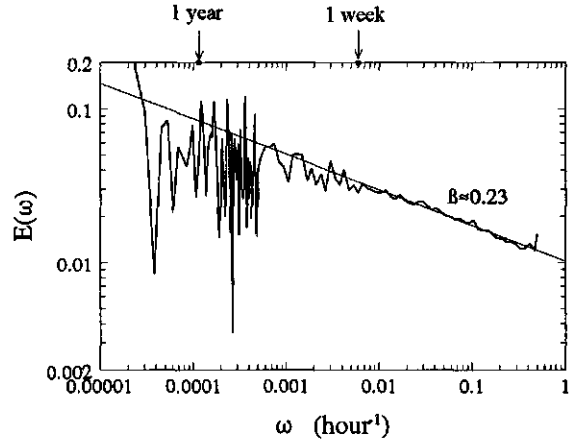

Figure 5.56 Energy spectrum obtained for hourly rainfall from Assink, from 1976 to 1986.

Scaling of the probability distributions

Figure 5.57 shows the log-log plot of the probability of exceeding rainfall intensity levels of singularity γ, observed on time scales from 1 hour (λ=1024) up to 42.7 days (λ=1), against the scale ratio λ. The orders of singularity γ of the rainfall intensity plotted in Figure 5.57 are indicated in the legend. The plot accumulates the statistics over 11 years. The scaling behaviour observed in Figure 5.57 is maintained from 1 hour up to at least 3 weeks.

Scaling of the moments

Figure 5.58 shows the log-log plot of the average q^{th} moments of the rainfall intensity ε_λ on time scales from 1 hour (λ=1024) up to 42.7 days (λ=1), against the scale ratio λ. Figure 5.58(a) shows moments larger than 1 and Figure 5.58(b) moments smaller than 1. The moments q plotted in Figure 5.58 are indicated in the legend. The plot accumulates the statistics of rainfall over 11 years.

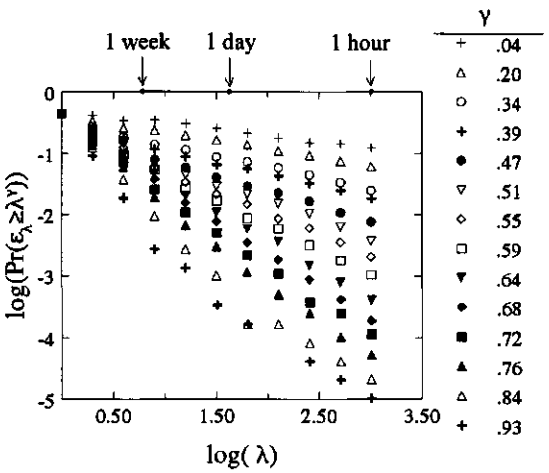

Figure 5.57 Log-log plot of the probability of exceeding rainfall intensity levels of singularity γ, observed on scales from 1 hour (λ=1024) up to 42.7 days (λ=1), against the scale ratio λ. The data are hourly rainfall from Assink, from 1976 to 1986. The legend indicates the order of singularity γ of the rainfall intensity ε_λ.

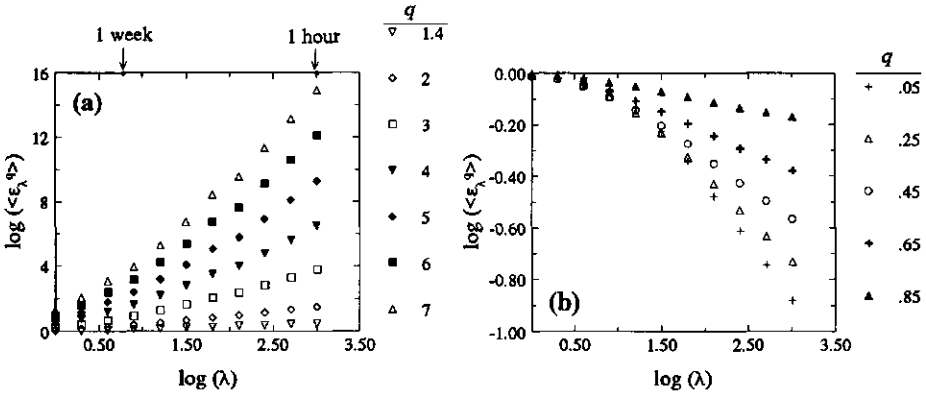

Figure 5.58 Log-log plot of the average q^{th} moments of the rainfall intensity ε_λ on scales between 1 hour (λ=1024) and 42.7 days (λ=1), against the scale ratio λ: (a) for moments larger than 1; and (b) for moments smaller than 1. The data are hourly rainfall from Assink, from 1976 to 1986.

In Figure 5.58, the scaling range seems to be smaller than it was suggested by the probability plot (see Figure 5.57). For moments larger than 1, the scaling range seems to extend from 1 hour up to at about one week. For some moments smaller than 1, which highlight the small intensities of the data, the scaling range is smaller. One expects that the scaling behaviour for the small moments is affected by an incorrect description of the rainfall process by the data,

over this range of the rainfall dynamics. This could result from the inability of the rainfall recording device to measure and/or to record rainfall intensities smaller than a characteristic value.

The scaling exponent functions

The study of the multifractality of the rainfall process is restricted to the range of scales from 1 hour up to 5.3 days. This is justified above.

Empirical codimension function

The empirical codimension function $c(\gamma)$, determined with the hourly rainfall for the range of scales from 1 hour up to 5.3 days, is plotted in Figure 5.59 (dotted line). The function consists of both non-linear and linear sections. This type of statistical behaviour indicates the presence of a first-order multifractal phase transition. The linear behaviour is observed for orders of singularity γ larger than around 0.80. The slope of this linear section of the function, of approximately 3.3, gives an estimate of the critical order of moments associated with the divergence of statistics; the intercept of this line gives an estimate of $K(q_D)\approx 1.13$. The divergence of moments larger than q_D is caused by rainfall intensities of certain (high) orders of singularity (i.e. for $\gamma > D$). This statistical behaviour leads to algebraic tails of the probability distributions of rainfall on single scales. The absolute value of the slope of these tails is q_D.

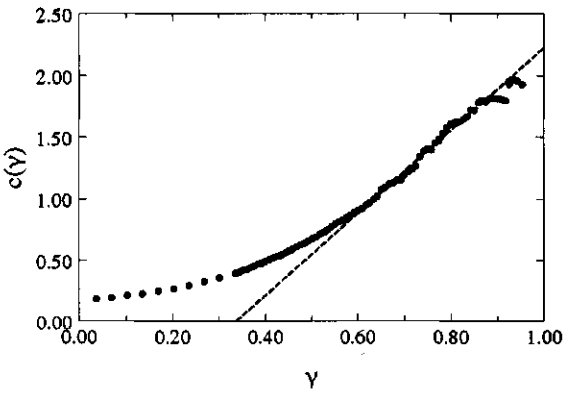

Figure 5.59 Empirical codimension function (dotted line), determined with hourly rainfall from Assink (from 1976 to 1986), for the range of scales from 1 hour up to 5.3 days.

Figure 5.60 shows, from top to bottom, the probability distributions of the rainfall intensity on scales of 1, 2, 4, and 8 hours. The histograms were offset vertically so as not to overlap. They exhibit algebraic tails, which confirms the divergence of moments. The absolute values of the slopes of the regression lines fitted to these tails are (also from top to bottom) 2.4, 2.6, 2.8, and 2.7. Thus, the estimate of the critical moment for divergence is $q_D\approx 2.6$.

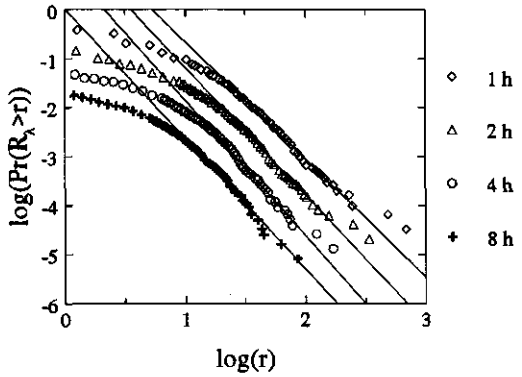

Figure 5.60 Histograms of rainfall on time scales of (from top to bottom) 1, 2, 4, and 8 hours (the histograms were offset vertically so as not to overlap). The absolute values of the slopes of the algebraic tails of the histograms are (also from top to bottom) 2.4, 2.6, 2.8, and 2.7. The histograms were obtained with hourly rainfall from Assink, from 1976 to 1986.

Empirical moments scaling function

The empirical moments scaling function $K(q)$, determined with the hourly rainfall for the range of scales from 1 hour up to 5.3 days, is plotted in Figure 5.61 (dotted line). The empirical function consists of both non-linear and linear sections. It exhibits linear behaviour for moments smaller than a critical order of around 0.7 to 0.8 (q_{min}). The slope of this linear section of the function is 0.42 (an estimate of γ_{min}), and the intercept is -0.42 (an estimate of $-c(\gamma_{min})$). The order of singularity γ_{min} represents the lower limit of the range of reliable

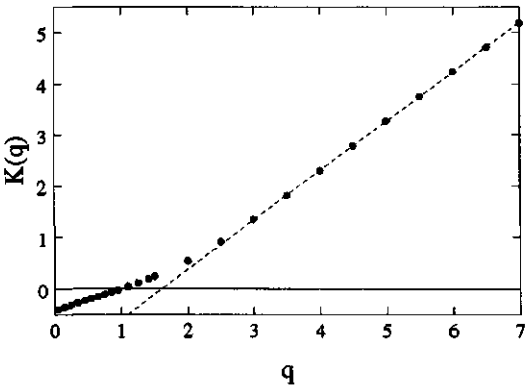

Figure 5.61 Empirical moments scaling function (dotted line) determined with hourly rainfall from Assink (from 1976 to 1986), for the range of scales from 1 hour up to 5.3 days.

γ-values present in the data. It indicates the presence of a minimum non-zero intensity in the data. The codimension $c(\gamma_{min})\approx 0.42$ corresponds to a geometric set, defined in the 1-dimensional space of time by the non-zero rainfall intervals, of fractal dimension $D=1-c(\gamma_{min})\approx 0.58$. This result is consistent with the box-counting analysis.

The function $K(q)$ also exhibits linear behaviour for moments larger than around 2.6, which is empirical evidence of a multifractal phase transition. The slope of this linear section yields an estimate of $\gamma_{max}\approx 0.96$ and the intercept an estimate of $c(\gamma_{max})\approx 1.55$. This singularity γ_{max} dominates the statistics. For $q_D=2.6$, one obtains the estimate of the dual critical singularity $\gamma_D=K'(q_D)$ of 0.87 (estimated from the empirical function $K(q)$). Also for $q_D=2.6$, the estimate of $D=K(q_D)/(q_D-1)$ is 0.62.

Another way to investigate the type of multifractal phase transition is to determine the empirical function $K(q)$ from samples of different sizes. The result is shown in Figure 5.62 for two samples with lengths of 11 years (black bullets) and 3.7 years (white bullets). Below a certain critical moment, the two empirical functions coincide; thus, they exhibit the same type of statistical behaviour. For the large moments (and above a certain critical order), both functions show linear and different behaviours.

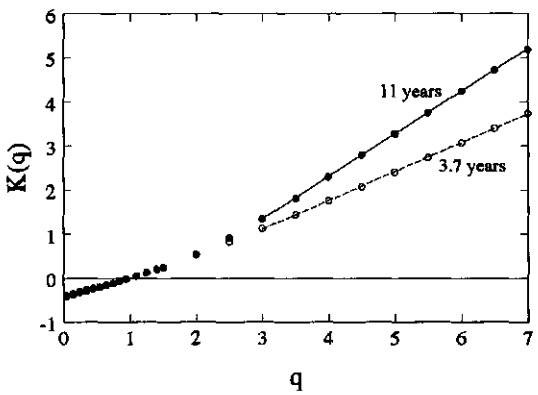

Figure 5.62 Comparing two empirical moments scaling functions (dotted lines), obtained with hourly rainfall from Assink, for the range of scales from 1 hour up to 5.3 days. The function represented with black bullets is for 11 years of rainfall (from 1976 to 1986) and the function represented with white bullets is for 3.7 years of rainfall (from 1976 to 1979).

In Figure 5.62, as the sample size increases, the slope of the linear part of the empirical function $K(q)$ for large moments also increases. The regression lines fitting the functions for moments $3\leq q\leq 7$ are represented by a solid line for the larger sample (the slope of the line is 0.96), and by a dashed line for the smaller sample (the slope of the line is 0.65). Their slopes give estimates of the largest order of the (*dressed*) singularities γ_{max} of the rain rate that are present in each of the samples, and that dominate the statistics of the corresponding sample.

Results illustrate the effect of the size of the sample on the observation of extreme and large events. The larger the sample, the larger the fraction of the probability space that is observed, and thus the chance of encountering rare and intense events. Estimates of the effective dimensions of the samples can be obtained from the intercept of the regression lines in Figure 5.62; they are 1.55 for the larger sample, and 0.85 for the smaller sample. Analysis of the critical moments in the empirical functions $K(q)$ may indicate the type of multifractal phase transition that is present in the statistics. If the critical moment does not vary with the sample size, then it follows from divergence of moments. In such a case, the intersection of the linear parts of the two empirical functions $K(q)$, in Figure 5.62, gives an estimate of the critical moment q_D associated with the divergence of moments. If the critical moments vary with the size of the sample, it indicates a second-order phase transition and the critical moment is then q_s. The behaviour observed in Figure 5.62 indicates the presence of a first-order phase transition. Figure 5.62 also illustrates that $K(q_D)=\infty$ is only observed for a very large sample (see Section 3.3.3). For finite samples, divergence of moments is observed as special linear forms in the function $K(q)$.

'Universal' multifractals

The DTM plot of $\log(|K(q,\eta)|)$ versus $\log(\eta)$ is shown in Figure 5.63 for a few q-moments (see legend). The plot is for rainfall on scales from 1 hour up to 5.3 days. It confirms the scaling and the 'universal' multifractal behaviour of rainfall over the range of moments limited by q_{min} and q_{max}. These critical moments can be estimated from the breaks in the scaling of the plot of $\log(|K(q,\eta)|)$ against $\log(\eta)$, in Figure 5.63. DTM analysis yielded estimates of the 'universal' multifractal parameters of $\alpha=0.67\pm0.11$ and $C_1=0.45\pm0.01$ (based on the study of the scaling of 12 q-moments).

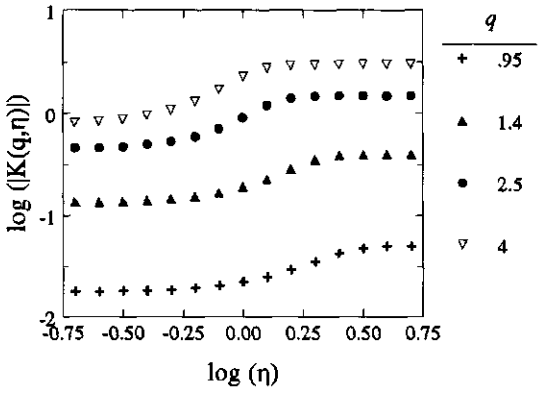

Figure 5.63 DTM plot of $\log(|K(q,\eta)|)$ versus $\log(\eta)$ estimated for the range of scales from 1 hour up to 5.3 days with hourly rainfall from Assink (from 1976 to 1986). The legend indicates the q-moments plotted.

Another estimate of C_1 can be obtained with the relation $K'(1)=C_1$; an approximation is $K'(1)\approx[K(1.1)-K(0.95)]/0.15=0.45$, which confirms the value obtained with the DTM technique.

Parameter H can be estimated with the relation $H=[\beta-1+K(2)]/2$, where $\beta\approx0.23$. Using the empirical $K(2)\approx0.54$ one obtains $H=-0.11$; using the theoretical value of $K(2)$ (with the parameters C_1 and α estimated above) it is also $H\approx-0.11$.

The 'universal' parameters can be used to estimate the critical moments q_s and q_D. Using Eq. (3.49), $q_s=[(D+D_s)/C_1]^{1/\alpha}=(1.55/0.45)^{1/0.67}\approx6.3$ which is well above the critical moment associated with the linear section of the function $K(q)$. For the smaller sample in Figure 5.62 the estimate is $q_s\approx2.7$, which is just above the estimate of the moment q_D.

With 'universal' multifractals the critical moment q_D can be estimated using the relation $C_1(q_D^{\alpha}-q_D)/[(\alpha-1)(q_D-1)]=D$ (in Eq. (3.50)). Using the average value of the estimates of D from the empirical function $K(q)$, $D\approx0.60$, one obtains an estimate of $q_D\approx2.7$. This value agrees well with the previous empirical estimate of this critical exponent. The statistical behaviour observed corresponds to a first-order phase transition. The estimate of the critical singularity with 'universal' multifractals yields $\gamma_D\approx0.7$.

Agreement between the empirical and theoretical multifractal exponent functions

Figure 5.64 shows the empirical (dotted line) and theoretical (solid line) codimension functions for this case (i.e. for the 11 years of data). The functions agree well for only a finite range of values (see also Figure 5.59). The limits are the critical orders of singularity discussed earlier. For the finite sample analyzed, and for singularities $\gamma>\gamma_D$ (with $\gamma_D=K'(q_D)$),

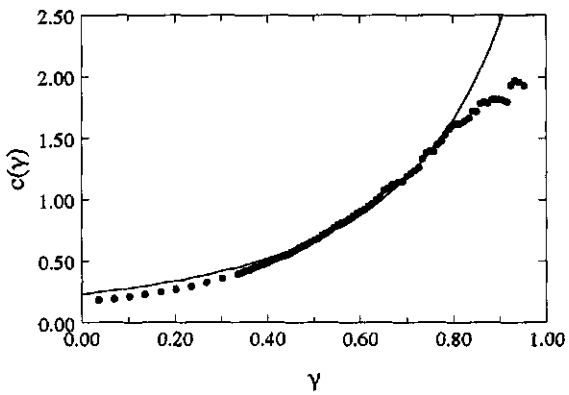

Figure 5.64 Empirical codimension function (dotted line) plotted with the 'universal' multifractal function (solid line) with parameter values $\alpha=0.67$, $C_1=0.45$, and $H=-0.11$. The empirical function was determined with hourly rainfall from Assink (from 1976 to 1986), for the range of scales from 1 hour up to 5.3 days.

the linear behaviour in the function $c(\gamma)$ (associated with divergence of moments of the rain rate) indicates the presence of orders of singularity larger than the values that can be estimated with a *bare* multiplicative cascade model, for the same probability of occurrence. This behaviour is only observed for sufficiently large samples since those high singularities are almost surely not present in small samples. The two codimension functions (theoretical and empirical) do not show good agreement for the small orders of singularity; the critical value agrees with the singularity $\gamma_{min} \approx 0.42$ studied above.

Figure 5.65 shows the theoretical (solid line) moments scaling function with parameter values $\alpha=0.67$ and $C_1=0.45$ plotted together with the empirical functions (dotted lines) obtained for the samples corresponding to 11 years and 3.7 years of hourly rainfall (see Figure 5.62). The theoretical and empirical functions show good agreement only for a finite range (see also Figure 5.61 and Figure 5.62). The limits are the critical order moments q_{min} and q_D.

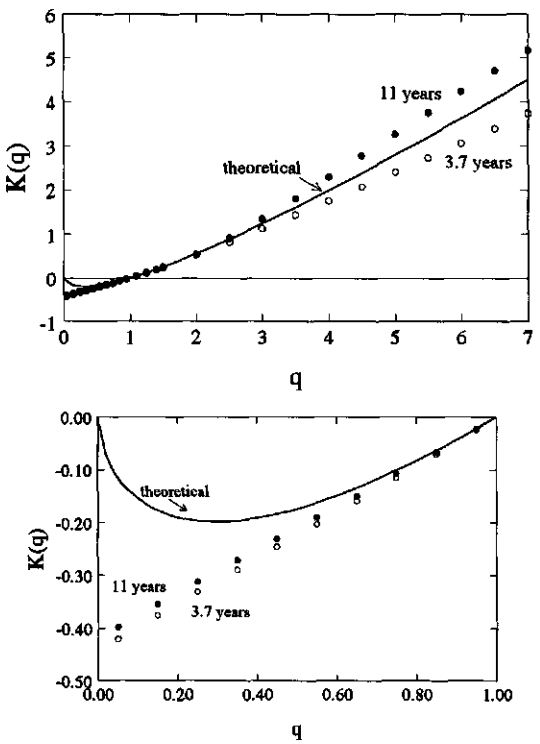

Figure 5.65 The 'universal' multifractal moments scaling function with parameter values $\alpha=0.67$ and $C_1=0.45$ (solid line), plotted with the empirical functions characterizing the statistics of 11 years of rainfall (black bullets) and 3.7 years of rainfall (white bullets). The lower plot shows a detail of the functions for $q<1$. The empirical functions were determined with hourly rainfall from Assink (from 1976 to 1986, and from 1976 to 1979), for the range of scales from 1 hour up to 5.3 days.

For $q>q_D$, comparison of the theoretical moments scaling function and the empirical functions obtained for the different sample sizes (see Figure 5.62) shows that: for the smaller sample, the theoretical function takes values larger than the empirical function; and, for the larger sample, the empirical function takes values larger than the theoretical function.

5.5 Analysis of rainfall from Nancy

This Section deals with the analysis of 4 years of rainfall data from Nancy (France), from 1988 to 1991. The average annual rainfall in this period is 827.8 mm. Details about the data are given in Section 4.4.

About the choice of the resolution of the pseudo time-series

The rainfall was measured with a tipping-bucket gauge; the capacity of the buckets was 0.2 mm of rainfall. This type of gauge does not have well-defined temporal and dynamic resolutions. Only the depth-capacity of the buckets is well defined. Nevertheless, rainfall (pseudo) time-series were 'reconstructed' from the records of the tipping-bucket gauge. This 'reconstruction' imposes a fixed time-resolution, which is in contrast to the rainfall record itself. In this procedure it was assumed that there is a constant rainfall-intensity between two consecutive 'tics' of the recording device (see Section 4.4). It leads to a time series without rainless periods (i.e. periods with zero rainfall) because the series were 'reconstructed' without any constraint in relation to the duration of low-intensity rainfall periods. This methodology introduces artificial features in the data with respect to the 'true' rainfall characteristics. An additional problem is the depth-capacity of the buckets. One would expect the depth-resolution of the measuring device to be one of the factors affecting the correctness of the description of the rainfall process by the data. This will necessarily affect the rainfall analysis, particularly the low-intensity events.

To gain more information about the type of data that are studied in this Section, some features of the Nancy data were investigated by means of a very rough empirical analysis of the time intervals recorded between two consecutive 'tics' of the recording device; only intervals of less than 6 hours were considered. Table 5.8 shows some information about those intervals (e.g. duration, rainfall-intensity).

About 44% of the time associated with intervals between 'tics' smaller than 6 hours was recorded, on average, with intervals of less than 1 hour. The average 'length' of such intervals is 8.34 ± 16.62 minutes. The study of the *sampling*-intervals below 30 minutes (which thus, contain the highest rainfall-intensities recorded) indicates that the rainfall process on these scales may be not described correctly by the data. This class shows the largest coefficient of variation, which may indicate the presence of measurement-induced problems in the rainfall data.

Table 5.8 Information on the different time intervals recorded with a tipping-bucket rain gauge. The gauge has a bucket-capacity of 0.2 mm of accumulated rainfall over time. The rainfall records are from Nancy, from 1988 to 1991.

duration of the interval between 'tips', Δt	contrib. to total recorded rainy-periods < 6h (%)	average duration of the intervals (in min)	average rainfall-intensity on the Δt (in mm/h)
$0 < \Delta t \leq 30$ min	31.3	6.29±18.67	9.209±8.729
30 min $< \Delta t \leq 1$ h	12.7	42.49±8.95	0.301±0.067
1 h $< \Delta t \leq 2$ h	16.6	85.04±10.35	0.150±0.024
2 h $< \Delta t \leq 3$ h	11.5	146.28±14.15	0.083±0.007
3 h $< \Delta t \leq 6$ h	27.9	259.35±23.86	0.049±0.002

It was to be expected that the intermittency of rainfall on small time-scales would not be properly recorded by the measuring device. For the lowest intensities, owing to the methodology used to reconstruct the time series, there would be problems in the description of the rainfall process up to time resolutions higher than an average of 4 hours.

Results of data analysis suggest that the rainfall measurement process might have introduced artificial characteristic scales into the data (i.e. scales not related to the rainfall process itself), which could be expected to be intensity dependent (see Table 5.8). This would lead typically to the observation of (artificial) breaks in the scaling.

The study of the rainfall data from Nancy presented in this Section focuses mainly on the analysis of 15-minute time series. The choice of the resolution of the time series was based on the previous analysis. Moreover, there is also interest in comparing the results of the multifractal analysis of this data set with the analysis of the high-resolution data from Vale Formoso (see Section 5.3.1). Data of 1-minute time resolution is also used to investigate the small-scale behaviour. Scaling problems are expected to occur during the analysis. This effect should be stronger for the low intensities. It is not possible to predict whether these problems will or will not be aggravated in relation to the problems that were observed previously during the analysis of rainfall from Vale Formoso (see Section 5.3.1). The main reasons are: i) the lowest rainfall resolution of the Nancy data (the digitization of the pluviographs from Vale Formoso provided data with an accuracy of 0.1 mm of rainfall whereas in this case there was a 0.2 mm rainfall resolution); ii) the human bias introduced by the digitization of the pluviographs from Vale Formoso is now absent, which is a favourable factor.

Box-counting analysis

The box-counting plot obtained with the 15-minute rainfall is shown in Figure 5.66. The rainfall threshold considered in the analysis was 0.1 mm/day. The plot displays time scales from 15 minutes up to 85.3 days, and it accumulates the statistics over 4 years. The plot exhibits 'saturation' both for scales smaller than 8 hours and larger than 3 weeks. For the intermediate scales, the absolute slope of the plot is 0.83. It yields an estimate of the fractal dimension that characterizes the set of rainfall occurrences of intensity larger than 0.1 mm/day defined in the 1-dimensional space of time. This result is clearly a consequence of the procedure used to reconstruct the rainfall time-series from the records of the tipping-bucket gauge. The critical small scale is different for different values of the intensity threshold.

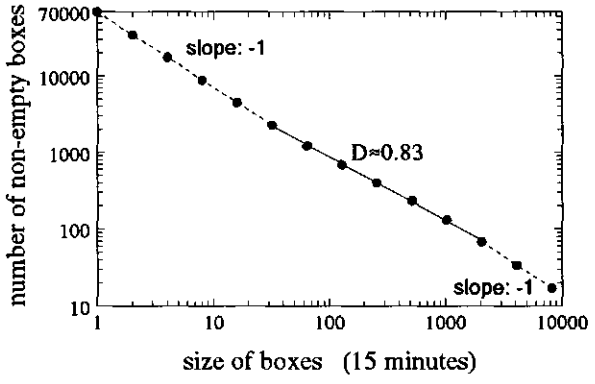

Figure 5.66 Box-counting log-log plot obtained with 15-minute rainfall from Nancy, from 1988 to 1991. A box of unit-size corresponds to 15 minutes. The plot displays time scales from 15 minutes up to 85.3 days.

Investigating scale-invariance with spectral analysis

The scale-invariant temporal structure of rainfall from Nancy is investigated here using the 1-minute (pseudo) time-series reconstructed from the tipping-bucket records (see above). The energy spectrum obtained for the 1-minute rainfall is shown in Figure 5.67. The spectrum has been smoothed for the high frequencies. The spectrum does not show a sharp peak corresponding to the annual cycle (at $\omega \approx 0.00011\ h^{-1}$), which is perhaps a consequence of the small size of the sample and/or the type of annual rainfall pattern shown in Figure 5.8. The spectrum exhibits power-law behaviour over a range of time scales extending at least up to about 3 weeks. The spectral slope is -0.21. This behaviour is maintained from 80 minutes up to at least 3 weeks. For the smaller time scales, a different behaviour is observed (see Figure 5.67). For scales smaller than 17 minutes, the spectral slope is -0.96. This behaviour is similar to the behaviour observed in the energy spectra of the 2-minute rainfall from Vale Formoso (see Section 5.3.1).

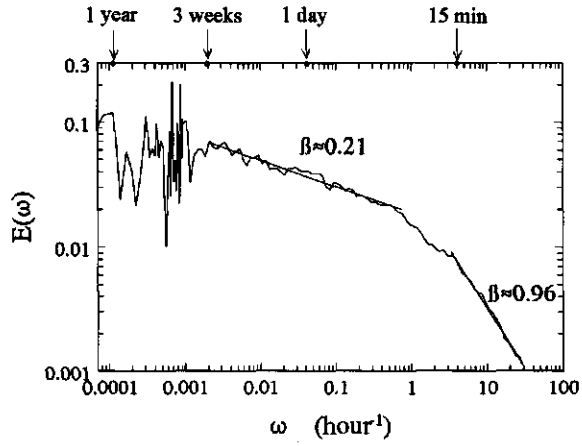

Figure 5.67 Energy spectrum obtained for 1-minute rainfall from Nancy, from 1988 to 1991.

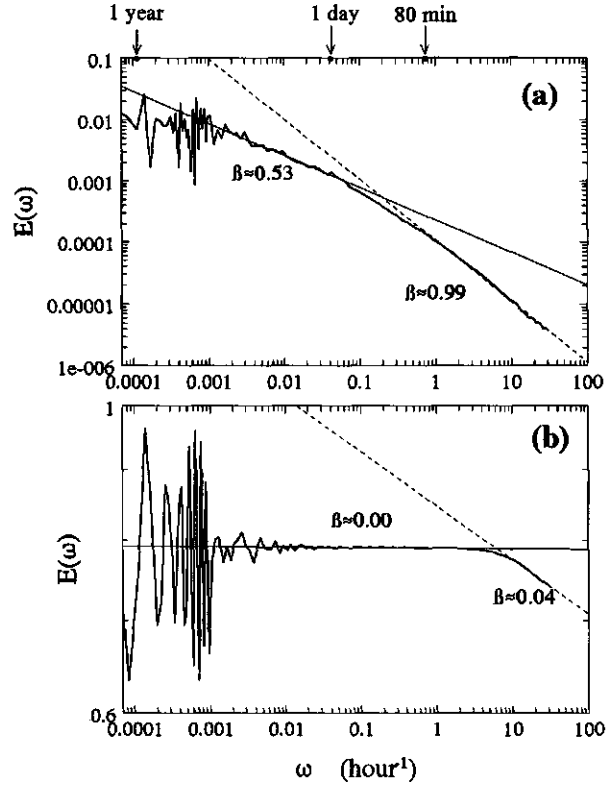

Figure 5.68 Energy spectra obtained for 1-minute rainfall from Nancy, from 1988 to 1991: (a) for the data renormalized with a power $\eta = 0.1$; and (b) for the data renormalized with a power $\eta = 10$.

The energy spectra of η-power renormalized versions of the rainfall intensity (see Section 3.5.4) were also investigated, and are shown in Figure 5.68. Figure 5.68(a) shows the spectrum for $\eta=0.1$ and Figure 5.68(b) shows the spectrum for $\eta=10$. The renormalizations of the data affect the energy spectra. Similarly to what was observed in the analysis of the data from Vale Formoso (see Section 5.3.1), the time scale corresponding to the spectral break observed at high frequencies is affected by the intensity of the process. The break occurs at different time-scales for different values of the moment η. In relation to the spectrum in Figure 5.67 (for $\eta=1$), the critical scale is shifted towards the lowest frequencies, for $\eta<1$, and towards the highest frequencies, for $\eta>1$. This is a qualitative result consistent with the hypothesis of scale-dependent measurement-problems in the data.

Studying the probability distributions

Figure 5.69 shows the log-log plot of the probability of exceeding rainfall intensity levels of singularity γ, observed on time scales of resolution λ, against the scale ratio λ. The study uses 15-minute rainfall, from 1988 to 1991. The scales represented in Figure 5.69 are from 15 minutes ($\lambda=8192$) up to about 2.84 months ($\lambda=1$). The orders of singularity γ plotted in Figure 5.69 are indicated in the legend. Results show that the probability distributions scale well (i.e. it follows closely a straight line) on time scales from 15 minutes up to about one-and-a-half months. However, this occurs for only a limited range of singularities. For the very small and the very large singularities, the plots deviate from the expected power-law. At scales varying between 30 minutes and 1 hour, the plots 'bend' in the upward direction, for the small singularities, and in the downward direction, for the high frequencies. This behaviour

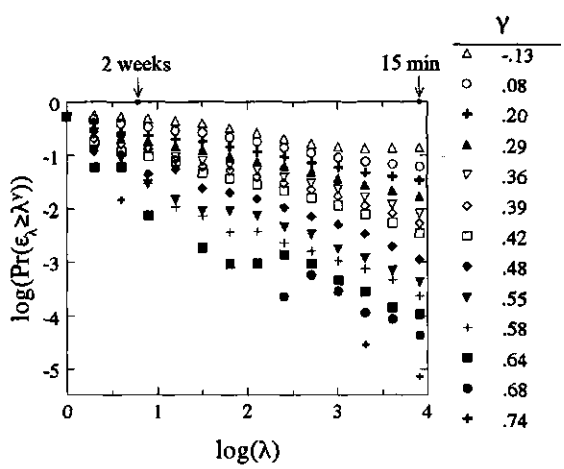

Figure 5.69 Log-log plot of the probability of exceeding rainfall intensity levels of singularity γ, observed on scales from 15 minutes ($\lambda=8192$) up to 2.84 months ($\lambda=1$), against the scale ratio λ. The data are 15-minute rainfall from Nancy, from 1988 to 1991. The legend indicates the order of singularity γ of the rainfall intensity ε_λ.

suggests that the low intensities in the data are overestimated and the high intensities are underestimated. The smallest intensity in the data corresponds to 0.2 mm of rain falling on a time interval of approximately 22 days. This may give some insight into the (incorrect) way rainfall is described sometimes by the time-series data. Over a number of scales, both the studies of certain (small) singularities of the rainfall intensity and of the associated statistical moments are necessarily affected by this rough description of the (true) process. This effect is stronger for small singularities (thus, also for small moments) and small time-scales. It 'diminishes' in a non-trivial way as the singularities (or the moments) of the rainfall intensity increase, in combination with the study of increasingly larger time-scales (see Figure 5.69). Such a problem should not be ignored in the analysis and interpretation of results.

The empirical codimension function that describes the scaling of the probability distributions of the rainfall intensity on scales from 15 minutes up to 10.7 days is shown in Figure 5.70. The choice of this range of scales was imposed by the scaling of the moments, below. There are some uncertainties in the estimates of the function $c(\gamma)$ both for the high and small singularities. These uncertainties occur perhaps because of the small size of the sample and the limitations of the dynamic range of the data, discussed above. These difficulties are influenced by the depth-capacity of the rain gauge buckets. They restrict this study to a limited range of singularities of the rainfall on small time-scales.

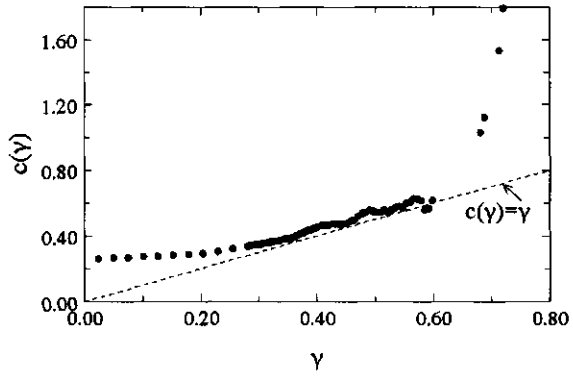

Figure 5.70 Empirical codimension function (dotted line) obtained for 15-minute rainfall from Nancy (from 1988 to 1991), for the range of scales from 15 minutes up to 10.7 days.

Figure 5.71 shows histograms of rainfall on different scales; from top to bottom, the histograms are for scales of 15 minutes, 30 minutes, 1 hour, 2 hours, and 4 hours. Some histograms were displaced along the vertical axis so as not to overlap. The histograms show algebraic fall-off. In Figure 5.71, the absolute values of the slopes of the regression lines fitted to the histograms tails are, from top to bottom, 1.95, 2.04, 2.13, 2.11, and 2.21. This indicates divergence of statistical moments of order larger than around 2.09 ± 0.10.

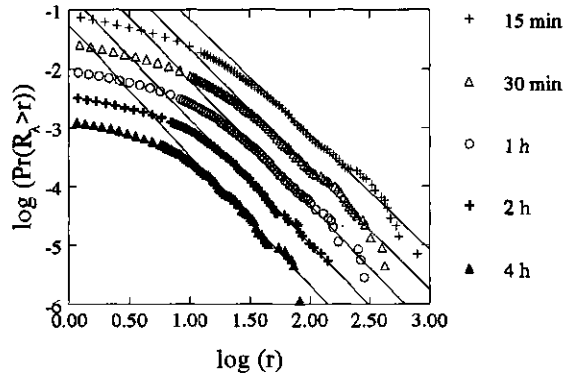

Figure 5.71 Histograms of rainfall on time scales of (from top to bottom) 15 minutes, 30 minutes, 1 hour, 2 hours, and 4 hours (the histograms were offset vertically so as not to overlap). The data are 15-minute rainfall from Nancy, from 1988 to 1991.

Studying the scaling of the moments

Figure 5.72 shows the log-log plot of the average q^{th} moments of the rainfall intensity ε_λ on time scales from 15 minutes (λ=8192) up to about 2.84 months (λ=1), against the scale ratio λ. The data are 15-minute rainfall from 1988 to 1991; the statistics are for 16 'samples' of 2.84 months. Figure 5.72(a) shows moments larger than 1 and Figure 5.72(b) shows moments smaller than 1. The q-moments plotted in Figure 5.72 are indicated in the legend.

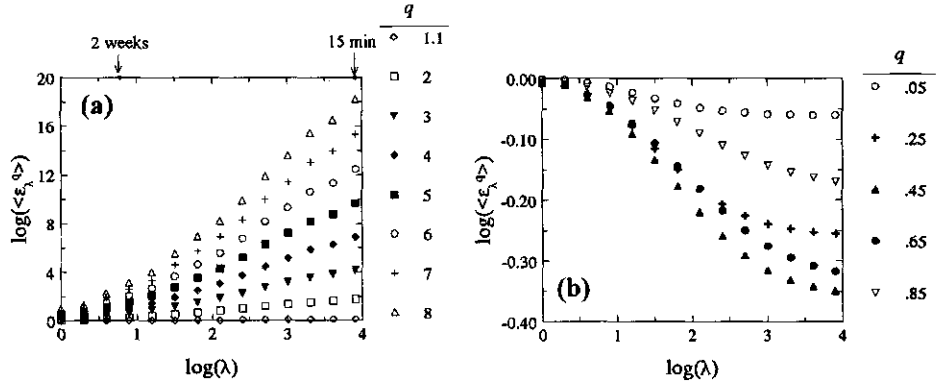

Figure 5.72 Log-log plot of the average q^{th} moments of the rainfall intensity ε_λ on time scales from 15 minutes (λ=8192) up to 2.84 months (λ=1), against the scale ratio λ: (a) for moments larger than 1; and (b) for moments smaller than 1. The data are 15-minute rainfall from Nancy, from 1988 to 1991.

The scaling range observed for the moments is smaller than for the probabilities. Power-law behaviour is observed from 15 minutes up to about one-and-a-half to two weeks. However, similarly to what was observed for other data sets, the scaling range is smaller for moments smaller than 1. The corresponding moments plots deviate from the expected power-laws indicating a overestimation of the low rainfall intensities. The critical scale is different for the moment analyzed, being larger for decreasing values of the moments. The behaviour observed for the larger moments indicate that the high rainfall intensities are better described by the data than in the case of the data from rain gauges of the float type.

The empirical moments scaling exponent function that describes the multifractal behaviour of rainfall on time scales from 15 minutes up to 10.7 days is plotted in Figure 5.73 (dotted line). The plot on the right-hand side of Figure 5.73 shows a detail for moments q smaller than 1. The empirical function $K(q)$ consists of both non-linear and linear sections. The linear behaviour for moments larger than about 2.5 is empirical evidence of a multifractal phase transition. The regression (dashed) line fitting to this section of the function (in Figure 5.73) has slope 0.80 (an estimate of the singularity γ_{max}) and intercept -1.18 (an estimate of the codimension $-c(\gamma_{max})$). If one accepts the previous estimate of $q_D \approx 2.1$, the dual critical singularity for divergence of moments is $\gamma_D \approx 0.68$. Moreover, one estimates $D=K(q_D)/(q_D-1) \approx 0.55$.

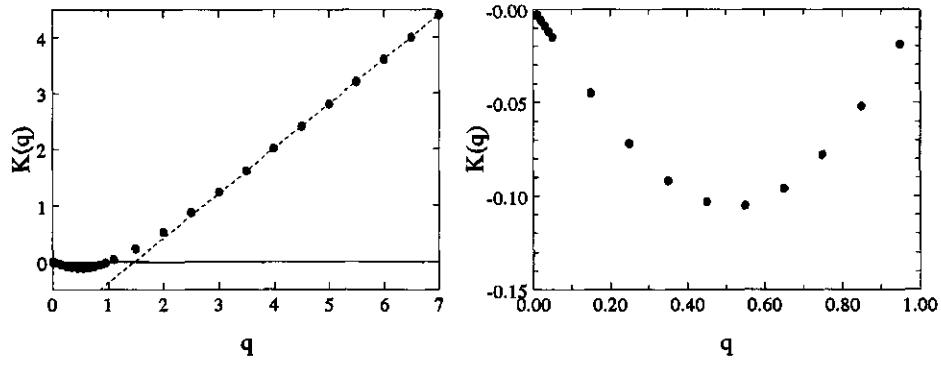

Figure 5.73 Empirical moments scaling function (dotted line) obtained for 15-minute rainfall from Nancy (from 1988 to 1991), for the range of scales from 15 minutes up to 10.7 days. The plot on the right-hand side shows a detail of the function for moments q smaller than 1.

The study of the empirical function $K(q)$, in Figure 5.73, near $q=0$ yields estimates of the singularity $\gamma_{min} \approx -0.29$, and codimension $-c(\gamma_{min})=K(0)=0$. The value obtained for the codimension $c(\gamma_{min})$ is consistent with the method used to 'reconstruct' the (pseudo) time-series from the tipping-bucket record, which yielded a time series without zero-rainfall periods. The data suggest that the rainfall process 'fills' the 1-dimensional space of time; therefore, one would expect the dimension of the (geometric) 'support' of the observed process to be 1.

'Universal' multifractals

The 'universal' parameters that are expected to characterize the multifractal temporal structure of rainfall, for this case, are estimated using the DTM method. The plot of $\log(|K(q,\eta)|)$ versus $\log(\eta)$ is shown in Figure 5.74 for a few of the q-moments investigated for testing the scaling (see legend). DTM analysis yields the estimates of the 'universal' multifractal parameters $\alpha=2$ and $C_1=0.20$. These values indicate a log-normal behaviour for the rainfall process, which does not agree with the results obtained for the other multifractal analysis of rainfall time-series conducted in this work (see Sections 5.3, 5.4, and 5.6). One will try to confirm the correctness of these results with other independent analyses and estimates.

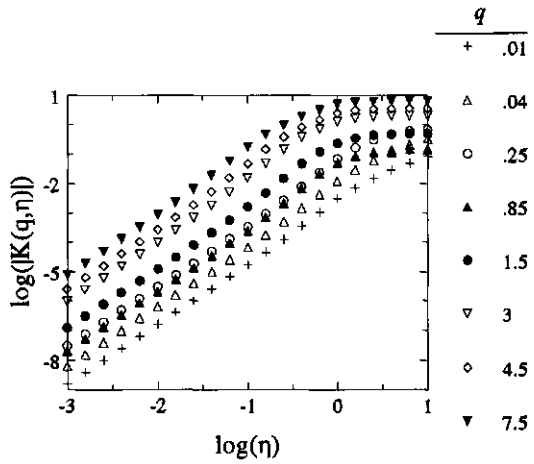

Figure 5.74 DTM plot of $\log(|K(q,\eta)|)$ versus $\log(\eta)$ estimated for the range of scales from 15 minutes up to 10.7 days, with 15-minute rainfall from Nancy (from 1988 to 1991). The legend indicates the q-moments plotted.

The 'universal' multifractal parameter C_1 can be estimated also from the first derivative of the moments scaling function at $q=1$. An approximation to the empirical $K'(1)=C_1$ is $K'(1)\approx[K(1.1)-K(0.95)]/0.15=(0.040+0.0192)/0.15=0.393$. This value, which is larger than the DTM estimate, is supported by the analysis of the empirical codimension function (see Figure 5.70). Although it is difficult to estimate the value of the parameters C_1 and H from the empirical codimension function in Figure 5.70 (it is $c'(C_1-H)=1$ and $c(C_1-H)=C_1$, in Eq. (3.30)), the value $C_1=0.20$ is rejected. Analysis of the empirical function $c(\gamma)$ yields an estimate of the parameter H of zero. Therefore, the DTM estimate for C_1 is not confirmed. Because of the strong non-linear correlations between parameters α and C_1, the DTM estimate of α may be also not correct.

Another method to estimate the multifractal parameters directly from the empirical functions uses non-linear regression techniques. In relation to the codimension function $c(\gamma)$, this study is

hampered by the poor estimate of the function outside a limited range of singularities γ. Non-linear fitting to the empirical function $K(q)$ for moments $0.65 \leq q \leq 2.5$ yielded estimates of $C_1=0.374$ and $\alpha=1.05$. This result agrees well with the previous estimate of the parameter C_1, obtained by analyzing the geometrical properties of the scaling functions. If one fixes the parameter $C_1=0.393$, obtained above, the non-linear fit yields $\alpha=0.93$. Without any claim on the correctness of these estimates, they do not confirm the previous DTM estimate of $\alpha=2$.

The inconsistency of the results and, moreover, the totally different magnitude of the value estimated here with the DTM method for the degree of multifractality α of the rainfall process needs more investigation.

Using Eq. (3.81), with $\beta=0.21$ and the empirical $K(2)=0.532$, one obtains the estimate $H\approx$-0.13. The same estimate of H is obtained with the other 'universal' parameters $\alpha=1.05$ and $C_1=0.37$. The empirical codimension function in Figure 5.70 suggests that H is smaller, $H\approx$-0.03.

Figure 5.75 shows the empirical codimension function plotted together with the theoretical function with parameter values $\alpha=2$, $C_1=0.20$ (DTM result), and $\alpha=1.05$, $C_1=0.37$ (non-linear regression result); in both cases parameter H is -0.03. The disparity between the empirical function and theoretical function with parameter values $\alpha=2$ and $C_1=0.20$ was expected. The theoretical function with parameter values $\alpha=1.05$ and $C_1=0.37$ agree well with the empirical function for only a very limited range of values. The upper limit of this range could be explained by uncertainties in the estimate of the empirical codimension function. The value of the regression coefficients above and below certain orders of singularity was uncertain; the corresponding estimates of the codimensions were not plotted in Figure 5.75. Similarly to what was observed for other cases (see Section 5.3.1), the empirical codimension function exhibits a 'flat' behaviour for $\gamma<0.2$. Such behaviour is associated with a minimum reliable singularity in the data, probably introduced by the measuring of the process. The left-hand section of the codimension function illustrates the manipulation of the data that occurred when time series were reconstructed from the records, in the way it is explained in Section 4.4. The lowest singularities in the data are artificially introduced by the procedure; their codimensions go to zero in an unlikely way. Rejecting the statistics of rainfall corresponding to the range of the smallest singularities in the data, one could estimate $c_{min}\approx0.26$.

Figure 5.76 shows the empirical moments scaling function plotted together with the theoretical function with parameter values $\alpha=2$, $C_1=0.20$ (DTM result), and $\alpha=1.05$, $C_1=0.37$ (non-linear regression result). The theoretical function with parameters $\alpha=1.05$ and $C_1=0.37$ agree well with the empirical function for only a limited range of values. The upper limit of this range is well explained by the presence of a multifractal phase transition. The lower limit, at approximately $q=0.7$, may be explained by the way the data were obtained and the consequences for the low intensities in the data that were discussed earlier. The estimate of the dual critical singularity, estimated from the empirical moments

function, is $K'(0.7)\approx 0.18$; this agrees very well with the behaviour of the codimension function and the presence of a critical small singularity.

Using the 'universal' multifractal characterization of the statistics of rainfall based on the parameter values $\alpha=1.05$ and $C_1=0.37$, the estimates of the critical moments q_s and q_D are the following: $q_s\approx(1.18/0.37)^{1/1.05}=3.0$; and $q_D\approx 2.2$, obtained using the estimate $D=0.55$. The estimate of the value of q_D obtained from the slope of the algebraic tails of the histograms was 2.1.

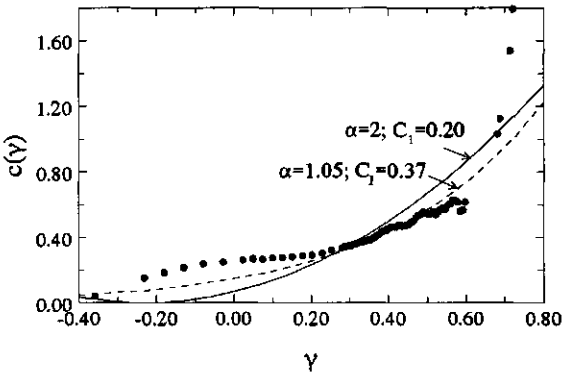

Figure 5.75 Empirical codimension function (dotted line) plotted together with the theoretical functions with parameter values $\alpha=2$, $C_1=0.20$ (DTM result), and $\alpha=1.05$, $C_1=0.37$ (non-linear regression result). In both cases is $H=-0.03$. The empirical function was determined with 15-minute rainfall from Nancy (from 1988 to 1991), for the range of scales from 15 minutes up to 10.7 days.

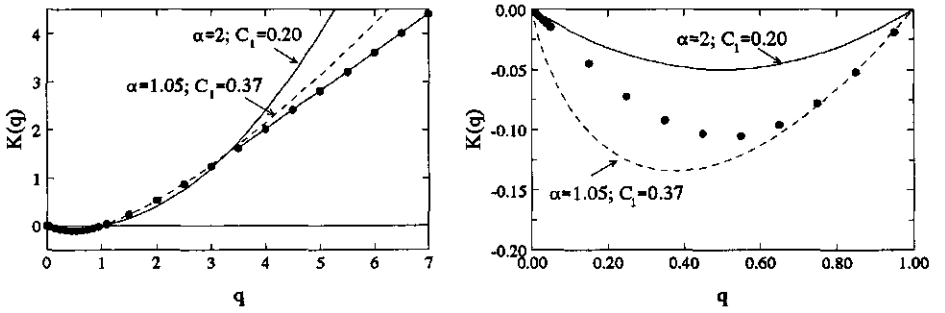

Figure 5.76 Empirical moments scaling function (dotted line) plotted together with the theoretical functions with parameter values $\alpha=2$, $C_1=0.20$ (DTM result), and $\alpha=1.05$, $C_1=0.37$ (non-linear regression result). The plot on the right-hand side shows a detail for moments q smaller than 1. The empirical function was determined with 15-minute rainfall from Nancy (from 1988 to 1991), for the range of scales from 15 minutes up to 10.7 days.

The DTM method yields values for the 'universal' parameters that are not completely consistent. It is still possible that the scale invariance in the data is of a 'universal' type. However, the DTM method does not permit us to draw this conclusion. Alternative analysis methods should be developed that avoid 'changing' the information in the records during the process of reconstructing the time series. Because the original data from tipping-bucket records has a fixed depth-resolution, this could be used as the quantity determining the resolution (Lovejoy, 1994).

The results obtained in this multifractal analysis question the appropriateness of the method of obtaining the data, including the procedure to reconstruct time series from the tipping-bucket records. It also showed that this type of analysis can detect 'anomalous' characteristics of a data set, because it 'explores' the whole of the dynamic range covered by the data.

5.6 Analysis of rainfall from Coimbra

This Section deals with the analysis of 90 years of monthly rainfall from Coimbra (Portugal), recorded from 1901 to 1990 (see Section 4.5). In this period, the average annual rainfall is 989.3 mm. The data were obtained by aggregating daily rainfall during monthly intervals. The daily rainfall was measured with a non-recording rain gauge.

The fractal structure of the monthly rainfall

The box-counting plot obtained with the monthly rainfall is shown in Figure 5.77. The plot displays time scales from 1 month up to 8 months; thus, it accumulates the statistics of 135 'samples' of 8 months. For scales larger than 1 month, the plot in Figure 5.77 exhibits linear behaviour of slope -1. This behaviour (i.e. the slope -1) indicates 'saturation' (see Section 3.2.3).

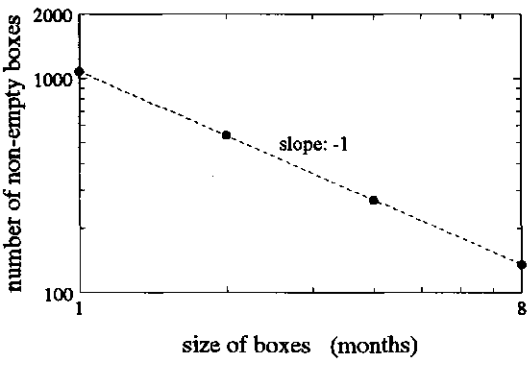

Figure 5.77 Box-counting log-log plot obtained with monthly rainfall from Coimbra, from 1901 to 1990. The plot displays time scales from 1 month up to 8 months.

Investigating scale-invariance with energy spectra

The energy spectrum for the monthly rainfall is given in Figure 5.78. The spectrum has been smoothed for the high frequencies. In the lowest frequency range (i.e. for the largest time scales), the spectrum starts rising with decreasing frequency. The adjacent region of the spectrum exhibits a nearly flat-power behaviour (i.e. $E(\omega)\approx\omega^0$). This plateau is observed now more clearly (in Figure 5.78) than when smaller samples were analyzed (see previous Sections). The behaviour observed for the lowest frequencies is expected to be related to climatic fluctuations (see e.g. Fraedrich and Larnder, 1993). It describes long-term variability. The slope of the regression line fitting to $\log(E(\omega))$ against $\log(\omega)$, for frequencies corresponding to time scales larger than 8.5 years, is -1.06.

A spectrum peak corresponding to the annual cycle frequency is clearly seen in the plot. This oscillation seems to 'emerge' on a scaling background, since the spectral slope remains unchanged on both sides of the annual peak. Other spectral peaks exhibiting strong signals are observed at approximately 4.7 and 11.4 years. The semi-annual peak has a quite weak signal.

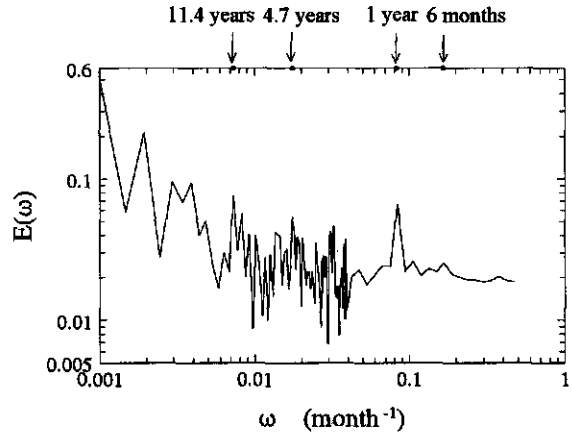

Figure 5.78 Energy spectrum obtained for monthly rainfall from Coimbra, from 1901 to 1990.

Scaling of the moments

Figure 5.79 shows the log-log plot of the average q^{th} moments of the rainfall intensity ε_λ on scales from 1 month (λ=32) up to 32 months (λ=1), against the scale ratio λ. Figure 5.79(a) shows moments larger than 1 and Figure 5.79(b) shows moments smaller than 1. The plots accumulate the statistics of 33 'samples' of 32 months. The (power-law) scaling behaviour exhibited by the moments is maintained from 1 month up to at least 16 months.

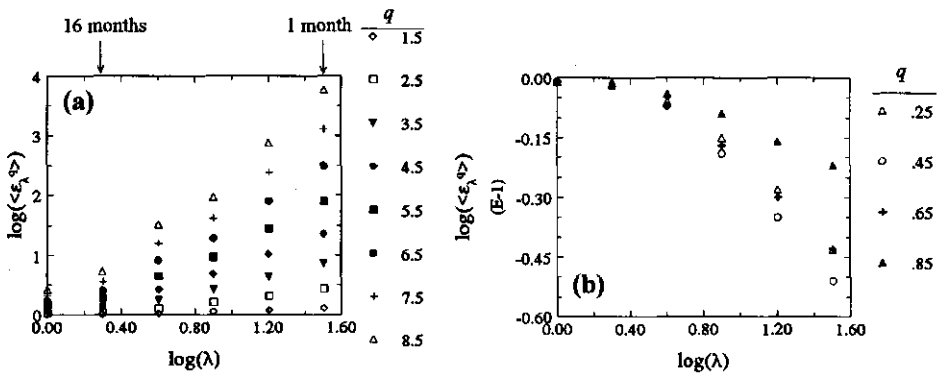

Figure 5.79 Log-log plot of the average q^{th} moments of the rainfall intensity ε_λ on scales between 1 month (λ=32) and 32 months (λ=1), against the scale ratio λ: (a) for moments larger than 1; and (b) for moments smaller than 1. The data are monthly rainfall from Coimbra (Portugal), from 1901 to 1990.

The empirical moments scaling exponent function

The empirical moments scaling exponent function that describes the multifractal behaviour of rainfall on scales from 1 month up to 16 months is plotted in Figure 5.80 (dotted line). The function exhibits a linear section for moments larger than around order 4 to 4.5. The slope of the straight (dashed) line fitting to this section of the function gives an estimate of γ_{max}=0.38 and the intercept an estimate of $c(\gamma_{max})$=0.73. This value is an estimate of the codimension of the maximum order of singularity γ_{max} that can be determined reliably, for the range of scales from 1 up to 16 months, from a sample of this size. The value of $-c_{min}=K(0)\approx 0$ (which yields an estimate of $D=1-c_{min}\approx 1$) agrees well with the fractal dimension determined with box-counting analysis for the range of scales of interest (from 1 month up to 16 months). The first derivative of the function $K(q)$ near q=0 is approximately -0.24 (γ_{min}); this is then an estimate of the smallest singularity of rainfall observed for this case.

Multifractal phase transitions

The linear behaviour of the empirical function $K(q)$ for moments larger than around 4 to 4.5 indicates the presence of a multifractal phase transition. To investigate the order of the phase transition, the empirical probability distributions of rainfall on different scales are analyzed. The histograms of rainfall on time scales of 1, 2, 4, and 8 months (in Figure 5.81) exhibit algebraic tails, which is an indication for divergence of moments. The absolute value of the slopes of the histograms tails are: 5.8 for 1 month, 5.8 for 2 months, 5.8 for 4 months, and 5.3 for 8 months. Theses slopes yield the estimate of the critical moment $q_D\approx 5.7$. The order of this critical moment is larger than the critical moment observed in the function $K(q)$. The phase transition is expected to be of the second order.

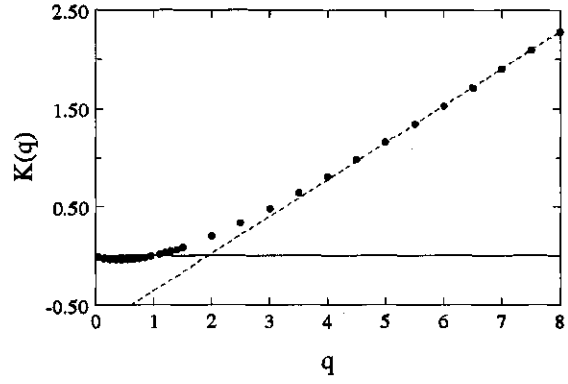

Figure 5.80 Empirical moments scaling function (dotted line) determined with monthly rainfall from Coimbra (from 1901 to 1990), for the range of scales from 1 up to 16 months.

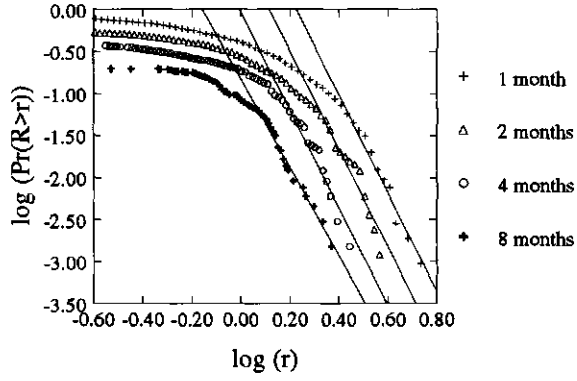

Figure 5.81 Histograms of rainfall on time scales of (from top to bottom) 1, 2, 4, and 8 months (the histograms were offset vertically so as not to overlap). The slope of the algebraic tails of the histograms are (also from top to bottom) 5.8, 5.8, 5.8 and 5.3. The data are monthly rainfall from Coimbra, from 1901 to 1990.

The estimate of the critical moment q_D is also larger than the value estimated earlier for monthly rainfall from Vale Formoso (see Section 5.3.3). One explanation for this difference is expected to be the distinct climates in Coimbra and Vale Formoso. The difference can not be attributed to the measuring device because the instrumentation used at both measuring sites is claimed to be of the same type (see Sections 4.2 and 4.5). The larger variability that characterizes the rainfall process in Vale Formoso was suggested already by the magnitude of

the coefficient of variation obtained for the monthly rainfall, which was 1.15, whereas it was of 0.90 for the monthly rainfall from Coimbra.

The maximum daily rainfall observed yearly in Coimbra, from 1901 to 1990, were used to investigate the tail of the probability distribution of the (extreme) daily rainfall events. This is shown in Figure 5.82. In this Figure the tail of the probability distribution for the daily rainfall from Vale Formoso is also plotted (see Section 5.3.2). The data were normalized with the corresponding average daily rainfall. Both probability plots exhibit algebraic tails. The absolute value of the slope of the tail of the probability distribution obtained with data from Coimbra is 4.27, which is an estimate of the critical order moment for divergence of the statistics of the daily rainfall. This value is smaller than the value estimated from the probability distributions of rainfall on scales larger than 1 month; this is consistent with the smaller variability observed in the rainfall process as the observation time-scale increases.

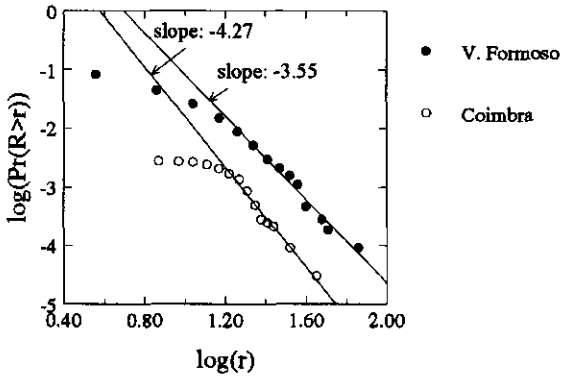

Figure 5.82 Probability of exceeding fixed thresholds r of daily rainfall. The plots were obtained from the maximum daily rainfall observed yearly in Coimbra, from 1901 to 1990 (thus, the corresponding plot was obtained from an 'incomplete' daily rainfall sample), and for the daily rainfall observed in Vale Formoso, from 1961 to 1990. The data were normalized with the corresponding average daily rainfall.

In Figure 5.82, the probability of occurrence of events smaller than a certain intensity-threshold are surely underestimated, because only the maximum values observed every year were considered (i.e. the analysis focuses on a selected part of the complete sample). This is not expected to be important for the behaviour displayed by the more extreme events, which is of interest here. Moreover, the correct value of those probabilities being larger would only lead to a larger absolute value of the slope of the tail of the probability plot (thus, to a larger estimate of the critical moment q_D).

The estimate of the critical exponent q_D, for the daily rainfall from Coimbra, is larger than the estimate for the data from Vale Formoso (the estimate for the daily data from Vale Formoso

was $q_D \approx 3.6$; see also Section 5.3.2). This result is consistent with what was observed when monthly rainfall was analyzed. The difference may have a climatic origin. The smaller value of q_D obtained for Vale Formoso can be associated with the more extreme rainfall events observed at this site, in relation to the 'mean' behaviour (see Sections 4.2 and 4.5). The maximum daily rainfall observed in Coimbra during the years 1901 to 1990 was 122.7 mm, and the average daily rainfall was 2.71 mm. In Vale Formoso, during the period from 1961 to 1990, the maximum daily rainfall record was 103.2 mm, and the average daily rainfall was 1.37 mm.

'Universal' multifractals

For the range of scales from 1 month up to 16 months, the DTM plot of $\log(|K(q,\eta)|)$ versus $\log(\eta)$ is shown in Figure 5.83, for a few q-moments. DTM analysis yields the estimates of the 'universal' multifractal parameters $C_1=0.12\pm0.01$ and $\alpha=1.34\pm0.03$ (the result relies on the study of 27 q-moments). The value of the parameter C_1 estimated with the DTM technique agrees with the value of C_1 that is estimated from the first derivative of the empirical function $K(q)$ at $q=1$. An approximation is $K'(1)=[K(1.1)-K(0.95)]/0.15=(0.014+0.006)/0.15\approx0.13$.

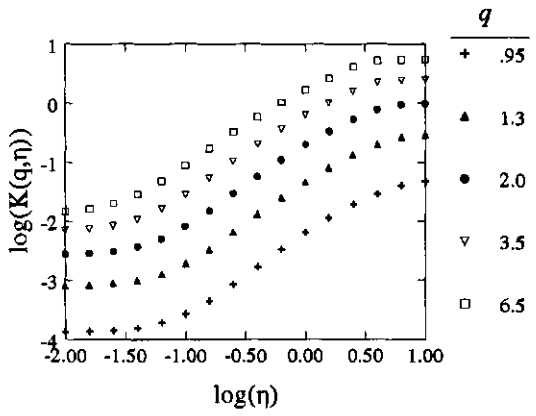

Figure 5.83 DTM plot of $\log(|K(q,\eta)|)$ versus $\log(\eta)$ estimated for the range of scales from 1 month up to 16 months. The data used are monthly rainfall from Coimbra, from 1901 to 1990. The legend indicates the q-moments plotted.

Agreement between the theoretical and empirical scaling functions

Figure 5.84 shows the empirical moments scaling function (dotted line) and the theoretical function (solid line) with parameter values $\alpha=1.34$ and $C_1=0.12$. The functions show good agreement up to a critical moment (see also Figure 5.80). This is the critical value of the order of the moments discussed before, of around 4. The agreement between the empirical and theoretical functions for moments smaller than 1 is quite good.

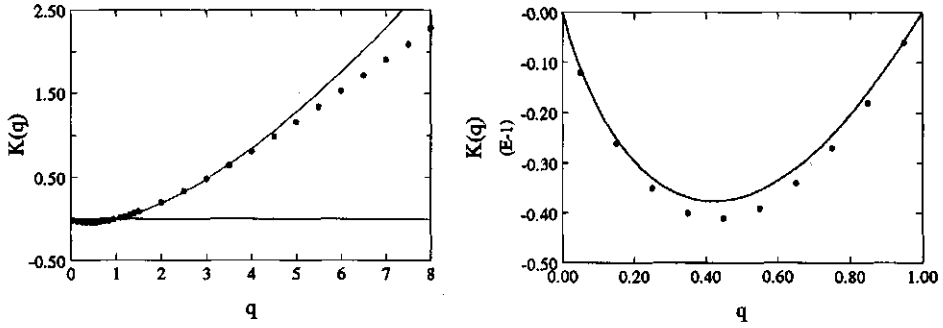

Figure 5.84 Empirical moments exponent function (dotted line) plotted with the 'universal' function with parameter values α=1.34 and C_1=0.12 (solid line). The plot on the right-hand side shows a detail for moments q smaller than 1. The empirical function was determined with monthly rainfall from Coimbra (from 1901 to 1990), for the range of scales from 1 up to 16 months.

Estimation of the critical moment q_s with 'universal' multifractals

The critical moment q_s can be estimated with Eq. (3.49). Let the effective dimension be estimated from the slope of the function $K(q)$ for larger moments; it is $c(\gamma_{max})=D+D_s\approx 0.73$. This yields an estimate of the critical moment $q_s=(0.73/0.12)^{1/1.34}\approx 3.9$. This estimate of the moment q_s agrees with the critical moment associated with the discontinuity observed in the empirical function $K(q)$, in Figure 5.80. This critical moment is smaller than the critical moment q_D for divergence of statistics that was estimated from the histograms in Figure 5.81. Thus, the behaviour of the moments scaling function is explained probably by a second-order multifractal phase transition, caused by undersampling.

5.7 Summary of results

This Section gives a summary of the results of the multifractal analysis of rainfall carried out in Sections 5.3 to 5.6. Table 5.9 summarizes the most important characteristics of the data sets that were analyzed.

Box-counting and functional box-counting analyses

The box-counting and functional box-counting methods were used to investigate scale-invariance in rainfall, and its multifractal character. The box-counting method was used to estimate the fractal dimensions that characterize the set of rainfall occurrences observed in the 1-dimensional space of time, over a range of scales. Table 5.10 summarizes the results obtained for the different cases. For the data from Vale Formoso, the estimates were obtained with rainfall data of different time-resolutions. The main problem found when applying the

Table 5.9 Main characteristics of the rainfall data sets analyzed in this work.

Data set	Measuring device	Depth/time resolution of the record	Temporal resolution	Sample size	Average annual rainfall (mm)
Vale Formoso (Portugal)	recording; float and syphon	0.1 mm/minute	2 min 15 min	23 years: 1963-1985	456.4
Vale Formoso (Portugal)	non-recording	0.1 mm/day	1 day	30 years: 1961-1990	498.8
Vale Formoso (Portugal)	non-recording	0.1 mm/day	1 month	59 years: 1932-1990	565.9
Coimbra (Portugal)	non-recording	0.1 mm/day	1 month	90 years: 1901-1990	989.3
Assink (The Netherlands)	recording; float	0.12 mm/15 minutes	1 hour	11 years: 1976-1986	826.0
Nancy (France)	recording; tipping-bucket	0.2 mm/second	1 min 15 min	4 years: 1988-1991	827.8

box-counting method to rainfall was 'saturation' above a certain critical scale. This scale was larger for the drier climates. 'Saturation' hampered the determination of the upper limit of the scaling range.

For the high-resolution rainfall, and below the lower limit of the scaling range indicated in Table 5.10, analysis was also hampered by a type of 'saturation;' this behaviour indicated some limitations of the data in relation to the description of the intermittence of rainfall. This type of 'saturation' was also observed by Hubert and Carbonnel (1988) and Olsson et al. (1992), among others.

Table 5.10 Fractal dimension that characterize the set of rainy periods observed in the 1-dimensional space of time, estimated with the box-counting method.

Data set	Temporal resolution	Threshold (method)	Range of scales	Fractal dimension
Vale Formoso	2 minutes	—	128 minutes - 11.4 days	0.50
Vale Formoso	1 day	—	1 day - 11 days	0.56
Vale Formoso	1 day	—	11 days - 4.2 months	0.80
Vale Formoso	1 month	—	1 month - 4 months	0.89
Coimbra	1 month	—	> 1 month	1 (saturation)
Assink	1 hour	—	1 hour - 4.5 days	0.56
Nancy	1 minute	0.1 mm/day	8 hours - 3 weeks	0.83

Spectral analysis

Scale-invariance was also investigated with spectral methods. The energy spectra exhibited power-law behaviour for the different cases, confirming the presence of scale invariance in the temporal structure of rainfall over a wide range of scales. However, it was difficult to estimate the upper and lower limits of the scaling range precisely. The estimate of the upper limit of the scaling range was sometimes affected by the size of the sample. For high-resolution rainfall it was difficult to determine the lower limit of the scaling range because of breaks in the scaling observed at the smaller scales. Similar breaks in the scaling (although at varying scales) are reported by e.g. Fraedrich and Larnder (1993), Olsson (1995, 1996), Onof et al. (1996). In this work these breaks were intensity-dependent, which indicates that they are not fundamental in nature. They suggest the presence of scale-dependent measurement problems in the data of the continuously recording rain gauges.

The spectral exponents estimated for the different cases are presented in Table 5.11. For the data from Vale Formoso, estimates of the spectral slope obtained for the data sets of different time-resolutions show good agreement. Results also indicate the presence of statistical variations that are attributable to the different size of the samples. Spectral exponents of intermittent data are difficult to estimate, requiring very large sample sizes.

The spectra of (sufficiently) long rainfall records exhibit a spectral plateau for time scales up to roughly one decade. This plateau is followed by another section (i.e. for even larger time scales), indicating large-scale climatic variability. Similar results have been reported by e.g. Ladoy et al. (1991), Fraedrich and Larnder (1993), Tessier et al. (1996), Svensson et al. (1996).

Table 5.11 Spectral exponents obtained for the rainfall data.

Data set	Time series resolution	Scaling range		Spectral exponent
		lower limit	upper limit	
Vale Formoso	2 minutes	6 hours	> 1 year	0.15
Vale Formoso	15 minutes	6 hours	> 1 year	0.15
Vale Formoso	1 day	1 day	>1 year	0.17
Vale Formoso	1 month	1 month	5 months	0.24
Coimbra	1 month	1 month	> 1 year	≈ 0
Assink	1 hour	1 hour	1 week	0.23
Nancy	1 minute	80 minutes	3 weeks	0.21

Multifractal behaviour

The multifractal behaviour of rainfall was investigated through the probability distributions and moments of the rainfall intensity. These analyses indicate that multifractal properties are maintained over a wide range of scales. The study of these properties was hampered by the behaviour observed for the very large and the very small intensities of the rainfall process. Over these ranges, breaks in the scaling occur. The cause of these breaks lies in either undersampling or the inability of the measuring device to capture the complete dynamic range of the rainfall process.

One can expect some uncertainty in the estimates of the very large and the very small empirical moments. The estimation of high-order empirical moments is dominated by large observations, and are therefore highly variable (see e.g. Kumar et al., 1994). The analysis of the very small moments, which highlight the contributions of the very small rainfall intensities, should be tackled carefully because these intensities are often not properly described by the rainfall data. Despite these difficulties, the analysis of both high and small moments is included in this study with the objective of 'exploring' the whole of the dynamic range covered by the data. In this way, one expects to identify the limitations of the data in describing properly the dynamics of the rainfall process.

For the data from the continuously recording rain gauges, the 'break' in the scaling occurs at a scale of roughly one to two hours. This break in the scaling was shown to be dependent upon the dynamic range investigated, perhaps because the measuring devices cannot capture the complete dynamic range characterizing the intensity of the rainfall process. The main problem here is their low accuracy in measuring low and/or high rainfall intensities. Moreover, the digitization of the pluviographs implies some human bias. Inaccuracies may thus be introduced in the data after the measurement and recording process itself, affecting the 'quality' and reliability of the data. Limitations on information about the true rainfall process affect the multifractal analysis of rainfall. An example of such a limitation is the analysis of (pseudo) time series with a resolution coarser than that of the original records. A negative consequence is that the multifractal behaviour of rainfall can only be studied over a limited range of scales. The expectation is that in some cases the true scaling range is much wider. To confirm this it would be necessary to analyze good quality, high-resolution rainfall data, and larger data sets.

Some results suggest that two different scaling regimes may govern the dynamics of rainfall above and below scales of around one to two weeks. This type of break in the scaling was observed at scales between 1 and 3 weeks by, for example, Ladoy et al. (1991, 1993), Tessier et al. (1996). These authors have explained such a break in terms of a synoptic maximum, which corresponds to temporal scales associated with structures of planetary size. Fraedrich and Larnder (1993) observed a break in the scaling at about 3 days.

The multifractal scaling exponent functions that characterize the statistics of rainfall over a range of scales were derived for the different cases. These functions displayed both non-linear and linear behaviours, indicating the presence of multifractal phase transitions. Discontinuities

in the empirical scaling functions can occur both at small and large values of the orders of singularity and moments. The nature of these phase transitions was investigated.

For high orders of the critical exponents, this special type of statistical behaviour is either explained by divergence of moments or undersampling (i.e. sample size limitations). Divergence of moments, which reveals a 'violent' behaviour of the rainfall process, occurs only for an infinite number of realizations. Experimentally, for a sample containing a large but finite number of realizations, divergence of moments is observed in the form of linear behaviour of the moments scaling function $K(q)$ and codimension function $c(\gamma)$, and algebraic tails of the histograms. The slope of the linear section of the function $K(q)$ increases logarithmically with the number of independent samples studied. The divergence of moments of experimental data (i.e. 'observables') is caused by the presence of large singularities. These data are averages (e.g. temporal averages at a certain resolution scale) of cascade processes developed down to the smallest and innermost scale of the process. The observation scale is often much larger than the true scale of homogeneity of processes.

In general, the values of the singularity γ_{max} observed for the different samples are larger than the values given by the slope of the linear sections (for large moments) of the empirical functions $K(q)$. These highest values of the orders of singularity of the rainfall process correspond to extremely rare events; their probability of occurrence is too low to contribute significantly to the statistical moments (see e.g. Lavallée et al., 1991a).

For the rainfall data analyzed, the critical statistical exponents were estimated with different and complementary methods. For a summary of results see Table 5.12. In this Table, discrepancies between the estimates obtained with different methods are indicated. The variation in the exponents has both statistical and systematic origins. For a comparison of the values of the statistical exponents with those found in other studies see, for example, Lovejoy and Schertzer (1995a, 1995b).

Results show empirically that the critical order q_D for divergence of moments is influenced by the measuring technique of the rainfall process, and the resolution of the observation scale. The critical order for divergence of moments is larger for coarser scales of observations. Because the integration of the small-scale variability occurs on a larger scale, the 'smoothing out' of the high small-scale variability is more 'effective.' Nevertheless, even at very large scales, this integration is still not sufficient to tame the contributions of the small-scale variability of the rainfall process. It leads to the divergence of moments, which occurs even at those large time-scales. This behaviour also means that the rainfall process is very intermittent, not only at smaller time-scales but also at larger ones. The smaller the value of q_D, the more 'violent' is the behaviour of the rainfall process.

Analyses of monthly rainfall from Vale Formoso and Coimbra show that the data from Vale Formoso lead to a smaller critical order q_D for divergence of moments. This behaviour is (qualitatively) consistent with the larger and more irregular fluctuations that are characteristic of the rainfall from Vale Formoso. This comparison of results is not

influenced by the type of data acquisition, because the instrumentation and the observation scale used at both sites were of the same respective types. The results may, however, be affected by the different scaling ranges analyzed.

The data from Vale Formoso were used to investigate seasonal variation in the multifractal temporal structure of rainfall. The exponent functions that describe the scaling of probabilities and moments of the rainfall intensity on different periods of the year were derived. The study indicates that there are differences between the multifractal properties of rainfall occurring during different periods of the year. However, the rainfall process observed throughout the year was found to belong to the same type of multifractal class, having, therefore, the same limiting behaviour. The effect on the results of the (effective) size of the samples and the different rainfall amounts associated with the different periods (which were used to renormalize the data in the corresponding periods) should be taken into consideration.

Table 5.12 Summary of estimates of the critical statistical exponents in the empirical functions that describe the scaling of the probability distributions and moments of the rainfall intensity. The symbols were defined earlier in this Chapter.

Data set	Time series resolution	Scaling range analyzed	γ_{min}	γ_D	γ_{max}	q_{min}	q_s	q_D	$c(\gamma_{min})$	$c(\gamma_{max})$
V. Formoso	15 min	15 min - 11 days	0.36 [1)] 0.30 [2)]	0.68	0.74	0.5	(4.1)	3.1	0.42 0.36	1.02 1.18
V. Formoso	1 day	1 day - 8 days	0.44 0.45	0.75	0.86	0.7	(6.0)	3.6	0.46 0.35	1.50
V. Formoso	1 day	8 days - 4 months	0.05	0.46	0.50 0.79	≈ 0	(4.4)	3.6	0.20 0.15	0.80 1.90
V. Formoso	1 month	1 - 4 months	- 0.03	0.41	0.42 0.88	≈ 0	(3.6)	3.6	0.11	0.66 2.25
Coimbra	1 month	1 - 16 months	- 0.24	—	0.38	≈ 0	3.9	(5.7)	0	0.73
Assink	1 hour	1 hour - 5 days	0.42	0.87	0.96	0.8	(6.3)	2.6	0.42	1.55 1.90
Nancy	15 min	15 min - 11 days	- 0.29	0.68	0.80	—	(3.0)	2.1	0	1.18 1.80

[1)] The top value presented in a cell was estimated from the function $K(q)$.
[2)] The bottom value presented in a cell was estimated from the function $c(\gamma)$.

'Universal' multifractal model

The adequacy of the 'universal' multifractal model (Schertzer and Lovejoy, 1987) for describing the empirical scaling exponent functions determined for the different cases was examined. The parameters of this model are: the Lévy index α; the codimension of the

singularity of the mean C_1; and the degree on non-conservation H. The estimates of the 'universal' parameters obtained with the Double Trace Moment method are given in Table 5.13. These parameters agree well with the estimates obtained by analyzing directly the empirical functions that describe the scaling of the moments and probability distributions of the rainfall intensity. The parameters of the 'universal' model were determined using different methods to increase the reliability of the estimates. For the parameter C_1, in particular, this verification can be carried out in a quite simple way.

Table 5.13 Summary of the 'universal' multifractal parameters, estimated directly using the DTM method, that characterize the statistics of the rainfall process over a range of scales.

Data set	Temporal resolution	Scaling range analyzed	'Universal' multifractal parameters		
			α	C_1	H
V. Formoso	15 minutes	15 min - 11 days	0.49±0.04	0.51±0.02	-0.02
V. Formoso	1 day	1 day - 8 days	0.48±0.08	0.51±0.03	-0.12
V. Formoso	1 day	8 days - 4 months	0.66±0.06	0.30±0.02	-0.03
V. Formoso	1 month	1 month - 4 months	0.82±0.06	0.23±0.01	-0.06
Coimbra	1 month	1 month - 16 months	1.34±0.03	0.12±0.01	—
Assink	1 hour	1 hour - 5 days	0.67±0.11	0.45±0.01	-0.11
Nancy	15 minutes	15 min - 11 days	2 (?)	0.20 (?)	-0.03

The 'universal' multifractal model could be used to describe the statistics of rainfall over only a limited range of values. Over this range, there was good agreement between the theoretical and the empirical exponent scaling functions. Above and below critical values, discrepancies between theoretical and empirical functions were observed for some of the cases studied. The upper limit of this range can be conveniently explained and estimated by means of the theory, which allows the estimation of the statistics of rainfall beyond this value. The critical values are the moments q_D, associated with first-order multifractal phase transitions, and q_s, associated with second-order multifractal phase transitions. These critical moments were estimated correctly with 'universal' multifractals. The lower limit is related to the presence of zero-values in the data, yielding empirical $K(0)\neq 0$, whereas for the theoretical function, $K(0)=0$ because the model implicitly assumes zero-free processes and data. Some of the zero-values in the rainfall data must be 'true' rain-free periods, in the sense that they are intrinsic to the physical process. Others are expected to be 'false,' because of what is known about the limitations of the measuring devices and the methods used to process the records (for example, to digitize the pluviographs). The magnitude of the minimum singularity γ_{min} is believed to be larger than the true value because of the 'assimilation' of very low rainfall rates to zero values (yielding rain-free periods); the data from the tipping-bucket gauge constitutes

an exception to this. This critical value γ_{min} is thus associated with the presence of a minimum non-zero singularity in the data. It will be necessary to study systematically the effect of the dynamic range and time resolution of the rainfall measuring device on the multifractal behaviour exhibited by the data.

The values obtained for the Lévy index show that the model describing the temporal structure of rainfall belongs to a class of models between the β-model ($\alpha=0$) and the log-normal model ($\alpha=2$). The result $\alpha=2$ obtained with the DTM method for the data from Nancy is discussed below. For the other cases, the rainfall process observed belongs to the class of multifractals where the parameter α lies within the interval $]0,1[$; these multifractals are classified as *conditionally soft/hard*. The exception is the monthly data set from Coimbra, which belongs to the class where the parameter α lies within the interval $]1,2[$; these multifractals are classified as *unconditionally hard*.

The *hard* behaviour of multifractals is related to the divergence of moments, which can occur for experimental data (i.e. 'observables'). In a D-dimensional observing space, this 'violent' behaviour is conditioned by the presence of singularities $\gamma>D$. Such singularities in the process are very rare and extreme (high) orders of singularities; they are expected to appear only for large samples. For the conditionally soft/hard multifractals, every statistical moment converges for sufficiently large D. For unconditionally hard multifractals, the critical divergence order q_D remains finite for any D.

The value of the parameter C_1 obtained in the analyses (see Table 5.13) is smaller for the rainfall regime occurring over the larger scales, which is consistent with what is known about the rainfall process. There are fewer zero-rainfall intervals when the process is observed at larger and larger scales.

Analyses of monthly rainfall from Vale Formoso and Coimbra show that the value of the parameter C_1 is larger for the data from the semi-arid climate of Vale Formoso. For the periods studied, the average annual rainfall observed at Vale Formoso is 57% of the rainfall observed at Coimbra. The larger value of the parameter C_1 indicates a process with greater intermittency.

Analysis of point-rainfall for periods of the year selected from an ensemble with marked seasonal fluctuations shows that multifractal analysis has the potential to distinguish between different physics of the rainfall.

The DTM method was not successful in estimating the 'universal' multifractal parameters that characterize the scaling exponent functions derived for the data from Nancy. These data consist of high-resolution rainfall, measured with a tipping-bucket rain gauge. The study focuses on the multifractal analysis of a pseudo time-series that was reconstructed from the record of the gauge. The procedure used to obtain the time series seems to have brought about spurious components in the data. The 'object' of the analysis could not be described by 'universal' multifractals over the range of small intensities of the process. DTM analysis yields $\alpha=2$ and $C_1=0.20$. Non-linear fitting to the empirical moments scaling function over a range

of values gave the estimates α=1.05 and C_1=0.37. The study of the empirical function $K(q)$ near q=1 indicated that was C_1=0.39, which led to α=0.95 using non-linear fitting algorithms. Thus, the DTM method yields values for the 'universal' parameters that are not supported by the other analyses. It is still possible that the scale invariance in the data is of a 'universal' type. However, the DTM method does not permit us to draw this conclusion.

Analysis of (pseudo) rainfall time-series derived from the records of continuously recording rain gauges should be tackled carefully. The cases studied here illustrate how data processing can affect the correct description of rainfall, and how it may introduce artificial orders of singularity of the rainfall intensity in the data. In particular, for data from tipping-bucket gauges, a more convenient way of dealing with this type of data would be to avoid the non-trivial transformation needed to obtain time series from the records. This implies the development of a different technique to analyze this type of data.

Chapter 6
Concluding remarks

The invariance of properties and multifractality of rainfall over a large range of scales lead to a quantification of the rainfall variability that could not be obtained from other approaches. This study of the temporal structure of rainfall contributes to the subject especially because of the long time-span of the records, and because of the various types of acquisition of the rainfall data analyzed. The data were recorded at four different sites in Europe, under different climatic conditions. The point-rainfall was measured with non-recording gauges, and with continuously recording gauges of both the float and the tipping-bucket types. The records have different resolutions over periods of different lengths.

Scaling ranges and scaling regimes in temporal rainfall

The temporal structure of rainfall analyzed in this work exhibits scale-invariant and multifractal behaviour over a wide range of scales. The scaling range was different for the various data sets analyzed. In general, the scaling ranges studied in this work are well above the average scaling ranges that are observed experimentally in many physical systems (see Avnir et al., 1998).

In multifractal studies of rainfall it is essential to have a correct estimate of the upper and lower limits of the scaling range. Nevertheless, it is not always easy to determine the precise values of these limits, nor to interpret breaks in the scaling. Such breaks can be either fundamental in nature, or they can be artefacts arising from limitations of the process sample. Causes of these limitations include the finite size of the sample and the small dynamic range of the measuring device. The existence of 'cut-offs' in the scaling is inherently associated with experimentation on real physical systems (see e.g. Avnir et al., 1998).

The high-resolution rainfall data exhibited a 'break' in the scaling at a scale of about one to two hours. Different analyses support the hypothesis that such a break in the scaling is not of a fundamental nature and is probably caused by the measuring device and data-processing procedures. On the one hand, the measuring device cannot capture the complete dynamic

range of the rainfall process, in particular the very high and the very low rainfall intensities. On the other hand, the processing of the records was found to 'change' the information about the rainfall process. These problems affect the correctness of the description of the rainfall process by the data.

Analyses indicate that two different scaling regimes govern the dynamics of the rainfall process. The critical scale is not always the same for the different rainfall data studied. This transition was found to be roughly at scales of five days and one-and-a-half weeks.

In the determination of the scaling range it is important to recognize that the scaling property can be broken, depending on individual realizations. The variability (intermittency) of processes is so pronounced that a large number of samples will be needed to obtain adequate approximations of the sample statistics. The application of the multifractal theory to the study of small samples may yield 'local' parameters or partial features of the process that do not embrace the full dynamics.

Statistical behaviour of temporal rainfall

The statistics of rainfall are described by multifractal exponent functions that characterize the scaling of probability distributions and moments of the rainfall intensity. These empirical functions show non-linear behaviour for only a limited range of the orders of singularity and moments of the rainfall rate. Above and below critical values, some of the scaling functions consist of linear sections. There are different explanations for this special type of statistical behaviour associated with the discontinuities in the scaling functions. For high orders of the critical exponents, the behaviour is understood to be caused by either divergence of moments or by undersampling (i.e. sample size limitations). For low orders of the critical exponents, the behaviour is caused by the presence of a minimum non-zero intensity in the data. In general, this lower limit of the dynamic range investigated is imposed by the technical limitations of both the measuring device and the methodology used to process the data.

The algebraic behaviour of the tail of the probability distributions is important for studying extreme values. This behaviour of the tail may indicate that the probability of exceeding certain events is greater than the probability predicted by more traditional models, such as the one devised by Gumbel (see e.g. Ladoy et al., 1991).

'Universal' multifractals

The adequacy of the (theoretical) 'universal' multifractal model (Schertzer and Lovejoy, 1987) in describing the statistics of rainfall was examined. This model is a multiplicative cascade model, based on Lévy stochastic variables. It provides analytical expressions for the multifractal exponent scaling functions involving only three parameters. These parameters are: the degree of multifractality α (Lévy index); the codimension of the singularity of the mean C_1; and the degree of non-conservation H.

The values obtained for the Lévy index show that the model that describes the temporal structure of rainfall belongs to a class of models between the β-model ($\alpha=0$) and the log-normal model ($\alpha=2$). For the different cases studied, the estimates of parameter α varied between 0.48 and 1.34, and those of parameter C_1 varied between 0.12 and 0.51. The values of parameter H were close to zero. These findings confirm the results of other researchers (see Sections 3.6 and 5.7). The multifractal parameters varied from location to location. In particular, parameter C_1 varied more strongly than parameter α. The model was 'sensitive' to the number of zeros in the data: the value of parameter α was larger for data with fewer zeros (i.e. rainless intervals).

Seasonal variations in the multifractal temporal structure of rainfall were investigated. Analysis was based on the comparison of scaling functions and 'universal' parameters derived for rainfall data over different periods of the year. Throughout the year, the dynamic behaviour of the rainfall process belongs to the same domain of attraction, thus to the same 'universality' class of multifractals. Nevertheless, the process has different multifractal properties.

Results show that the 'universal' multifractal model provides good descriptions of rainfall statistics over a limited range of orders of singularity and moments of the rainfall rate. The critical values are associated with multifractal phase transitions. In general, the upper limit of this range can be conveniently explained and estimated with the theory. Thus, the statistics of rainfall can be described over a large dynamic range.

The multiplicative cascade processes described by the theoretical 'universal' multifractal model do not show the high variability found in experimental data of the rainfall process observed from sufficiently large samples. The theoretical cascade is a truncated process, in the sense that it is obtained after a finite number of cascade steps. For this process, the moments are always finite. The higher variability of the rainfall process causes divergence of statistics above a certain critical order. Thus, the probability of occurrence of high singularities of the rainfall rate (i.e. of extreme events) is greater than that predicted by the theoretical model. This difference has to be kept in mind in multifractal studies of rainfall.

The disparity between empirical and theoretical scaling functions for small orders of singularity and moments is related to the presence of zeros in the rainfall data; the model implicitly assumes zero-free processes and data. The distinction between true rainless periods (intrinsic to the rainfall process) and false zeros is unclear in certain cases because the limitations of the measuring devices and data-processing procedures are often unknown. The estimate of the critical exponents requires knowledge of the type of data and characteristics of the rainfall measuring device. It will be necessary to study systematically the effect of the dynamic range and time resolution of the measuring device upon the statistical properties of the rainfall data. Such a study should involve the analysis of large data sets from high-resolution measuring devices, so that a large dynamic range is covered.

The critical exponents discussed above (associated with multifractal phase transitions) determine the range of validity of the theoretical 'universal' model for describing the

multifractal scaling exponent functions that characterize the statistics of rainfall. Thus, the 'universal' multifractal parameters and the critical exponents associated with multifractal phase transitions describe the moments and probability distributions of the rainfall rate over a range of scales. These parameters fully characterize the statistics of the rainfall process. Their determination enables the convenient exploration of the invariance of properties across scales.

At present, the statistical properties of some multifractal techniques are not yet well established. In this study, the validity of the multifractal analysis of rainfall was checked by comparison of the results obtained with different methods. The existence of two statistical descriptions that are linked by Legendre transformations makes it possible to cross-check the results. This is important and necessary because there are as yet no statistical tests that can be used to assess the correctness of the results of the multifractal analysis of experimental data.

Developments in the study of rainfall

Special attention should be paid to mechanisms leading to artificial breaks in the scaling. The effect on the statistics of rainfall of the various methods and devices, used both to measure and process rainfall data, deserves more study. Some procedures may introduce an unquantifiable bias in the data. Results suggest that the characteristics of the devices (e.g. their temporal and intensity resolutions) can be associated with critical exponents in the multifractal description of the statistics of rainfall. This is particularly important because of the diversity of measuring standards used world-wide. This diversity can hinder the comparison of the analyses of rainfall recorded with different devices, especially when sufficiently detailed information about the data is lacking.

Results suggest that the investigation of scale invariance and multifractal behaviour in the temporal structure of rainfall can be useful in testing a rainfall-data set to decide whether it is suitable for certain studies. The 'quality' of such a set is important because it can affect the results of investigations of rainfall-induced processes (e.g. runoff and soil erosion). This type of analysis can also contribute to improving the selection of the resolution for data collection, and the type of measuring device. It can also help in evaluating the different procedures that are used to process rainfall records from continuously-recording devices.

Further investigation of the multifractal temporal structure of the rainfall process requires the availability of high-quality data, data with different resolutions, and large data sets. Analysis of the dependency of the multifractal behaviour on climatological and geographical factors is essential and requires a systematic study of rainfall from different origins. This will allow one to relate multifractal behaviour to rainfall-generating mechanisms (see e.g. Svensson et al., 1996; Harris et al., 1996). An important issue is the physical basis of the multifractal behaviour observed.

It is believed that the 'universal' multifractal model can be useful in generating synthetic rainfall data. This application needs more study, because, as this dissertation shows, there are difficulties caused by the presence of (true or false) zeros in the rainfall data, and

intensity-dependent measurement features. The suitability of 'universal' multifractals as a model for high-resolution rainfall is limited, unless some artificial thresholding for the lower intensities is implemented. This is also important to simulate lower resolution rainfall, depending on the climate.

The lack of suitable rainfall data is claimed to be one of the main obstacles to progress in many hydrological studies. The temporal and spatial resolutions of available rainfall data often hamper the detailed modelling of complex hydrological processes. Thus, multifractal simulations of rainfall may play an important role in the study of other hydrological processes (e.g. rainfall induced soil erosion, overland flow, river flow). Multifractals may also offer an alternative approach to the direct study of such hydrological processes (see e.g. Tessier et al., 1996; Gupta et al., 1996; Pandey et al., 1998). Multifractal characterization of different hydrological processes may increase the understanding of their interactions, which are a source of the non-linear behaviour of the Earth´s system.

The knowledge of precipitation variability is fundamental to understanding the behaviour (and changes) of the climate system. Research is focusing on the investigation of trends, in precipitation variability, over the past century. Some studies (e.g. Tsonis, 1996) report that the global mean precipitation has not changed, but that the fluctuations about the mean have increased significantly (on decade to multi-decade time scales). Extremes have become more probable. It is thus important to analyze rainfall with methods that have the potential to assess the full range of rainfall fluctuations. Multifractal theory and methods can certainly play an important role in such studies. The multifractal characterization of rainfall not based on any type of theoretical probability distribution may be a practical tool for assessing correctly the probability of occurrence of extreme events. Such events are often referred to as 'outliers' in the more traditional studies of rainfall.

Appendix I
Generalized central limit theorem; Lévy variables

Gaussian variables are obtained by applying the central limit theorem. This theorem assumes that the variance of stable variables, under addition, is finite. Lévy random variables, which are stable by addition (e.g. Feller, 1971), are a generalization of the Gaussian variables. They have infinite variance. Some features of Lévy stable variables are reviewed briefly in this Appendix. More detailed discussions can be found in Schertzer and Lovejoy (1989; 1993), and Wilson et al. (1991), for example.

Fixed points for sums of independent and identically distributed random variables

Stable fixed points of renormalized sums are defined as follows:

> *The random variables $X_i =^d X_1$ with $i=1,n$ ($=^d$ means equality in probability distributions) are stable points under renormalized sum iff for any integer $n \geq 2$, there exists a positive b_n and a real a_n such that*

$$\sum_{i=1}^{n} X_i =^d b_n X_1 + a_n \tag{I.1}$$

The Gaussian case, with finite variance, corresponds to

$$\langle X_1^2 \rangle \leq \infty \quad \rightarrow \quad b_n = n^{1/2}, \quad a_n = (n-1)\langle X_i \rangle \tag{I.2}$$

where the angular brackets mean ensemble average.

The limit $n \rightarrow \infty$ of the renormalized sum in Eq. (I.3) corresponds to the usual central limit theorem:

$$X = \lim_{n \rightarrow \infty} \frac{\left(\sum_{i=1}^{n} X_i \right) - a_n}{b_n} \tag{I.3}$$

This limit converges to a Gaussian variable X, even if the X_i are not Gaussian, but are of finite variance, i.e.:

$$\langle X^2 \rangle = \langle X_i{}^2 \rangle \leq \infty \quad \rightarrow \quad b_n = n^{1/2}, \quad a_n = n\langle X_i \rangle - \langle X \rangle \tag{I.4}$$

Hence, the Gaussian law is attractive; the variable X is completely independent of the details of the distribution of X_i (as long as $\langle X_i^2 \rangle < \infty$).

Lévy generalized the Gaussian case by relaxing the hypothesis of finite variance for the X_i (which implies that every statistical moment for the limit is finite). Lévy introduced an order of divergence for the moments, α, of the random variables X_i which satisfies either Eq. (I.1) or Eq. (I.3):

$$\langle |X_i|^q \rangle < \infty, \quad \text{for } q < \alpha \tag{I.5a}$$

$$\langle |X_i|^q \rangle = \infty, \quad \text{for } q \geq \alpha \quad (\text{i.e. } \Pr(|X_i| \geq s) \approx s^{-\alpha}, \quad s >> 1) \tag{I.5b}$$

with

$$b_n = n^{1/\alpha} \quad (\text{and, for } \alpha > 1, \; a_n = n\langle X_i \rangle - \langle X \rangle) \tag{I.6}$$

The order of divergence for the moments, α, is called the Lévy index ($0 < \alpha < 2$). The variables X_i are called *hyperbolic* variables due to the algebraic fall-off of their probability distribution tails. Hence, Lévy variables are the stable and fixed points of (renormalized) sums of i.i.d. *hyperbolic* variables. The Gaussian case appears as the regular case $\alpha = 2$, for which the divergence of moments is suppressed.

Characteristic functions of Lévy variables

The probability distributions of Lévy (stable) variables are not expressible in a closed form with elementary functions, with the exceptions $\alpha = 2$, 1, 0.5. However, the second (Laplace) characteristic function can be given in a closed form due to the basic properties of stability.

The function $K(q)$ is the logarithm of the first characteristic function $Z(q)$, which is the (Laplace) transform of the probability distribution $dP(x)$:

$$e^{K(q)} = Z(q) = \langle e^{qX} \rangle = \int e^{qx} dP(x) \tag{I.7}$$

where the argument q is real. The fundamental property of the fixed point (Eq. (I.1)) is transposed easily to the characteristic functions:

The variables X_i ($=^d X_1$, $i=1,n$) of second characteristic function $K(q)$ are stable points under renormalized sum iff, for any integer $n \geq 2$, there exists a positive b_n and a real a_n such that:

$$n\,K(q) = K(b_n q) + a_n q \tag{I.8}$$

The limit theorems correspond to

$$K(q) = \lim_{n\to\infty} n\left[K_i\left(\frac{q}{b_n}\right) - \frac{q\,a_n}{n\,b_n}\right] \tag{I.9}$$

where K_i is the second characteristic function of the variables X_i, and K is the second characteristic function of X. These characteristic functions, up to the recentring term, should be power laws with exponent α bounded above by 2, and must be positive to avoid divergence at q=0. Thus (see details in e.g. Schertzer and Lovejoy, 1989, 1993; Wilson et al., 1991), one obtains

$$K(q) = \lambda_\alpha q^\alpha \tag{I.10}$$

where λ_α is a constant analogous to the variance determining the amplitude of the random variables. The condition $\alpha \le 2$ follows: α=2 is the (extreme) regular Gaussian case; if $\alpha>2$ then $\langle X_i^2\rangle<\infty$ and a Gaussian limit is obtained.

Divergence of moments; the break-down of the law of large numbers

Estimation of the q^{th} order moment of a random variable x, using the standard method, yields (e.g. Schertzer and Lovejoy, 1993)

$$\mu_q = \frac{1}{n}\sum_{i=1}^{n} x_i{}^q \tag{I.11}$$

being the estimated ensemble average $\langle x^q\rangle$ using n independent empirical observations. The (usual) convergence $n\to\infty$, $\mu_q\to\langle x^q\rangle$ is guaranteed by the law of large numbers; it is only true when $\langle x^q\rangle<\infty$. If, however, the variable x is *hyperbolic* with exponent q_D, then the variable x^q is *hyperbolic* with exponent q_D/q. The generalized central limit theorem (for $q>q_D$) leads to

$$\sum_{i=1}^{n} x_i{}^q \to \;\approx\; L_\alpha\, n^{1/\alpha} \tag{I.12}$$

where $\alpha=q_D/q$ (thus, is $\alpha<1$) and L_α is a Lévy random variable (index α). Hence,

$$\mu_q \approx L_\alpha\, n^{\frac{1}{\alpha}-1}, \quad \text{as } n\to\infty \tag{I.13}$$

The estimated q^{th} moment is finite for finite n, but will diverge with sample size. The variable L_α is a very 'wild' random variable; it is *hyperbolic* with exponent α (since $\alpha<1$, it is $\langle L_\alpha\rangle=\infty$). For fixed n, there will be large fluctuations among different experimental estimates (μ_q), and each sample of n values is expected to have a few extreme values that will dominate the estimate of μ_q. These values are referred to as 'outliers'.

Appendix II
Another multifractal formalism

In parallel, two multifractal formalisms have been developed: the *turbulence* formalism (the formalism used in this work; see Chapter 3 for references), and the *strange attractor* formalism (Hentschel and Procaccia, 1983; Grassberger, 1983; Halsey et al., 1986). The *strange attractor* formalism deals with the fractal dimensions of the geometric sets associated with singularities of measures. The singularities of the measures are usually denoted by the symbol α_D, and the corresponding dimensions by $f_D(\alpha_D)$. The *turbulence* formalism deals instead with the singularities of the densities, γ.

The *strange attractor* notation $(f_D(\alpha_D), \tau_D(q))$ is related to the *turbulence* notation $(c(\gamma), K(q))$ as follows (e.g. Schertzer and Lovejoy, 1989; 1993; Schmitt, 1993; see also Chapter 3). The relation between the singularities α_D and γ is

$$\alpha_D = D - \gamma \tag{II.1}$$

where D is the dimension of the space where the process occurs. Moreover, is

$$f_D(\alpha_D) = D - c(\gamma) \tag{II.2}$$

$$\tau_D(q) = (q-1)D - K(q) \tag{II.3}$$

where: $c(\gamma)$ is the codimension function (i.e. the exponent function that describes the scaling of probability distributions, in Eq. (3.22)); q is the order of the statistical moment; $K(q)$ is the moment scaling exponent function (in Eq. (3.23)), of the *turbulence* formalism; and $\tau_D(q)$ is the scaling exponent function for the moments, of the *strange attractor* formalism.

Another important relation of the *strange attractor* formalism is

$$D_q = \frac{\tau(q)}{q-1} \tag{II.4}$$

where D_q is the *generalized dimension* (Hentschel and Procaccia, 1983). This relation leads to the following equivalence in notation:

$$D_q = D - \frac{K(q)}{q-1} \tag{II.5}$$

The representations (f_D, α_D) and (D_q, q) are equivalent. Legendre transforms establish (dual) relations between these exponents (Frisch and Parisi, 1985; Halsey et al., 1986). The original *strange attractor* notation does not have the subscript D; sometimes this subscript is used to indicate that the variables of the *strange attractor* formalism depend on the dimension of the observing space D. This is in contrast with the *turbulence* formalism which is independent of D. The D-dependency makes the *strange attractor* notation and formalism not suitable for dealing with stochastic processes and an infinity of dimensional spaces (e.g. Schertzer et al., 1991). The *strange attractor* notation is useful to deal with multifractal probability measures in low-dimensional phase-spaces.

List of references

Almeida-Teixeira, M. E., R. Fantechi, R. Moore, and V. M. Silva (eds.), 1994. *Advances in radar hydrology*. Proceedings International Workshop, November 11-13, 1991, Lisbon. European Commission, Luxembourg. Report EUR 14334 EN, 361 p.

Avnir, D., O. Biham, D. Lidar, and O. Malcai, 1998. Is the geometry of nature fractal?. Science, 279: 39-40.

Barnsley, M. F., 1993. *Fractals everywhere*. Academic Press Professional, Boston, USA, 531 p. (second edition).

Bärring, L., 1993. The need for a global database of sub-hour rainfall measurements. In: Sevruk, B., and M. Lapin (eds.), *Precipitation Measurement & Quality Control*. Proceedings of the Symposium "Precipitation and Evaporation", September 20-24, 1993, Bratislava, Slovakia, vol. 1, 78-81.

Bell, T. L., and P. K. Kundu, 1996. A study of the sampling error in satellite rainfall estimates using optimal averaging of data and a stochastic model. Journal of Climate, 9(6): 1251-1268.

Bendjoudi, H., P. Hubert, D. Schertzer, and S. Lovejoy, 1997. Multifractal point of view on rainfall intensity-duration-frequency curves. C. R. Acad. Sci. Paris, Série II, Fasc. A, 325(5): 323-326.

Benzi, R., G. Paladin, G. Parisi, and A. Vulpiani, 1984. On the multifractal structure of fully developed turbulence. Journal Physics A, 17: 3521-3531.

Beven, K. J., 1991. Scale considerations. In: Bowles, D. S., and P. E. O'Connell (eds.), *Recent advances in the modeling of hydrological systems*. NATO ASI Series, Serie C: Mathematical and physical sciences, vol. 345. Kluwer Academic Publishers, Dordrecht, The Netherlands, 357-371.

Blöschl, G., and M. Sivapalan, 1995. Scale issues in hydrological modelling: a review. In: Kalma, J. D., and M. Sivapalan (eds.), *Scale issues in hydrological modelling*. John Wiley & Sons, Chichester, UK, 9-48.

Bogárdi, J. J., L. Duckstein, and O. H. Rumambo, 1988. Practical generation of synthetic rainfall event time series in a semi-arid climatic zone. Journal of Hydrology, 103: 357-373.

Box, G. E. P., and G. M. Jenkins, 1976. *Time series analysis: forecasting and control*. Holden-Day, San Francisco, USA, 575 p.

Buishand, T. A., 1977. *Stochastic modelling of daily rainfall sequences*. Ph.D. dissertation (Agricultural University of Wageningen), H. Veenman & Zonen, Wageningen, The Netherlands, 212 p.

Buishand, T. A., 1978. Some remarks on the use of daily rainfall models. Journal of Hydrology, 36: 295-308.

Burlando, P., and R. Rosso, 1996. Scaling and multiscaling models of depth-duration-frequency curves for storm precipitation. Journal of Hydrology, 187(1-2): 45-64.

Carey, D. I., and C. T. Haan, 1978. Markov process for simulating daily point rainfall. Journal Irrigation & Drainage Division, ASCE, 104(IRI): 111-125.

Cârsteanu, A., and E. Foufoula-Georgiou, 1996. Assessing dependence among weights in a multiplicative cascade model of temporal rainfall. Journal of Geophysical Research, 101(D21): 26363-26370.

Caskey, J. E., 1963. A Markov chain model for the probability of precipitation occurrence in intervals of various lengths. Monthly Weather Review, 91(6): 298-301.

Chang, T. J., M. L. Kavvas, and J. W. Delleur, 1984. Daily precipitation modeling by discrete autoregressive moving average processes. Water Resources Research, 20(5): 565-580.

Chin, E. H., 1977. Modeling daily precipitation occurrence process with Markov chain. Water Resources Research, 13(6): 949-956.

Chow, V. T., D. R. Maidment, and L. W. Mays, 1988. *Applied Hydrology*. McGraw-Hill, New York, 572 p.

Colenbrander, H. J., and J. M. I. Verstraate, 1967. Een registrerende grondregenmeter, waarvan de gegevens automatisch kunnen worden verwerkt. Cultuurtechnisch Tijdschrift, 6e Jaargang (1966/1967), 83-93.

Collier, C. G., 1997. The measurement of rainfall. In: Sorooshian, S., H. V. Gupta and S. C. Rodda (eds.), *Land surface processes in hydrology: trials and tribulations of modeling and measuring*. Springer-Verlag, Berlin, Germany. NATO ASI Series, Vol. I 46, 75-111.

Cox, D. R., and V. Isham, 1980. *Point processes*. Monographs on applied probability and statistics. Chapman and Hall, London, UK, 188 p.

Dahmen, E. R., and M. J. Hall, 1990. *Screening of hydrological data: tests for stationarity and relative consistency*. ILRI, Wageningen, The Netherlands, Publ. 49, 58 p.

Davis, A., A. Marshak, W. Wiscombe, and R. Cahalan, 1994. Multifractal characterization of nonstationarity and intermittency in geophysical fields: observed, retrieved, or simulated. Journal of Geophysical Research, 99(D4): 8055-8072.

Desaulniers-Soucy, N., S. Lovejoy, M. R. Ducan, and D. Schertzer, 1995. The multiscaling properties of the spatial distribution of raindrops and ice crystals and the basis of cloud physics. Fifth International Conference on Precipitation "Space-time variability and dynamics of rainfall" (Abstract volume), Elounda, Crete, June 14-16, 1995, 4.18.

DGRN — Direcção-Geral dos Recursos Naturais, undated. '*Água em Portugal*'. Publication of the 'Gabinete Nacional Campanha Educativa da Água' - DGRN, Secretaria de Estado do Ambiente e dos Recursos Naturais, Portugal.

Dingman, S. L., 1993. *Physical hydrology*. Prentice Hall, Englewood Cliffs, New Jersey, 575 p.

Dooge, J. C. I., 1986. Looking for hydrologic laws. Water Resources Research, 22(9): 46S-58S.

Eagleson, P. S., 1970. *Dynamic hydrology*. McGraw-Hill, New York, 462 p.

Eagleson, P. S., 1978. Climate, soil and vegetation 2: The distribution of annual precipitation derived from observed storm sequences. Water Resources Research, 14(5): 713-721.

Eigel, J. D., and I. D. Moore, 1983. A simplified technique for measuring raindrop size and distribution. Transactions of the ASAE, 26(4): 1079-1084.

Engman, E. T., and R. J. Gurney, 1991. Recent advances and future applications of remote sensing for hydrologic modeling. In: Bowles, D. S., and P. E. O'Connel (eds.), *Recent advances in the modeling of hydrologic systems*. Kluwer Academic Publishers, Dordrecht, The Netherlands, 471-495.

Falconer, K. J., 1990. *Fractal geometry: mathematical foundations and applications*. John Wiley & Sons, Chichester, England, 288 p.

Feder, J., 1988. *Fractals*. Plenum Press, New York, 283 p.

Feller, W., 1971. *An introduction to probability theory and its applications*. John Wiley & Sons, New York, USA, vol. II (second edition), 669 p.

Ferrazza, J., W. Bartell, and R. Schick, 1992. *Spray nozzle drop size: How to evaluate measurement techniques and interpret data and reporting procedures*. Spraying Systems Co., Wheaton, USA, Bulletin no. 336.

Ferreira, I. M. M., A. J. R. Ferreira, and D. A. Sims, 1984. *Preliminary analysis of runoff plot data from the Vale Formoso research station, for the years 1962/63 to 1979/80, in terms of the Universal Soil Loss Equation*. Drainage and Soil Conservation Project for the Alentejo Region, Direcção de Hidráulica e Engenharia Agrícola, Lisbon, Portugal.

Feyerherm, A. M., and L. D. Bark, 1967. Goodness of fit of a Markov chain model for sequences of wet and dry days. Journal of Applied Meteorology, 6: 770-773.

Foufoula-Georgiou, E., and K. P. Georgakakos, 1991. Hydrologic advances in space-time precipitation modeling and forecasting. In: Bowles, D. S., and P. E. O'Connell (eds.), *Recent advances in the modeling of hydrologic systems*. NATO ASI Series, Serie C: mathematical and physical sciences, vol. 345. Kluwer Academic Publishers, Dordrecht, The Netherlands, 47-65.

Foufoula-Georgiou, E., and P. Guttorp, 1986. Compatibility of continuous rainfall occurrence models with discrete rainfall observations. Water Resources Research, 22(8): 1316-1322.

Foufoula-Georgiou, E., and D. P. Lettenmaier, 1986. Continuous-time versus discrete-time point process models for rainfall occurrence series. Water Resources Research, 22(4): 531-542.

Foufoula-Georgiou, E., and D. P. Lettenmaier, 1987. A Markov renewal model for rainfall occurrences. Water Resources Research, 23(5): 875-884.

Fraedrich, K., and C. Lamder, 1993. Scaling regimes of composite rainfall time series. Tellus, 45A(4): 289-298.

Frisch, U., and G. Parisi, 1985. Fully developed turbulence and intermittency. In: Ghil, M., R. Benzi, and G. Parisi (eds.) *Turbulence and predicability in geophysical fluid dynamics and climate dynamics*. Proceedings of the International School of Physics "Enrico Fermi", Course LXXXVIII, Italian Physical Society, North-Holland, Amsterdam.

Frisch, U., P. L. Sulem, and M. Nelkin, 1978. A simple dynamical model of intermittentcy in fully developed turbulence. Journal of Fluid Mechanics, 87, 719-724.

Gabriel, K. R., and J. Neumann, 1957. On a distribution of weather cycles by lengths. Quart. J. R. Meteor. Soc., 83: 375-380.

Gabriel, K. R., and J. Neumann, 1962. A Markov chain model for daily occurrences at Tel Aviv. Quart. J. R. Meteor. Soc., 88: 90-95.

Gabriel, P., S. Lovejoy, D. Schertzer, and G. L. Austin, 1988. Multifractal analysis of resolution dependence in satellite imagery. Geophysical Research Letters, 15(12): 1373-1376.

Galloy, E., A. Le Breton, and S. Martin, 1981. A model for weather cycles based on daily rainfall occurrences. In: Cosnard, M. (ed.), *Rhythms in biology and other fields of application*. Springer Lectures Notes in Biomathematics, 49: 303-318.

Georgakakos, K. P., and M. L. Kavvas, 1987. Precipitation analysis, modeling, and prediction in hydrology. Reviews of Geophysics, 25(2): 163-178.

Grassberger, P., 1983. Generalized dimensions of strange attractors. Physics Reviews Letters, 97A(6): 227-230.

Green, J. R., 1964. A model for rainfall occurrences. Journal Roy. Statist. Society, B, 26: 345-353.

Gupta, V. K., and L. Duckstein, 1975. A stochastic analysis of extreme droughts. Water Resources Research, 12(2): 221-228.

Gupta, V. K., and E. Waymire, 1991. On lognormality and scaling in spatial rainfall averages? In: Schertzer, D., and S. Lovejoy (eds.), *Non-linear variability in Geophysics: scaling and fractals*. Kluwer Academic Publishers, The Netherlands, 175-183.

Gupta, V. K., and E. Waymire, 1993. A statistical analysis of mesoscale rainfall as a random cascade. Journal of Applied Meteorology, 32: 251-267.

Gupta, V. K., and E. C. Waymire, 1997. Reply to 'Universal Multifractals do exist!'. Journal of Applied Meteorology, 36(9): 1304.

Gupta, V. K., I. Rodríguez-Iturbe, and E. F. Wood, 1986. *Scale problems in hydrology*. D. Reidel, Dordrecht, The Netherlands, 246 p.

Gupta, V. K., S. L. Castro, and T. M. Over, 1996. On scaling exponents of spatial peak flows from rainfall and river network geometry. Journal of Hydrology, 187(1-2): 81-104.

Haan, C. T., 1977. *Statistical methods in hydrology*. The Iowa State University Press/Ames, 378 p.

Haan, C. T., D. M. Allen, and J. O. Street, 1976. A Markov chain model of daily rainfall. Water Resources Research, 12(3): 443-449.

Halsey, T. C., M. H. Jensen, L. P. Kadanoff, I. Procaccia, and B. I. Shraiman, 1986. Fractal measures and their singularities: the characterization of strange sets. Physics Reviews Letters, 33A(2): 1141-1151.

Harris, D., M. Menabde, A. Seed, and G. Austin, 1996. Multifractal characterization of rain fields with a strong orographic influence. Journal of Geophysical Research, 101(D21): 26405-26414.

Hastings, H. M., and G. Sugihara, 1993. *Fractals: a user's guide for the natural sciences*. Oxford University Press, Oxford, UK, 235 p.

Hentschel, H. G. E., and I. Procaccia, 1983. The infinite number of generalized dimensions of fractals and strange attractors. Physica, 8D: 435-444.

Hochstadt, H., 1971. *The functions of mathematical physics*. Wiley-Interscience, New York.

Hopkins, J. W., and P. Robillard, 1964. Some statistics from the canadian prairie provinces. Journal of Applied Meteorology, 3: 600-602.

Hubert, P., 1992. Analyse multifractale de champs temporels d'intensité des précipitations. Rencontres hydrologiques Franco-Roumaines, UNESCO, Paris, 3-6 September, 1991. SC/92/WS/48, 379-386.

Hubert, P., 1995. Fractals et multifractals appliqués à l'étude de la variabilité temporelle des précipitations. In: Feddes, R. A. (ed.), *Space and time scale variability and interdependencies in hydrological processes*. Cambridge University Press, UK, 175-181.

Hubert, P., and J.-P. Carbonnel, 1988. Caractérisation fractale de la variabilité et de l'ánisotropie des précipitations intertropicales. C. R. Acad. Sci. Paris, Série II, 307: 909-914.

Hubert, P., and J.-P. Carbonnel, 1989. Dimensions fractales de l'occurrence de pluie en climat soudano-sahélien. Hydrologie Continental, 4(1): 3-10.

Hubert, P., and J.-P. Carbonnel, 1991. Fractal characterization of intertropical precipitations variability and anisotropy. In: Schertzer, D., and S. Lovejoy (eds.), *Non-linear variability in Geophysics: scaling and fractals*. Kluwer Academic Publishers, The Netherlands, 209-213.

Hubert, P., and J.-P. Carbonnel, 1993. Analyse multifractale et précipitations extrêmes. Proceedings of the Sixth Scientific Assembly of the International Association of Meteorology and Atmospheric Physics and Fourth Scientific Assembly of the International Association of Hydrological Sciences, Yokohama, Japan, July 11-23, 1993.

Hubert, P., Y. Tessier, S. Lovejoy, D. Schertzer, F. Schmitt, P. Ladoy, J. P. Carbonnel, S. Violette, and I. Desurosne, 1993. Multifractals and extreme rainfall events. Geophysical Research Letters, 20(10): 931-934.

Huff, F. A., 1967. Time distribution of rainfall in heavy storms. Water Resources Research, 3(4): 1007-1019.

Huff, F. A., and S. A. Changnon Jr., 1964. A model 10-inch rainstorm. Journal of Applied Meteorology, 3: 587-599.

Ison, N. T., A. M. Feyerherm, and L. D. Bark, 1971. Wet period precipitation and the gamma distribution. Journal of Applied Meteorology, 10(4): 658-665.

Jones, J. A. A., 1997. *Global hydrology: processes, resources and environmental management*. Longman, England, 399 p.

Kalma, J. D., and M. Sivapalan (eds.), 1995. Scale issues in hydrological modelling. John Wiley & Sons, Chichester, UK, 489 p.

Kavvas, M. L., and J. W. Delleur, 1981. A stochastic cluster model of daily rainfall sequences. Water Resources Research, 17(4): 1151-1160.

Khanal, N. N., and R. L. Hamrick, 1974. A stochastic model for daily rainfall data synthesis. Proceedings of the Symposium on "Statistical Hydrology", 1971, Tucson, Arizona. U.S. Dept. of Agric., Publ. no. 1275, 197-210.

Klemeš, V., 1983. Conceptualisation and scale in hydrology. Journal of Hydrology, 65: 1-23.

Kohnke, H., and A. R. Bertrand, 1959. *Soil Conservation*. McGraw-Hill, New York, 298 p.

Kolmogorov, A. N., 1962. A refinement of previous hypotheses concerning the local structure of turbulence in a viscous incompressible fluid at high Reynolds number. Journal of Fluid Mechanics, 13: 82-85.

Koutsoyiannis, D., and D. Pachakis, 1996. Deterministic chaos versus stochasticity in analysis and modeling of point rainfall series. Journal of Geophysiscal Research, 101(D21): 26441-26451.

Krajewski, W. F., E. N. Anagnoustou, and G. J. Ciach, 1996. Effects of the radar observation process on inferred rainfall statistics. Journal of Geophysical Research, 101(D21): 26493-26502.

Kumar, P., P. Guttarp, and E. Foufoula-Georgiou, 1994. A probability-weighted moment test to assess simple scaling. Stochastic Hydrology and Hydraulics, 8(3): 173-183.

Ladoy, P., S. Lovejoy, and D. Schertzer, 1991. Extreme variability of climatological data: scaling and intermittency. In: Schertzer, D., and S. Lovejoy (eds.), *Non-linear variability in Geophysics: scaling and fractals*. Kluwer Academic Publishers, The Netherlands, 241-250.

Ladoy, P., F. Schmitt, D. Schertzer, and S. Lovejoy, 1993. Variabilité temporelle multifractale des observations pluviométriques à Nîmes. C. R. Acad. Sci. Paris, Série II, 317: 775-782.

Lavallée, D., 1991. *Multifractal techniques: analysis and simulation of turbulent fields*. Ph.D. dissertation, McGill University, Montreal, Canada.

Lavallée, D., D. Schertzer, and S. Lovejoy, 1991a. On the determination of the codimension function. In: Schertzer, D., and S. Lovejoy (eds.), *Non-linear variability in Geophysics: scaling and fractals*. Kluwer Academic Publishers, The Netherlands, 99-110.

Lavallée, D., S. Lovejoy, D. Schertzer, and P. Ladoy, 1991b. Nonlinear variability and landscape topography: analysis and simulation. In: Cola, L. de, and N. Lam (eds.), *Fractals in geography*. Kluwer, 171-205.

Lavallée, D., S. Lovejoy, D. Schertzer, and F. Schimtt, 1992. On the determination of universal multifractal parameters in turbulence. In: Moffat, K., M. Tabor, and G. Zaslavsky (eds.), Topological aspects of the dynamics of fluids and plasmas. Kluwer, Dordrecht, 463-478.

Larson, L. W., and E. L. Peck, 1974. Accuracy of precipitation measurements for hydrologic modelling. Water Resources Research, 10(4): 857-863.

Lima, J. L. M. P. de, 1990. The effect of oblique rain on inclined surfaces: a nomograph for the rain-gauge correction factor. Journal of Hydrology, 115: 407-412.

Lima, M. I. P. de, P. J. J. F. Torfs, and J. J. Bogardi, 1993. Multifractal analysis of rainfall time series. International Conference "Nonlinear Variability in Geophysics 3 - Scaling and multifractal processes" (Abstract volume), September 10-17, 1993, Cargèse, France.

Lima, M. I. P. de, S. Lovejoy, and D. Schertzer, 1994. Empirical analysis of multifractal phase transitions observed for temporal rainfall processes. Annales Geophysicae, Vol. 12, Supplement II, C482.

Lima, M. I. P. de, and J. J. Bogardi, 1995. Multifractals in hydrological studies: the analysis of rainfall time series. In: Proceedings of the UNESCO International Conference "Statistical and bayesian methods in hydrological sciences", September 11-13, 1995, UNESCO, Paris, France, vol. II.

Lima, M. I. P. de, S. Lovejoy, D. Schertzer, and J. J. Bogardi, 1995. The influence of the type of rainfall measuring device on the multifractal analysis of temporal rainfall processes. Annales Geophysicae, Vol. 13, Supplement II, C465.

Lovejoy, S., 1981. The statistical characterization of rain areas in terms of fractals. In: Proceedings of the 20th Conference on "Radar Meteorology", November 30 - December 3, 1981, Boston, USA, sponsored by American Meteorological Society, 476-483.

Lovejoy, S., 1982. The area-perimeter relationship for rain and cloud areas. Science, 216: 185-187.

Lovejoy, S., 1983. La géométrie fractale des nuages et des régions de pluie et les simulations aléatoires. La Houille Blanche, n° 5/6, 431-435.

Lovejoy, S., 1994. Personal communication.

Lovejoy, S., and B. B. Mandelbrot, 1985. Fractal properties of rain, and a fractal model. Tellus, 37A: 209-232.

Lovejoy, S., and D. Schertzer, 1985a. Rainfronts, fractals and rainfall simulations. In: Goodison, B.E. (ed.), *Hydrological applications of remote sensing and remote data transmission*. Proceedings of the Hamburg Symposium, August 1983. IAHS Publication n° 145, 323-334.

Lovejoy, S., and D. Schertzer, 1985b. Generalized scale invariance in the atmosphere and fractal models of rain. Water Resources Research, 21(8): 1233-1250.

Lovejoy, S., and D. Schertzer, 1990a. Multifractals, universality classes and satellite and radar measurements of cloud and rain fields. Journal of Geophysical Research, 95(D3): 2021-2034.

Lovejoy, S., and D. Schertzer, 1990b. Our multifractal atmosphere: a unique laboratory for non-linear dynamics. Physics in Canada, 46(4): 62-71.

Lovejoy, S., and D. Schertzer, 1990c. Fractals, raindrops and resolution dependence of rain measurements. Journal of Applied Meteorology, 29: 1167-1170.

Lovejoy, S., and D. Schertzer, 1991. Multifractal analysis techniques and the rain and cloud fields from 10^{-3} to 10^{6} m. In: Schertzer, D., and S. Lovejoy (eds.), *Non-linear variability in Geophysics: scaling and fractals*. Kluwer Academic Publishers, The Netherlands, 111-144.

Lovejoy, S., and D. Schertzer, 1992. *Multifractals in Geophysics*. Lecture notes, AGU-CGU-MSA Spring Meeting, May 11, 1992, Canada.

Lovejoy, S., and D. Schertzer, 1995a. Multifractals and rain. In: Kunzewicz, Z. W. (ed.), *New Uncertainty Concepts in Hydrology and Water Resources*. UNESCO series in Water Sciences, Cambridge University Press, New York, 62-103.

Lovejoy, S., and D. Schertzer, 1995b. How bright is the Coast of Brittany? In: Wilkinson, G., I. Kanellopoulos, and J. Mégier (eds.), *Fractals in Geoscience and remote sensing*. Proceedings of Joint JRC/EARSeL Expert Meeting, Ispra, Italy, April 1994. Image Understanding Research, vol. 1, 102-151.

Lovejoy, S., D. Schertzer, and A. A. Tsonis, 1987. Functional box-counting and multiple elliptical dimensions in rain. Science, 235: 1036-1038.

Lovejoy, S., D. Schertzer, P. Silas, Y. Tessier, and D. Lavallée, 1993. The unified scaling model of atmospheric dynamics and systematic analysis of scale invariance in cloud radiances. Annales Geophysicae, 11: 119-127.

Mandelbrot, B., 1967. How long is the Coast of Britain? Statistical self-similarity and fractional dimension. Science, 156: 636-639.

Mandelbrot, B., 1974. Intermittent turbulence in self-similar cascades: divergence of high moments and dimension of the carrier. Journal of Fluid Mechanics, 62, part II: 331-358.

Mandelbrot, B., 1975. *Les objects fractals: forme, hasard et dimension*. Flammarion, Paris.

Mandelbrot, B., 1977. *Fractals: form, chance and dimension*. Freeman, San Francisco, 365 p.

Mandelbrot, B., 1982. *The fractal geometry of nature*. Freeman, San Francisco, 460 p.

Mandelbrot, B. B., 1989. A class of multinomial multifractal measures with negative (latent) values for the "dimension" f(α). In: Pietronero, L. (ed.), *Fractals' physical origin and properties*. Plenum Press, New York, 3-29.

Mandelbrot, B. B., 1991. Random multifractals: negative dimensions and the resulting limitations of the thermodynamical formalism. Proc. R. Soc. London A 434, 79.

Marsan, D., D. Schertzer, and S. Lovejoy, 1996. Causal space-time multifractal processes: predictability and forecasting of rain fields. Journal of Geophysical Research, 101(D21): 26333-26346.

McIlveen, R., 1992. *Fundamentals of weather and climate*. Chapman & Hall, London, UK, 497 p.

McLeod, A. I., and K. W. Hipel, 1995. Exploratory spectral analysis of hydrological times series. Stochastic Hydrology and Hydraulics, 9: 171-205.

Menabde, M., D. Harris, A. Seed, G. Austin, and D. Stow, 1997. Multiscaling properties of rainfall and bounded random cascades. Water Resources Research, 33(12): 2823-2830.

Mielke, P. W., Jr., 1973. Another family of distributions for describing and analyzing precipitation data. Journal of Applied Meteorology, 10(2): 275-280.

Mielke, P. W., Jr., and E. S. Johnson, 1974. Some generalized Beta distributions of the second kind having desirable application features in hydrology and meteorology. Water Resources Research, 10(2): 275-280.

Monfort, M. A. J. van, and J. V. Witter, 1986. The generalized Pareto distribution applied to rainfall depths. Hydrological Sciences Journal, 31(2): 151-162.

NRC — National Research Council, 1991. *Opportunities in the hydrologic sciences*. National Academy Press, Washington, DC, USA, 348 pp.

Novikov, E. A., and R. Stewart, 1964. Intermittency of turbulence and spectrum of fluctuations in energy dissipation. Izv. Akad. Nauk. SSSR Ser. Geofiz., 3, 408-412.

Obeysekera, J. T. B., G. O. Tabios III, and J. D. Salas, 1987. On parameter estimation of temporal rainfall models. Water Resources Research, 23(10): 1837-1850.

Obukhov, A. M., 1962. Some specific features of atmospheric turbulence. Journal of Fluid Mechanics, 13: 77-81.

Olsson, J., 1995. Limits and characteristics of the multifractal behaviour of a high-resolution rainfall time series, Nonlinear Processes in Geophysics, 2(1): 23-29.

Olsson, J., 1996. Validity and applicability of a scale-independent, multifractal relationship for rainfall. Journal of Atmospheric Research, 42: 53-65.

Olsson, J., and J. Niemczynowicz, 1994. Multifractal relations in rainfall data. In: Kettunen, J., K. Granlund, M. Paasonen-Kivekäs, and H. Sirviö (eds.), *Spatial and temporal variability and interdependencies among hydrological processes*. Proceedings Nordic Seminar, September 14-16, 1994, Kirkkonummi, Finland. NHP Report No. 36, 110-119.

Olsson, J., and J. Niemczynowicz, 1996. Multifractal analysis of daily spatial rainfall distributions. Journal of Hydrology, 187(1-2): 29-43.

Olsson, J., J. Niemczynowicz, R. Berndtsson, and M. Larson, 1992. An analysis of the rainfall time structure by box counting: some practical implications. Journal of Hydrology, 137(1-4): 261-277.

Onof, C., P. Northrop, H. S. Wheater, and V. Isham, 1996. Spatiotemporal storm structure and scaling property analysis for modeling. Journal of Geophysical Research, 101(D21): 26415-26425.

Over, T. M., and V. K. Gupta, 1994. Statistical analysis of mesoscale rainfall: dependence of a random cascade generator on large-scale forcing. Journal of Applied Meteorology, 33: 1526-1542.

Over, T. M., and V. K. Gupta, 1996. A space-time theory of mesoscale rainfall using random cascades. Journal of Geophysical Research, 101(D21): 26319-26331.

Pandey, G., S. Lovejoy, and D. Schertzer, 1998. Multifractal analysis of daily river flows including extremes for basins of five to two million square kilometres, one day to 75 years. Journal of Hydrology, 208(1-2): 62-81.

Perica, S., and E. Foufoula-Georgiou, 1996a. Linkage of scaling and thermodynamic parameters of rainfall: results from midlatitude mesoscale convective systems. Journal of Geophysical Research, 101(D3): 7431-7448.

Perica, S., and E. Foufoula-Georgiou, 1996b. Model for multiscale disaggregation of spatial rainfall based on coupling meteorological and scaling descriptions. Journal of Geophysical Research, 101(D21): 26347-26361.

Pilgrim, D., and I. Cordery, 1975. Rainfall temporal patterns for design floods. Journal Hydraulics Engineering, 101(HY1): 81-95.

Press, W. H., B. P. Flannery, S. A. Teukolsky, and W. T. Vetterling, 1989. *Numerical recipes, The art of scientific computing* (Fortran version). Cambridge University Press, Cambridge, UK, 702 p.

Richardson, C. W., 1981. Stochastic models of rainfall precipitation, temperature, and solar radiation. Water Resources Research, 17(1): 182-190.

Richardson, C. W., 1982. A comparison of three distributions for the generation of daily rainfall amounts. In: Singh, V. P. (ed.), *Statistical analysis of rainfall and runoff*. Proc. Intern. Symposium on Rainfall-Runoff Modeling, May 18-21, 1981, Mississippi State University, Mississipi. Water Resources Publications, Littleton, Colorado, USA, 67-78.

Rodda, J. C., 1997. Data, data everywhere, nor any drop to drink. In: Sorooshian, S., H. V. Gupta, and J. C. Rodda (eds.), *Land surface processes in hydrology: trials and tribulations of modeling and measuring*. Springer-Verlag, Berlin, Germany. NATO ASI Series, vol. I46, 3-18.

Rodríguez-Iturbe, I., and V. K. Gupta (eds.), 1983. Scale problems in hydrology. Journal of Hydrology, vol. 65 (special issue).

Rodríguez-Iturbe, I., V. K. Gupta, and E. Waymire, 1984. Scale considerations in the modelling of temporal rainfall. Water Resources Research, 20(11): 1611-1619.

Rodríguez-Iturbe, I., D. R. Cox, and V. Isham, 1987a. Some models for rainfall based on stochastic point processes. Proc. R. Soc. Lond., A, 410: 269-288.

Rodríguez-Iturbe, I., B. Febres de Power, and J. B. Valdes, 1987b. Rectangular pulses point process models for rainfall: analysis of empirical data. Journal of Geophysical Research, 92(D8): 9645-9656.

Rodríguez-Iturbe, I., D. R. Cox, and V. Isham, 1988. A point process model for rainfall: further developments. Proc. R. Soc. Lond., A, 417: 283-298.

Rodríguez-Iturbe, I., B. Febres de Power, M. B. Sharifi, and K. P. Georgakakos, 1989. Chaos in rainfall. Water Resources Research, 25(7): 1667-1675.

Roldán, J., and D. A. Woolhiser, 1982. Stochastic daily precipitation models, 1: A comparison of occurrence processes. Water Resources Research, 18(5): 1451-1459.

Roxo, M. J., P. C. Casimiro, and R. S. de Brito, 1996. Inner Lower Alentejo field site: cereal cropping, soil degradation and desertification. In: Brandt, C. J., and J. B. Thornes (eds.), *Mediterranean desertification and land use*. John Wiley & Sons, Chichester, England, 111-135.

Salas, J. D., 1993. Analysis and modeling of hydrologic time series. In: Maidment, D. R. (ed.), *Handbook of hydrology*. McGraw-Hill, New York, 19.1-19.72.

Salas, J. D., J. W. Delleur, V. Yevjevich, and W. L. Lane, 1980. *Applied modeling of hydrologic time series*. Water Resources Publications, Littleton, USA, 484 p.

Schertzer, D., and S. Lovejoy, 1983. Elliptical turbulence in the atmosphere. In: Proceedings of the Fourth Symposium on "Turbulent shear flows", Karlshule, West Germany, 11.1-11.8.

Schertzer, D., and S. Lovejoy, 1984. On the dimension of atmospheric motions. In: Tatsumi, T. (ed.), *Turbulence and chaotic phenomena in fluids*. Elsevier Science Publishers, 505-512.

Schertzer, D., and S. Lovejoy, 1985. The dimension and intermittency of atmospheric dynamics. In: Bradbury, L. J. S., F. Durst, B. E. Launder, F. W. Schmidt, and J. H. Whitelaw (eds.), *Turbulent shear flow 4*. Selected papers from the Fourth International Symposium on "Turbulent Shear Flows", Springer-Verlag, Berlim, 7-33.

Schertzer, D., and S. Lovejoy, 1987. Physical modeling and analysis of rain and clouds by anisotropic scaling multiplicative processes. Journal of Geophysical Research, 92(D8): 9693-9714.

Schertzer, D., and S. Lovejoy, 1988. Multifractal simulations and analysis of clouds by multiplicative processes. Atmospheric Research, 21: 337-361.

Schertzer, D., and S. Lovejoy, 1989. Nonlinear variability in Geophysics: multifractal simulations and analysis. In: Pietronero, L. (ed.), *Fractals' physical origin and properties*. Plenum Press, New York, 49-79.

Schertzer, D., and S. Lovejoy (eds.), 1991a. *Non-linear variability in Geophysics: scaling and fractals*. Kluwer Academic Publishers, The Netherlands. 318 p.

Schertzer, D., and S. Lovejoy, 1991b. Nonlinear geodynamical variability: multiple singularities, universality and observables. In: Schertzer, D., and S. Lovejoy (eds.), *Non-linear variability in Geophysics: scaling and fractals*. Kluwer Academic Publishers, The Netherlands, 41-82.

Schertzer, D., and S. Lovejoy, 1992. Hard and soft multifractal processes. Physica A, 185, 187-194.

Schertzer, D., and S. Lovejoy, 1993. *Nonlinear variability in Geophysics 3: scaling and multifractal processes*. Lecture notes, AGU/EGS Conference, September 10-17, 1993. Cargèse, France.

Schertzer, D., and S. Lovejoy, 1994. Multifractal generation of self-organized criticality. In: Novak, M. (ed.), *Fractals in the natural and applied sciences*. Elsevier, North-Holland, 325-339.

Schertzer, D., and S. Lovejoy, 1995a. From scalar cascades to lie cascades: joint multifractal analysis of rain and cloud processes. In: Feddes, R. A. (ed.), *Space and time scale variability and interdependencies in hydrological processes*. Cambridge University Press, UK, 153-173.

Schertzer, D., and S. Lovejoy, 1995b. Standard and advanced multifractal techniques in remote sensing. In: Wilkinson, G., I. Kanellopoulos, and J. Mégier (eds.), *Fractals in Geoscience and remote sensing*. Proceedings of Joint JRC/EARSeL Expert Meeting, Ispra, Italy, April 1994. Image Understanding Research, vol. 1, 11-40.

Schertzer, D., and S. Lovejoy, 1997. Universal multifractals do exist!: Comment on 'A statistical analysis of mesoscale rainfall as a random cascade'. Journal of Applied Meteorology, 36(9): 1296-1303.

Schertzer, D., S. Lovejoy, R. Visvanathan, D. Lavallée, and J. Wilson, 1988. Universal multifractals in turbulence. In: Weitz, D. A., L. M. Sander, and B. B. Mandelbrot (eds.), *Fractal aspects of materials: disordered systems*. Materials Research Society, Pittsburg, 267.

Schertzer, D., S. Lovejoy, D. Lavallée, and F. Schmitt, 1991. Universal hard multifractal turbulence: theory and observations. In: Sagdeev, R. Z., U. Frisch, F. Hussain, S. S. Moiseev, and N. S. Erokhin (eds.), *Nonlinear dynamics of structures*. World Scientific, 213-235.

Schertzer, D., S. Lovejoy, and D. Lavallée, 1993. Generic multifractal phase transitions and self-organized criticality. In: Perdang, J. M., and A. Lejeune (eds.), *Cellular Automata: prospects in astronomy and astrophysics*. World Scientific, Singapore.

Schertzer, D., S. Lovejoy, and F. Schmitt, 1995. Structures in turbulence and multifractal universality. In: Meneguzzi, M., A. Pouquet, and P. L. Sulem (eds.), *Small scale structures in 3D hydro and MHD turbulence*. Lecture notes in physics, 462: 137-144.

Schmitt, F., 1993. *Turbulence développée et multifractals universels en soufflerie et dans l'atmosphère*. Ph.D. dissertation, L'Université Pierre et Marie Curie (Paris VI), Paris, France, 273 p.

Schmitt, F., D. Lavallée, D. Schertzer, and S. Lovejoy, 1992a. Empirical determination of universal multifractal exponents in turbulent velocity fields. Physical Review Letters, 68(3): 305-308.

Schmitt, F., D. Lavallée, S. Lovejoy, D. Schertzer, and C. Hooge, 1992b. Estimations directes des indices de multifractals universels dans le champ de vent et de température. C. R. Acad. Sci. Paris, Série II, 314: 749-754.

Schmitt, F., D. Schertzer, S. Lovejoy, and Y. Brunet, 1993. Estimation of universal multifractal indices for atmospheric turbulent fields. Fractals, 1(3): 568-575.

Schuster, H. G., 1988. *Deterministic chaos: an introduction*. VCH, New York, 270 p.

Seyhan, E., 1977. *Fundamentals of hydrology*. Geografisch Instituut der Rijksuniversiteit te Utrecht, Utrecht, The Netherlands.

Sevruk, B. (ed.), 1989. *Precipitation measurements*. Proceedings of WMO/IAHS/ETH International Workshop on "Precipitation Measurements", December 3-7, 1989, St. Moritz, Switzerland.

Sevruk, B., 1993a. Spatial and temporal inhomogeneity of global precipitation data. In: Sevruk, B., and M. Lapin (eds.), *Precipitation measurement & quality control*. Proceedings of Symposium on "Precipitation and Evaporation", September 20-24, 1993, Bratislava, Slovakia, 15-19.

Sevruk, B., 1993b. WMO precipitation measurement intercomparisons. In: Sevruk, B., and M. Lapin (eds.), *Precipitation measurement & quality control*. Proceedings of Symposium on "Precipitation and Evaporation", September 20-24, 1993, Bratislava, Slovakia, 120-121.

Sevruk, B., 1993c. Physics of precipitation gauges. In: Sevruk, B., and M. Lapin (eds.), *Precipitation measurement & quality control*. Proceedings of Symposium on "Precipitation and Evaporation", September 20-24, 1993, Bratislava, Slovakia, 135-142.

Sevruk, B., and S. Klemm, 1989. Types of standard precipitation gauges. In: Sevruk, B. (ed.), *Precipitation measurements*. Proceedings of WMO/IAHS/ETH International Workshop on "Precipitation Measurements", December 3-7, 1989, St. Moritz, Switzerland, 227-232.

SGHB — Study Group 'Hupselse Beek', 1971. *Report of the hydrologic research in the Catchment of the Hupselse Beek (period November 1968/March 1970)*. Bi-annual Report 1.

SGHB — Study Group 'Hupselse Beek', 1972. *Second report of the hydrologic research in the Catchment of the Hupselse Beek (period April 1970/April 1972)*. Bi-annual Report 2.

Sharon, D., 1980. The distribution of hydrologically effective rainfall incident on sloping ground. Journal of Hydrology, 46, 165-188.

Sharon, D., and A. Arazi, 1993. An empirical basis for modeling the effect of watershed topography on the local distribution of wind-driven rainfall. In: Sevruk, B., and M. Lapin (eds.), *Precipitation measurement & quality control*. Proceedings of Symposium on "Precipitation and Evaporation", September 20-24, 1993, Bratislava, Slovakia, 159-164.

Sharon, D., J. Morin, and Y. Moshe, 1988. Micro-topographical variations of rainfall incident on ridges of a cultivated field. Transactions of the ASAE, 31(6), 1715-1722.

Shaw, E. M., 1983. *Hydrology in practice*. Van Nostrand Reinhold (International), London, 539 p.

Siebesma, A. P., 1989. *Multifractals in condensed matter*. Ph.D. dissertation, The Cheese Press, Edam, The Netherlands, 143 p.

Singh, V. P. (ed.), 1982. *Statistical analysis of rainfall and runoff*. Proc. Intern. Symposium on Rainfall-Runoff Modeling, May 18-21, 1981, Mississippi, USA Water Resources Publications, Littleton, Colorado, USA, 700 p.

Singh, V. P., 1992. *Elementary Hydrology*. Prentice-Hall, New Jersey, USA, 973 p.

Small, M. J., and D. J. Morgan, 1986. The relationship between a continuous-time renewal model and a discrete Markov Chain model of precipitation occurrence. Water Resources Research, 22(10): 1422-1430.

Smith, J. A., 1993. Precipitation. In: Maidment, D. R. (ed.), *Handbook of hydrology*. McGraw-Hill, New York, 3.1-3.47.

Smith, J. A., and A. F. Karr, 1983. A point process model of summer season rainfall occurrence. Water Resources Research, 19(1): 95-103.

Smith, R. E., and H. A. Schreiber, 1973. Point processes of seasonal thunderstorm rainfall, Part 1: Distribution of rainfall events. Water Resources Research, 9(4): 871-884.

Smith, R. E., and H. A. Schreiber, 1974. Point processes of seasonal thunderstorm rainfall, Part 2: Rainfall depth probabilities. Water Resources Research, 10(3): 418-423.

Sokollek, V., H. Haamann, and A. Meuser, 1989. Precipitation measurement errors as a function of the degree of gauge site exposure to wind. In: Sevruk, B. (ed.), *Precipitation measurement*. Procedings of the WMO/IAHS/ETH International Workshop on "Precipitation Measurement", December 3-7, 1989, St. Moritz, Switzerland, 109-116.

Stedinger, J. R., R. M. Vogel, and E. Foufoula-Georgiou, 1993. Frequency analysis of extreme events. In: Maidment, D. R. (ed.), *Handbook of hydrology*. McGraw-Hill, New York, 18.1-18.66.

Stem, R. D., and R. Coe, 1984. A model fitting analysis of rainfall data. Journal Roy. Statist. Society, Ser. A. 147: 1-34.

Svensson, C., J. Olsson, and R. Berndtsson, 1996. Multifractal properties of daily rainfall in two different climates. Water Resources Research, 32(8): 2463-2472.

Tél, T., 1988. Fractals, multifractals, and thermodynamics: an introductory review. Z. Naturforsch., 43a: 1154-1174.

Tessier, Y., S. Lovejoy, and D. Schertzer, 1988. Multifractal analysis of global rainfall from 1 day to 1 year. Nonlinear Variability in Geophysics 2 (Abstract volume), Paris.

Tessier, Y., S. Lovejoy, and D. Schertzer, 1992. Universal multifractals: theory and observations for rain and clouds. In: Proceedings of 11th International Conference on "Clouds and Precipitation", Montreal, Canada, vol. 2, 1098-1101.

Tessier, Y., S. Lovejoy, and D. Schertzer, 1993. Universal multifractals: theory and observations for rain and clouds. Journal of Applied Meteorology, 32(2): 223-250.

Tessier, Y., S. Lovejoy, and D. Schertzer, 1994. Multifractal analysis and simulation of the global meteorological network. Journal of Applied Meteorology, 33(12): 1572-1586.

Tessier, Y., S. Lovejoy, P. Hubert, D. Schertzer, and J.-P. Carbonnel, 1995. Multifractal relations between rainfall and river flows. Fifth International Conference on Precipitation "Space-time variability and dynamics of rainfall" (Abstract volume), Elounda, Crete, June 14-16, 1995, 4.20.

Tessier, Y., S. Lovejoy, P. Hubert, D. Schertzer, and S. Pecknold, 1996. Multifractal analysis and modeling of rainfall and river flows and scaling, causal transfer functions. Journal of Geophysical Research, 101(D21): 26427-26440.

Todorovic, P., and D. A. Woolhiser, 1974. Stochastic model of daily rainfall. In: Proceedings of the USDA-IASPS Symposium on "Statistical Hydrology", Tucson, Arizona, held in 1971. USDA, Misc. Publ. n° 1275, 232-246.

Todorovic, P., and V. Yevjevich, 1969. Stochastic processes of precipitation. Colorado State Univ., Hydrology Paper 35, 1-61.

Tomás, P. M. P. P., 1992. *Estudo da erosão hídrica em solos agrícolas: aplicação à região sul de Portugal*. M.Sc. dissertation, Instituto Superior Técnico, Universidade Técnica de Lisboa, Lisboa, 194 p.

Torfs, P. J. J. F, 1998. Personal communication.

Tsonis, A. A., 1996. Widespread increase in low-frequency variability of precipitation over the past century. Nature, 382(6593): 700-702.

Tsonis, A. A., G. N. Triantafyllou, and K. P. Georgakakos, 1996. Hydrological applications of satellite data - 1. Rainfall estimation. Journal of Geophysical Research, 101(D21): 26517-26525.

Valdes, J. B., I. Rodríguez-Iturbe, and V. K. Gupta, 1985. Approximations of temporal rainfall from a multidimensional model. Water Resources Research, 21(8): 1259-1270.

Viessman, W., Jr., and G. L. Lewis, 1996. *Introduction to hydrology*. HarperCollins College Publishers, New York, USA, 760 p. (fourth edition).

Warmerdam, P. M. M., J. Kole, and J. Chormanski, 1997. Modelling rainfall-runoff processes in the Hupselse Beek research area. In: Viville, D., and I. G. Littlewood (eds.), *Ecohydrological processes in small basins*. Proceedings of the Sixth Conference of the European Network of Experimental and Representative Basins, September 24-26, 1996, Strasbourg, France. IHP-V (UNESCO, Paris), Technical Documents in Hydrology, No. 14, 155-160.

Waymire, E., 1985. Scaling limits and self-similarity in precipitation fields. Water Resources Research, 21(8): 1271-1281.

Waymire, E., and V. K. Gupta, 1981a. The mathematical structure of rainfall representations, 1: A review of stochastic rainfall models. Water Resources Research, 17(5): 1262-1272.

Waymire, E., and V. K. Gupta, 1981b. The mathematical structure of rainfall representations, 2: A review of the theory of point processes. Water Resources Research, 17(5): 1273-1285.

Waymire, E., and V. K. Gupta, 1981c. The mathematical structure of rainfall representations, 3: Some applications of the point process theory to rainfall processes. Water Resources Research, 17(5): 1287-1294.

Weatherhead, E. C., G. C. Reinsel, G. C. Tiao, X.-L. Meng, D. Choi, W.-K. Cheang, T. Keller, J. DeLuisi, D. J. Wuebbles, J. B. Kerr, A. J. Miller, S. J. Oltmans, and J. E. Frederick, 1998. Factors affecting the detection of trends: statistical considerations and applications to environmental data. Journal of Geophysical Research, 103(D14): 17149-17161.

Weiss, L. L., 1964. Sequences of wet and dry days described by a Markov chain model. Monthly Weather Review, 92: 169-176.

Wilson, J., D. Schertzer, and S. Lovejoy, 1991. Continuous multiplicative cascade models of rain and clouds. In: Schertzer, D., and S. Lovejoy (eds.), *Non-linear variability in Geophysics: scaling and fractals*. Kluwer Academic Publishers, The Netherlands, 185-207.

Witter, J. V., 1984. *Heterogeneity of Dutch rainfall*. Ph.D. dissertation, Wageningen Agricultural University, Wageningen, The Netherlands, 204 p.

Wischmeier, W. H., 1976. Use and misuse of the universal soil loss equation. Journal of Soil and Water Conservation, 31(1): 5-9.

Wischmeier, W. H., and D. D. Smith, 1978. *Predicting rainfall erosion losses — a guide to conservation planning*. U. S. Department of Agriculture, Agriculture Handbook nr. 537.

Wood, E. F., M. Sivapalan, and K. Beven, 1990. Similarity and scale in catchment storm response. Reviews of Geophysics, 28(1): 1-18.

Woolhiser, D. A., and G. G. S. Pegram, 1979. Maximum likelihood estimation of Fourier coefficients to describe seasonal variations of parameters in stochastic daily precipitation models. Journal of Applied Meteorology, 8(1): 34-42.

Woolhiser, D. A., and J. Roldán, 1982. Stochastic daily precipitation models, 2: A comparison of distributions of amounts. Water Resources Research, 18(5): 1461-1468.

Woolhiser, D. A., E. Rovey, and P. Todorovic, 1975. Temporal and spatial variation of parameters for the distribution of n-day precipitation. In: *Floods and droughts*, Proceedings of the Second International Symposium on "Hydrology". Water Resources Publications, Ft. Collins, Colorado, 605-614.

Wu, B., 1973. *Mathematical models for the simulation of cyclonic storm sequences and precipitation.* Ph.D. dissertation, University of California, Davis, USA.

Yang, D., B. E. Goodison, S. Ishida, and C. S. Benson, 1998. Adjustment of daily precipitation data at 10 climate stations in Alaska: application of World Meteorological Organization intercomparison results. Water Resources Research, 34(2): 241-256.

List of symbols and abbreviations

Symbols:

The symbols used in this work were defined throughout the text. The most relevant symbols are listed below. The variables associated with these symbols are non-dimensional, unless it is stated otherwise.

A	-	fractal set of dimension D
A_λ	-	sub-set of an arbitrary set A, at resolution λ
c	-	(fractal) codimension of an arbitrary set A
$c(\gamma)$	-	codimension function, defined for the singularities γ of the density of a process
$c_b(\gamma)$	-	codimension function characterizing a 'bare' process
$c(\gamma,\eta)$	-	codimension function of a η-power renormalized process
C_1	-	multifractal parameter quantifying the degree of non-homogeneity of a process, defined as the singularity of the mean of a process
C_t	-	parameter of an empirical parametrization of the function $c(\gamma)$
$C(q)$	-	codimension function for the moments q, dual to the function $c(\gamma)$
d	-	Euclidean dimension (d=1, 2, 3) of the geometric entity in which an arbitrary fractal set A is embedded; also subscript referring to 'dressed' quantities; also derivative
D	-	dimension of the space embedding an arbitrary set A
D_A	-	fractal dimension of an arbitrary set A
D_s	-	sampling dimension
$D(q)$	-	dimension function defined for the moments q of the density of a process
$D(\gamma)$	-	(fractal) dimension function defined for the singularities γ of the density of a process
$E(\omega)$	-	energy (power) spectrum
$E_\Gamma(\omega)$	-	energy (power) spectrum of the multifractal generator Γ
f	-	parameter in the spectral exponent of the stable extremal Lévy noise ($1/f$ noise)
$f(\gamma)$	-	proportionality factor given as a function of the singularity γ
H	-	multifractal parameter quantifying the degree of non-conservation of a process
$K(q)$	-	moments scaling exponent function
$K_b(q)$	-	empirical moments scaling exponent function characterizing a 'bare' process

$K(q,\eta)$ - double-moment scaling exponent function characterizing a η-power renormalized process ($\eta \neq 1$)
L - size of a geometric object defined in a 1-dimensional space; the dimensions/units depend on the nature of the embedding space, e.g. [L], [T]
L_α - Lévy random variable (index α)
$M(\ )$ - Mellin transform
$M^{-1}(\ )$ - inverse Mellin transform
N_s - finite number of (independent) samples
N_∞ - infinite number of (independent) samples
N_λ - number of non-overlapping 'cubes' of side λ^{-1} necessary to cover a bounded part of the D-dimensional space containing an arbitrary set A
$N_{\lambda,A}$ - number of non-overlapping 'cubes' of side λ^{-1} needed to cover the fractal set A embedded in a D-dimensional space
$N_\lambda(\gamma)$ - number of 'cubes' of side λ^{-1} satisfying $\varepsilon_\lambda \geq \lambda^\gamma$
$p(\gamma)$ - multiplicative factor given as a function of γ
q - order of statistical moment
q_D - critical order for divergence of statistical moments
q_s - critical order of the statistical moments caused by undersampling
q_γ - moment related to the order of singularity γ: $K'(q_\gamma)=\gamma$
q_{max} - critical moment defined as $q_{max}=\min(q_s, q_D)$
q_{min} - critical moment of the exponent function $K(q)$, with $0<q_{min}<1$
r - reducing factor; **also** (non-dimensional) intensity threshold
R_λ - rainfall intensity at resolution λ [$L T^{-1}$]
R_o - radius of curvature of a function
$\mathbb{R}$ - set of real numbers
s - subscript referring to quantities estimated from finite samples
t - time [T]; **also** subscript indicating tangent
T - time, denotes the largest duration of the observation period [T]
T_{hr} - intensity threshold
Tr_λ - trace moments, ensemble average for the set A at resolution λ
x - non-negative random variable; **also** orthogonal axis
X_i - random variable, with $i=1,n$
$Z(q)$ - first characteristic function

α - parameter quantifying the degree of multifractality, the Lévy index
α-model - a multifractal cascade model
α' - parameter related to the Lévy index α by the relation $1/\alpha+1/\alpha'=1$
β - spectral exponent
β-model - a monofractal cascade model
Γ - generator of a multifractal process, a random noise with infinite band-width $[1,\infty[$
Γ_λ - multifractal generator of the density ε_λ of a process, $\Gamma_\lambda=\ln(\varepsilon_\lambda)$
γ - order of singularity of the intensity of a process
γ_1 - order of singularity characterizing the mean of a process
γ_q - order of singularity related to the moment q: $c'(\gamma_q)=q$
γ_{max} - upper boundary for the orders of singularities γ
γ^+ - parameter greater than 0, yielding a 'boost' in the α-model
γ^- - parameter smaller than 0, yielding a 'decrease' in the α-model

γ_s - maximum order of singularity of the intensity of a process, likely to be observed in a finite number N_s of samples

γ_D - critical order of singularity associated with divergence of statistical moments of order larger than q_D

γ_t - parameter of an empirical parametrization of the function $c(\gamma)$

δ - scale of homogeneity

ε - (non-dimensional) intensity (or density) of a process

ε_d - (non-dimensional) intensity (or density) of a 'dressed' process

ε_h - 'hidden' (small-scale) intensity (or density) contributing to the 'dressed' intensity $\varepsilon_d=\varepsilon\varepsilon_h$, where ε is the intensity of a 'bare' process

ε_λ - (non-dimensional) intensity (or density) of a process on a scale of resolution λ

$\varepsilon_{\lambda,i}$ - all (non-dimensional) intensities of a process observed on a D-dimensional space, at a scale of resolution λ, with $i=1,\lambda^D$

$\varepsilon_{\lambda'}^{(\eta)}$ - η-power renormalized intensity (or density) of a process on the finest scale of resolution λ'

η - moment used to renormalize a process

(η) - superscript indicating renormalization with moments η

λ - scale ratio, defined as the quotient between the largest scale of interest and the homogeneity scale

λ' - scale ratio corresponding to the finest (known) resolution of a process

λ_α - constant analogous to the variance, determining the amplitude of random variables

μ - (random) multiplicative 'increment' or factor

μ_q - estimated ensemble average $\langle x^q \rangle$ obtained using n independent empirical observations; the units depend on the observation

τ - time interval [T]

ω - wave-number, for temporal processes, $\omega=1/\tau$ [T^{-1}]

$\Pi_\lambda(A)$ - total flux over an arbitrary set A of dimension D, at the scale of homogeneity λ^{-1}

$\Pi_{\lambda'}(A_\lambda)$ - flux density over the set A_λ (sub-set of the set A of dimension D, at resolution λ), where λ' corresponds to the finest (known) homogeneity scale of resolution $\lambda'>\lambda$

$\Pi_{\lambda'}^{(\eta)}(A_\lambda)$ - renormalized η-flux density over the set A_λ (sub-set of the set A of dimension D, at resolution λ), where λ' corresponds to the finest (known) resolution

$\Pi_\infty(A)$ - regular limit for the total flux $\Pi_\lambda(A)$, when $\lambda\to\infty$

$\langle ... \rangle$ - ensemble average

$=^d$ - sign that means equality in probability distributions

$\approx$ - sign that means approximately equal to, and which 'absorbs' proportionality constants

Abbreviations:

The abbreviations used frequently in this work are listed below.

DTM - 'Double Trace Moment' (method)

i.i.d. - independent and identically distributed

IM - *Instituto de Meteorologia* (Portugal)

PDMS - 'Probability Distribution/Multiple Scaling' (method)

TM - 'Trace Moment' (method)

WAU - Wageningen Agricultural University (The Netherlands)

Acknowledgements

The author would like to express her gratitude to Prof. Dr.-Ing. J. J. Bogardi and Prof. Dr. Ir. J. Grasman, of the Wageningen Agricultural University, for their supervision and support during the period dedicated to this research.

The author is grateful to Prof. Dr. S. Lovejoy (McGill University, Canada) for the stimulating discussions and continued encouragement during various stages of this work. The author also thanks Dr. D. Schertzer and Dr. F. Schmitt (Pierre et Marie Curie University, France) for their interest in this research.

Thanks are given to several staff members of the Sub-department of Water Resources (Department of Environmental Sciences) of the Wageningen Agricultural University, where the present work was partly conducted. The author is particularly grateful to Drs. P.J.J.F. Torfs and Dr. Ir. R.W.R. Koopmans for their comments on Chapter 2, to Ing. A. Dommerholt for his assistance in preparing some figures, and to Ir. P.M.M. Warmerdam for his help regarding administrative matters.

Junta Nacional de Investigação Científica e Tecnológica (Portugal) and the Wageningen Agricultural University (The Netherlands) are acknowledged for financial support of this research. The opportunity given to the author by the *Escola Superior Agrária*, of the *Instituto Politécnico de Coimbra* (Portugal), to conduct this research at the Wageningen Agricultural University is also acknowledged.

Thanks are extended to *Direcção Geral de Hidráulica e Engenharia Agrícola*, from the Portuguese Ministry of Agriculture, for allowing the author to use the data collected at the Erosion Experimental Station of Vale Formoso (Portugal). The assistance of Mrs. A. Jacobs, during the visits of the author to the Experimental Station, is appreciated. The digitized rainfall data from Vale Formoso were kindly provided by Prof. Dr. M. A. Coutinho of the *Instituto Superior Técnico* (Lisbon, Portugal). The rainfall data from Assink (Hupsel), The Netherlands, were provided by the Sub-department of Water Resources of the Wageningen Agricultural University. The data from Nancy, France, were kindly made available to the author by Dr. S. Lovejoy and Dr. D. Schertzer. The data are part of a data collection programme established by Prof. Dr. I. Roussel (Lille University, France).

A word of appreciation goes also to Darko Milutin, and to Meredith and Han Naeff. Finally, sincere thanks go to Rui and João.

About the author

Maria Isabel Mendes Leal Pereira Pedroso de Lima was born in Leiria, Portugal, on the 18 November 1960.

In 1983 she graduated in Civil Engineering at the Faculty of Science and Technology of the University of Coimbra (Portugal).

From 1983 to 1986 she worked, as an engineer, for the *Direcção Geral dos Recursos e Aproveitamentos Hidráulicos* of the Portuguese Ministry of Public Works.

In 1985 she participated on the 24th International Course on Land Drainage, held in Wageningen (the Netherlands), and organized by the International Institute for Land Reclamation and Improvement (ILRI) and the International Agricultural Centre. In 1986/87 she undertook a 7-month training period at ILRI.

In 1987 she joined the M.Sc. Course on Soil Science and Water Management of the Wageningen Agricultural University (WAU), and graduated in 1989 in the specialization Agrohydrology.

Since December 1989 she has been working as a lecturer at the *Escola Superior Agrária* of the Politechnical Institute of Coimbra, teaching courses related to civil and rural engineering. During several periods over this time, she was given the opportunity to conduct her doctoral research at the Department of Environmental Sciences, Sub-department of Water Resources, of the WAU, under the supervision of Prof. Dr.-Ing. J. J. Bogardi and Prof. Dr. Ir. J. Grasman, of that University.

Her present address is: *Departamento Florestal*
Escola Superior Agrária
Instituto Politécnico de Coimbra
Bencanta, 3040 Coimbra, Portugal.

e-mail: iplima@mail.esac.pt